UNIVERSIDADE FEDERAL DE CAMPINA GRANDE
CENTRO DE SAÚDE E TECNOLOGIA RURAL
UNIDADE ACADÊMICA DE MEDICINA VETERINÁRIA
PROGRAMA DE PÓS-GRADUAÇÃO EM CIÊNCIA E SAÚDE ANIMAL

Ana Yasha Ferreira de La Salles

Anatomia óssea do macaco-prego (*Sapajus libidinosus Spix*, 1823): Análise comparativa macroscópica, radiográfica e tomográfica

PATOS - PB
2022

Ana Yasha Ferreira de La Salles

Anatomia óssea do macaco-prego (*Sapajus libidinosus* Spix, 1823): Análise comparativa macroscópica, radiográfica e tomográfica

Tese submetida ao Programa de Pós-Graduação em Ciência e Saúde Animal, da Universidade Federal de Campina Grande, como requisito parcial para obtenção do grau de Doutor em Ciência e Saúde Animal.

Prof. Dr. Danilo José Ayres de Menezes

Patos/PB
2022

L111a La Salles, Ana Yasha Ferreira de.
Anatomia óssea do macaco-prego (*Sapajus libidinosus* Spix, 1823): análise comparativa macroscópica, radiográfica e tomográfica / Ana Yasha Ferreira de La Salles. – Patos, 2022.
183f. : il. color

Tese (Doutorado em Ciência e Saúde Animal) - Universidade Federal de Campina Grande, Centro de Saúde e Tecnologia Rural, 2022.
"Orientação: Prof. Dr. Danilo José Ayres de Menezes".
Referências.

1. Anatomia. 2. Osteologia. 3. Primates. 4. Radiologia Digital. 5. Tomografia. I. Menezes, Danilo José Ayres de. II. Título.

CDU 591.4(043)

FICHA CATALOGRÁFICA ELABORADA PELA BIBLIOTECÁRIA ITAPUANA SOARES DIAS GONÇALVES CRB-15/93

MINISTÉRIO DA EDUCAÇÃO
UNIVERSIDADE FEDERAL DE CAMPINA GRANDE
PÓS-GRADUACAO EM CIÊNCIA E SAÚDE ANIMAL
Rua Aprigio Veloso, 882, - Bairro Universitario, Campina Grande/PB, CEP 58429-900

FOLHA DE ASSINATURA PARA TESES E DISSERTAÇÕES

ANA YASHA FERREIRA DE LA SALLES

ANATOMIA ÓSSEA DO MACACO-PREGO (*Sapajus libidinosus* SPIX, 1823): ANÁLISE COMPARATIVA MACROSCÓPICA, RADIOGRÁFICA E TOMOGRÁFICA

Tese apresentada ao Programa de Pós-Graduação em Ciência e Saúde Animal como pré-requisito para obtenção do titulo de Doutor em Ciência e Saúde Animal.

Aprovada em: 14/02/2022

BANCA EXAMINADORA:

Prof. Dr. Danilo José Ayres de Menezes (Orientador - UFRN)

Prof. Dr. Marcelo Jorge Cavalcanti de Sá (Examinador Interno - PPGCSA/UFCG)

Profa. Dra. Marcia Almeida de Melo (Examinadora Interna - PPGCSA/UFCG)

Prof. Dr. José Rômulo Soares dos Santos (Examinador Externo - FACENE/FAMENE)

Prof. Dr. Gildenor Xavier Medeiros (Examinador Externo - UFCG)

OBSERVAÇÕES:

1 - Por não possuir cadastro como usuário externo no SEI, o examinador José Rômulo Soares dos Santos receberá cópia do presente documento e dará ciência e aprovação dos termos por e-mail.

2 - Os examinadores internos signatários certificam que o examinador externo acima identificado participou da defesa da tese e tomou conhecimento do teor deste documento.

Documento assinado eletronicamente por **MARCIA ALMEIDA DE MELO**, **PROFESSOR DO MAGISTERIO SUPERIOR**, em 14/02/2022, às 12:03, conforme horário oficial de Brasília, com fundamento no art. 8º, caput, da Portaria SEI nº 002, de 25 de outubro de 2018.

Documento assinado eletronicamente por **MARCELO JORGE CAVALCANTI DE SA**, **PROFESSOR DO MAGISTERIO SUPERIOR**, em 14/02/2022, às 12:08, conforme horário oficial de Brasília, com fundamento no art. 8º, caput, da Portaria SEI nº 002, de 25 de outubro de 2018.

Documento assinado eletronicamente por **DANILO JOSE AYRES DE MENEZES**, **Usuário Externo**, em 14/02/2022, às 12:11, conforme horário oficial de Brasília, com fundamento no art. 8º, caput, da Portaria SEI nº 002, de 25 de outubro de 2018.

Documento assinado eletronicamente por **GILDENOR XAVIER MEDEIROS**, **PROFESSOR DO MAGISTERIO SUPERIOR**, em 15/02/2022, às 14:11, conforme horário oficial de Brasília, com fundamento no art. 8º, caput, da Portaria SEI nº 002, de 25 de outubro de 2018.

A autenticidade deste documento pode ser conferida no site https://sei.ufcg.edu.br/autenticidade, informando o código verificador **2115210** e o código CRC **F35B6A8D**.

Dedicatória

Aos meus pais, primeiros educadores, formadores e professores, e a fonte de amor mais pura.

Ao meu esposo, pelo incentivo, encorajamento, compreensão, e tanto amor a mim dedicado.

AGRADECIMENTOS

A Deus, fonte inesgotável de amor e misericórdia, por ter sido luz em toda a minha estrada, pela coragem e discernimento.

Aos meus irmãos, tios, primos, sobrinhos, sogros, cunhados, avós (*in memorian*), pelo amor, orgulho e vibração de sempre.

Ao meu orientador, Prof. Danilo, grande responsável pelo meu crescimento acadêmico, por todo acompanhamento, ensinamento e encorajamento.

A todos os professores que passaram pela minha trajetória. Um pouco de cada um de vocês está em mim, a cada passo mais alto que dou.

À pequena (grande) equipe de experimento. Obrigada por todo empenho, compromisso e amizade. Sem vocês, certamente seria bem mais difícil.

A toda a equipe do CETAS/Natal, em especial a Tiago e Douglas, à UNP, em nome da professora Luanna Fernandes Silva, e ao IRV, em nome do Dr. Marcius Alessandro Peçanha Klem, por todo apoio para que a pesquisa fosse realizada.

A todos que fazem parte do Ligamorfa e do Laboratório de Anatomia Animal da UFRN. Obrigada pela vivência, descontração e ajuda sempre que precisei.

Aos meus amigos Potiguares e também aos "Patoenses de coração". Obrigada por todo apoio e incentivo. Obrigada pela vibração a cada conquista e por se fazerem sempre perto.

À Coordenação de Aperfeiçoamento de Pessoal de Nível Superior (CAPES) pela concessão da bolsa.

SUMÁRIO

Página

RESUMO

Estudos anatômicos de base, voltados à descrição de estruturas, são muitas vezes negligenciados, e, por consequência, escassos na literatura, apesar de representarem o alicerce para tantas outras áreas da medicina. O objetivo desse estudo foi descrever a anatomia óssea de *Sapajus libidinosus*, macroscopicamente, e em imagens de tomografia e radiografia. Para isso, um total de quatro cadáveres foram utilizados na análise macroscópica e cinco animais para os exames de imagem, sendo que destes, quatro foram eutanasiados e somados à etapa macroscópica. Para os exames de imagem, os animais foram mantidos anestesiados. Todos os ossos foram documentados com câmera fotográfica digital e as estruturas descritas com base na *Nomina Anatomica Veterinaria* e comparadas com dados da literatura de primatas humano e não humanos. Teste t de Student para amostras independentes foi realizado. Não houve diferença estatística significativa entre machos e fêmeas, quanto ao comprimento das vértebras, esterno, costelas e ossos apendiculares. A coluna vertebral do *Sapajus libidinosus* consiste em sete vértebras cervicais, 13 ou 14 torácicas, cinco ou seis lombares, duas ou três sacrais e 23 ou 24 caudais, com um animal com 16 vértebras. Foi possível constatar a eficiência dos métodos de diagnóstico por imagem em *Sapajus libidinosus*, demonstrando ser possível a identificação das estruturas ósseas com bastante precisão, quando comparado às imagens das peças ósseas. Quanto à região vertebral, a identificação de estruturas foi bastante dependente da presença ou não de sobreposição óssea, assim como, da robustez das vértebras, apresentando maior nitidez ao ponto que segue em sentido caudal. O esterno pôde ser bem descrito por meio da radiografia e reconstrução 3D, sendo este último método de melhor identificação das estruturas das costelas. Estruturas como o sulco para o nervo espinhal, nas vértebras cervicais e cartilagem xifoidea do esterno, não foram claramente visualizadas em nenhum método de imagem. A maioria das estruturas ósseas da escápula foram bem identificadas nos métodos de imagem, sendo mais restrita na projeção ventrodorsal. Já a clavícula apresentou visualização bem limitada. O úmero, assim como o rádio e a ulna, não foram bem retratados em suas epífises proximal e distal pela radiografia, no entanto, foram bem identificados na tomografia. O mesmo foi observado para o fêmur, tíbia e fíbula. Todas as estruturas descritas na imagem macroscópica de carpo, metacarpo, tarso e metatarso puderam ser identificadas por meio da radiografia e tomografia. O osso coxal foi amplamente bem descrito por meio dos métodos de imagem. Um pequeno osso peniano está presente na extremidade do pênis, e pôde ser identificado por todos os métodos analisados. Estruturas mais sutis, como a incisura poplítea, na tíbia e tuberosidade glútea, linha pectínea e face áspera, no osso coxal, não foram identificadas. Estruturas presentes nas superfícies articulares dos ossos ficaram limitadas à análise macroscópica. O *Sapajus libidinosus* apresentou, no geral, características anatômicas estruturalmente e morfologicamente mais semelhantes a da infraordem Simiiformes, incluindo o homem, sendo um ótimo indicador de modelo experimental nestas espécies.

PALAVRAS-CHAVE: Anatomia; osteologia; Primates; radiologia digital; tomografia

ABSTRACT

Basic anatomical studies, aimed at describing structures, are often neglected, and, consequently, scarce in the literature, despite representing the foundation for so many other areas of medicine. The aim of this study was to describe the bone anatomy of *Sapajus libidinosus*, macroscopically, and in tomography and radiography images. For this, a total of four cadavers were used in the macroscopic analysis and five animals in the imaging exams, four of which were euthanized and added to the macroscopic stage. For imaging exams, animals were kept anesthetized. All bones were documented with a digital camera and the structures described based on the *Nomina Anatomica Veterinaria* and compared with data from the literature on human and non-human primates. Student t-test for independent samples was performed. There was no statistically significant difference between males and females, regarding the length of vertebrae, sternum, ribs and appendicular bones. The spinal column of *Sapajus libidinosus* consists of seven cervical vertebrae, 13 or 14 thoracic, five or six lumbar, two or three sacral and 23 or 24 caudal, with one animal with 16 vertebrae. It was possible to verify the efficiency of diagnostic imaging methods in *Sapajus libidinosus*, demonstrating that it is possible to identify bone structures with great precision, when compared to images of bone pieces. As for the vertebral region, the identification of structures was highly dependent on the presence or not of bone overlap, as well as on the robustness of the vertebrae, with greater sharpness in the caudal direction. The sternum can be well described by means of radiography and 3D reconstruction, the latter being a method of better identification of rib structures. Structures such as the sulcus for the spinal nerve, cervical vertebrae and xiphoid cartilage of the sternum were not clearly visualized in any imaging method. Most of the bone structures of the scapula were well identified in the imaging methods, being more restricted in the ventrodorsal projection. The clavicle showed very limited visualization. The humerus, as well as the radius and ulna, were not well portrayed in their proximal and distal epiphysis by radiography, however, they were well identified on tomography. The same was observed for the femur, tibia and fibula. All structures described in the macroscopic image of the carpus, metacarpal, tarsus and metatarsus could be identified by means of radiography and tomography. The thigh bone has been extensively described using imaging methods. A small penile bone is present at the end of the penis, and could be identified by all methods analyzed. More subtle structures, such as the popliteal notch, in the tibia and gluteal tuberosity, pectineal line and scratchy face, in the thigh bone, were not identified. Structures present on the articular surfaces of bones were limited to macroscopic analysis. *Sapajus libidinosus* presented, in general, anatomical characteristics structurally and morphologically more similar to those of the infraorder Simiiformes, including humans, being a great indicator of an experimental model in these species.

KEY-WORDS: Anatomy; osteology; Primates; digital radiology; tomography

LISTA DE TABELAS

CAPÍTULO I

CAPÍTULO II

CAPÍTULO III

LISTA DE FIGURAS

CAPÍTULO I

Página

CAPÍTULO II **Página**

LISTA DE ABREVIATURAS E SIGLAS

2D	Bidimensional
3D	Tridimensional
ASP	American Society of Primatologists
C1	Primeiro par de nervo cervical
C3-C7	Vértebras cervicais
Ca	Vértebra coccígea ou caudal
CETAS	Centro de Triagem de Animais Silvestres
CEUA	Comitê de Ética no Uso de Animais
CR	Radiologia computadorizada
DICOM	Digital Imaging and Communications in Medicine
DR	Radiologia digital
F1-F4	Animais fêmeas de 1 a 4
IAC	Infusão alvo-controlada
IBAMA	Instituto Brasileiro do Meio Ambiente e dos Recursos Naturais Renováveis
ICMBio	Instituto Chico Mendes de Conservação da Biodiversidade
IM	Intramuscular
IP	Imaging plate
IRV	Instituto de Radiologia de Natal
LL	Laterolateral
L1-L6	Vértebras lombares
M1-M4	Animais machos de 1 a 4
Micro-CT	Microtomografia por raios-X
MPR	Reconstrução multiplanar
Pixel	Picture element
RX	Radiografia
S1-S3	Vértebras sacrais
SISBIO	Sistema de Autorização e Informação em Biodiversidade
T1-T14	Vértebras torácicas
TC / CT	Tomografia computadorizada / Computed tomography
UFCG	Universidade Federal de Campina Grande
UFRN	Universidade Federal do Rio Grande do Norte
UnP	Universidade Potiguar
VD	Ventrodorsal

LISTA DE SÍMBOLOS

%	Porcentagem
&	“e” comercial/ampersand
±	Mais ou menos
®	Marca registrada
g	Grama
G	Gauge
kg	Quilograma
km^2	Quilômetro quadrado
kV	Quilovolt
m^2	Metro quadrado
mA	Miliampere
Mean	Média
mg	Miligrama
min	Minuto
mL	Mililitro
mm	Milímetro
n.º	Número
s	Segundo
SD	Desvio Padrão

INTRODUÇÃO GERAL

A grande semelhança encontrada entre primatas não humanos e o homem, a dificuldade de procedimentos experimentais invasivos em humanos e a indisponibilidade de métodos alternativos na pesquisa científica, têm justificado o uso desses animais (RIBEIRO, 2002), com atenção ao refinamento e à redução como exigência absoluta, para garantir o respeito do Princípio dos 3Rs, de acordo com Russell e Burch (1959). No entanto, considerando que pesquisas com primatas são amplamente limitadas pelos comitês de ética e legislações (SHARP, 2017), a utilização de roedores ainda vem se sobrepondo.

Para estudos osteológicos, a uniformidade nos resultados de dados de roedores em comparação com o homem é dificultada, não sendo considerados modelos adequados nas pesquisas que envolvem, principalmente, estudo das propriedades estruturais do osso (NUNAMAKER, 1998). Primatas não humanos são mais amplamente caracterizados como modelos para a biologia esquelética humana do que qualquer outra ordem animal e, particularmente, o macaco-prego (*Sapajus libidinosus*) se assemelha ao homem quanto à estrutura óssea e remodelação, tornando-o um excelente modelo animal de primata não humano para estudos osteológicos (PRITZKER; KESSLER, 2012). As pesquisas nesse ramo utilizando macacos-prego são escassas, mas incluem trabalhos com osteoporose (CAMARGO et al., 2013), displasia coxofemoral (FONTELES et al., 2010), maloclusão e osteodistrofia (PINTO, 2016).

Com a chegada da radiologia e, mais tarde, das demais modalidades de imagem, como a tomografia computadorizada, na medicina veterinária, a identificação e avaliação das estruturas internas dos animais tornou-se mais prática. Entretanto, a análise de exames de imagem, como a radiografia e a tomografia, depende estreitamente do conhecimento anatômico macroscópico da espécie animal para que haja reconhecimento das estruturas naturais e alteradas (CUBAS et al., 2014; GOODENOUGH et al., 2012). Ainda hoje, apesar do surgimento de novas modalidades de imagem, a radiografia continua a ser a mais rápida e econômica modalidade de imagem para primatas não humanos usados em laboratórios em todo o mundo (XIE et al., 2014).

A espécie em estudo, o *Sapajus libidinosus*, é um primata do Novo Mundo (Infraordem Platyrrhini, família Cebidae) com comprimento do corpo de 35 cm a 48 cm e comprimento da cauda, de 37 cm a 55 cm (BICCA-MARQUES, 2006). Esses animais arbóreos diurnos são os que apresentam maior distribuição geográfica dentre as espécies neotropicais e pesam entre 1,5 a 4,0 kg (MARTINS et al., 2021; KINZEY, 1997). Eles são onívoros e se alimentam

naturalmente com frutos, insetos, sementes, flores, brotos e pequenos vertebrados (ROCHA, 1992). Tanto em seus habitats naturais quanto em cativeiro, vivem em grupos sociais que variam de seis a 35 indivíduos, com composição estável e geralmente apenas um ou dois machos adultos, sendo também observados com frequência indivíduos solitários (BICCA-MARQUES et al., 2006). Depois de uma gravidez de aproximadamente 150 dias, nasce um único filhote, exclusivamente dependente da mãe para nutrição e transporte, pelo menos até o segundo mês de vida (VERDERANE; IZAR, 2019). A maturidade sexual é atingida na idade de quatro a cinco anos para fêmeas e sete anos para machos, e a expectativa de vida de animais em cativeiro é de 40-50 anos (FRAGASZY et al., 2004).

Apesar de seu uso crescente na pesquisa biomédica, as características específicas do esqueleto desta espécie são mal documentadas. Schwartz e Yamada (1998) oferecem um breve relato sobre a anatomia do carpo de macaco-prego, em estudo que abrange primatas no geral. Molina et al. (2016) utilizou pontos ósseos na obtenção da via de melhor acesso para bloqueio anestésico do plexo braquial e La Salles et al. (2021) utilizaram a identificação da clavícula, para determinação do melhor ponto para anestesia de plexo por via supraclavicular. Young & Heard-Booth (2016) analisaram a ontogenia das proporções intrínsecas das mãos e dos pés de macacos-prego. Cordeiro et al. (2014) estudaram o segmento toraco-lombar do macaco-prego visando saber a localização do cone medular para anestesia epidural na espécie. Além disso, como nenhum estudo apresenta parâmetros de radiografia e tomografia óssea completa em *Sapajus libidinosus*, é essencial construir índices de referência de parâmetros baseados para esta espécie.

Diante disso, devido à escassez de dados osteológicos e imagiológicos específicos, o primeiro capítulo foi destinado à descrição das vértebras, esterno e costelas e suas particularidades. O segundo capítulo foi direcionado à descrição do membro torácico e suas particularidades. E o terceiro capítulo foi aplicado à descrição do membro pélvico e suas particularidades. Ambos os estudos foram comparados com imagens tomográficas e de radiografia. Diante disso, o texto enfocou as principais características do esqueleto da espécie, enquanto as imagens ilustraram as várias particularidades com mais detalhes. A terminologia anatômica comum em português foi usada em todo o texto, enquanto as legendas das figuras também forneceram os termos oficiais em latim.

REFERÊNCIAS

BICCA-MARQUES, J. C.; SILVA, V. M.; GOMES, D. F. Ordem Primates. In: REIS, N. R.; PERACCHI, A. L.; PEDRO, W. A.; LIMA, I. P. (Org.). **Mamíferos do Brasil**. 5. ed. Londrina: UEL, 2006. p. 101-148.

CAMARGO, N. I.; SILVA, I. C. C.; SANTOS, M. S.; COSTA, L. A. V. S.; COSTA, F. S. Osteoporose estabelecida em macaco-prego galego (*Cebus flavius*) – Relato de caso. **Archives of Veterinary Science**, v. 18, supl.1, Resumo 006, 2013.

CORDEIRO, J. F.; SANTOS, J. R. S.; DANTAS, S. B. A.; FONSECA, S. S.; DIAS, R. F. F.; MEDEIROS, G. X.; NÓBREGA NETO, P. I.; MENEZES, D. J. A. Anatomia do cone medular aplicada à via epidural de administração de fármacos em macacos-prego (*Sapajus libidinosus*). **Pesquisa veterinária brasileira**, v. 34, Supl.1, p. 29-33, 2014.

CUBAS, Z. S.; SILVA, J. C. R.; CATÃO-DIAS, J. L. **Tratado de animais selvagens**: Medicina Veterinária. 2. ed. São Paulo: Editora GEN/Roca, 2014.

FONTELES, Z. G. C.; QUESSADA, A. M.; ALCANTARA, D. S.; SOUSA, J. M. Aspectos radiográficos da displasia coxofemoral em um *Cebus libidinosus*: Relato de caso. **PUBVET**, v. 4, n. 24, ed. 129, art. 874, p. 1-6, 2010.

FRAGASZY, D. M.; VISALBERGHI, E.; FEDIGAN, L. **The complete capuchin**: The biology of the genus *Cebus*. Cambridge: Cambridge University Press, 2004.

GOODENOUGH, A. E; SMITH, A. L.; STUBBS, H.; WILLIAMS, R.; HART, A. G. Observer variability in measuring animal biometrics and fluctuating asymmetry when using digital analysis of photographs. **Annales Zoologici Fennici**, v. 49, n. 1-2, p. 81-92, 2012.

KINZEY, W. G. *Cebus*. In: KINZEY, W. G. (Org.). **New World Primates**: Ecology, evolution, and behavior. New York: Aldine de Gruyter, 1997.

LA SALLES, A. Y. F; ANDRADE, J. K.; CORDEIRO, J. F.; CARREIRO, A. N.; FALCÃO, B. M. R.; FREITAS, K. B.; MENEZES, D. J. A. Assessment of the technique of the anesthetic block of the brachial plexus by supraclavicular approach in *Sapajus libidinosus* (SPIX, 1823). **Journal of Medical Primatology**, v. 50, n. 1, p. 29-35, 2021.

MARTINS, A. B.; FIALHO, M. S.; JERUSALINSKY, L.; VALENÇA-MONTENEGRO, M. M.; BEZERRA, B. M.; LAROQUE, P. O.; MELO, F. R.; LYNCH ALFARO, J. W. *Sapajus libidinosus* (amended version of 2019 assessment). **The IUCN Red List of Threatened Species**, 2021. Disponível em: <https://dx.doi.org/10.2305/IUCN.UK.2021-1.RLTS.T136346A192593226.en>.

MOLINA, J. M.; DIAS, R. F. F.; VASCONCELOS, K. F.; ROCHA, E. F.; SANTOS, J. R. S.; LA SALLES, A. Y. F.; CARREIRO, A. N.; MEDEIROS, G. X.; MENEZES, D. J. A. Bases anatômicas para o bloqueio anestésico do plexo braquial de macacos-prego (*Sapajus libidinosus*). **Acta Scientiae Veterinariae**, v. 44, p. 1-6, 2016.

NUNAMAKER, D. M. Experimental models of fracture repair. **Clinical Orthopaedics and Related Research**, v. 355, p. 56-65, 1998.

PINTO, A. L. M. F. T. **Levantamento clínico e radiológico da prevalência de doenças dentárias em primatas no parque zoológico de Goiânia.** Orientador: Naida Cristina Borges. 2016. 65 f. Dissertação (Mestrado) - Ciência Animal, Escola de Veterinária e Zootecnia, Universidade Federal de Goiás, Goiás, 2016.

PRITZKER, K. P. H.; KESSLER, M. J. Arthritis, muscle, adipose tissue, and bone diseases of nonhuman primates. In: ABEE, C. R.; MANSFIELD, K.; TARDIF, S.; MORRIS, T. (Org.). **Nonhuman primates in biomedical research**: Diseases. 2. ed. San Diego: Academic Press, 2012. p. 415-459.

RIBEIRO, A. R. **Estudo anatômico do plexo braquial do macaco *Cebus apella***: origem, composição e nervos resultantes**.** Orientador: Irvenia Luiza de Santis Prada. 2002. 145 f. Dissertação (Mestrado) Anatomia dos Animais Domésticos, Faculdade de Medicina Veterinária e Zootecnia, Universidade de São Paulo, São Paulo, 2002.

ROCHA, V. J. Macaco-prego, como controlar esta nova praga florestal? **Floresta**, v. 30, n. 1, p. 95–99, 2000.

RUSSELL, W. M. S.; BURCH, R. L. **The principles of humane experimental technique**. London: Methuen & Company, 1959.

SHARP, L. A. The moral lives of laboratory monkeys: television and the ethics of care. **Culture, medicine, and psychiatry**, v. 2, n. 41, p. 224-244, 2017.

SCHWARTZ, J. H.; YAMADA, T. K. Carpal anatomy and primate relationships. **Anthropological Science**, v. 106, p. 47-65, 1998.

VERDERANE, M. P.; IZAR, P. Estilos de cuidado materno em primatas: Considerações a partir de uma espécie do Novo Mundo. **Psicologia USP**, v. 30, 2019.

XIE, L.; ZHOU, Q.; LIU, S.; W. U, Q.; JI, Y.; ZHANG, L.; XU, F.; GONG, W.; MELGIRI, N. D.; XIE, P. Normal thoracic radiographic appearance of the cynomolgus monkey (*Macaca fascicularis*). **PLOS ONE**, v. 9, n. 1, p. 1-6, 2014.

YOUNG, J. W.; HEARD-BOOTH, A. N. Grasping primate development: Ontogeny of intrinsic hand and foot proportions in capuchin monkeys (*Cebus albifrons* and *Sapajus apella*). **American Journal of Physical Anthropology**, v. 161, n. 1, p. 104-115, 2016.

CAPÍTULO I:

Anatomy applied to diagnostic imaging of the vertebrae, sternum and ribs of the capuchin monkey (Cebidae: Primates)

Trabalho submetido à revista Journal of Anatomy
ISSN: 1469-7580; Fator de impacto: 2.610; Qualis A2

Anatomy applied to diagnostic imaging of the vertebrae, sternum and ribs of the capuchin monkey (Cebidae: Primates)

Anatomy of the vertebrae, sternum and ribs of the capuchin monkey

Ana Yasha Ferreira de La Salles[1], Jéssica Kária de Andrade[2], Joyce Galvão de Souza[1], Kelvis de Brito Freitas[3], Artur da Nóbrega Carreiro[1], Edson Vinícius Leite Veloso[1], Ediane Freitas Rocha[1], Marcius Alessandro Pessanha Klem[4], Fábio Tatian Moura Mendonça[5], Danilo José Ayres de Menezes[1,6*]

[1]Postgraduate Program in Animal Science and Health, Federal University of Campina Grande, Center for Rural Health and Technology, 58708-110. Patos, Paraiba, Brazil.

[2]Veterinary Doctor, Postgraduate in Veterinary Anesthesiology at Instituto Qualittas, 60175-020. Fortaleza, Ceará, Brazil.

[3]Graduate Program in Structural and Functional Biology, Federal University of Rio Grande do Norte, 59078-220. Natal, Rio Grande do Norte, Brazil.

[4]Veterinarian specialized in Diagnostic Imaging, managing partner of the Institute of Veterinary Radiology, 59080-101. Natal, Rio Grande do Norte, Brazil.

[5]Veterinary Doctor, Tutor of Diagnostic Imaging Practices, Veterinary Health Center, Universidade Potiguar, 59052-000. Natal, Rio Grande do Norte, Brazil.

[6]Department of Morphology, Federal University of Rio Grande do Norte, 59078-970. Natal, Rio Grande do Norte, Brazil.

*Corresponding author: Danilo José Ayres de Menezes, Campus Universitário UFRN, Av. Senador Salgado Filho, 3000, Lagoa Nova, Natal/RN, 59064-741, Telephone: +55 84 98101-9198, mdanayres@gmail.com.

Abstract

Anatomical studies applied to veterinary medical knowledge, and which contribute to intervention in the areas of surgery, anesthesia, and diagnostic imaging are crucial for a correct assessment and approach to the animal. The black-striped capuchin monkey is a New World monkey and an excellent animal model for studies of the bone system. Therefore, the aim of this study was to describe the structures of the vertebrae, sternum and ribs of the capuchin monkey in anatomical pieces, identifying them in radiographic and tomographic images. For this, four cadavers were used in the macroscopic analysis and five animals for the imaging exams, of which four were euthanized and added to the macroscopic stage. For imaging exams, the animals were anesthetized. All bones were documented with a digital camera, the structures were described and compared with data from the literature of human and non-human primates. Student's t-test for independent samples was performed. There was no statistical difference between males and females regarding the length of the vertebral and sternum segments. The vertebral column of the capuchin monkey comprises seven cervical, 13 or 14 thoracic, five or six lumbar, two or three sacral, and 23 or 24 caudal vertebrae, with one animal having 16 vertebrae, which was cut. The atlas is characterized by having three foramina on the wing, the sixth cervical vertebra can be easily recognized by its ventral lamina and the seventh cervical vertebra in one specimen had a transverse foramen. The anticlinal vertebra is always the penultimate thoracic one, the ninth pair of ribs is always the last sternal pair, and the last two are buoyant. The sternum presented its body divided into five or six sternebrae. The lumbar vertebrae had a bifurcated spinous process and a well-developed accessory process. Three different sacral morphologies were observed, and the first five caudal ones are of differentiated structure. The structures identified macroscopically, in general, could be well determined through radiographic and tomographic images. The capuchin monkey presented anatomical characteristics, in terms of particularities, very similar to those of man, and, in terms of shape, similar to those of New World monkeys, being an excellent indicator of an experimental model in studies in man. Knowledge through gross anatomy and tomographic and radiological exams may contribute to a better evaluation of therapeutic agents, regional anesthesia, skeletal diseases, osteometabolic diseases, and bone clinical-surgical interventions.

Key words

3D reconstruction, digital radiology, osteology, Platyrrhini, tomography

1 INTRODUCTION

In the last 30 years, research involving non-human primates has been conducted with great interest, a point attributed to the anatomical, physiological and ethological similarity of these animals to the human species (Auricchio, 1995). For osteological studies, the black-striped capuchin monkey (*Sapajus libidinosus*) resembles humans in bone structure and remodeling, making it an excellent non-human primate animal model for this line of research (Pritzker & Kessler, 2012).).

Sapajus libidinosus is a New World monkey (Infraorder Platyrrhini, family Cebidae) with a body length of 35 cm to 48 cm, and a tail length of 37 cm to 55 cm (Bicca-Marques, 2006). These diurnal arboreal animals are the most geographically distributed among Neotropical species and weigh between 1.5 and 4.0 kg (Kinzey, 1997; Martins et al., 2021).

Among the areas that have shown great growth in veterinary medicine in recent years, imaging has been praised given its considered evolution (Krautwald-Junghanns et al., 2001). The analysis of imaging tests, such as radiography and tomography, depends closely on the macroscopic anatomical knowledge of the animal species so that natural and altered structures can be recognized. With the arrival of radiology and, later, other imaging modalities, such as computed tomography, in veterinary medicine, the identification and evaluation of the internal structures of animals became more practical, opening the field of vision for the veterinary diagnosis and anatomical studies (Cubas et al., 2014; Goodenough et al., 2012).

The inclusion of these new modalities allowed the execution of imaging studies in wild animals, including primates (Bortolini, 2013; Tranquilim, 2012). However, there is still a limited number of studies performed on specimens of *Sapajus libidinosus*, focused on the area of macroscopic anatomy compared with imaging methods, which are relevant for clinical studies, research centers, and primatologists.

Despite its increasing use in biomedical research, the specific skeletal features of this species are poorly documented, and little has been reported on aspects of the vertebrae, ribs and sternum. Barros et al. (2003), in a study on the constitution of the lumbar plexus of the black-striped capuchin monkey, offer a brief report on the anatomy of the region. Alves et al. (2012) also discuss the vertebral anatomy in a study that points out the anatomical and radiographic appearance of the thoracic cavity of this monkey. Cordeiro et al. (2014) analyzed the number of vertebrae in a study aimed at determining the anatomy of the medullary cone in *S. libidinosus*.

Therefore, due to the scarcity of specific osteological and imaging data, and based on the importance of anatomical description, as well as imaging modalities for the biological

knowledge of primates, this study aimed to recognize the structures of the vertebrae, sternum and ribs of *Sapajus libidinosus* in anatomical parts, radiographic and tomographic images, to serve as an anatomical guide for future biomedical research.

2 MATERIAL AND METHODS

2.1 Animals and Study Site

The macroscopic stage of the study was conducted at the Laboratory of Animal Anatomy, Department of Morphology, Federal University of Rio Grande do Norte (UFRN), Natal-RN. The CT scans and part of the radiographs were performed at the Institute of Veterinary Radiology (IRV), Natal-RN, and the other radiographs, in partnership with the Potiguar University (UnP), Natal-RN.

The methodological protocols were approved by the Ministry of the Environment, through the Biodiversity Authorization and Information System-SISBIO of the Chico Mendes Institute-ICMBio (n.º 70606-2), CEUA/UFCG (n.º 121/2019), and CEUA/UFRN protocol 074/2019, certificate n.º 209.074/2019.

Four animal cadavers, males, two juveniles, aged less than 10 years, and two adults estimated to be 10-15 years old, kept frozen, donated by CETAS/IBAMA/Natal-RN, were used for the macroscopic study of the vertebrae, sternum and ribs.

For radiography (RX) and tomography (CT), five specimens of *Sapajus libidinosus* were selected, an adult male, estimated at 10-15 years, and four elderly females, estimated at 20-30 years, weighing in average 2.21 kg, from the Wild Animal Screening Center (CETAS/IBAMA), in the city of Natal/RN. The monkeys were submitted to 4 hours of water fasting and 8 hours of food fasting before the anesthetic procedure. After the imaging tests, the females were euthanized with 19.1% potassium chloride (Equiplex®, Brazil), at a dose of 1 mL/kg, intravenously, and added to the macroscopic study, totaling eight animals at this stage. The adult male animal was destined only for the examinations and returned to CETAS.

2.2 Preparation of the parts and bone description

In the eight animals destined for the macroscopic stage, a dissection technique associated with maceration was performed, according to Ladeira & Höfling (2007). The region of interest was separated into ribs and vertebral column (cervical, thoracic and lumbar), and sacral and caudal vertebrae, and stored in bags made of mesh fabric, to facilitate the identification after maceration. In the vertebral column, a wire was inserted through the vertebral foramen,

following the order of the vertebrae. The sternum underwent an alternation between freezing and daily dissection until obtaining the appropriate piece. The bones were separated by animal and, to join them together, Araldite® Hobby epoxy glue and instant superglue (Tekbond®, Brazil) were used.

The lengths of the various segments of the vertebral column (cervical, thoracic, lumbar, sacral and caudal), from the most cranial to the most caudal extremity, the total length of the vertebral column, from cervical to lumbar, and the length of the sternum, from the manubrium to the xiphoid, were determined in the eight animals destined for macroscopic description.

All bones were described, following the recommendations of the *Nomina Anatomica Veterinaria* (International Committee On Veterinary Gross Anatomical Nomenclature, 2017).

2.3 Imaging exams

Five animals were destined for this stage. One adult male and one female for tomography and radiography exams, and the other females only for radiography exams. For the examinations, the animals were referred to the IRV and UnP, sedated with a combination of tiletamine hydrochloride and zolazepam hydrochloride (Telazol® 10%, Zoetis, Brazil) at a dose of 6 mg/kg, administered intramuscularly (La Salles et al. al., 2019, 2021). Upon arrival, access to the caudal saphenous vein was obtained (La Salles et al., 2017) for anesthetic induction, which was performed with intravenous propofol (Provive 1%, União Química, Brazil) in a target-controlled infusion (IAC), with a VP50 infusion pump (MedRena®, Guangdong, China), at a dose of 2-5mg/kg, followed by anesthetic maintenance at an initial dose of 0.25-0.5 mg/kg/min, reduced during the experiment. The animal was kept breathing room air, and in the 3rd anesthetic stage, between the 2nd and 3rd plane, so that there was no movement during the exams. Monitoring was performed using a multiparameter monitor (Model DL 1000, Deltalife, Brazil).

After the exams, euthanasia was performed, except for one male animal that was donated only for the examinations. The corpses of the four euthanized females were sent to the Animal Anatomy Laboratory/UFRN to be added to the macroscopic study.

2.3.1 Radiography

At the Veterinary Hospital of UnP, radiographic examinations were performed using a conventional radiodiagnostic device, model VET500, (X-RAD X-Ray equipment, Brazil), with a capacity of 500 mA and 125 kV, equipped with a radiographic table with an anti-diffusion device and X-ray tube, and the images acquired with the CR digital system, with an IP cassette

plate, CC type (24 cm x 30 cm) (Fujifilm, Japan) and FCR PRIMA T2 Image Reader photostimulable phosphor plate scanner, model CR-IR 392 (Fujifilm, Japan). The radiographic technique used was 44-46 kV, 0.05 s and 200 mA, under the same focus-film distance. The images were saved in PDS files and analyzed using the PD-S Viewer software, version 1.4.0.0.

To obtain better image definition, two animals were referred to the IRV and the images were performed using a conventional radiodiagnostic device, Intecal, CR 500 mAs – Casa do Radiologista, equipped with a radiographic table with anti-diffusion grid, "Potter-Bucky ", and IAE X-ray tube (Italy) with rotating anode and the images were acquired using the DR digital system, with a VIEWORKS digitizer plate, model CESIO 1417WA, with 2560 x 3072 pixels. The radiographic technique used was 55 kV, 0.06 s and 300 mA, under the same focus-film distance. After the acquisition, the radiographic images were saved in DICOM files, and transferred and analyzed online using the postDICOM program (Herten, Netherlands). All radiographic examinations were performed in compliance with the radiological protection standards.

The animals were positioned directly on the radiographic tables. Ventrodorsal and laterolateral projections of the cervical, thorax, abdomen, pelvis and tail were made, with emphasis on the entire spine region.

The radiographic exams were individually analyzed, identifying all the bones and particularities observed in the skeletal system already described in the macroscopic stage, and a comparison of the three study methods was performed.

2.3.2 Computed tomography

For this examination, a helical computed tomography device, model XVision EX, single slice (Toshiba, Japan) was used. Before the scan, sagittal radiographic images of each region and sub-region to be studied of each animal were acquired (topogram), to define the extent of the study (the beginning and end of the scan) and the variation of the slices. Once the area was defined, transverse planes with predetermined section thickness and table increment were performed.

The imaging parameters used for the cervical, thoracic, lumbar, sacral and caudal regions were: 2.0 mm slice thickness, 2.0 table increment, 100 mA and 120 kV. To perform the CT, the animals were positioned in sternal recumbency, with the caudal extension of the thoracic and pelvic limbs.

The tomographic images were transferred to the Horos software version 1.1.7 (United States) for the analysis of transverse plane images and multiplanar reconstructions (MPR) in the sagittal and dorsal planes. A 3D reconstruction to illustrate bone anatomy was also obtained.

The tomographic images were individually analyzed, identification of the bones and particularities already described macroscopically was performed, and a comparison of the three methods of the study was performed.

2.4 Statistical analysis

During the study, the results obtained were documented with a digital camera, and, later, described and compared with data from the literature, about human and non-human primates. Mean and standard deviation of bone lengths were determined. Student's t-test was performed for independent samples using the Past software version 4.03.

3 RESULTS

The vertebral column consists of seven cervical vertebrae, 13 or 14 thoracic vertebrae, five or six lumbar vertebrae, two or three sacral vertebrae and 23 or 24 caudal vertebrae. There was an animal with 16 vertebrae because its tail was cut off (Table 1). The sum of the thoracic and lumbar vertebrae does not reach an exact number in all animals.

TABLE 1 Number of vertebrae from each region of four males (M1-M4) and four females (F1-F4) of *Sapajus libidinosus*.

	M1	M2	M3	M4	F1	F2	F3	F4
Cervical Vertebrae	7	7	7	7	7	7	7	7
Thoracic Vertebrae	14	13	14	14	13	14	14	13
Lumbar Vertebrae	6	6	5	5	6	6	5	6
Sacral Vertebrae	3	2	3	3	2	3	3	3
Caudal Vertebrae	24	23	23	24	23	16	23	23

Measurements of the cervical, thoracic, lumbar, sacral and caudal regions, from the most cranial to the most caudal extremity, and the sternum, from the manubrium to the xiphoid process, are distributed in Table 2. For the statistical analysis, only seven specimens were used to obtain values of means and standard deviation in the caudal segment. The animal with the cut-off tail was discarded.

TABLE 2 Length in millimeters (mm) of the vertebral and sternum regions and total length of the vertebral column (from cervical to lumbar) of four males (M1-M4) and four females (F1-F4) of *Sapajus libidinosus*, arranged on average (Mean), standard deviation (SD), mean of males (Mean M) and mean of females (Mean F).

	Mean	**SD**	**Mean M**	**Mean F**
Cervical Region	36.0	3.34	34.5	37.5
Thoracic Region	110.1	13.00	104.8	115.5
Lumbar Region	84.6	11.29	78.5	90.8
Sacral Region	39.8	6.30	37.8	41.8
Tail	421.4	33.25	422.3	420.3*
Sternum	75.4	11.87	68.3	82.5
Vertebral Column	225.5	24.87	210.8	240.3
Value of t			0.657	
Value of p			1.68	

[1] Means do not differ statistically from each other when compared by the t-test ($p < 0,05$).
*Means of three females in the study, excluding the specimen (F2) with the tail cut off.

Data from table 2 demonstrate that there is no statistically significant difference between males and females regarding the length of the vertebral and sternum segments.

The bodies of the cervical vertebrae are short and narrow. The atlas is characterized by small rectangular wings and a large vertebral foramen. Three more foramina are found, the transverse foramen, in the most medial portion of the wing, the alar foramen, and the lateral vertebral foramen, both on the dorsal surface, the first with an external opening and the second with an opening into the vertebral canal (Figure 1).

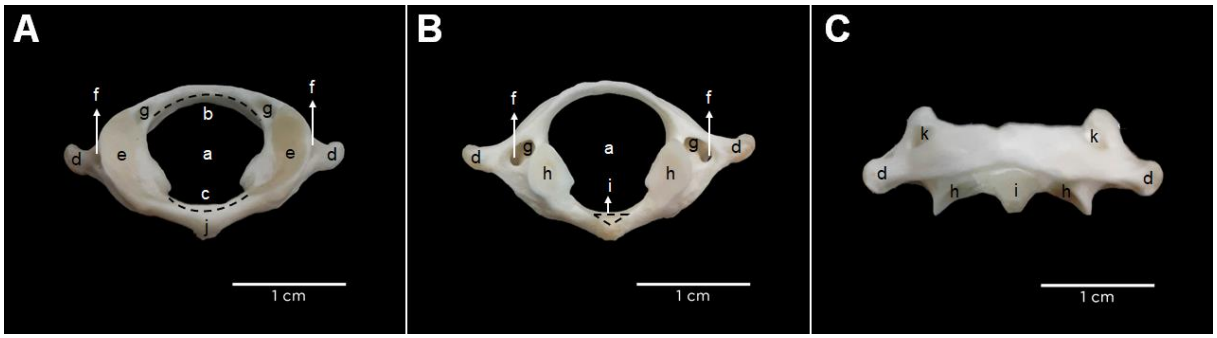

FIGURE 1 First cervical vertebra (Atlas). Cranial view (A), Caudal view (B), Dorsal view (C). a. Vertebral canal (*Canalis vertebralis*); b. Dorsal arch (*Arcus dorsalis*); c. Ventral arch (*Arcus ventralis*); d. Atlas wing (*Ala atlantis*); e. Cranial articular fovea (*Fovea articularis cranialis*); f. Transverse foramen (*Foramen transversarium*); g. Lateral vertebral foramen (*Foramen vertebrale laterale*); h. Caudal articular fovea (*Fovea articularis caudalis*); i. Fovea dentis (*Fovea dentis*); j. Ventral tubercle (*Tuberculum ventralis*); k. Alar foramen (*Foramen alare*).

The axis has a very prominent odontoid process and a triangular spinous process much more robust than the other cervical vertebrae. Among the foramina, only the transverse remains (Figure 2).

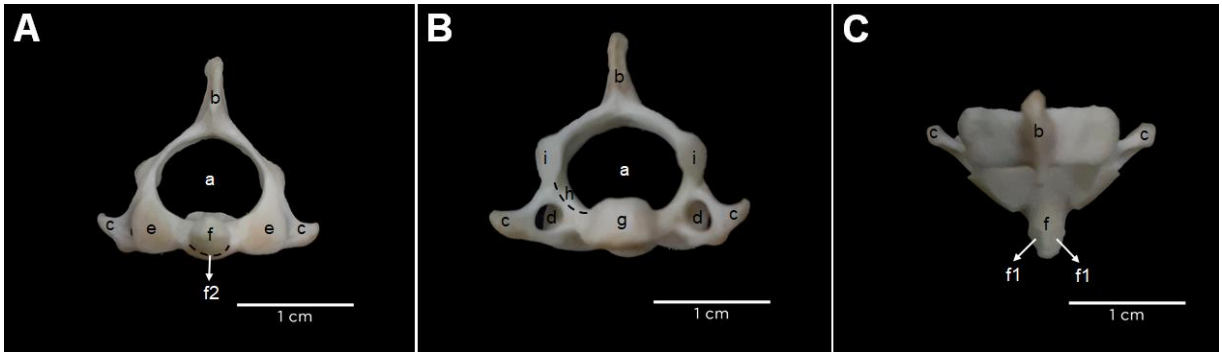

FIGURE 2 Second cervical vertebra (Axis). Cranial view (A), Caudal view (B), Dorsal view (C). a. Vertebral canal (*Canalis vertebralis*); b. Spinous process (*Processus spinosus*); c. Transverse process (*Processus transversus*); d. Transverse foramen (*Foramen transversarium*); e. Cranial articular process (*Processus articularis cranialis*); f. Odontoid process (*Dens*); f1. Dorsal articular surface (*Facies articularis dorsalis*); f2. Ventral articular surface (*Facies articularis ventralis*); g. Caudal end (*Extremitas caudalis*); h. Caudal vertebral notch (*Incisura vertebralis caudalis*); i. Caudal articular process (*Processus articularis caudalis*).

The spinous processes gradually increase in length from the third to the seventh cervical vertebrae and are quite narrow. From the axis to the last cervical vertebra, the caudal ends are quite robust and fit perfectly with the corresponding cranial ends, with their well-developed uncinate processes. The third, fourth and fifth cervical vertebrae have similar morphology (Figure 3). All cervical vertebrae have a groove for the spinal nerve, which is more visible from C3-C6 (Figure 3A).

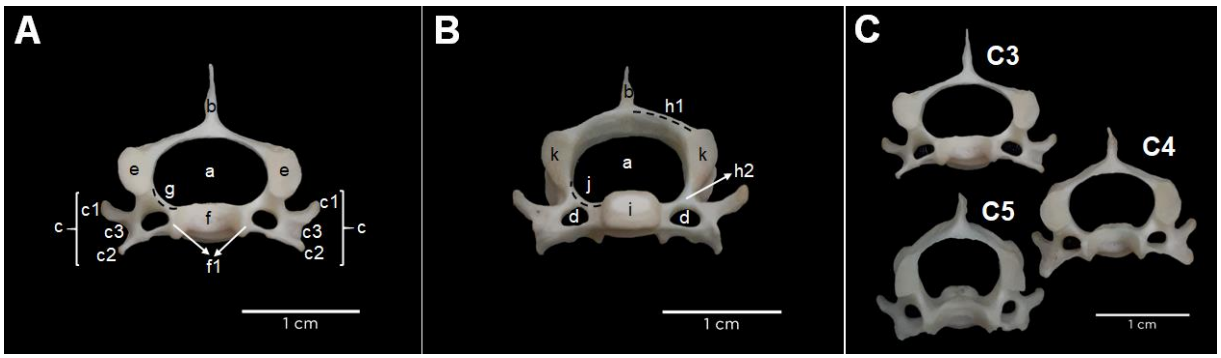

FIGURE 3 Cranial view of the 3rd cervical vertebra - C3 (A), Caudal view of the 3rd cervical vertebra - C3 (B), Cranial view of the C3, C4 and C5 (C). a. Vertebral canal (*Canalis vertebralis*); b. Spinous process (*Processus spinosus*); c. Transverse process (*Processus transversus*); c1. Dorsal tubercle (*Tuberculum dorsale*); c2. Ventral tubercle (*Tuberculum ventrale)*; c3. Sulcus for the spinal nerve (*Sulcus n. spinalis*); d. Transverse foramen (*Foramen transversarium*); e. Cranial articular process (*Processus articularis cranialis*); f. Cranial extremity (*Extremitas cranialis*); f1. Uncinate process (*Unci corporis*); g. Cranial vertebral notch (*Incisura vertebralis cranialis*); h. Vertebral arch (*Arcus vertebrae*); h1. Lamina (*Lamina arcus vertebrae*); h2. Pedicle (*Pediculus arcus vertebrae*); i. Caudal end (*Extremitas caudalis*); j. Caudal vertebral notch (*Incisura vertebralis caudalis*); k. Caudal articular process (*Processus articularis caudalis*).

The sixth cervical vertebra can be easily recognized by its ventral lamina (Figure 4). The seventh cervical vertebra does not have a transverse foramen and has only one tip in the transverse process (Figures 5A and 5B), except for one animal that had a foramen and two tips in the transverse process, the dorsal and ventral tubercle (Figure 5C).

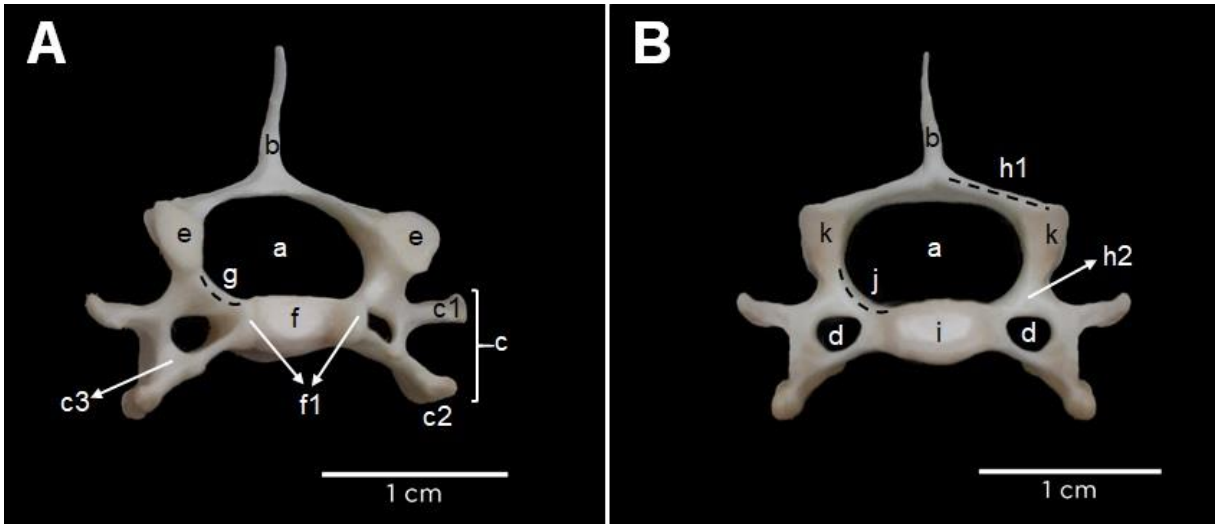

FIGURE 4 Sixth cervical vertebra (C6). Cranial view (A), Caudal view (B). a. Vertebral canal (*Canalis vertebralis*); b. Spinous process *(Processus spinosus*); c. Transverse process (*Processus transversus*); c1. Dorsal tubercle (*Tuberculum dorsale*); c2. Ventral lamina (*Lamina ventralis*); c3. Sulcus for the spinal nerve (*Sulcus n. spinalis*); d. Transverse foramen (*Foramen transversarium*); e. Cranial articular process (*Processus articularis cranialis*); f. Cranial extremity (*Extremitas cranialis*); f1. Uncinate process (*Unci corporis*); g. Cranial vertebral notch (*Incisura vertebralis cranialis*); h. Vertebral arch (*Arcus vertebrae*); h1. Lamina (*Lamina arcus vertebrae*); h2. Pedicle (*Pediculus arcus vertebrae*); i. Caudal end (*Extremitas caudalis*); j. Caudal vertebral notch (*Incisura vertebralis caudalis*); k. Caudal articular process (*Processus articularis caudalis*).

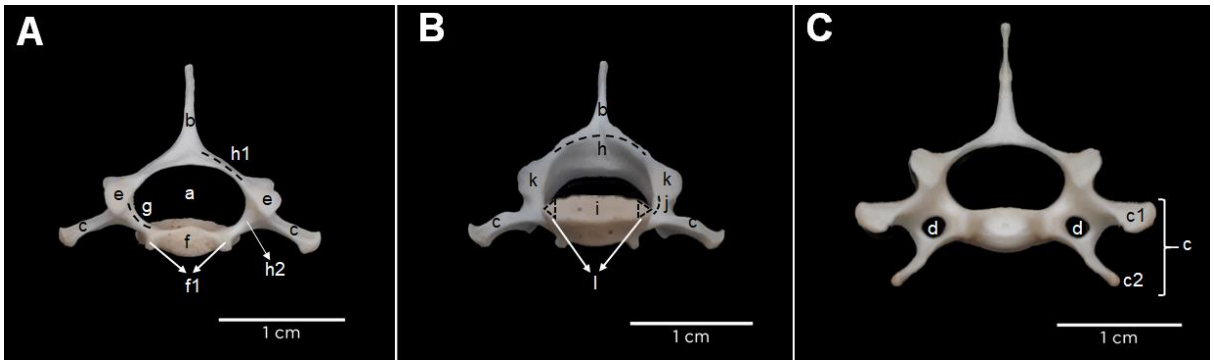

FIGURE 5 Seventh cervical vertebra (C7). Cranial view (A), Caudal view (B), Cranial view of C7 with different morphology (C). a. Vertebral canal (*Canalis vertebralis*); b. Spinous process (*Processus spinosus*); c. Transverse process (*Processus transversus*); c1. Dorsal tubercle (*Tuberculum dorsale*); c2. Ventral tubercle (*Tuberculum ventrale*); d. Transverse foramen (*Foramen transversarium*); e. Cranial articular process (*Processus articularis cranialis*); f. Cranial extremity (*Extremitas cranialis*); f1. Uncinate process (*Unci corporis*); g. Cranial vertebral notch (*Incisura vertebralis cranialis*); h. Vertebral arch (*Arcus vertebrae*); h1. Lamina (*Lamina arcus vertebrae*); h2. Pedicle (*Pediculus arcus vertebrae*); i. Caudal end

(*Extremitas caudalis*); j. Caudal vertebral notch (*Incisura vertebralis caudalis*); k. Caudal articular process (*Processus articularis caudalis*); l. Caudal costal fovea (*Fovea costalis caudalis*).

Most of the bony structures of the cervical vertebrae are visible in radiographic images, in both projections, and the 3D reconstruction (Figures 6 and 7). In the laterolateral projection (LL), structures such as the foramina and transverse process are better identified in the 3D reconstruction (Figure 6B), whereas interosseous structures are more clearly observed in the radiographic examination (Figure 6A). The vertebral canal, dorsal and ventral tubercle of the transverse process, and vertebral notches were only visible in the transverse section of the CT scan (Figures 7B and 7D). In the cervical region, the identification of some structures becomes more difficult because the vertebral bodies are narrow and the vertebrae are intimately articulated, without interarcual spaces. A structure such as the groove for the spinal nerve was not clearly visualized in any imaging method.

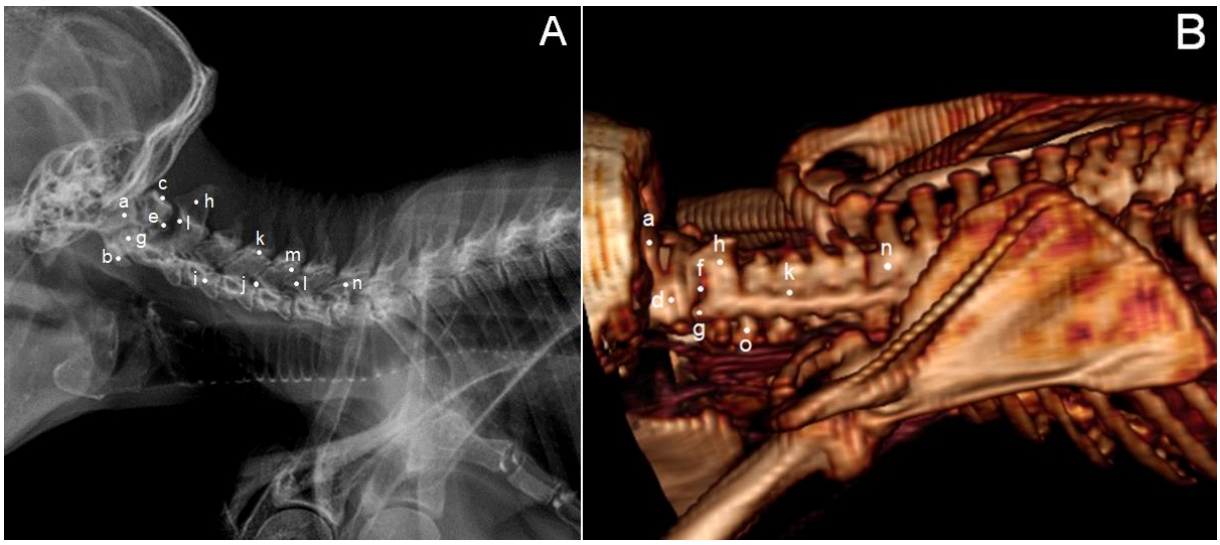

FIGURE 6 Radiographic image (A) and 3D reconstruction (B) in laterolateral projection of the cervical region of *Sapajus libidinosus*. a. Occipital condyle; b. Ventral tubercle of the atlas; c. Atlas dorsal arch; d. Alar foramen; e. Caudal articular fovea; f. Atlanto-axial joint; g. Odontoid process; h. Spinous process of the Axis; i. Body of the C3 vertebra; j. Intervertebral foramen; k. Vertebral arch blade; l. Cranial articular process; m. Caudal articular process; n. 7th cervical vertebra; o. Transverse process.

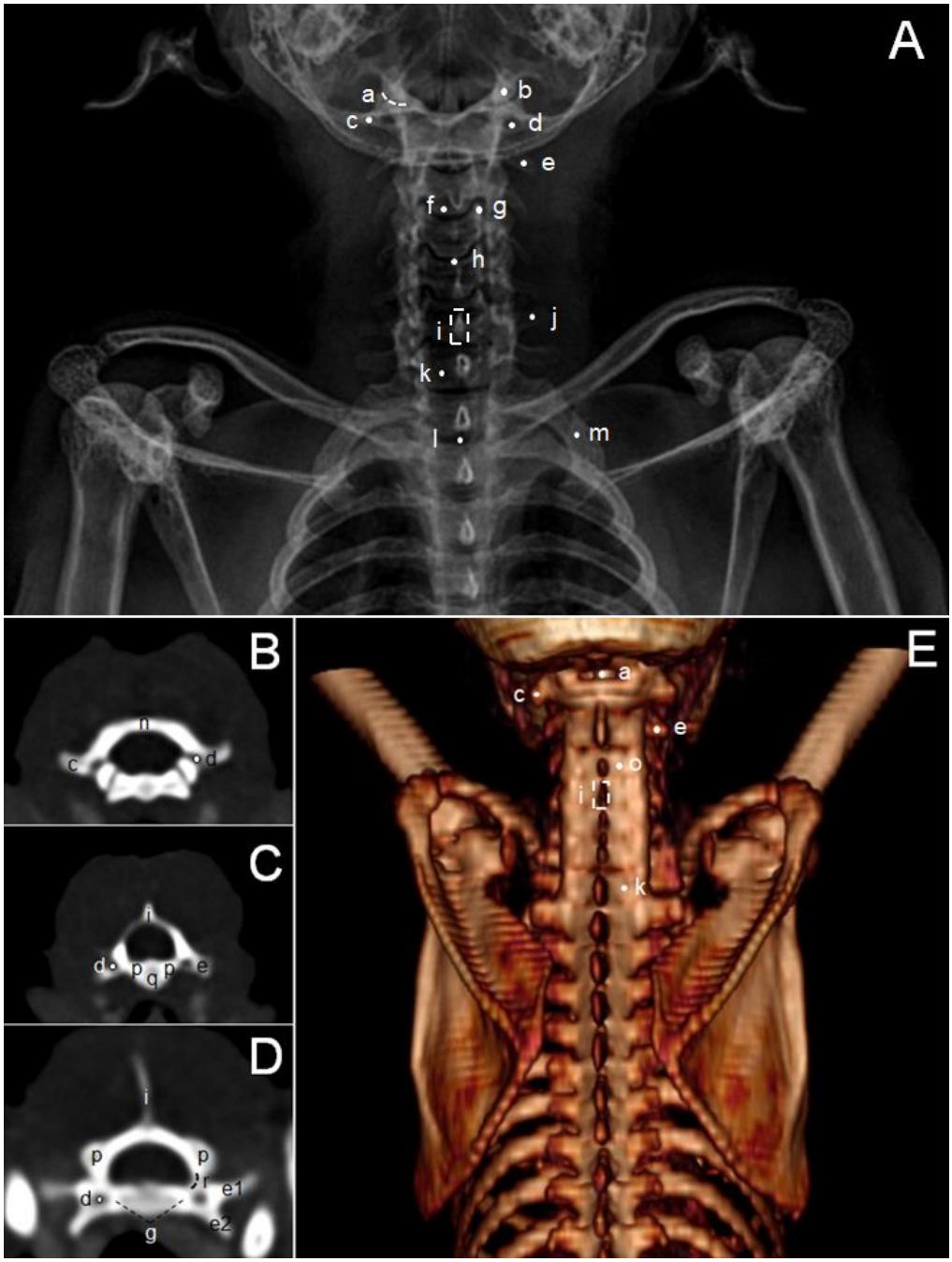

FIGURE 7 Ventrodorsal radiographic image (A), cross-sectional tomographic image at the level of the atlas (B), axis (C) and C6 (D), and 3D reconstruction (E) of the cervical region of *Sapajus libidinosus*. a. Atlanto-occipital joint; b. Occipital condyle; c. Wing of the atlas; d. Transverse foramen of the atlas; e. Transverse process; e1. Dorsal tubercle; e2. Ventral tubercle; f. Caudal end of the 3rd cervical; g. Uncinate process; h. Intervertebral disc; i. Spinous process; j. Ventral lamina of the 6th cervical; k. 7th cervical vertebra; l. Interarcual space; m. Body of the 1st rib; n. Vertebral arch; o. Vertebral arch lamina; p. Cranial articular process; q. Odontoid process; r. Cranial vertebral notch.

The bodies of the thoracic vertebrae elongate towards the lumbar region, while the spinous processes widen in the last three thoracic vertebrae. The anatomy of this vertebra is shown in Figures 8 and 9. Caudally bifurcated spinous process is found from the penultimate

thoracic vertebra to the penultimate lumbar vertebra, gradually assuming a more ventral position, except for two animals that did not present bifurcation in the spinous process of the thoracic vertebrae. These processes point caudally to the 11th-12th thoracic vertebra. The spinous processes of the last thoracic vertebra, as well as those of the lumbar vertebrae, point slightly cranially. As a result, the anticlinal vertebra is T13 in animals with 14 thoracic vertebrae and T12 in animals with 13 vertebrae (Figure 9C). Large interarcual spaces are observed between the last four thoracic vertebrae, and narrow spaces between the remaining vertebrae of the thoracic segment.

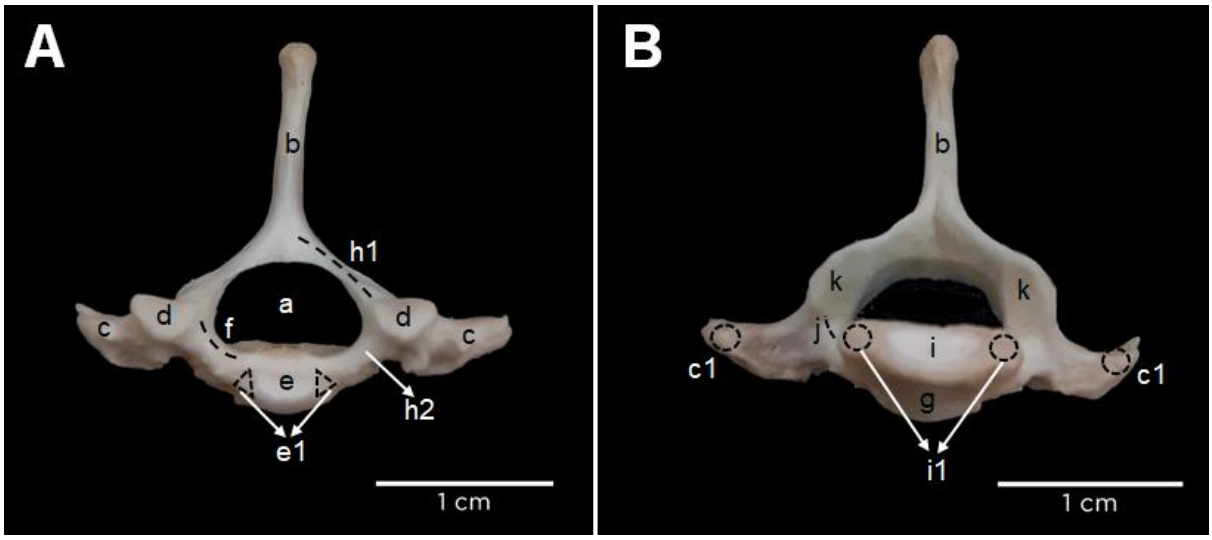

FIGURE 8 First thoracic vertebra (T1). Cranial view (A), Caudal view (B). a. Vertebral canal (*Canalis vertebralis*); b. Spinous process (*Processus spinosus*); c. Transverse process (*Processus transversus*); c1. Costal fovea of the transverse process (*Fovea costalis processus transversi*); d. Cranial articular process (*Processus articularis cranialis*); e. Cranial extremity (*Extremitas cranialis*); e1. Cranial costal fovea (*Fovea costalis cranialis*); f. Cranial vertebral notch (*Incisura vertebralis cranialis*); g. Ventral crest (*Crista ventralis*); h. Vertebral arch (A*rcus vertebrae*); h1. Lamina (*Lamina arcus vertebrae*); h2. Pedicle (*Pediculus arcus vertebrae*); i. Caudal end (*Extremitas caudalis*); i1. Caudal costal fovea (*Fovea costalis caudalis*); j. Caudal vertebral notch (*Incisura vertebralis caudalis*); k. Caudal articular process (*Processus articularis caudalis*).

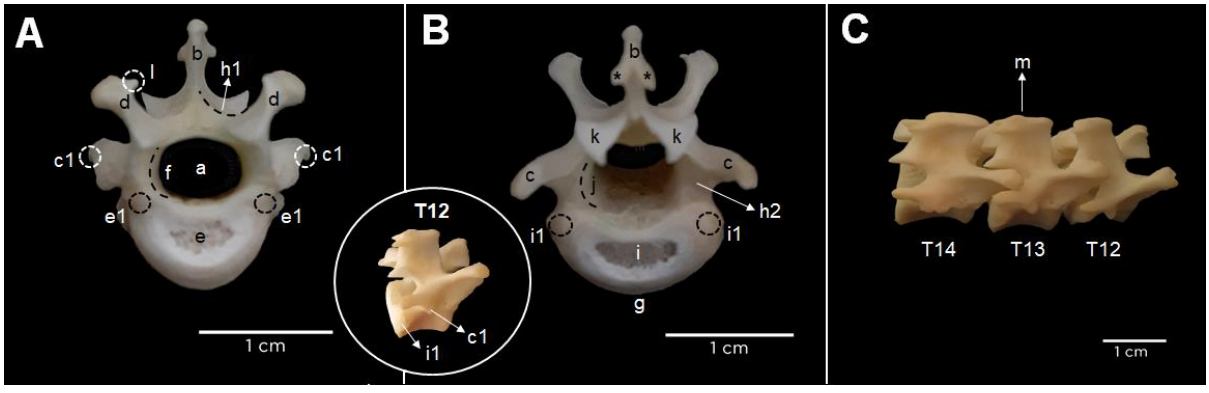

FIGURE 9 13th thoracic vertebra (T13). Cranial view (A), Caudal view (B), T12, T13 and T14 vertebrae, with emphasis on the anticlinal vertebra (C). a. Vertebral canal (*Canalis vertebralis*); b. Spinous process with bifurcation (*) (*Processus spinosus*); c. Transverse process (*Processus transversus*); c1. Costal fovea of the transverse process (*Fovea costalis processus transversi*); d. Cranial articular process (*Processus articularis cranialis*); e. Cranial extremity (*Extremitas cranialis*); e1. Cranial costal fovea (*Fovea costalis cranialis*); f. Cranial vertebral notch (*Incisura vertebralis cranialis*); g. Ventral crest (*Crista ventralis*); h. Vertebral arch *(Arcus vertebrae*); h1. Lamina (*Lamina arcus vertebrae*); h2. Pedicle (*Pediculus arcus vertebrae*); i. Caudal end (*Extremitas caudalis*); i1. Caudal costal fovea (*Fovea costalis caudalis*); j. Caudal vertebral notch (*Incisura vertebralis caudalis*); k. Caudal articular process (*Processus articularis caudalis*); l. Processus mamillaris (*Processus mamillaris*); m. Anticlinal vertebra (*Vertebra anticlinalis*).

The thoracic region suffers a lot of image overlap in the radiographic examination, in its cranial portion, of the scapula, and its entirety, of the ribs (Figure 10). However, due to its more robust body, when compared to the cervical vertebrae, the identification of bone structures is clearer, being even better when visualized in the 3D reconstruction (Figure 11). In the radiographic image of the sternum, it is possible to identify most structures. The xiphoid process is not clearly visualized because of the overlapping costal cartilages. Proximal structures of the rib are also not visible on radiographic examination, only the body and costochondral joint are observed (Figure 10).

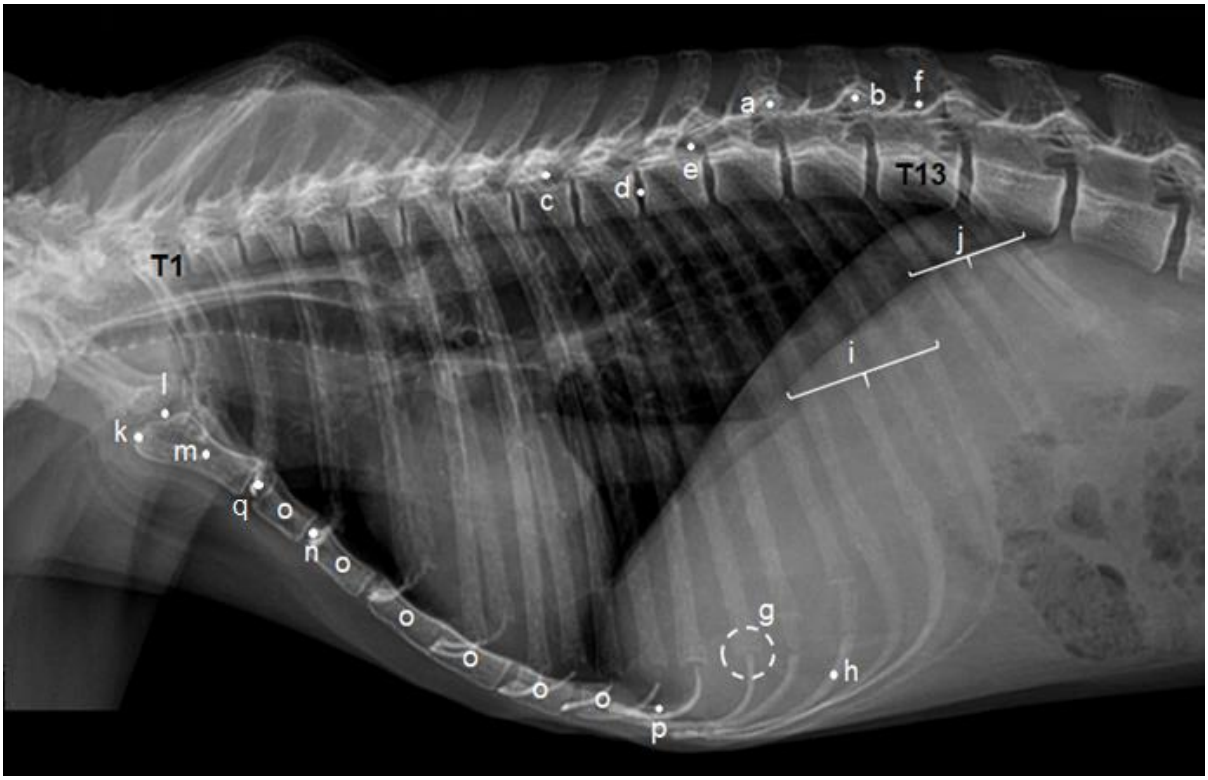

FIGURE 10 Laterolateral radiographic image of the thoracic segment, sternum and ribs of *Sapajus libidinosus*. a. Cranial articular process; b. Caudal articular process; c. Caudal vertebral

notch; d. Intervertebral disc; e. Intervertebral foramen; f. Vertebral arch blade; g. Costochondral joint; h. Costal cartilage; i. Sternal ribs; j. Floating ribs; k. Jugular notch; l. Clavicular notch; m. Manubrium of the sternum; n. Intersternal cartilage; o. Sternebrae; p. Xiphoid process; q. Manubriosternal symphysis.

Thoracic segment structures such as transverse processes, articular processes, and costal foveas are best identified in the 3D reconstruction. Interosseous structures, such as the vertebral canal, are visible only in the transverse tomographic section, others, such as the vertebral arch, notches, and extremities, are also better visualized by this means (Figure 11). The bifurcation of the spinous process was not observed in the images. The sternum can be well described using 3D reconstruction, and structures such as the jugular notch and costal notch were better visualized by this method (Figure 11B). In the 3D reconstruction of the rib, it was possible to identify some main structures, such as the head, the costal tubercle, the body, and the costochondral joint (Figure 11A). It was not possible to identify the xiphoid cartilage in any of the imaging methods.

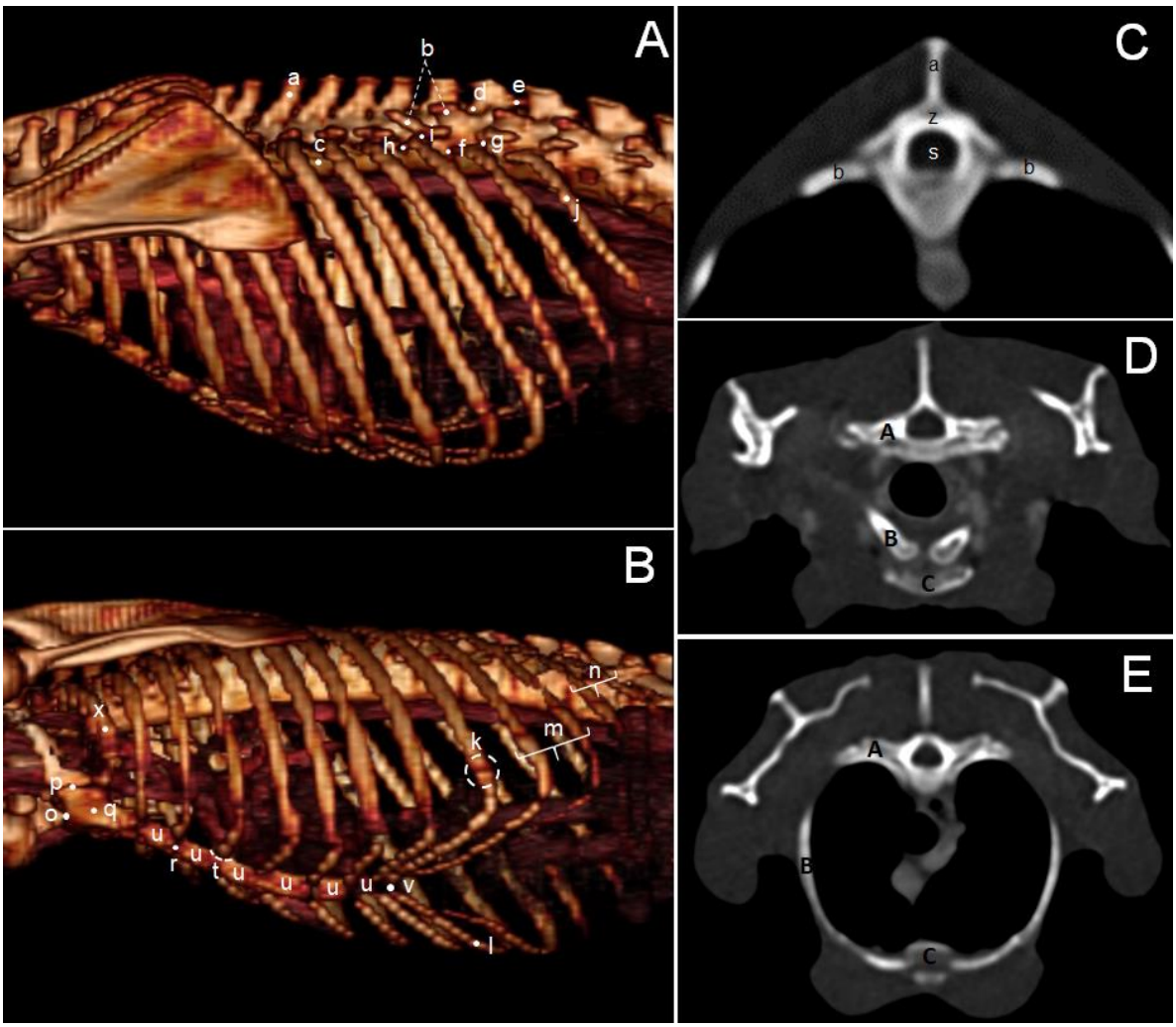

FIGURE 11 3D reconstruction in laterolateral (A) and lateroventral (B) projection of the thoracic region and tomographic image in cross section at the level of the cranial (C), middle (D) and caudal (E) thoracic segments of *Sapajus libidinosus*. A. Thoracic vertebra; B. Rib; C. Sternum. a. Spinous process; b. Transverse process; c. Vertebral body; d. Cranial articular process; e. Caudal articular process; f. Caudal costal fovea; g. Costal fovea of the transverse process; h. Head of the rib; i. Costal tubercle; j. Body of the rib; k. Costochondral joint; l. Costal cartilage; m. Sternal ribs; n. Floating ribs; o. Jugular notch; p. Clavicular notch; q. Manubrium of the sternum; r. Intersternal cartilage; s. Spinal canal; t. Costal notch; u. Sternebrae; v. Xiphoid process; x. First rib; z. Vertebral arch.

The number of ribs depends on the number of thoracic vertebrae and varies between 13 and 14 pairs. However, the number of 14 thoracic vertebrae is predominant, as only three of the eight *Sapajus libidinosus* investigated in this study had 13 thoracic vertebrae. The first rib is short and more robust than the others, presenting a more detailed cranial end, with a well-developed costal tubercle. The other ribs are narrower, with a pronounced costal groove, but the tip is more subtle, with less detail (Figure 12). The ninth pair of ribs is always the last sternal pair that is directly connected to the sternum by the costal cartilage. In animals with 14 ribs, the three caudal pairs are sternal ribs, which have indirect connections with the sternum, since their costal cartilages are attached to those of the anterior rib. Animals with 13 ribs have two pairs of sternal ones. The last two pairs of ribs are short and floating, without any connection to the sternum, in all animals. Each rib ends ventrally in cartilage, and the sternal ribs join the sternum through the costochondral joint.

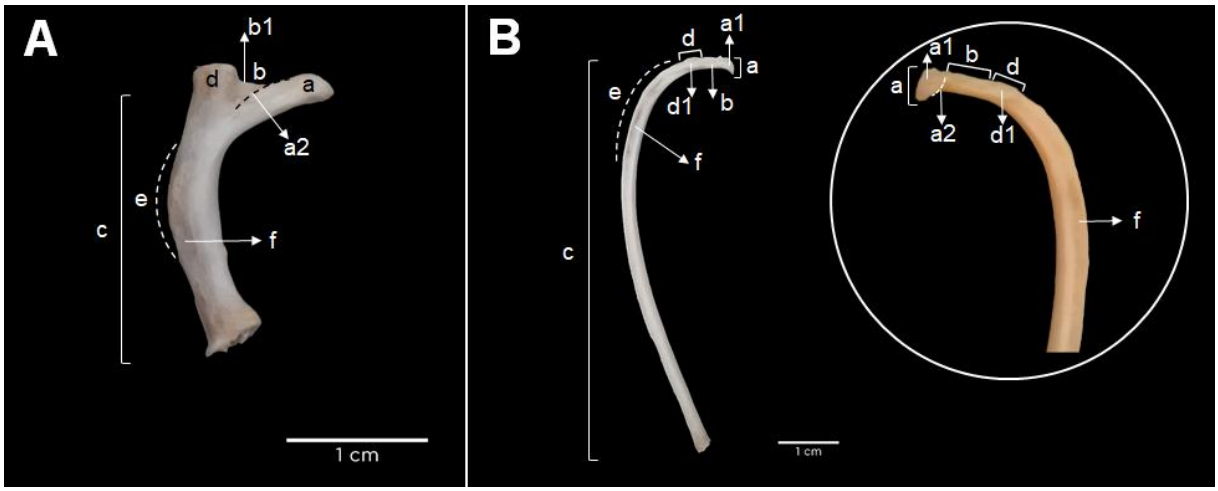

FIGURE 12 First rib (A) and eighth rib (B). a. Head of the rib (*Caput costae*); a1. Articular surface of the head of the rib (*Facies articularis capitis costae*); a2. Crest of the coastal head (*Crista capitis costae*); b. Neck of the rib (*Collum costae*); b1. Crest of the neck of the rib (*Crista colli costae*); c. Body of the rib (*Corpus costae*); d. Costal tubercle (*Tuberculum costae*); d1. Articular face of the costal tubercle (*Facies articularis tuberculi costae*); e. Costal angle (*Angulus costae*); f. Costal sulcus (*Sulcus costae*).

The sternum is composed of a broad manubrium, five or six cuboidal sternebrae related to the number of thoracic vertebrae, and a thin xiphoid process with xiphoid cartilage. It does not have a sternal crest. The articular surfaces of the clavicles are located bilaterally on the craniolateral surfaces of the manubrium, called the clavicular notch (Figure 13A). Caudally to these, the costal cartilages of the first pair of ribs are attached. The subsequent sternebrae are connected to each other by intervertebral cartilages to which the costal cartilages are attached by means of costal notches. Symphyses between the manubrium and the second sternebra, and between the last sternebra and the xiphoid process are observed (Figure 13B).

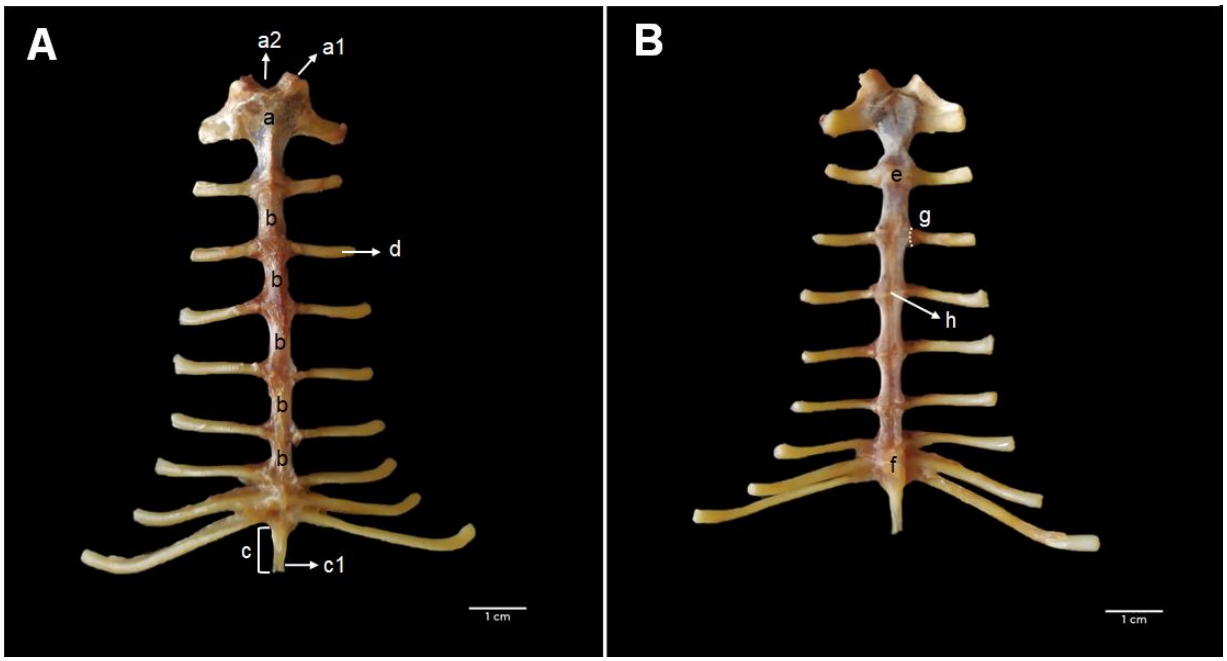

FIGURE 13 Sternum. Dorsal view (A), Ventral view (B). a. Manubrium of the sternum (*Manubrium sterni*); a1. Clavicular notch (*Incisura clavicularis*); a2. Jugular notch (*Incisura jugularis*); b. Sternebrae (*Sternebrae*); c. Xiphoid process (*Processus xiphoideus*); c1. Xiphoid cartilage (*Cartilago xiphoidea*); d. Costal cartilage (*Cartilago costalis*); e. Symphysis manubriosternal (*Symphysis manubriosternal*); f. Symphysis xylosternal (*Symphysis xylosternal*); g. Costal notch (*Incisura costalis*); h. Intertenebral cartilage (*Cartilago interternebral*).

Although the number of lumbar vertebrae is only half that of the thoracic vertebrae, the lengths of the thoracic and lumbar regions are similar (Table 2). The lumbar vertebrae have a well-developed body and prominent transverse processes (Figures 14A and 14B), becoming larger towards the sacrum, except for the last one, which is slightly narrower (Figure 14C). In four animals, the transverse process of the first vertebra was arranged craniocaudally and the others were inclined in the opposite direction; in the other animals this differentiation did not occur. The spinous processes of these vertebrae are also well developed.

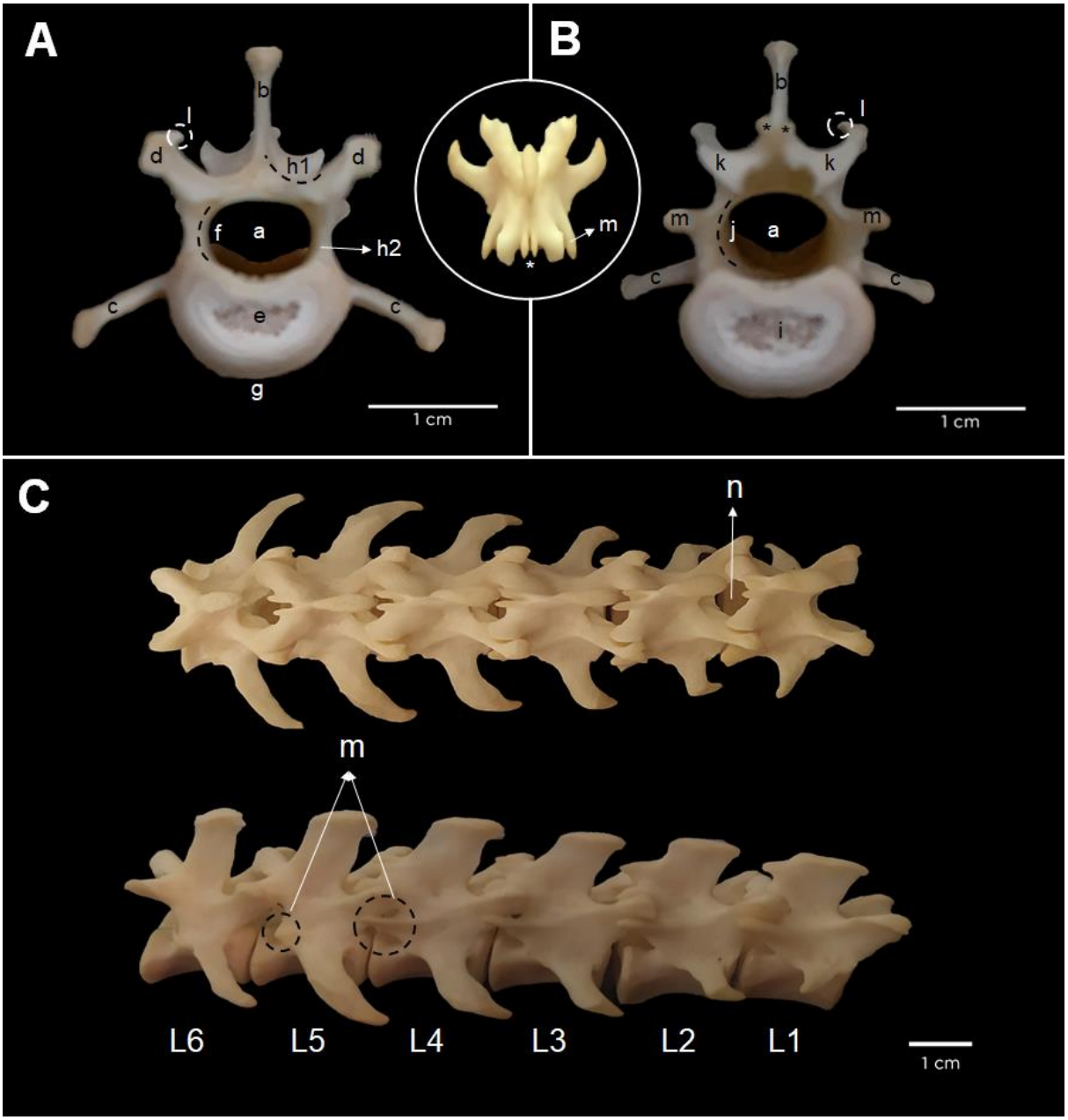

FIGURE 14 Third lumbar vertebra (L3). Cranial view (A), Caudal view (B), Sequence of lumbar vertebrae (C). a. Vertebral canal (*Canalis vertebralis*); b. Bifurcated spinous process (*) (*Processus spinosus*); c. Transverse process (*Processus transversus*); d. Cranial articular process (*Processus articularis cranialis*); e. Cranial extremity (*Extremitas cranialis*); f. Cranial vertebral notch (*Incisura vertebralis cranialis*); g. Ventral crest (*Crista ventralis*); h. Vertebral arch (*Arcus vertebrae*); h1. Lamina (*Lamina arcus vertebrae*); h2. Pedicle (*Pediculus arcus vertebrae*); i. Caudal end (*Extremitas caudalis*); j. Caudal vertebral notch (*Incisura vertebralis caudalis*); k. Caudal articular process (*Processus articularis caudalis*); l. Processus mamillaris (*Processus mamillaris*); m. Accessory process (*Processus accessorius*); n. Interarcual space (*Spatium interarcuales*).

The first three or four lumbar vertebrae, in animals that have five or six vertebrae, respectively, have well-developed accessory processes, which articulate with the lateral margin of the cranial articular process of the subsequent vertebra, the penultimate vertebra has a

rudimentary accessory process and the last one does not present it (Figure 14C). This is characterized as one point of differentiation in the thoracolumbar transition. Large interarcual spaces are seen between all lumbar vertebrae (Figure 14C), and between the most caudal lumbar vertebra and the sacrum.

The sacral vertebrae are three in number and fused by the vertebral body. In one animal, only two sacral vertebrae were present (Figure 15C). A transitional vertebra between the second sacral vertebra and the tail was seen once (Figure 15C). The transverse processes, facing laterally, fuse at the ends between one vertebra and another, cranially forming the sacral wing, which is connected to the auricular surface of the ilium. Each vertebra can be recognized individually, delimited by transverse lines on the face of the pelvis. The sacral foramina are large, the more caudal ones being larger, two of them on both sides, except for the two animals that presented different morphology. The spinous processes are similar to those of the lumbar vertebrae and are not fused. There is a median, intermediate and lateral sacral crest (Figures 15A and 15B).

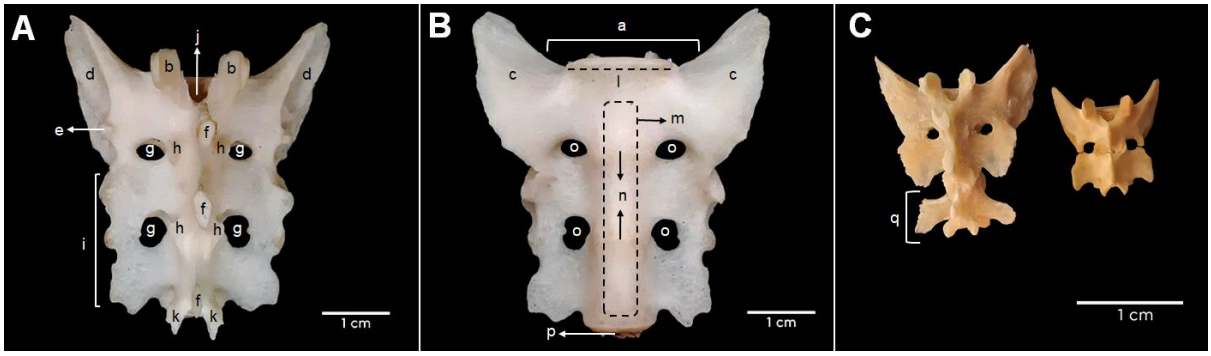

FIGURE 15 Sacral bone. Dorsal view (A), Ventral view (B), Sacral entities with differentiated morphology (C). a. Base of the sacral bone (*Basis ossis sacri*); b. Cranial articular process (*Processus articularis cranialis*); c. Sacral wing (*Ala sacralis*); d. Auricular surface (*Facies auriculares*); e. Sacral tuberosity (*Tuberositas sacralis*); f. Median sacral crest (*Crista sacralis mediana*); g. Dorsal sacral foramen (*Foramina sacralia dorsalia*); h. Intermediate sacral crest (*Crista sacralis intermedia*); i. Lateral sacral crest (*Crista sacralis lateralis*); j. Sacral canal (*Canalis sacralis*); k. Sacral horn (*Cornu sacralis*); l. Promontory (*Promontorium*); m. Pelvic surface (*Facies pelvina*); n. Transverse line (*Lineae transversae*); o. Ventral sacral foramen (*Foramina sacralia ventralia*); p. Caudal articular process (apex) (*Processus articularis caudalis*); q. Transition vertebra.

In the radiographic image of the lumbar vertebrae, it is possible to clearly identify most of the bone structures, due to the robust body of their vertebrae and the absence of bone overlap, which are even better observed in the 3D reconstruction. Except for the interarcual space, all other structures observed in the macroscopic analysis could be identified in the image analysis

as well (Figures 16 and 17). Structures not visible in the thoracic region, such as the bifurcation of the spinous process, could be identified in the lumbar region (Figure 16B).

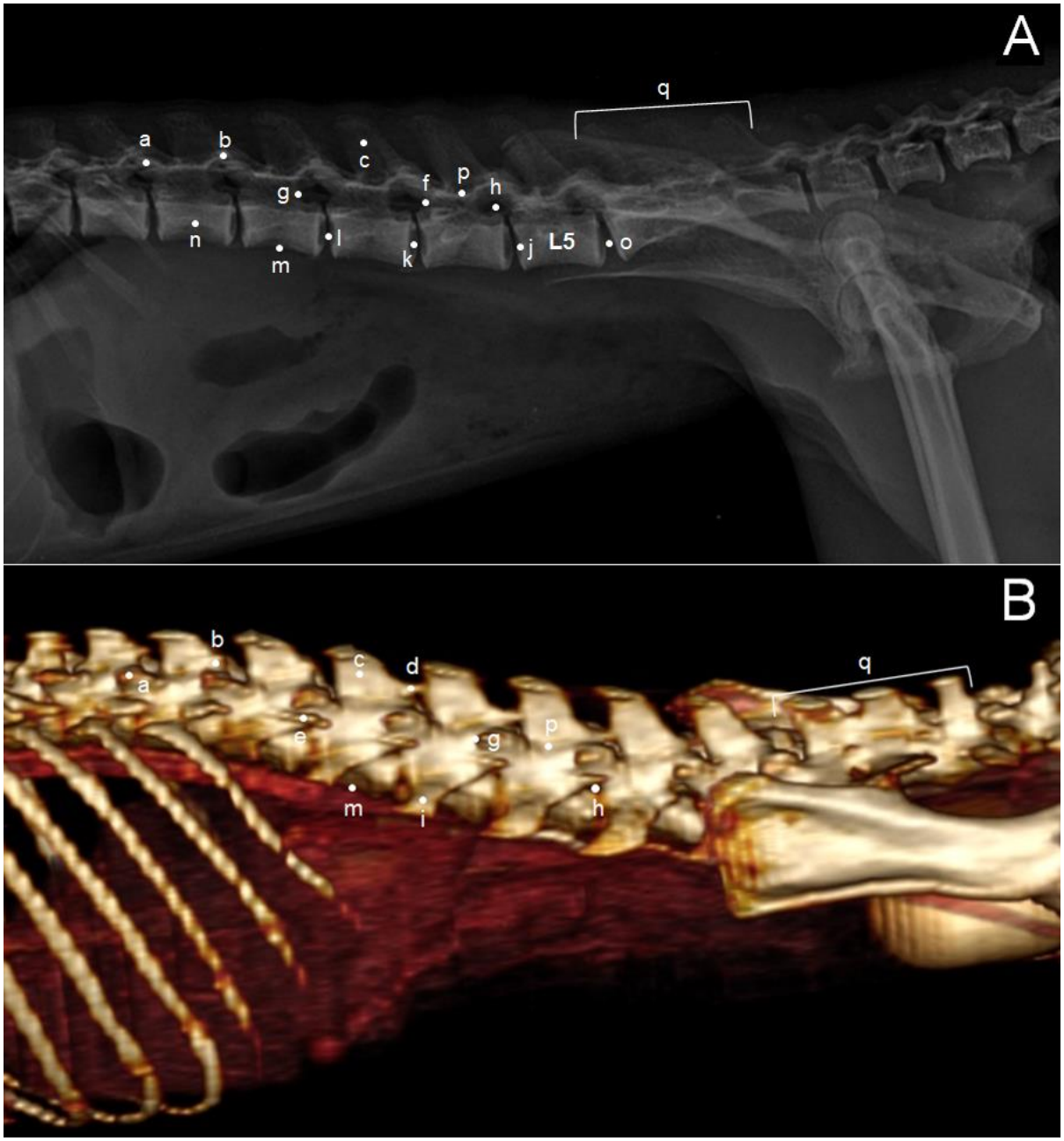

FIGURE 16 Radiographic image (A), and 3D reconstruction (B) in laterolateral projection of the lumbosacral region of *Sapajus libidinosus*, pointing out the main structures observed. a. Cranial articular process; b. Caudal articular process; c. Spinous process; d. Bifurcated spinous process; e. Accessory process; f. Cranial vertebral notch; g. Caudal vertebral notch; h. Intervertebral foramen; i. Transverse process; j. Cranial extremity; k. Caudal end; l. Intervertebral disc; m. Ventral crest; n. Body of the 1st lumbar; o. Lumbosacral joint; p. Vertebral arch lamina; q. Sacrum.

The cross-section of the CT scan allows us to identify more clearly structures such as the vertebral canal, notches, extremities, and the vertebral arch, some of which have already

been identified in other projections (Figure 17B1). The sacrum, on its dorsal surface, allows identification of most of its structures, both in the radiographic image and in the 3D reconstruction, in the ventrodorsal projection (Figures 17A and 17B). However, its ventral face was not visible. The sacral canal is identified in the cross-section of the tomographic image (Figure 17B2).

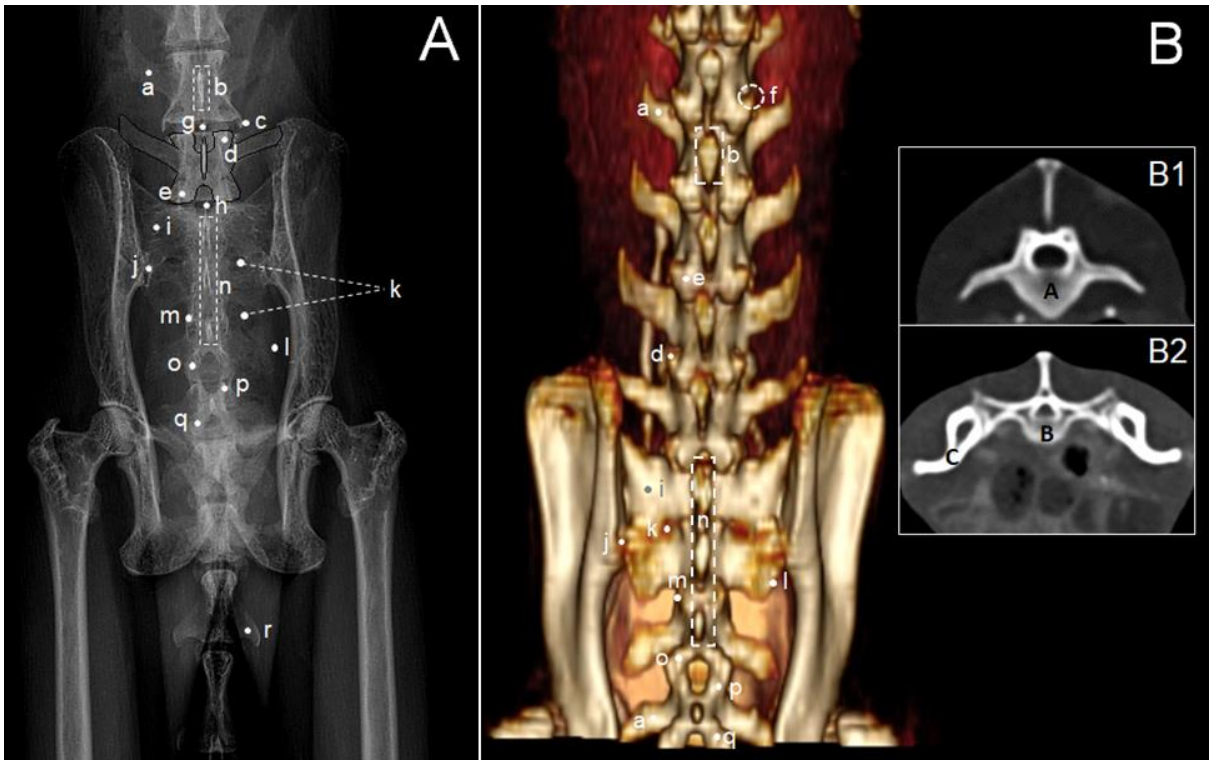

FIGURE 17 Radiographic image (A) and 3D reconstruction (B) in ventrodorsal projection of the lumbosacral region, and tomographic image in cross section at the level of L2 (B1) and sacral vertebra (B2) of *Sapajus libidinosus*. A. Lumbar vertebra; B. Sacrum; C. Coxal bone. a. Transverse process; b. Spinous process; c. Accessory process; d. Cranial articular process; e. Caudal articular process; f. Processus mamillaris; g. Intervertebral disc; h. Lumbosacral joint; i. Sacral wing; j. Sacral tubercle; k Sacral foramen; l. Lateral sacral crest; m. Intermediate sacral crest; n. Median sacral crest; o. Sacral horn; p. Cranial articular process of the 1st caudal vertebra; q. Caudal articular process of the 1st caudal vertebra; r. Transverse process of the 4th caudal vertebra.

The first five caudal vertebrae have differentiated anatomy, more similar to the lumbar vertebrae, even with the presence of a vertebral canal (Figures 18A and 18B). Both in the sacrocaudal transition and between these vertebrae, there are still interarcual spaces. Subsequent caudal vertebrae lose the vertebral canal and assume a more cylindrical shape (Figure 18C), elongating towards the middle of the tail, where they begin to shorten again until the last, smallest vertebra (Figure 18D). The haemal arches are open and larger in the more

cranial vertebrae (Figure 18C), decreasing in size to the most caudal ones, and can be recognized from the fourth or fifth to the last caudal vertebra, macroscopically.

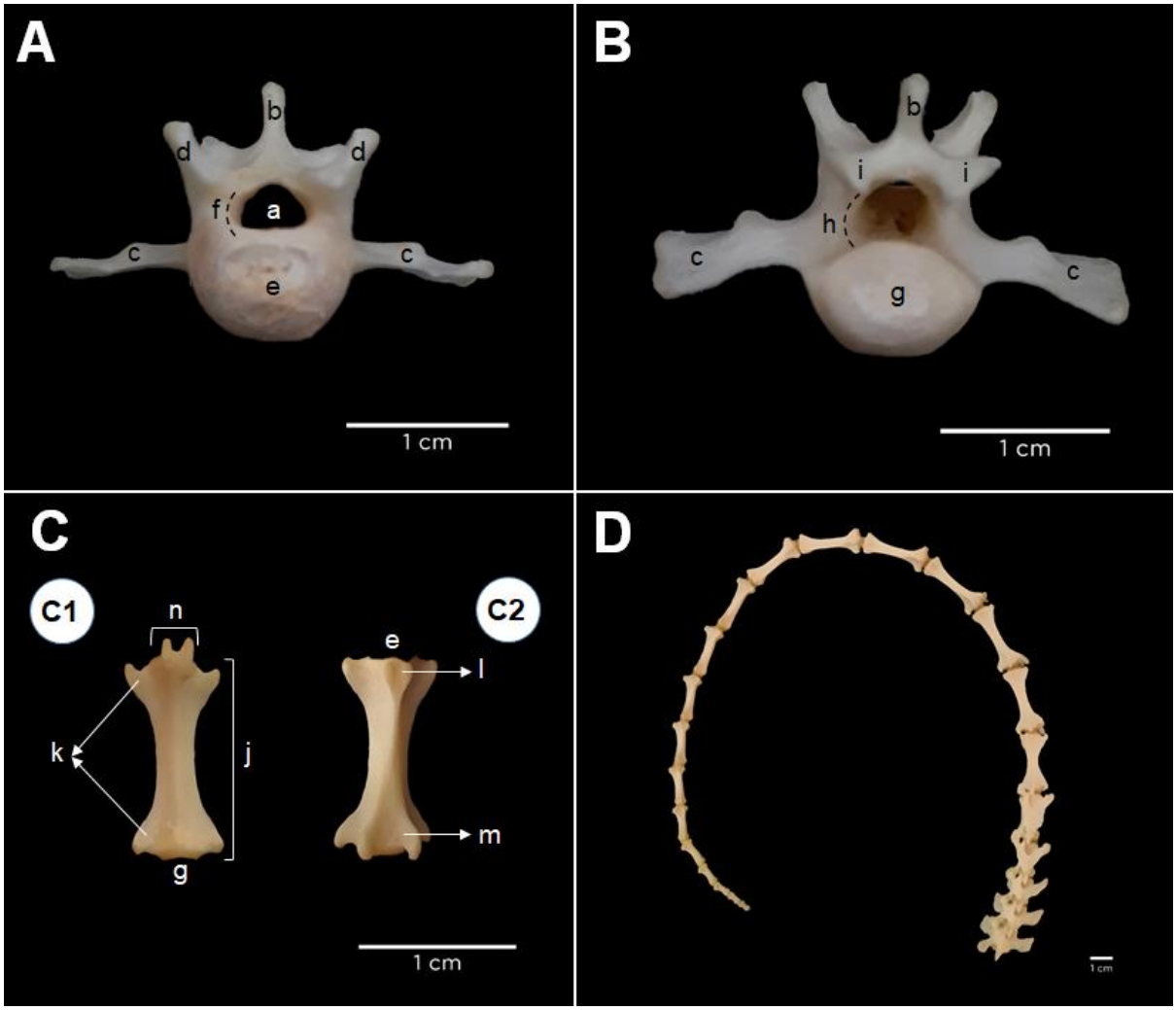

FIGURE 18 Ca1. Cranial view (A), Caudal view (B); Ca8 (C) Ventral view (C1), Dorsal view (C2); Sequence of caudal vertebrae (D). a. Vertebral canal (*Canalis vertebralis*); b. Spinous process (*Processus spinosus*); c. Transverse process (Processus transversus); d. Cranial articular process (*Processus articularis cranialis*); e. Cranial extremity (*Extremitas cranialis*); f. Cranial vertebral notch (*Incisura vertebralis cranialis*); g. Caudal end (*Extremitas caudalis*); h. Caudal vertebral notch (*Incisura vertebralis caudalis*); i. Caudal articular process (*Processus articularis caudalis*); j. Vertebral body (*Corpus vertebrae*); k. Remnant of the transverse process (*Reliquiae processus transversus*); l. Remnant of the cranial articular process (*Reliquiae processus articularis cranialis*); m. Remnant of the caudal articular process (*Reliquiae processus articularis caudalis*); n. Haemal arch (*Arcus hemalis*).

The radiographic image of the caudal vertebrae presents clear bone structures for identification, mainly in the laterolateral projection, allowing the visualization of all bone structures (Figure 19A). In the ventrodorsal view, the vertebrae are best identified from the fourth caudal vertebra, since the first three are in the pubic region (Figure 17A). In the 3D reconstruction, the structures are well visualized and identified in the two projections (Figures

17B and 19B). It is possible to observe, especially through the 3D image, that the haemal arches are present from the second caudal vertebra, a structure that detaches from the most cranial vertebrae during maceration and therefore is not observed in the macroscopic analysis (Figure 19). Radiographic examination of this region is an excellent method of identifying fractures, including three females in the study with tail fractures, which were clearly observed with this method (Figure 20).

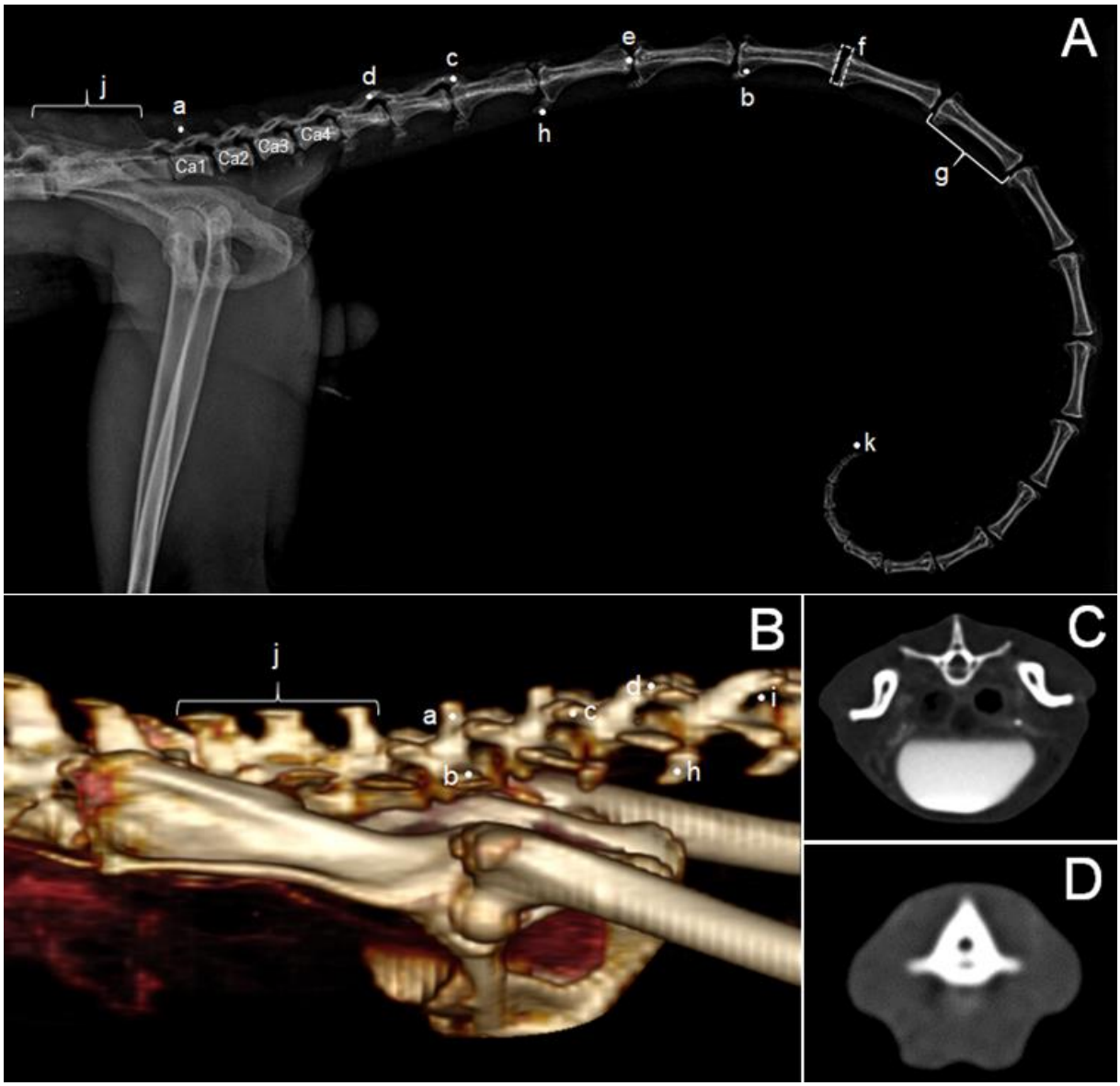

FIGURE 19 Radiographic image (A) and 3D reconstruction (B) in laterolateral projection of the caudal region, and tomographic image in cross section of the morphology of the vertebrae at the level of Ca2 (C) and Ca10 (D) of *Sapajus libidinosus*. a. Spinous process; b. Transverse process; c. Cranial articular process; d. Caudal articular process; e. Caudal end; f. Intervertebral disc; g. Vertebral body; h. Haemal arch; i. Intervertebral foramen; j. Sacrum; k. Last caudal vertebra.

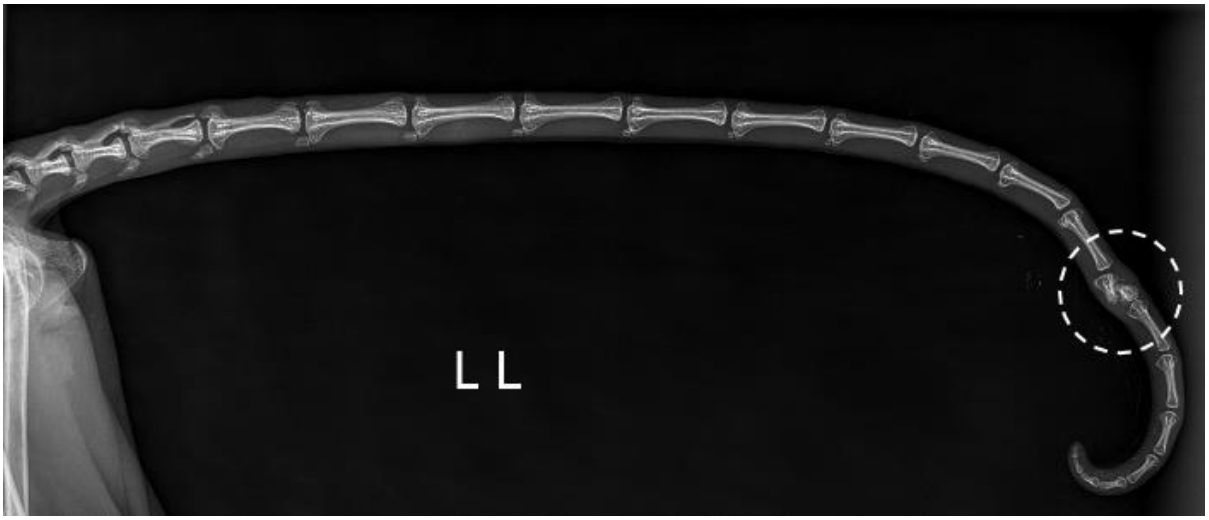

FIGURE 20 Fracture in the distal segment of the tail, identified in a female *Sapajus libidinosus*, identification F1.

4 DISCUSSION

Non-human primates are more widely characterized as models for human skeletal biology than any other animal order, having been widely used to evaluate, for example, therapeutic agents for osteoporosis, with results fully consistent with clinical data (Jerome & Peterson, 2001); vertebral injuries; as models for studying injuries and concussions (Kazarian, 1975; Kohno et al., 1979; Life & Pince, 1968); among others. Although primates such as the crab-eating macaque (*Macaca fascicularis*) and the rhesus macaque (*Macaca mulatta*) may be the best choice for translating experimental data to humans, their use is restricted by their high cost, human safety considerations, need for staff training, and limited availability (Bagi et al., 2007; Ludlage and Mansfield, 2003). Therefore, it can be considered that *Sapajus libidinosus* proves to be a valuable research model in a cost-benefit analysis.

The main particularities of the cervical vertebrae of *Sapajus libidinosus* consist of the presence of vertebral foramen in the atlas, which is not observed in humans (Sobotta, 2000), but is present in other primates, such as *Callithrix jacchus* (Casteleyn et al., 2012), *Alouatta seniculus* (Mesquita et al., 2019) and *Callimico goeldii* (Hill, 1959), and the presence of an alar foramen, also in the first cervical vertebra, not described in any of the aforementioned studies. Animals that have the wing of the atlas wider in the craniocaudal direction, especially at the cranial end, required the creation of an alar foramen, aligned with the lateral vertebral foramen, for the passage of the first pair of cervical nerves (C1). This nerve, unlike the other cervical ones, does not emerge through the first intervertebral foramina but through the lateral vertebral foramina, so there are 8 pairs of them and 7 cervical vertebrae, in most mammals. From this,

the alar foramen appears as a guide foramen, directing this pair of nerves out of the vertebral canal. This morphological aspect is commonly observed in domestic mammals (Konig & Liebich, 2016).

Bifid transverse processes, divided into dorsal and ventral tubercles observed in this study, were also described in humans (Sobotta, 2000), *Callimico goeldii* (Hill, 1959) and from C4-C6 in *Alouatta seniculus* (Mesquita et al., 2019), not being described in *Callithrix jacchus* (Casteleyn et al., 2012). The pattern of the seventh cervical vertebra (C7) without transverse foramen, corroborates the studies by Hill (1959) and Casteleyn et al. (2012), however, the animal that presented C7 transverse foramen in this study follows the pattern observed in humans (Sobotta, 2000) and *Alouatta seniculus* (Mesquita et al., 2019), which are larger primates.

The number of cervical vertebrae in the *Sapajus libidinosus* analyzed was equal to seven, in all animals. With few individual exceptions, this number is the rule in both living and fossil mammals. Since no evolutionary change has considerably affected the number of cervical segments in any of the primates, the cervicothoracic transition is characterized by remarkable stability (Burmeister, 1854). The rare variation in the number of cervical vertebrae in primates is exemplified by the fact that the literature contains only four articles recording such cases: eight cervical vertebrae were found in a siamang (Weber, 1890), a gorilla (Struthers, 1893), and a gibbon (Schultz & Straus Jr., 2015), six cervical vertebrae were registered in a *Perodicticus potto* (Nayak, 1933), and six and a half cervical vertebrae were found in a monkey, an orangutan and a gorilla. Still, a considerable number of human skeletons with six cervical vertebrae and some with eight have been described, but the percentage of these variations is not published in the literature (Schultz & Straus Jr., 2015).

Due to the greater stability in the cervical segment, already reported, little is studied about the functional morphology of these vertebrae in non-human primates (Manfreda et al., 2006; Mercer, 1999; Nalley, 2013), when compared to other vertebral segments. Furthermore, this lack of information is considered surprising given the importance of the neck as the bridge between the head and the trunk, playing several biomechanical roles related to posture and locomotion, including stabilizing head movement, and providing a bony platform for the soft tissues of the pectoral girdle and forelimb (Nalley & Grider-Potter, 2017). The same authors performed a functional analysis of the primate upper cervical spine, at the atlas and axis level, and reported, through studies (Graf et al., 1995a, 1995b), the importance of imaging and anatomical knowledge in identifying postures during locomotion, in the functional aspect and the mechanics of the cervical segment.

More than 50% of the records of spinal cord injury are in the cervical spine (Majdan et al., 2016; Sekhon & Fehlings, 2001) mainly in men (Ferro et al., 2017; Joseph et al., 2017; Kriz et al., 2015; Mirzaeva et al., 2019; Moshi et al., 2017). However, due to anatomical and neurological differences between rodents and humans, treatments that are effective in the former are difficult to translate to the latter (Courtine et al., 2007; Nardone et al., 2017). Potential advantages of non-human primate models include genetic similarities, similar spinal cord caliber, and length, as well as biological and physiological responses to injuries that are more similar to those of humans. Therefore, the non-human primate as a model of spinal cord injury is seen with greater significance in the development of treatment strategies, making it necessary to use imaging methods for injury assessments (Kwon et al., 2015).

Thoracic vertebrae show greater variation in terms of their number than in structures, which follow the same pattern, with small variations in size and arrangement in this study, in humans (Sobotta, 2000), *Callithrix jacchus* (Casteleyn et al., 2012), *Alouatta seniculus* (Mesquita et al., 2019), and *Callimico goeldii* (Hill, 1959). At the caudal edge of the base of the spinous process, in the last thoracic vertebrae, a V-shaped bifurcation for the attachment of a well-developed yellow ligament is present in both *Sapajus libidinosus* and *Cebupithecia sarmientoi* (Meldrum & Lemelin, 1991). According to the same author, in quadrupedal jumpers, this ligament is well developed and serves as an elastic recoil mechanism, tending to extend the flexed spine at the beginning of a jump.

As for the variation in the number of thoracic vertebrae, in the present study, it was possible to analyze a small variation, between 13-14 vertebrae, but within the Primate Order a much greater variation can be seen. In contrast to the number of cervicals, this segment varies widely among mammals in general, and primates, in particular. Since, as mentioned earlier, the cervicothoracic border is comparatively stable, certainly, the thoracolumbar border is easily displaced, being responsible for the differentiation in the number of segments that form the thoracic region of the spine. Thirteen thoracic vertebrae are assumed to represent the primitive ancestral number of primates, however, among them, phylogenetic disruptions have occurred to both increase and decrease this number (Keith, 1903).

The first thoracic segment is the eighth vertebra of the spine, with very few exceptions, but the last thoracic segment can be represented by any vertebra between the eleventh one in the genera *Myoxicebus*, *Semnopithecus*, and *Homo*, and the eighteenth one, in *Nycticebus*, among recent primates (Schultz & Straus Jr., 2015). In *Alouatta seniculus*, 14 vertebrae were observed in one analyzed specimen (Mesquita et al., 2019). In man, the modal number of thoracic vertebrae, among higher primates, is 12 (Sobotta, 2000), this same number is observed

in orangutan (Schultz & Straus Jr., 2015), *Callimico goeldii* (Hill, 1959) and *Callithrix jacchus* (Casteleyn et al., 2012), the latter maintaining a commonly observed variation between 12 and 13 vertebrae. In humans and orangutans, extreme reduction to 11 thoracic segments occurs with significant frequency (Schultz & Straus Jr., 2015).).

None of the thoracic vertebrae presented a transverse foramen in the analyzed animals. The data corroborate studies of other platyrrhines (Casteleyn et al., 2012; Hill, 1959; Mesquita et al., 2019), however, the presence of a transverse foramen was reported in five specimens of *Pithecia monachus* from a bone collection (Meldrum & Lemelin, 1991), a fact hitherto only seen in primates of the Lorisidae family (Ankel-Simons, 1983; Mivart, 1865), presumably for the passage of a spinal nerve.

As for the anticlinal vertebra, in *Sapajus libidinosus* we have observed that, in all animals, it was equivalent to the penultimate thoracic vertebra, in opposition to other studies with platyrrhines, in which it is described that the anticlinal vertebra usually invades the thoracic region cranially for two to four segments (Erikson, 1963). This information is confirmed by researchers when analyzing some specimens of New World monkeys, such as *Pithecia pithecia*, with 12 thoracic vertebrae and an anticline at the T10 level; *Pithecia monachus*, with 12 or 13 thoracic ones, and anticline at T10 or T11; *Cacajao* and *Chiropotes*, with an average of 13 thoracic vertebrae and an anticline at the T11 level (Meldrum & Lemelin, 1991). The same pattern is observed in *Callithrix jacchus*, with 12-13 thoracic vertebrae and anticline at T9 or T10 (Casteleyn et al., 2012), and in *Callimico goeldii*, with a segment of 12 thoracic vertebrae and anticline at T9 (Hill, 1959).

As for imaging aspects, it is described that conventional radiography remains the basis of any diagnostic investigation of the thoracic spine, and that it must precede any complex imaging procedure (EI-Khoury & Whitten, 1992). The same authors report that data from human studies prove that fractures in the upper thoracic spine (T1-T10) are not uncommon. In a retrospective study, with 2,416 patients presenting acute spinal fractures admitted to the Center for Acute Spinal Injuries at Northwestern University, between 1972 and 1986, 16% involved the upper thoracic spine (Meyer Jr., 1989). Radiographic examination was also performed to determine normal radiographic anatomy and establish reference values in *Macaca fascicularis* (Xie et al., 2014), *Lemur catta* (Makungu et al., 2014) and *Chlorocebus sabaeus* (Young et al., 2013).

Computed tomography was used to analyze structural differences in vertebral bodies at T8 between humans and Old World monkeys, to identify why osteoporosis-related spinal fractures are the most common fractures in humans but are not seen in monkeys, even in cases

of severe osteopenia. Bone strength, bone morphology through macroscopic bone analysis, trabecular microarchitecture, and bone mass were determined, concluding that human vertebrae are more porous and weaker than those of monkeys in young adulthood, and even modest amounts of bone loss related to age make them susceptible to vertebral fracture, whereas, in monkeys, large amounts of bone loss could be required before a vertebral fracture becomes likely (Cotter et al., 2011). The authors further argued that these differences are related to evolutionary adaptations associated with bipedalism.

The number of ribs is associated with the number of thoracic vertebrae, and as a result, it also varies greatly among primates. *Sapajus libidinosus*, for the most part, followed the pattern identified in humans (Sobotta, 2000), with three pairs of sternal ribs and two pairs of floating ones. Differently from what was observed in this study, in *Callithrix jacchus,* four pairs of asternal ribs and only one pair of floating ones were described (Casteleyn et al., 2012), and in *Callimico goeldii*, three pairs of asternal ribs and one pair of floating ones were identified (Hill, 1959).

As for the structures identified, the ribs of *Sapajus libidinosus* follow the pattern identified in humans (Sobotta, 2000), *Cebupithecia sarmientoi* (Meldrum & Lemelin, 1991), *Callithrix jacchus* (Casteleyn et al. 2012), *Alouatta seniculus* (Mesquita et al., 2019), and *Callimico goeldii* (Hill, 1959). However, in relation to its morphology, it presents greater similarity with the last three. In humans (Sobotta, 2000) and *Cebupithecia sarmientoi*, as well as in *Pithecia monachus*, there is the presence of broader ribs. In the latter, this is so evident that they are almost in contact at the costal angle (Meldrum & Lemelin, 1991). One study proposed that broad ribs in some primates are somehow part of a mechanism to generate trunk stability, however, this hypothesis has not yet been proven (Jenkins, 1970).

The sharpness of the radiographic and tomographic images of the ribs of *Sapajus libidinosus* showed that it is possible to immediately identify any morphological deformity that indicates even a minor crack. This is important data for the species, since several studies in humans portray the severity that a rib fracture can cause, such as pneumonia, morbidity, and mortality, and how the knowledge of anatomy and early recognition of life-threatening injuries is important for an immediate intervention (Bulger et al., 2000; Garcia et al., 1990; Sharma et al., 2008; Stawicki et al., 2004). Research states that for each additional rib fracture in the elderly, mortality increases by 19% and the risk of pneumonia by 27% (Bulger et al., 2000). And it is not just for the elderly. A study evaluating the importance of multiple rib fractures as a marker of serious injury in children showed that there were 14 deaths among 33 children with rib fractures, a mortality rate of 42%, and that although these fractures are rare injuries in

childhood, they are associated with a high risk of death (Garcia et al., 1990). In view of this, authors state that the radiological examination constitutes the basis for the evaluation of these lesions, which, for the most part, are easily detected by imaging (Lonergan et al., 2003).).

Due to the phylogenetic proximity, we know that the risk of injury to the ribs in primates is similar to that described in humans, with a natural case described in chimpanzees (Jurmain, 1997), and several other ones, using primates as models, for the study of injuries and concussions, that present similar results to those observed in humans (Kazarian, 1975; Kohno et al., 1979; Life & Pince, 1968).

The sternum of *Sapajus libidinosus* is very similar to that of man, in terms of the particularities observed (Sobotta, 2000), however, morphologically, the sternal body of the human is a unique structure, without the presence of sternebrae and intersternebral cartilages, being much wider than that of small primates, such as *Sapajus libidinosus*, *Callithrix jacchus* (Casteleyn et al., 2012), and *Callimico goeldii* (Hill, 1959). The absence of a ventral crest is unanimous among the works analyzed with primates. This characteristic is directly related to the development of the pectoral muscles, which originate from the sternum and to the shape of the rib cage. It is observed that primates have a shorter thorax and do not develop large chests, these muscles are more concentrated in the cranial portion, presenting greater growth in the laterolateral direction, due to the support of the limbs and the execution of adduction and abduction actions in large amplitude (Konig & Liebich, 2016; Sobotta, 2000).

The number of sternebrae is little variable among the small New World monkeys. In this study, we have found five to six sternebrae in the animals analyzed, as opposed to four to five in *Callithrix jacchus* (Casteleyn et al., 2012) and five in *Callimico goeldii* (Hill, 1959).

As for injuries of the sternum, it is frequently twisted or fractured in patients with trauma to the upper thoracic spine, called indirect sternal injury. It can also undergo direct trauma, where forces applied to the front of the chest later displace the lower sternal fragment. For both, radiographic analysis and knowledge of normal anatomy are necessary. Radiographically, the pattern of the two lesions differs and should alert radiologists to serious pathologies in the thoracic spine (Fowler, 1957; Gopalakrishnan & El Masri, 1986).

As for the particularities in the lumbar segment identified in *Sapajus libidinosus*, attention turns to a particular structure, the accessory process. Observed from the first to the penultimate lumbar vertebra in a well-developed manner, it is not found in humans (Sobotta, 2000), nor has it been described in *Callithrix jacchus* (Casteleyn et al., 2012), but it can be identified in *Alouatta seniculus* (Mesquita et al., 2019) and *Callimico goeldii* (Hill, 1959).

Another particularity of the animals in this study was the well-developed spinous processes in the lumbar segment. In this regard, it is reported that this particularity is not limiting for procedures to access the lumbosacral space, but limits dorsal flexion of the lumbar region, since the cranial part of the spinous processes are locked at the V-shaped end, preventing backward movement, and this condition may be associated with the use of the tail as a fifth limb since it provides greater stability to the trunk (Ankel-Simons, 2007).

A small variation between five and six lumbar vertebrae was observed in the animals of this study, being within the considered modal number in primates, which are six vertebrae in this segment. Some genera maintained this pattern in most of their specimens, such as *Tarsius*, *Galago* and *Perodicticus*, among the prosimians, and *Pithecia*, *Cacajao*, *Alouatta*, *Saimiri*, *Cebus* and *Lagothrix*, among the platyrrhines. This number increased to seven, eight, or even nine, in most lemurid genera, ten lumbar vertebrae were found in only one genus, *Lepidolemur* and less than six lumbar vertebrae occurred in the platyrrhine subfamilies, *Alouattinae* and *Atelinae*, and in all higher primates (Schultz & Straus Jr., 2015).

The great apes, or Pongidae, are the only primates to show extreme individual reductions to just three lumbar vertebrae. According to the literature, this reduction can occasionally be even greater. For example, there is a report of two gorillas with only one and a half lumbar vertebrae (Fick, 1933), and another case of gorillas containing two lumbar vertebrae (Randall, 1944).

Man, with an average of five lumbar vertebrae, has undergone a smaller phylogenetic change than many other primates, with few reports of specimens with 4 and 6 vertebrae (Schultz & Straus Jr., 2015). Transitional, or half lumbar vertebrae, occur more frequently at the cranial end than at the caudal end, indicating that the lumbosacral border is more stable than the thoracolumbar border (Elliot, 1913).

Although the number of lumbar vertebrae is only half that of the thoracic vertebrae in the animals in this study, the lengths of the thoracic and lumbar regions are similar. This elongation and strength of the lumbar region are associated with jumping adaptations in primates (Erikson, 1963; Fleagle, 1977), an association demonstrated in a study with *Pithecia pithecia* and *Chiropotes satanas* (Fleagle & Meldrum, 1988). In several Cebidae genera, the number of thoracic + lumbar vertebrae remained virtually unchanged, resulting in 19 (Schultz & Straus Jr., 2015). Six of the eight animals analyzed in this study showed this disposition.

It is important to know the lumbar segment in *Sapajus libidinosus*, as well as the sacral and even coccygeal segment, in other primate species, for the knowledge of the topography of the medullary cone in these animals, important for performing epidural anesthesia, a technique

of regional anesthesia used with great frequency, due to its ease and relative safety, which is generally required in interventions in the rectum, anus, vagina, umbilical cord fistula, cesarean section, caudectomy or even in the pelvic limbs (Santos et al., 2009).

Study data in black-striped capuchin monkeys, report the location of the medullary cone between L2 and L5 (Cordeiro et al., 2014) and in *Callithrix jacchus* (La Salles et al., 2017), between L3 and L6, both using the spinous process of the first sacral vertebra as one of the palpable bone projections to identify the space, and allowing access to the epidural space through the lumbosacral joint, since the apex of the cone does not go beyond the lumbar segment (Tranquilli et al., 2007). In comparison with other smaller neotropical primate species, a report in *Saguinus midas* highlights the presence of a medullary cone from L4 to S2 (Martins, 2013) and a study in *Saimiri sciureus*, describes it from L7 to Ca1 (Lima, 2011). These results show us the importance of knowing the vertebral segments in the access to regional anesthesia routes.

In a study of lumbar facet joints in humans, computed tomography (CT) was requested as an essential test in the identification of treatable abnormalities (Carrera et al., 1980). Researchers claim that images are difficult to obtain with conventional radiographic techniques of the lumbar joints, and that the use of CT is necessary in patients with sciatica or low back pain (Inman et al., 1942). These same authors analyzed a series of 100 consecutive cases of sciatica and low back pain by means of CT, and abnormal facet joints were found in 65 of them. Accordingly, it is reported that facet joint disorder is rarely diagnosed because appropriate radiographic techniques for imaging these joints have not been developed. In the images generated in *Sapajus libidinosus*, we could clearly observe this joint, characterized by the connection between the surfaces of the cranial and caudal articular processes, confirming that the species under study can serve as a model for the development of techniques for the treatment or prevention of this type of lesions.

The sacrum of *Sapajus libidinosus* was mostly rectangular in shape, with a wider base and a narrower caudal portion of the apex, similar to what was observed in *Callithrix jacchus* (Casteleyn et al., 2012), *Callimico goeldii* (Hill, 1959) and *Alouatta seniculus* (Mesquita et al., 2019). Structurally, it presented the same particularities identified in man (Sobotta, 2000).

Most of the animals analyzed followed a pattern of three sacral vertebrae, considered the modal number in most primate genera and particularly modal for platyrrhines, although there may be a variation between three and six vertebrae in primates in general. C*allithrix jacchus* (Casteleyn et al., 2012) and *Callimico goeldii* (Hill, 1959) maintained the pattern of three sacral vertebrae, however, only two vertebrae were observed in a specimen of *Alouatta*

seniculus (Mesquita et al., 2019), in one specimen of *Callithrix jacchus* (Casteleyn et al., 2012) and two specimens from this study, considering the animal that presented a transitional vertebra. This number increased to five or even six in just two groups of primates, the Lorisinae, of the suborder Lemuroidea and all higher primates of the infraorder Simiiformes. This can be considered an example of convergent evolution, as the same phylogenetic tendency to increase the number of sacral segments independently affected two quite distinct groups of primates (Schultz & Straus Jr., 2015).).

An increase in the number of vertebrae that participate in the formation of the sacrum can occur at the expense of the lumbar and caudal region. In one of the animals in this study, the presence of a caudal transition vertebra was observed next to the sacrum. In this case the first caudal vertebra came very close to forming sacral foramina along with the last true sacral segments. This same observation was identified in a study with *Cercocebus* and *Macaca* (Schultz, 1944), *Alouatta seniculus* (Mesquita et al., 2019) and *Callithrix jacchus* (Casteleyn et al., 2012). There are also reports in the *Oedipomida* and *Pan* genera of unilateral transformation of a lumbar vertebra into a sacral one, in which the number of lumbar vertebrae was reduced by half a segment, hence, it can be said that the sacral region invaded the lumbar region (Schultz & Straus Jr., 2015). These same authors reported that, despite the difficulty in distinguishing between the last sacral vertebra and the first caudal vertebra, transitional vertebrae are comparatively rare at the caudal end of the sacrum.

Computed tomography of the lumbar and sacral region of *Sapajus libidinosus* showed anatomical details to support the diagnosis of lesions and even malformations, from the most subtle, which are often invisible on radiographs, to the most severe, with structural and functional damage. This diagnostic technology has been important for the identification of important morphological alterations, such as spina bifida, an alteration commonly observed in the lumbosacral region. Despite being one of the most common malformations in humans and other animal species (Mitchell et al., 2004), there is only one report of spina bifida occulta in *Callithrix penicillata* (Marques et al., 2012), from T2 to T4, considered an uncommon site, and a report of spontaneously occurring spina bifida cystica in a female *Macaca nigra* in S1 (Meire et al., 1978), both with diagnosis confirmed by computed tomography examination. Spina bifida can affect any vertebra (Marques et al., 2012), but is most often seen in the lumbosacral region (Oliver et al., 2011). In the occult form, the picture is asymptomatic as the spinal cord and meninges remain in the normal position. When the meninges are distended by fluid, the change is called spina bifida cystica (Sinowatz, 2010) and, in these cases, it can cause

neurological deficits (Moore & Persuad, 2004), being an alert condition and important to be identified.

The caudal region is the most variable part of the entire vertebral column, and its number of segments underwent phylogenetic alteration with apparent ease and rapidity, given that even closely related species can differ widely in the number of caudal segments. In *Sapajus libidinosus*, we have observed a variation of 23-24 sacral vertebrae, with an animal that had its tail cut off and presented 16 vertebrae, however, studies report that the caudal region of primates can contain from zero, in a specimen of the genus *Hylobates*, up to 34 vertebrae in the genus *Ateles* (Schultz & Straus Jr., 2015).

The mean number of coccygeal vertebrae in man was 4.2 in 745 cases in the literature (Schultz, 1930). Data from the same genus under study, *Cebus*, with a distinction of number of caudal vertebrae of 22-26 has been described (Schultz & Straus Jr., 2015). Researchers observed 24, 27 and 28 caudal vertebrae, respectively, in three *Tupaia* skeletons and 22 in a *Tupaia tana* specimen (Lyon Jr., 1913). A record of 26 vertebrae has been reported in a *Tupaia* (Flower, 1884), 27 segments in a *Dendrogale* (Davis, 1938) and 31 to 33 segments in *Ptilocercus specimens* (Gregory, 1913; Le Gros Clark, 2009). There were 26–29 caudal vertebrae described in *Callithrix jacchus* (Casteleyn et al., 2012), 29 in *Callimico goeldii* (Hill, 1959) and 25 in *Cebupithecia sarmientoi* (Meldrum & Lemelin, 1991). This represents a much higher variability than that found in other regions of the spine and the total number of vertebrae is mainly influenced by the variable number in this segment. There is no doubt that these numerical variations are related to the major evolutionary change in the tail region of higher primates and could also be a potential point for further changes.

In the analyzed animals, the first five caudal vertebrae presented a different morphology, more structurally related to the lumbar vertebrae. Contradicting what has been observed, researchers report that the initial segment of the tail in larger platyrrhines, such as *Cebupithecia*, *Pithecia* and *Chiropotes*, comprises a total of four elements, whereas in smaller platyrrhines, such as callitrichids, five elements are generally observed, while in prehensile-tailed monkey it ranges from six in *Cebus* to eight in Atelines (Ankel-Simons, 1972).

From the sixth vertebra, in *Sapajus libidinosus*, a differentiated morphology is assumed, also following a regression in terms of size, up to the last and smallest vertebra. In this regard, it is described that the absolute lengths of the caudal vertebrae of any primate decrease in a similar way (German, 1982). However, when the proportions of average or proximal width, in relation to the length of the vertebrae are analyzed, changes in vertebral dimensions occur in two distinct patterns, which separate primates with prehensile tails, such as *Cebus*, *Alouatta* and

Ateles, from those with non-prehensile tails, such as *Pithecia* and *Chiropotes* (Meldrum & Lemelin, 1991). In this regard, it has been proven that the degree of development of the transverse processes in the caudal vertebrae of the distal region; as well as the strong development of specific caudal muscles, such as the intertransverse muscles of tail in the distal part of the tail and the medial and lateral flexors; is an excellent indicator of prehensile function in platyrrhine tails, and contrasts dramatically with the condition of these muscles in non-prehensile-tailed monkeys (Lemelin, 1989).

It is possible to visualize haemal arches on the ventral surface of the caudal vertebrae in the three methods analyzed in this study. This structure is responsible for protecting vessels and nerves in the ventral region of the tail and serves for the insertion of muscle fibers, being still important in caudectomy surgeries, since its location, in the cranial limit of the vertebra, usually constitutes the region of the surgical incision in the muscle (Ankel-Simons, 2007).

Researchers, when estimating the proportion of injured and disabled individuals between sexes and age classes in a National Park, of four genera of the Cercopithecidae family, observed that, among bone fractures, those of the tail were the most common in adult females (Arlet et al., 2009). Reports also show that, in nature, susceptibility to fracture is associated in part both with the type of locomotion, for example, long tails in *Ateles*, *Cebus* and *Callithrix*, used as a fifth limb, and long and fragile arms in gibbons, as well as with body parts that are targeted by attackers (Schultz, 1944; McGraw et al., 2006).

Among the animals analyzed in this study, three females presented a fracture in the tail, one in the medial distal portion, and two in the distal portion, even within another reality, in captivity. Consistent with this, one study described that females participate in group defense, and may also be injured when trying to protect their babies from infanticidal males, and this applies both in captivity and in the wild (Harris, 2002). However, knowledge in the anatomy of the caudal segment is necessary in clinical interventions.

High-resolution computed tomography was used to perform three-dimensional reconstructions of each element of a partial skeleton of an *Australopithecus afarensis* fossil, making it possible to visualize and quantify the internal and external anatomical structures (Haile-Selassie & Su, 2016). According to the same authors, the computed tomography has been applied to a variety of contexts within the fields of biological anthropology and paleoanthropology, and its technology provides non-destructive access to the internal structure of objects with various material compositions (Denison & Carlson, 1997; Ketcham & Carlson, 2001) and has been used successfully in anatomical analyzes of fossil materials (Alemseged et

al., 2006; Carlson et al., 2011; Leakey et al., 2012; Suwa et al., 2009; Thompson & Illerhaus, 2012; 1998).

Radiography has also been widely used in the primatological routine. An archival survey of radiographic images associated with nutritional osteoporosis in non-human primates was performed, noting, through anatomic-radiographic analysis, that 94% of the exams referred to cases of bone demineralization and 35% to pathological fractures (Bruno et al., 2020). These and many other works already mentioned, lead us to recognize the important role of basic anatomical knowledge and imaging exams in the veterinary routine and, particularly, in the routine of primates.

5 CONCLUSION

By presenting detailed anatomical and imaging data on the axial skeleton of *Sapajus libidinosus*, this study contributes to the science education of laboratory animals. It was possible to verify the efficiency of imaging diagnostic methods in the species under study, demonstrating that it is possible to identify bone structures with great precision, when compared to images of bone pieces. *Sapajus libidinosus* presented anatomical characteristics that were structurally very similar to humans, and, morphologically, to those of New World monkeys, being an excellent indicator of an experimental model for human studies. Knowledge through gross anatomy and tomographic and radiological exams can contribute to a better evaluation of therapeutic agents, regional anesthesia, skeletal diseases, osteo-metabolic diseases, and bone clinical-surgical interventions in primates in general, resulting in the refinement of research protocols and possibly in a reduction of animals in experiments as well.

AKNOWLEDGMENTS

The authors would like to thank CETAS/IBAMA-Natal, on behalf of the environmental analyst and Veterinary Doctor Tiago Saulo Freire Costa, for their help and agreement in the use of animals and the Coordination for the Improvement of Higher Education Personnel (CAPES) for the doctoral scholarship. They would also like to thank the staff of the Instituto de Radiologia de Natal (IRV), for all the support in carrying out the tomography and Rx exams, and the Potiguar University (UnP), for the partnership established and competence in carrying out the radiographic exams.

CONFLICT OF INTEREST

All authors declare that there is no conflict of interest in the present study.

AUTHOR CONTRIBUTION

SAYFLS, JKA, JGS, KBF, ANC, EVLV, MAPK, FTMM and DJAM have contributed to the concept/design and data acquisition; AYFLS, MAPK and DJAM have contributed to the analysis/interpretation of data; AYFLS has contributed to the writing of the manuscript; AYFLS, MAPK and DJAM have contributed to the critical review of the manuscript. All authors gave final approval of the article before submission.

DATA AVAILABILITY STATEMENT

Data supporting the results of this study are available from the corresponding author upon reasonable request.

ORCID

Ana Yasha Ferreira de La Salles https://orcid.org/0000-0003-2104-3539
Jéssica Kária de Andrade https://orcid.org/0000-0002-0039-8456
Joyce Galvão de Souza https://orcid.org/0000-0001-5492-6317
Kelvis de Brito Freitas https://orcid.org/0000-0002-4851-0734
Artur da Nóbrega Carreiro https://orcid.org/0000-0002-2131-7432
Edson Vinícius Leite Veloso https://orcid.org/0000-0002-1533-8499
Ediane Freitas Rocha https://orcid.org/0000-0003-4671-3906
Marcius Alessandro Pessanha Klem https://orcid.org/0000-0002-9097-6175
Fábio Tatian Moura Mendonça https://orcid.org/0000-0001-9770-2997
Danilo José Ayres de Menezes https://orcid.org/0000-0001-6089-3283

REFERENCES

Alemseged, Z., Spoor, F., Kimbel, W.H. et al. (2006) A juvenile early hominin skeleton from Dikika, Ethiopia. *Nature*, 443, 296–301.

Ankel-Simons, F. (2007) Primate Anatomy: an introduction. 3 ed. Unite States: Elsevier Inc.

998 Ankel-Simons, F. (1972) Vertebral morphology of fossil and extant primates. In: Tuttle, R.H.
999 (Ed.) *The Functional and Evolutionary Biology of the Primates*. Chicago: Aldine Press, pp.
1000 223-240.
1001
1002 Ankel-Simons, F. (1983) A Survey of living primates and their anatomy. New York:
1003 Macmillan.
1004
1005 Alves, F.R., Costa, F.B., Machado, P.P. et al. (2012) Anatomical and radiographic appearance
1006 of the capuchin monkey thoracic cavity (*Cebus apella*). *Pesquisa Veterinária Brasileira*, 32,
1007 1345-1350.
1008
1009 Arlet, M.E., Carey, J.R. & Molleman, F. (2009) Species, age and sex differences in type and
1010 frequencies of injuries and impairments among four arboreal primate species in Kibale National
1011 Park, Uganda. *Primates*, 50, 65–73.
1012
1013 Auricchio, P. (1995) Primatas do Brasil. São Paulo: Terra Brasilis.
1014
1015 Bagi, C.M., Volberg, M., Moalli, M. et al. (2007) Age-related changes in marmoset trabecular
1016 and cortical bone and response to alendronate therapy resemble human bone physiology and
1017 architecture. *The Anatomical Record*, 290, 1005–1016.
1018
1019 Barros, R.A.C., Prada, I.L.S., Silva, Z., Ribeiro, A.R. & Silva, D.C.O. (2003) Constituição do
1020 plexo lombar do macaco *Cebus apella*. *Brazilian Journal of Veterinary Research and Animal*
1021 *Science*, 40, 373-381.
1022
1023 Bicca-Marques, J.C., Silva, V.M. & Gomes, D.F. (2006) Ordem Primates. In: Reis, N.R.,
1024 Peracchi. A.L., Pedro, W.A. & Lima, I.P. (Eds.) *Mamíferos do Brasil*. Londrina: UEL, pp. 101-
1025 148.
1026
1027 Bortolini, Z. (2013) Ressonância magnética na avaliação das estruturas encefálicas do *Alouatta*
1028 *fusca* (Bubio-ruivo – Geoffroy Saint-Hilaire, 1812). Tese de doutorado. Universidade Estadual
1029 Paulista, Faculdade de Medicina Veterinária e Zootecnia, Botucatu, Brasil.

Bruno, S.F., Albuquerque, G.L., Carvalho, L.C.R., Pollis, E.S.C. & Romão, M.A.P. (2020) Estudo retrospectivo de alterações anatomo-radiográficas consequentes da osteoporose nutricional em saguis (Primates: Callitrichidae) no setor de animais selvagens da Universidade Federal Fluminense – UFF. *Brazilian Journal of Development*, 6, 363-374.

Bulger, E.M., Arneson, M.A., Mock, C.N. & Jurkovich, G.J. (2000) Rib fractures in the elderly. *The Journal of Trauma: Injury, Infection, and Critical Care*, 48, 1040-1047.

Burmeister, H. (1894) Ueber die arten der gattung *Cebus*. Halle: Abhandlungen der Naturforschenden Gesellschaft zu Halle.

Carlson, K.J, Stout, D., Jashashvili, T. et al. (2011) The endocast of MH1, *Australopithecus sediba*. *Science*, 333, 1402–1407.

Carrera, G.F., Haughton, V.M., Syvertsen, A. & Williams, A.L. (1980) Computed tomography of the lumbar facet joints lumbar facet joints. *Radiology*, 134, 145-148.

Casteleyn, C., Bakker, J., Breugelmans, S. et al. (2012) Anatomical description and morphometry of the skeleton of the common marmoset (*Callithrix jacchus*). *Laboratory Animals*, 46, 152–163.

Cordeiro, J.F., Santos, J.R.S., Dantas, S.B.A. et al. (2014) Anatomia do cone medular aplicada à via epidural de administração de fármacos em macacos-prego (*Sapajus libidinosus*). Pesquisa veterinária brasileira, 34, 29-33.

Cotter, M.M., Loomis, D.A., Simpson, S.W., Latimer, B. & Hernandez, C.J. (2011) Human evolution and osteoporosis-related spinal fractures. *Plos One*, 6, 1-11.

Courtine, G., Bunge, M.B., Fawcett, J.W. et al. (2007) Can experiments in nonhuman primates expedite the translation of treatments for spinal cord injury in humans? *Nature Medicine*, 13, 561–566.

Cubas, Z.S., Silva, J.C.R. & Catão-Dias, J.L. (2014) Tratado de animais selvagens: Medicina Veterinária. São Paulo: Editora GEN/Roca.

1064 Davis, D.D. (1938) Notes on the anatomy of the treeshrew *Dendrogale*. *Field Museum of*
1065 *Natural History - Zoological series*, 20, 383-404.
1066
1067 Denison, C. & Carlson, W.D. (1997) Three-dimensional quantitative textural analysis of
1068 metamorphic rocks using high-resolution computed X-ray technology: Part I. Methods and
1069 techniques. *Journal of Metamorphic Geology*, 15, 29–44.
1070
1071 Elliot, D.G. (1913) A review of the primates. Monograph series, v. 3. New York: American
1072 Museum of Natural History.
1073
1074 Ei-Khoury, G.V. & Whitten, C.G. (1993) Trauma to the upper thoracic spine: Anatomy,
1075 biomechanics, and unique imaging features. *American journal of roentgenology*, 160, 95-102.
1076
1077 Erikson, G.E. (1963) Brachiation in New World monkeys and in anthropoid apes. *Symposium*
1078 *of the Zoological Society of London*, 10, 135-163.
1079
1080 Ferro, S., Cecconi, L., Bonavita, J., Pagliacci, M.C., Biggeri, A. & Franceschini, M. (2017)
1081 Incidence of traumatic spinal cord injury in Italy during 2013–2014: a population-based study.
1082 *Spinal Cord*, 55, 1103–1107.
1083
1084 Fick, R. (1933) Untersuchungen an der wirbelsaule der menschenaffen. Preuss. Akad. Wiss.
1085 Phys. Math. Ki., 77, 167-239.
1086
1087 Fleagle, J.G. (1977) Locomotor behavior and muscular anatomy of sympatric Malaysian leaf-
1088 monkeys (*Presbytis obscura* and *Presbytis melalophos*). *American Journal of Physical*
1089 *Anthropology*, 46, 297-308.
1090
1091 Fleagle, J.G. & Meldrum, D.J. (1988) Locomotor behavior and skeletal morphology of two
1092 sympatric pitheciine monkeys, *Pithecia pithecia* and *Chiropotes satanas*. *American Journal of*
1093 *Primatology*, 16, 1-23.
1094
1095 Flower, W.H. (1884) Catalogue of the specimens illustrating the osteology and dentition of
1096 vertebrated animals, recent and extinct, contained in the Museum of the Royal College of
1097 Surgeons of England. Part II, Mammalia. London: Palala Press.

1098 Fowler, A.W. (1957) Flexion-compression injury of the sternum. *Journal of Bone and Joint*
1099 *Surgery*, 39-B, 487-496.
1100
1101 Garcia, V.F., Gotschall, C.S., Eichelberger, M.R. & Bowman, L.M. (1990) Rib fractures in
1102 children: a marker of severe trauma. *The Journal of Trauma*, 30, 695-700.
1103
1104 German, R.Z. (1982) The functional morphology of caudal vertebrae in New World monkeys.
1105 *American Journal of Physical Anthropology*, 58, 453-459.
1106
1107 Goodenough, A.E., Smith, A.L., Stubbs, H., Williams, R. & Hart, A.G. (2012) Observer
1108 variability in measuring animal biometrics and fluctuating asymmetry when using digital
1109 analysis of photographs. *Annales Zoologici Fennici*, 49, 81-92.
1110
1111 Gopalakrishnan, K.C. & El Masri, W. (1986) Fractures of the stemum associated with spinal
1112 injury. *Journal of Bone and Joint Surgery*, 68-B, 178-181.
1113
1114 Graf, W., De Waele, C. & Vidal, P.P. (1995a) Functional anatomy of the head-neck movement
1115 system of quadrupedal and bipedal mammals. *Journal of Anatomy*, 186, 55-74.
1116
1117 Graf, W., De Waele, C., Vidal, P.P., Wang, D.H. & Evinger, C. (1995b) The orientation of the
1118 cervical vertebral column in unrestrained awake animals. *Brain, Behavior and Evolution*, 45,
1119 209-231.
1120
1121 Gregory, W.K. (1913) Relationship of the Tupaiidae and of the Eocene lemurs, especially
1122 *Notharctus*. *Bulletin of Geological Society of America*, 24, 247-252.
1123
1124 Haile-Selassie, Y. & Su, D.F. (2016) The postcranial anatomy of *Australopithecus afarensis* -
1125 New Insights from KSD-VP-1/1. Dordrecht: Springer Netherlands.
1126
1127 Harris, T.R. (2002) Infanticide and subsequent mating behavior in a black and white colobus
1128 monkey group. AAPA poster and presentation schedule. *American Journal of Physical*
1129 *Anthropology*, 117, 17-67.

1130 Hill, W.C.O. (1959) The Anatomy of *Callimico goeldii* (Thomas): A Primitive American
1131 Primate. *Transactions of the American Philosophical Society, New Series*, 49, 1-116.
1132
1133 Inman, V.T. & Saunders, J.B. (1942) The clinico-anatomical aspects of the lumbosacral region.
1134 *Radiology*, 38, 669-678.
1135
1136 *International Committee on Veterinary Gross Anatomical Nomenclature*. (2017) Nomina
1137 Anatomica Veterinária. 6 ed. Hanover, Ghent, Columbia, MO, Rio de Janeiro: Editorial
1138 Committee.
1139
1140 Jenkins, F.A. (1970) Anatomy and function of expanded ribs in certain edentates and primates.
1141 *Journal of Mammalogy*, 51, 288-301.
1142
1143 Jerome, C.P. & Peterson, P.E. (2001) Nonhuman primate models in skeletal research. *Bone*, 29,
1144 1-6.
1145
1146 Joseph, C., Andersson, N. & Bjelak, S. et al. (2017) Incidence, aetiology and injury
1147 characteristics of traumatic spinal cord injury in Stockholm, Sweden: A prospective,
1148 population-based update. *Journal of Rehabilitation Medicine*, 49, 431–436.
1149
1150 Jurmain, R. (1997) Skeletal evidence of trauma in African apes, with special reference to the
1151 gombe chimpanzees. *Primates*, 38, 1-14.
1152
1153 Kazarian, L. (1975) The primate as a model for crash injury. SAE Technical Paper 751175,
1154 Proceedings of the 19th Stapp Car Crash Conference - Society of Automotive Engineers,
1155 Warrendale, PA.
1156
1157 Keith, A. (1903) The extent to which the posterior segments of the body have been transmuted
1158 and suppressed in the evolution of man and allied primates. *Journal of Anatomy and Physiology*,
1159 37, 18-40.
1160
1161 Kinzey, W.G. (1997) *Cebus*. In: Kinzey, W.G. (Ed.). *New World Primates: Ecology, Evolution,*
1162 *and Behavior*. New York: Aldine de Gruyter, pp. 248-257.

1163 Ketcham, R.A. & Carlson, W.D. (2001) Acquisition, optimization and interpretation of X-ray
1164 computed tomographic imagery: applications to the geosciences. *Computers and Geosciences*,
1165 27, 381–400.
1166
1167 Kohno, H., Nakamura, N., Hirakawa, K. et al. (1979) Experimental head injury and concussion:
1168 morphologic changes and pathophysiologic responses following translational acceleration in
1169 primates. *Neurologia medico-chirurgica*, 19, 781-791.
1170
1171 König, H.E. & Liebich, H.G. (2016) Anatomia dos animais domésticos: texto e atlas colorido.
1172 6 ed. Porto Alegre: Artmed.
1173
1174 Krautwald-Junghanns, M.E., Zebisch, K., Enders, F., Pees, M. & Willuhn, J. (2001) Diagnoses
1175 of liver disease in birds by radiography and ultrasonography: under special consideration of
1176 ultrasound-guided liver biopsies. *Seminars in Avian and Exotic Pet Medicine*, 10, 153-161.
1177
1178 Kriz, J., Kulakovska, M., Davidova, H., Silova, M. & Kobesova, A. (2017) Incidence of acute
1179 spinal cord injury in the Czech Republic: a prospective epidemiological study 2006–2015.
1180 *Spinal Cord*, 55, 870–874.
1181
1182 Kwon, B.K., Streijger, F., Hill, C.E. et al. (2015) Large animal and primate models of spinal
1183 cord injury for the testing of novel therapies. *Experimental Neurology*, 269, 154–168.
1184
1185 Ladeira, L.M.C.E.B. & Höfling, E. (2007) Osteologia craniana de Bucconidae. *Boletim do*
1186 *Museu Paraense Emílio Goeldi Ciências Naturais*, 2, 117-153.
1187
1188 La Salles, A.Y.F., Cordeiro, J.F., Santos, J.R.S., Carreiro, A.N., Medeiros, G.X. & Menezes,
1189 D.J.A. (2017) Anatomical description of the main vessels for venipuncture in the black-striped
1190 capuchin monkey (*Sapajus libidinosus*, Silva Junior, 2002). *Journal of Medical Primatology*,
1191 46, 320-326.
1192
1193 La Salles, A.Y.F., Andrade, J.K., Lemos, K.K.A. et al. (2019) Electrocardiographic parameters
1194 of *Sapajus libidinosus* (SPIX, 1823) after chemical immobilization with tiletamine-zolazepam.
1195 *Journal of Medical Primatology*, 48, 154-160.

1196 La Salles, A.Y.F., Andrade, J.K., Cordeiro, J.F. et al. (2021) Assessment of the technique of
1197 the anesthetic block of the brachial plexus by supraclavicular approach in *Sapajus libidinosus*
1198 (SPIX, 1823). *Journal of Medical Primatology*, 50, 29-35.
1199
1200 Le Gros Clark, W.E. (2009) On the anatomy of the pentailed tree-shrew (*Ptilocercus lowii*).
1201 *Journal of Zoology*, 96, 1179-1309.
1202
1203 Leakey, M.G., Spoor, F., Dean, M.C. et al. (2012) New fossils from Koobi Fora in northern
1204 Kenya confirm taxonomic diversity in early Homo. *Nature*, 488, 201–204.
1205
1206 Lemelin, P. (1989) Functional myology of the platyrrhine prehensile tail. *American Journal of*
1207 *Physical Anthropology*, 78, 331-458.
1208
1209 Leutenegger, W. (1970) Beziehungen zwischen der neugeborenengriisse und dem
1210 sexualdimorphismue am becken bei simischen primaten. *Folia Primatologica*, 12, 224-235.
1211
1212 Life, J.S. & Pince, B.W. (1968) Comparative responses of small and medium sized primates,
1213 both live and embalmed, to impact stress. *Stapp Car Crash Conference Proceedings*, 76, 2941-
1214 2951.
1215
1216 Lima, A.R., Fioretto, E.T., Fontes, R.F., Imbeloni, A.A., Muniz, J.A.P.C. & Branco, E. (2011)
1217 Caring about medullary anesthesia in *Saimiri sciureus*: the conus medullaris topography. *Anais*
1218 *da Academia Brasileira de Ciências*, 83, 1339-1343.
1219
1220 Lonergan, G.J., Baker, A.M., Morey, M.K. & Boos, S.C. (2003) Child Abuse: Radiologic-
1221 Pathologic Correlation. *AFIP Archives*, 23, 811-845.
1222
1223 Ludlage, E. & Mansfield, K. (2003) Clinical care and disease of the common marmoset
1224 (*Callithrix jacchus*). *Comparative Medicine*, 53, 369–382.
1225
1226 Lyon Jr., N.W. (1913) Treeshrews: An account of the mammalian family Tupaiidae.
1227 *Proceedings of the United States National Museum*, 45, 1-18.

1228 Mcgraw, W.S., Cooke, C. & Shultz, S. (2006) Primate remains from African crowned eagle
1229 (*Stephanoaetus coronatus*) nests in Ivory coast's Tai forest: implications for primate predation
1230 and early hominid taphonomy in South Africa. *American Journal of Physical Anthropology*,
1231 131, 151-165.
1232
1233 Majdan, M., Brazinova, A. & Mauritz, W. (2016) Epidemiology of traumatic spinal cord
1234 injuries in Austria 2002-2012. *European Spine Journal*, 25, 62–73.
1235
1236 Makungu, M., Plessis, W.M., Barrows, M., Groenewald, H.B. & Koeppel, K.N. (2014)
1237 Radiographic thoracic anatomy of the ring-tailed lemur (*Lemur catta*). *Journal of Medical*
1238 *Primatology*, 43, 144-152.
1239
1240 Manfreda, E., Mitteroecker, P., Bookstein, F.L. & Schaefer, K. (2006) Functional morphology
1241 of the first cervical vertebra in humans and nonhuman primates. *Anatomical record - Part B -*
1242 *New anatomista*, 289, 184-194.
1243
1244 Martins, A.B., Fialho, M.S., Jerusalinsky, L., Valença-Montenegro, M.M., Bezerra, B.M.,
1245 Laroque, P.O., Melo, F.R. & Lynch Alfaro, J.W. (2021). *Sapajus libidinosus* (amended version
1246 of 2019 assessment). *The IUCN Red List of Threatened Species*. 10.2305/IUCN.UK.2021-
1247 1.RLTS.T136346A192593226.en.
1248
1249 Martins, D.M., Pinheiro, L.L., Lima, A.R., Pereira, L.C. & Branco, E.R. (2013) Topografia do
1250 cone medular do sauim (*Saguinus midas*). *Ciência Rural*, 43, 1092-1095.
1251
1252 Meldrum, D.J. & Lemelin, P. (1991) Axial skeleton of *Cebupithecia sarmientoi* (Pitheciinae,
1253 Platyrrhini) from the middle Miocene of La Venta, Colombia. *American Journal of*
1254 *Primatology*, 25, 69-89.
1255
1256 Meire, J.E., Boyce, W.L. & Silverman, N.R. (1978) Spina bifida occulta in a *Celebes* crested
1257 macaque. *Journal of the American Veterinary Medical Association*, 173, 1236-1238.
1258
1259 Mercer, S. (1999) Functional morphology of the lower cervical spine in nonhuman primates.
1260 Ph.D Dissertation, University of Pittsburgh, Pittsburgh, Pensilvânia.

1261 Mesquita, V.A., Souza, A.N.A., Sousa, E.L., Pinheiro, G.G., Silva, W.A. & Marques, D.A.
1262 (2019) Atlas simplificado de osteologia de *Alouatta seniculus*. 1 ed. Manaus: Instituto Federal
1263 de Educação, Ciência e Tecnologia do Amazonas.
1264
1265 Meyer Jr., P.R. (1989) Fractures of the thoracic spine: T1 to T10. In: Meyer Jr., P.R. (Ed.)
1266 *Surgery of spine trauma*. New York: Churchill Livingstone, pp. 525-571.
1267
1268 Mitchell, L.E., Adzick, N.S., Melchionne, J., Pasquariello, P.S., Sutton, L.N. & Whitehaed,
1269 A.S. (2004) Spina bifida. *Lancet*, 364, 1885-1895.
1270
1271 Mirzaeva, L., Gilhus, N.E., Lobzin, S. & Rekand, T. (2019) Incidence of adult traumatic spinal
1272 cord injury in Saint Petersburg, Russia. *Spinal Cord*, 57, 692–699.
1273
1274 Mivart, G. (1865) Contributions toward a more complete knowledge of the axial skeleton in
1275 primates. *Proceedings of the Zoological Society of London*, 33, 545-592.
1276
1277 Moore, K.L. & Persuad, T.V.N. (2004) Embriologia Clínica. 5 ed. Rio de Janeiro: Guanabara
1278 Koogan.
1279
1280 Moshi, H., Sundelin, G., Sahlen, K.G. & Sörlin, A. (2017) Traumatic spinal cord injury in the
1281 north-east Tanzania – describing incidence, etiology and clinical outcomes retrospectively.
1282 *Global Health Action*, 10, 1-9.
1283
1284 Nardone, R., Florea, C., Höller, Y. et al. (2017) Rodent, large animal and non-human primate
1285 models of spinal cord injury. *Zoology (Jena)*, 123, 101–114.
1286
1287 Nalley, T.K. (2013) Positional behaviors and the neck: a comparative analysis of the cervical
1288 vertebrae of living primates and fossil hominoids. Ph.D. Dissertation in Philosophy, Arizona
1289 State University, Arizona, Unite States.
1290
1291 Nalley, T.K. & Grider-Potter, N. (2017) Functional analyses of the primate upper cervical
1292 vertebral column. *Journal of Human Evolution*, 107, 19-35.

Nayak, U.V. (1933) Note on an unusual type of cervical rib in a lemur. *Journal of Anatomy*, 68, 119-121.

Oliver, J.E., Lorenz, M.D. & Korenegay, J.N. (2011) Pelvic limb paresis, paralysis, or ataxia. In: Lorenz, M.D., Coates, J.R., Kent, M. (Eds). *Handbook of veterinary neurology*. 5 ed. Missouri: W.B. Saunders Co., pp. 109-161.

Pritzker, K.P.H. & Kessler, M.J. (2012) Arthritis, muscle, adipose tissue, and bone diseases of nonhuman primates. In: Abee, C.R., Mansfield, K., Tardif, S. & Morris, T. (Eds). *Nonhuman Primates in Biomedical Research: Diseases*. San Diego: Academic Press, pp. 629-697.

Randall, F.E. (1944) The skeletal and dental development and variability of the *Gorilla*. *Human Biology*, 16, 307-308.

Santos, G.J., Pirajá, G.V., Dias, L.G.G.G. & Pereira, D.M. (2009) Anestesia epidural em pequenos animais. *Revista científica eletrônica de Medicina Veterinária*, 12.

Sekhon, L.H.S. & Fehlings, M.G. (2001) Epidemiology, Demographics, and Pathophysiology of Acute Spinal Cord Injury. *Spine*, 26, 2–12.

Schultz, A.H. (1961) Vertebral column and thorax. In: Hofer, H., Schultz, A.H., Stark, D. *Primatologia*. Basel: Karger Publishers, pp. 1-66.

Schultz, A.H. (1944) Age changes and variability in gibbons. *American Journal of Physical Anthropology*, 2, 1-129.

Schultz, A.H. (1930) The skeleton of the trunk and limbs of higher primates. *Human Biology*, 2, 303-438.

Schultz, A.H. & Straus Jr., W.L. (1945) The numbers of vertebrae in primates. *Proceedings of the American Philosophical Society*, 89, 601-626.

Sharma, O.P., Oswanski, M.F., Jolly, S., Lauer, S.K., Dressel, R. & Stombaugh, H.A. 2008. Perils of Rib Fractures. *The American Surgeon*, 74, 310-314.

Silva, T.C.F.; Valença-Montenegro, M.M.; Lucas, J.L.B.; Wagner, P.G.C.; Ferreira, J.G.; Ferreira, D.R.A.; Jerusalinsky, L.; Martins, A.B.; Senna, M.B. & Laroque, P.O. (2009) Morfometria de *Cebus libidinosus* SPIX, 1823 (Primates, Cebidae). In: XIII Congresso Brasileiro de Primatologia. Livro de Resumos do XIII Congresso Brasileiro de Primatologia.

Sinowatz, F. (2010) Teratology. In: Hyttel, P., Sinowatz, F., Vejlsted, M. (Eds). *Essentials of Domestic Animals Embriology*. Philadelphia: W.B. Saunders Co., pp. 338-382.

Sobotta, J. (2000) Atlas de Anatomia Humana. 21 ed. Rio de Janeiro: Guanabara Koogan.

Stawicki, S.P., Grossman, M.D., Hoey, B.A., Miller, D.L. & Reed, J.F. (2004) Rib Fractures in the Elderly: A marker of injury severity. *Journal of the American Geriatrics Society*, 52, 805-808.

Struthers, J. (1893) On the articular processes of the vertebrae in the *Gorilla* compared with those in man, and on costo-vertebral variation in the *Gorilla*. *Journal of Anatomy and Physiology*, 27, 131-138.

Suwa, G., Asfaw, B., Kono, R.T., Kubo, D., Lovejoy, C.O. & White, T.D. (2009) The *Ardipithecus ramidus* skull and its implications for hominid origins. *Science*, 326, 68e1–68e7.

Thompson, J.L. & Illerhaus, B. (1998) A new reconstruction of the Le Moustier 1 skull and investigation of internal structures using 3-D- μCT data. *Journal of Human Evolution*, 35, 647-665.

Tranquilim, M.V. (2012) Análise do líquido cefalorraquidiano, tomografia computadorizada craniana e angiotomografia cerebral de *Alouatta guariba* – Geoffroy Saint-Hilaire, 1812 (Bugio Ruivo). Tese de Doutorado, Faculdade de Medicina Veterinária e Zootecnia, Universidade Estadual Paulista, Botucatu, Brasil.

Tranquilli, W.J., Thurmon, J.C. & Grimm, K.A. (2007) Lumb and jones veterinary anesthesia and analgesia. Iowa: Blackwell Publishing.

1359 Weber, M. (1890) Zoologische Ergebnisse Einer Reise In Niederländisch Ost-indien, Leiden:
1360 Brill Archive.
1361
1362 Xie, L., Zhou, Q., Liu, S. et al. (2014) Normal thoracic radiographic appearance of the
1363 cynomolgus monkey (*Macaca fascicularis*). *Plos One*, 9, 1-6.
1364
1365 Young, A.N., Plessis, W.M., Rodriguez, D. & Beierschmitt, A. (2013) Thoracic radiographic
1366 anatomy in vervet monkeys (*Chlorocebus sabaeus*). *Journal of Medical Primatolology*, 42,
1367 310-317.

CAPÍTULO II:

Anatomy applied to image diagnosis of the forelimb of the black-striped capuchin (*Sapajus libidinosus* Spix, 1823)

Trabalho submetido à revista The Anatomical Record
ISSN: 1932-8494; Fator de Impacto: 2.064; Qualis A4

Anatomy applied to image diagnosis of the forelimb of the black-striped capuchin (*Sapajus libidinosus* Spix, 1823)

Running title: Anatomy of the forelimb in the black-striped capuchin

Ana Yasha F. de La Salles[1], Jéssica K. de Andrade[2], Joyce G. de Souza[1], Kelvis de B. Freitas[3], Artur da N. Carreiro[1], Edson Vinícius L. Veloso[1], Ediane F. Rocha[1], Marcius Alessandro P. Klem[4], Felipe V. Câmara[5], Danilo José A. de Menezes[1,6*]

[1]Postgraduate Program in Animal Science and Health, Federal University of Campina Grande, Center for Rural Health and Technology, 58708-110. Patos, Paraiba, Brazil.

[2]Veterinary Doctor, Postgraduate in Veterinary Anesthesiology at Instituto Qualittas, 60175-020. Fortaleza, Ceara, Brazil.

[3]Graduate Program in Structural and Functional Biology, Federal University of Rio Grande do Norte, 59078-220. Natal, Rio Grande do Norte, Brazil.

[4]Veterinarian specialized in Diagnostic Imaging, managing partner of the Institute of Veterinary Radiology, 59080-101. Natal, Rio Grande do Norte, Brazil.

[5]Veterinary Doctor, Master in Animal Science, Professor at Universidade Potiguar, 59056-000. Natal, Rio Grande do Norte, Brazil.

[6]Department of Morphology, Federal University of Rio Grande do Norte, 59078-970. Natal, Rio Grande do Norte, Brazil.

*Corresponding author: Danilo José Ayres de Menezes, Campus Universitário UFRN, Av. Senador Salgado Filho, 3000, Lagoa Nova, Natal/RN, 59064-741. Telephone: +55 84 98101-9198. E-mail: mdanayres@gmail.com

CONFLICT OF INTERESTS

All authors declare that there is no conflict of interest in the present study.

DATA AVAILABILITY STATEMENT

Data supporting the results of this study are available from the corresponding author upon reasonable request.

DECLARATION OF ETHICS

All procedures were in agreement with the ethical standards of the Federal University of Campina Grande (UFCG) and Federal University of Rio Grande do Norte (UFRN), and with the federal regulations of the Ministry of the Environment, Brazil. Post-mortem samples were collected and processed under Authorization Documents from the Wild Animal Screening Centers of the Brazilian Institute for the Environment and Renewable Natural Resources (CETAS/IBAMA) with the approval and supervision of the UFCG Ethics Committee for the Use of Animals and UFRN. This article does not contain analysis of human samples.

ORCID

Ana Yasha Ferreira de La Salles https://orcid.org/0000-0003-2104-3539
Jéssica Kária de Andrade https://orcid.org/0000-0002-0039-8456
Joyce Galvão de Souza https://orcid.org/0000-0001-5492-6317
Kelvis de Brito Freitas https://orcid.org/0000-0002-4851-0734
Artur da Nóbrega Carreiro https://orcid.org/0000-0002-2131-7432
Edson Vinícius Leite Veloso https://orcid.org/0000-0002-1533-8499
Ediane Freitas Rocha https://orcid.org/0000-0003-4671-3906
Marcius Alessandro Pessanha Klem https://orcid.org/0000-0002-9097-6175
Felipe Venceslau Câmara https://orcid.org/0000-0002-2089-5206
Danilo José Ayres de Menezes https://orcid.org/0000-0001-6089-3283

Abstract

Macroscopic bone analysis and evaluation through imaging methods are essential in the recognition of natural and altered structures. Therefore, this study aimed at describing the structures of the thoracic limb of *Sapajus libidinosus* in anatomical pieces, identifying them in radiographic and tomographic images. For this, four cadavers were used in the macroscopic analysis and five animals for the imaging exams, of which four were euthanized and added to the macroscopic stage. For imaging exams, the animals were kept anesthetized. All bones were documented, structures described, and compared with literature data from human and non-human primates. There was no statistical difference between males and females regarding the length of the forelimb bones. Most of the bone structures of the scapula were well identified in the imaging methods, being more restricted in the ventrodorsal projection. The clavicle presented very limited visualization. The humerus, as well as the radius and ulna, were not well portrayed in their proximal and distal epiphyses by radiography, however, they were well identified on tomography. All structures described in the macroscopic image of the carpal and metacarpal bones could be identified through radiography and tomography, and the radiographic examination of this region is an excellent method for identifying fractures. The glenoid notch of the scapula was not visualized by any imaging method. *Sapajus libidinosus* presented anatomical characteristics more similar to those of neotropical primates and man, being a great indicator of an experimental model for studies in these species.

Keywords

anatomy, Cebidae, digital radiology, osteology, Primates, tomography

1 INTRODUCTION

Anatomy studies are of great importance, whether for teaching or research, as they allow the understanding of the constitution and development of beings in an organized way (Dangelo & Fattini, 2011). The growing emergence of research centers with primate breeding, animal screening centers, and the increase in illegal trafficking and apprehension of these wild animals from human coexistence, increased the demand for veterinary care, and the knowledge of anatomy and imaging exams emerges as an important tool in for diagnosis and in the successful choice of the appropriate clinical and surgical procedure (Bortolini et al., 2013).

Among the most common primate species kept under human care in Brazil, the black-striped capuchin stands out, a medium-sized neotropical primate, weighing between 1.5 and 4.0 kg, endemic to Brazil and belonging to the infraorder Platyrrhini and family Cebidae. They are arboreal and diurnal, with great behavioral and ecological flexibility, easily adapting to different areas in free life and, as a result, they have the widest geographic distribution among Neotropical species, with an extension of occurrence greater than 20.000 km² (Bicca-Marques et al., 2006; Kinzey, 1997; Martins et al., 2021).

Keeping in captivity can favor the occurrence of several conditions in primates, among which are those that affect bone and joint structures, such as vitamin D3 deficiency, pathological fractures, skeletal deformities, and fractures resulting from traumatic events, power disputes and joint degenerative processes (Gros-Louis et al., 2003; Johnson-Delaney, 1994; Rangel et al., 2013).

Among the areas that have shown great growth in veterinary medicine in recent years, imaging has been praised given its evolution (Krautwald-Junghanns et al., 2001). Radiography is widely used in the description and anatomical identification of wild animals in general, and its affordability makes it the most used modality for bone assessment (Armbrust, 2010). With the advancement of technology, tomography has also become a widely used resource, because of its very enlightening imaging methods that provide a more accurate diagnosis, opening the field of vision for better clinical management and possibilities for anatomical studies, besides being an excellent model for morphofunctional investigation (Tidwell, 2010).

The inclusion of new modalities of imaging exams allowed the execution of studies in greater proportion in wild animals, including primates (Bortolini, 2013; Tranquilim, 2012). However, the number of studies on *Sapajus libidinosus*, focused on the area of gross anatomy compared with imaging methods, is still limited.

Despite being a genus that has been widely used as a biological model over the years, the specific characteristics of the *Sapajus* skeleton are still poorly documented, and little has been reported on aspects of the forelimb, such as the neonatal skeletal development of the genus *Cebus* and other primates (Watts, 1990) and intrinsic hand ontogeny, in capuchin monkeys (Young & Heard-Booth, 2016). The genus *Cebus*, among other primates, was also analyzed in a study of the evolution of the hand (Godinot & Beard, 1991) and the sesamoid bone of the musculus abductor pollicis longus (Le Minor, 1994).

Therefore, due to the scarcity of specific osteological and imaging data, and based on the importance of knowing the anatomical description and imaging tests for better medical intervention in primates, this study aimed at recognizing the structures of the forelimb of the black-striped capuchin monkey (*Sapajus libidinosus*) in anatomical parts, and radiographic and tomographic images, to serve as an anatomical guide for future biomedical research.

2 MATERIAL AND METHODS

2.1 Animals and Study Site

The macroscopic stage of the study was conducted at the Laboratory of Animal Anatomy, Department of Morphology, Federal University of Rio Grande do Norte (UFRN), Natal-RN. The CT scans and part of the radiographs were performed at the Institute of Veterinary Radiology (IRV), Natal-RN, and the other radiographs, in partnership with the Potiguar University (UnP), Natal-RN.

The methodological protocols were approved by the Ministry of the Environment, through the Biodiversity Authorization and Information System-SISBIO of the Chico Mendes Institute-ICMBio (n.º 70606-2), CEUA/UFCG (n.º 121/2019) and CEUA/UFRN protocol 074/2019, certificate n.º 209.074/2019.

Four corpses of black-striped capuchin monkeys (*Sapajus libidinosus*), males, two juveniles, aged less than 10 years, and two adults estimated to be 10-15 years old, kept frozen, donated by CETAS/IBAMA/Natal-RN, were used for the macroscopic study of the forelimb.

For the stage of radiography (RX) and tomography (CT), five specimens of *Sapajus libidinosus* were selected, an adult male, with an estimated age of 10-15 years, and four elderly females, with an estimated age of 20-30 years, weighing in average 2.21 kg, from the Wild Animal Screening Center (CETAS/IBAMA), in the city of Natal/RN. The monkeys were submitted to 4 hours of water fasting and 8 hours of food fasting before the anesthetic procedure.

After the imaging tests, the females were euthanized with 19.1% potassium chloride (Equiplex®, Brazil), at a dose of 1 mL/kg, intravenously, and added to the macroscopic study, totaling eight animals at this stage. The adult male animal was destined only for the examinations and returned to CETAS.

2.2 Preparation of parts and bone description

In the eight animals destined for the macroscopic stage, a dissection technique associated with maceration was performed, according to Ladeira & Höfling (2007). The region of interest was separated into right and left thoracic limbs and stored in bags made of mesh-like tissue, to facilitate the identification of the bones after maceration. The bones were separated by animal and we have used Araldite® Hobby epoxy glue and instant superglue (Tekbond®, Brazil) to put them together.

The lengths of the bones of the forelimb, from the most cranial to the most caudal extremity, or the most proximal to the most distal, were determined in the eight animals destined for macroscopic description. The right antimere was defined as the standard for measurement.

All bones were described, following the recommendations of the *Nomina Anatomica Veterinaria* (International Committee on Veterinary Gross Anatomical Nomenclature, 2017) and the structures of the clavicle were described based on the *Terminologia Anatomica Humana* (Federative International Program on Anatomical Terminologies & Verlag, 1998).

2.3 Imaging exams

Five animals were destined for this stage. One adult male and one female for tomography and radiography exams, and the other females were only for radiography exams. For the examinations, the animals were referred to the IRV and UnP, sedated with a combination of tiletamine hydrochloride and zolazepam hydrochloride (Telazol® 10%, Zoetis, Brazil) at a dose of 6 mg/kg, administered intramuscularly (La Salles et al. al., 2019; 2021). Upon arrival, access to the caudal saphenous vein was obtained (La Salles et al., 2017) for the anesthetic induction, which was performed with intravenous propofol (Provive 1%, União Química, Brazil) in a target-controlled infusion (TCI), with a VP50 infusion pump (MedRena®, Guangdong, China), at a dose of 2-5 mg/kg, followed by anesthetic maintenance at an initial dose of 0.25-0.5 mg/kg/min, reduced during the experiment. The animal was kept breathing room air, and in the 3rd anesthetic stage, between the 2nd and 3rd plane, so that there was no movement during the

exams. Monitoring was performed using a multiparameter monitor (Model DL 1000, Deltalife, Brazil).

After the exams, euthanasia was performed. One male animal was donated only for the examinations and was not euthanized. The corpses of the four euthanized females were sent to the Animal Anatomy Laboratory/UFRN to be added to the macroscopic study.

2.3.1 Radiography

At the Veterinary Hospital of UnP, radiographic examinations were performed using a conventional radiodiagnostic device, model VET500, (X-RAD X-Ray equipment, Brazil), with a capacity of 500 mA and 125 kV, equipped with a radiographic table with an anti-diffusion device and X-ray tube, and the images were acquired with the CR digital system, with an IP cassette plate, CC type (24 cm x 30 cm) (Fujifilm, Japan) and FCR PRIMA T2 Image Reader photostimulable phosphor plate scanner, model CR-IR 392 (Fujifilm, Japan). The radiographic technique used was 44 kV, 0.045-0.05 s, and 200 mA, under the same focus-film distance. The images were saved in PDS files and analyzed using the PD-S Viewer software, version 1.4.0.0.

To obtain better image definition, two animals were referred to the IRV, and the images were performed using a conventional radiodiagnostic device, Intecal, CR 500 mAs – Casa do Radiologista, equipped with a radiographic table with anti-diffusion grid, "Potter-Bucky ", and IAE X-ray tube (Italy) with rotating anode and the images were acquired using the DR digital system, with a VIEWORKS digitizer plate, model CESIO 1417WA, with 2560 x 3072 pixels. The radiographic technique used was 55 kV, 0.06 s and 300 mA, under the same focus-film distance. After the acquisition, the images were saved in DICOM files, transferred, and analyzed online using the postDICOM program (Herten, Netherlands). All radiographic examinations were performed in compliance with the radiological protection standards.

The animals were positioned directly on the radiographic tables. The forelimb was radiographed under the mediolateral and craniocaudal projections, in the arm and forearm regions, with the evaluation of the scapula also in the first projection, and dorsopalmar, in the hand region. A ventrodorsal projection of the thorax was performed to observe the clavicle.

The radiographic exams were individually analyzed, identifying all the bones and particularities observed in the skeletal system already described in the macroscopic stage, and a comparison of the three study methods was performed.

2.3.2 Computed tomography

For this examination, a helical computed tomography device, model XVision EX, single slice (Toshiba, Japan) was used. Before the scan, sagittal radiographic images of each region and sub-region to be studied of each animal were acquired (topogram), to define the extent of the study (the beginning and end of the scan) and the variation of the slices. Once the area was defined, transverse planes with predetermined section thickness and table increment were performed.

The imaging parameters used for the forelimb were: 2.0 mm slice thickness, 2.0 table increment, 100 mA and 120 kV, for the clavicle, and 1.0 mm slice thickness, 1.0 table increment, 150 mA and 120 kV, for the other regions. To perform the CT, the animals were positioned in sternal recumbency, with the caudal extension of the thoracic and pelvic limbs.

The tomographic images were transferred to the Horos software version 1.1.7 (United States) for the analysis of transverse plane images and multiplanar reconstructions (MPR) in the sagittal and dorsal planes. A 3D reconstruction to illustrate bone anatomy was also obtained.

The tomographic images were individually analyzed, identification of the bones, of particularities already described macroscopically, and a comparison of the three methods of study were performed.

2.4 Statistical analysis

During the study, the results obtained were documented with a digital camera, and, later, described and compared with data from the literature, about human and non-human primates. Mean and standard deviation of the lengths of the right antimere of the bones of the forelimb were determined. Student's t-test was performed for independent samples using the Past software version 4.03.

3 RESULTS

The bones of the forelimb comprise the scapula, clavicle, humerus, radius, ulna, carpus, metacarpal and phalanges. The measurements of the bone lengths of the right antimere, from the most cranial to the most caudal end of the scapula and the most proximal to the most distal end of the long bones, are distributed in Table 1.

TABLE 1 Length in millimeters (mm) of the bones of the right antimere of the forelimb of four males (M1-M4) and four females (F1-F4) of *Sapajus libidinosus*, arranged in mean (Mean) and standard deviation (SD).

	Mean	SD	Mean M*	Mean F**
Scapula	65.6	7.19	62.0	69.3
Clavicle	38.6	4.25	37.6	39.5
Humerus	100.8	7.41	97.4	104.1
Radius	96.1	9.47	91.1	101.1
Ulna	106.9	8.14	103.4	110.4
Value of t			0.3925	
Value of p			2.012	

[1] * Mean of males, **Mean of females.
[2] Means do not differ statistically from each other when compared by the t-test (p <0,05).

Data from Table 1 demonstrate that there was no statistically significant difference between males and females regarding the length of the forelimb bones. No differences were observed among the study specimens regarding the analyzed bones.

The scapula appears as a triangular bone, dorsoventrally long, with a domed cranial margin, a flat subscapular face, and a cranially displaced spine. It is characterized by a prominent coracoid process and a well-developed acromion that connects with the clavicle, which is sigmoid in shape. The other articular surface of the clavicles is bilaterally connected to the craniolateral surfaces of the manubrium of the sternum. The scapula also has a tubercle on the spine, small cartilage in its caudal angle, supraglenoid and infraglenoid tubercles. In the clavicle, it is possible to observe very subtle structures, such as the conoid tubercle, the trapezoid line, and the sulcus of the subclavius muscle. The impression of the costoclavicular ligament may be well-demarcated (Figs. 1, 2).

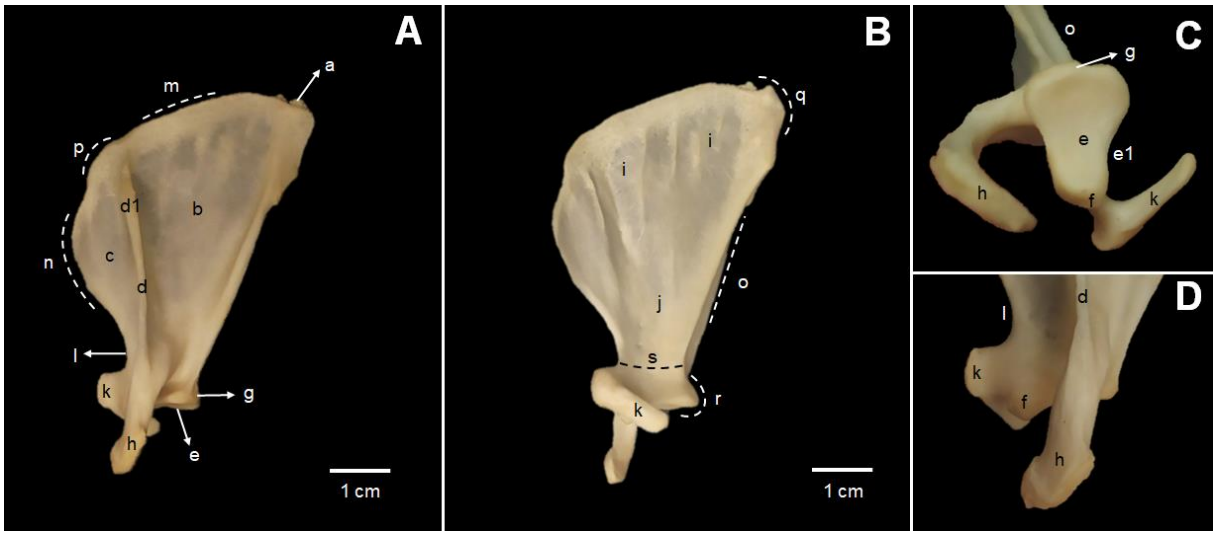

FIGURE 1 Left scapula. Lateral view (A), Medial view (B), Ventral joint surface (C), Lateral view of the distal end (D). a. Scapula cartilage (*Cartilago scapulae*); b. Infraspinatus fossa

(*Fossa infraspinata*); c. Supraspinatus fossa (*Fossa supraspinata*); d. Spine of the scapula (*Spina scapulae*); d1. Tuber of the spine of the scapula (*Tuber spinae scapulae*); e. Glenoid cavity (*Cavitas glenoidis*); e1. Glenoid notch (*Incisura glenoidis*); f. Supraglenoid tubercle (*Tuberculum supraglenoidale*); g. Infraglenoid tubercle (*Tuberculum infraglenoidale*); h. Acromion (*Acromion*); i. Facies serrata (Facies serrata); j. Subscapular fossa (*Fossa subscapularis*); k. Coracoid process (*Processus coracoideus*); l. Notch of the scapula (*Incisura scapulae*); m. Dorsal margin (*Margo dorsalis*); n. Cranial margin (*Margo cranialis*); o. Caudal margin (*Margo caudalis*); p. Cranial angle (*Angulus cranialis*); q. Caudal angle (*Angulus caudalis*); r. Ventral angle (*Angulus ventralis*); s. Neck of the scapula (*Collum scapulae*).

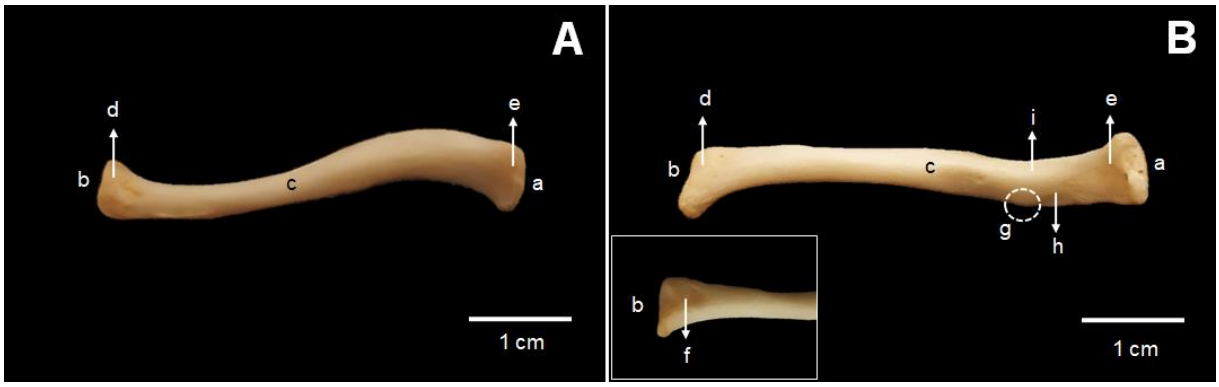

FIGURE 2 Left clavicle. Dorsal view (A), Ventral view (B). a. Sternal articular surface (*Facies articularis sternalis*); b. Scapular acromial articular surface (*Facies articularis acromialis*); c. Body of the clavicle (*Corpus claviculae*); d. Sternal extremity (*Extremitas sternalis*); e. Acromial extremity (*Extremitas acromialis*); f. Impression for the costoclavicular ligament (*Impressio ligamenti costoclavicularis*); g. Conoid tubercle (*Tuberculum conoideum*); h. Trapezoid line (*Linea trapezoidea*); i. Subclavian sulcus (*Sulcus musculi subclavii*).

Most bone structures of the scapula are visible both in radiographic images, in both projections, and 3D reconstruction (Figs. 3, 5 and 6). In the ventrodorsal (VD) projection, the view is more restricted because of the dorsal positioning of the scapula (Fig. 3), which, in the laterolateral projection (LL) and the 3D reconstruction, are better identified (Figs. 5 and 6). Structures such as the subscapular fossa and the face of the serratus were only visualized in the 3D reconstruction, due to the amplitude of visualization of the medial face of the bone, which is not observed through radiography (Fig. 6). On the other hand, the infraglenoid tubercle was only visible through the radiographic image (Fig. 5). The glenoid notch was the only structure not visualized by any imaging method. In the cross-sectional image of the region, it was possible to identify the scapula, clavicle, humerus and cervical vertebra (Fig. 4).

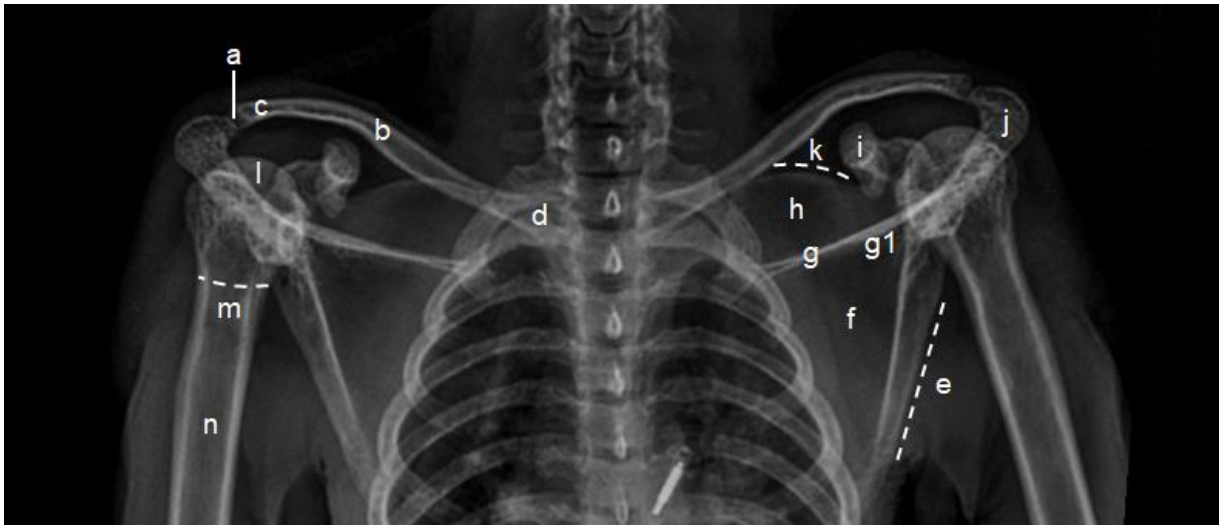

FIGURE 3 Radiographic image in ventrodorsal projection, highlighting the region of the clavicle, scapula and humerus. a. Scapular acromial articular surface; b. Body of the clavicle; c. Acromial extremity; d. Sternal extremity; e. Caudal margin; f. Infraspinous fossa; g. Spine of the scapula; g1. Tuberosity of the spine of the scapula; h. Supraspinous fossa; i. Coracoid process; j. Acromion; k. Cranial margin; l. Humeral head; m. Humeral neck; n. Humeral body.

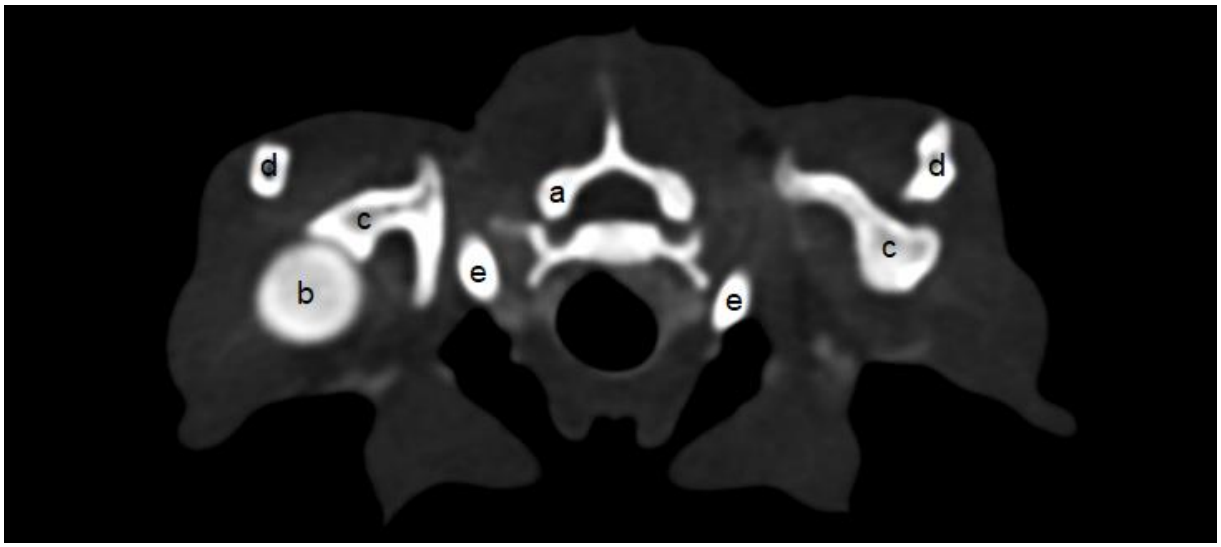

FIGURE 4 Cross-sectional tomographic image at the level of the cervical segment, highlighting the humerus, scapula and clavicle. a. Cervical vertebra; b. Humerus; c. Shoulder blade; d. Acromial end of the clavicle; e. Sternal end of clavicle.

The clavicle was best described by macroscopy. The structures identified in the imaging methods were limited to the body and acromial and sternal extremities (Figs. 3, 5 and 6). The conoid tubercle can be seen through the radiographic image, but not in the 3D reconstruction (Fig. 5).

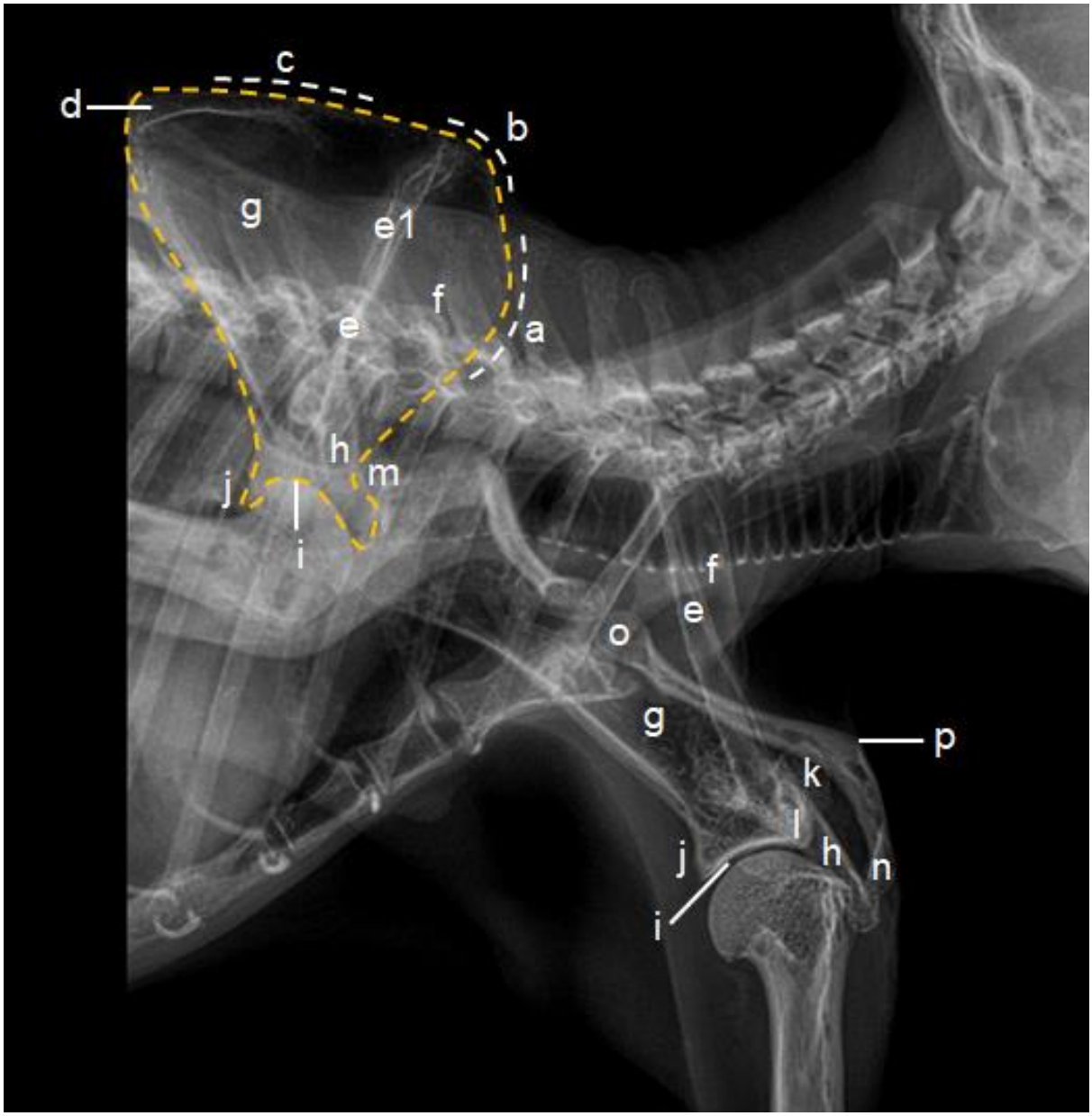

FIGURE 5 Radiographic image in mediolateral projection of the left antimere, highlighting the scapula and clavicle. a. Cranial margin of the scapula; b. Cranial angle of the scapula; c. Dorsal margin of scapula; d. Scapular cartilage; e. Spine of the scapula; e1. Tuberosity of the spine of the scapula; f. Supraspinous fossa; g. Infraspinous fossa; h. Acromion; i. Glenoid fossa; j. Infraglenoid tubercle; k. Coracoid process; l. Supraglenoid tubercle; m. Notch of the scapula; n. Acromial end of the clavicle; o. Sternal articular surface; p. Conoid tubercle.

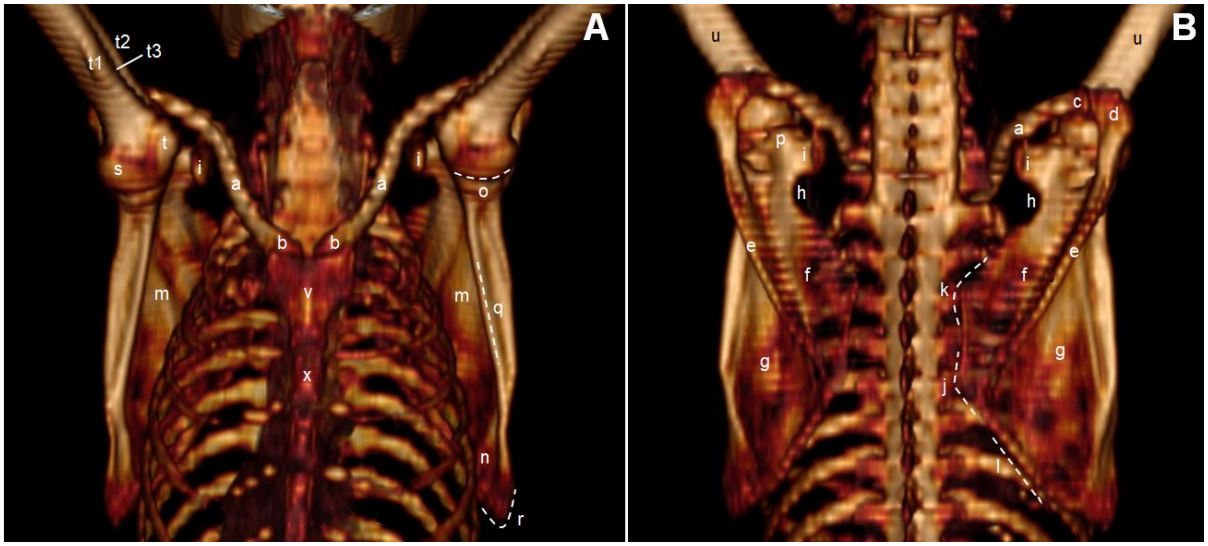

FIGURE 6 3D reconstruction image in ventrodorsal (A) and dorsoventral (B) projection, highlighting the humerus, scapula and clavicle. a. Clavicle body; b. Sternal extremity; c. Acromial extremity; d. Acromion; e. Spine of the scapula; f. Supraspinous fossa; g. Infraspinal fossa; h. Notch of the scapula; i. Coracoid process; j. Cranial angle of the scapula; k. Cranial margin of the scapula; l. Dorsal margin of scapula; m. Subscapularis fossa; n. Facies serrata; o. Glenoid cavity; p. Supraglenoid tubercle; q. Caudal margin of the scapula; a. Caudal angle of the scapula; s. Humeral head; t. Lesser tubercle; t1. Lesser tubercle crest; t2. Greater tubercle crest; t3. Intertubercular sulcus; u. Humerus body; v. Manubrium of the sternum; x. Second sternebra.

The humerus is quite robust and shows a discrete cranial deltoid tuberosity, as a continuous projection of the crest of the greater tubercle (Fig. 8B). In contrast, it has lateral and medial supra-epicondylar ridges, which join the well-developed epicondyles, in particular, the medial epicondyle has a greater projection (Figs. 7A and 8C). A large oblique entepicondylar foramen crossing the medial supra-epicondylar crest was observed. There is a well-defined olecranon fossa, coronoid fossa and radial fossa (Figs. 8C, D). Greater and lesser tubercles and their well-developed ridges were also observed, in particular, that of the greater tubercle, and a very prominent intertubercular groove (Fig. 8A). A triceps line is arranged on the caudal margin of the caudal part of the greater tubercle (Fig. 8B). A radial nerve sulcus is formed along the edge of the lateral supra-epicondylar ridge, in the caudal view (Fig. 7B). Although the supratrochlear region is very thin, no supratrochlear foramen was observed among the animals.

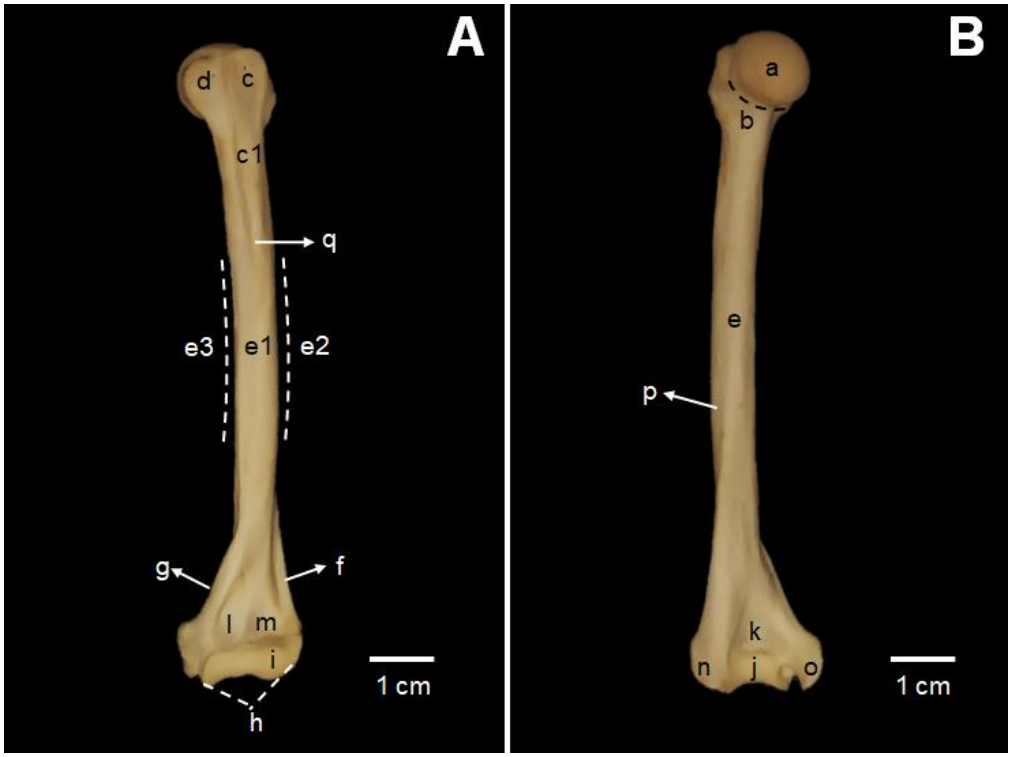

FIGURE 7 Left humerus. Cranial view (A), Caudal view (B). a. Humeral head (*Caput humeri*); b. Humeral neck (*Collum humeri*); c. Greater tubercle (*Tuberculum majus*); c1. Greater tubercle crest (*Crista tuberculi majoris*); d. Lesser tubercle (*Tuberculum minus*); e. Humeral body (*Corpus humeri*); e1. Cranial face (*Facies cranialis*); e2. Lateral face (*Facies lateralis*); e3. Medial face (*Facies medialis*); f. Lateral supraepicondylar crest (*Crista supraepicondylaris lateralis*); g. Medial supraepicondylar ridge (*Crista supraepicondylaris medialis*); h. Condyle of the humerus (*Condylus humeri*); i. Capitulum of the humerus (*Capitulum humeri*); j. Trochlea of the humerus (*Trochlea humeri*); k. Olecranon fossa (*Fossa olecrani*); l. Coronoid fossa (*Fossa coronoidea*); m. Radial fossa (*Fossa radialis*); n. Lateral epicondyle (*Epicondylus lateralis*); o. Medial epicondyle (*Epicondylus medialis*); p. Radial nerve sulcus (*Sulcus nervi radialis*); q. Deltoid tuberosity (*Tuberositas deltoidea*).

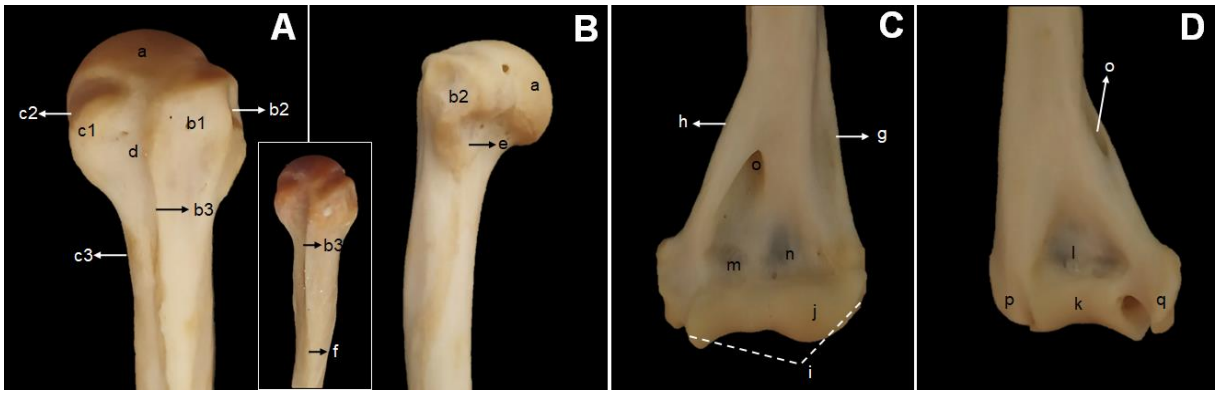

FIGURE 8 Left humerus. Cranial surface of the proximal epiphysis (A), Lateral view of the proximal epiphysis (B), Cranial view of the distal epiphysis (C), Caudal view of the distal epiphysis (D). a. Humeral head (*Caput humeri*); b. Greater tubercle (*Tuberculum majus*); b1. Cranial part (*Pars cranialis*); b2. Caudal part (*Pars caudalis*); b3. Greater tubercle crest (*Crista tuberculi majoris*); c. Lesser tubercle (*Tuberculum minus*); c1. Cranial part (*Pars cranialis*); c2. Caudal part (*Pars caudalis*); c3. Lesser tubercle crest (*Crista tuberculi minoris*); d. Intertubercular sulcus (*Sulcus intertubercularis*); e. Line of the tricipitis muscle (*Linea m.*

tricipitis); f. Deltoid tuberosity (*Tuberositas deltoidea*); g. Lateral supraepicondylar crest (*Crista supraepicondylaris lateralis*); h. Medial supraepicondylar ridge (*Crista supraepicondylaris medialis*); i. Condyle of the humerus (*Condylus humeri*); j. Capitulum of the humerus (*Capitulum humeri*); k. Trochlea of the humerus (*Trochlea humeri*); l. Olecranon fossa (*Fossa olecrani*); m. Coronoid fossa (*Fossa coronoidea*); n. Radial fossa (*Fossa radialis*); o. Entepicondylar foramen (*Entepicondylar foramen*); p. Lateral epicondyle (*Epicondylus lateralis*); q. Medial epicondyle (*Epicondylus medialis*).

The radius and ulna are separated by a wide interosseous space and are not fused (Fig. 11). The radius is thinner and has a fovea on the articular surface of the proximal epiphysis, and a single radial tuberosity on the interosseous margin (Figs. 9A, 9E and 11A). In its distal epiphysis, four grooves are observed for the passage of muscle tendons. A transverse ridge is observed at the distal limit of the bone, on the caudal surface. The articular surface of the distal epiphysis, in addition to presenting the surface for articulation with the carpus, also presents a lateral ulnar notch (Fig. 9). The ulna is well developed, being the third-largest bone in the body, with a robust olecranon tubercle. We have also observed robust anconeus and coronoid processes, a trochlear notch for articulation with the trochlea of the humerus, and a radial notch, to which the radial head articulates (Fig. 10). A very marked styloid process of the ulna and radius were described (Fig. 11). Both bones have a slight curvature at their interosseous margins.

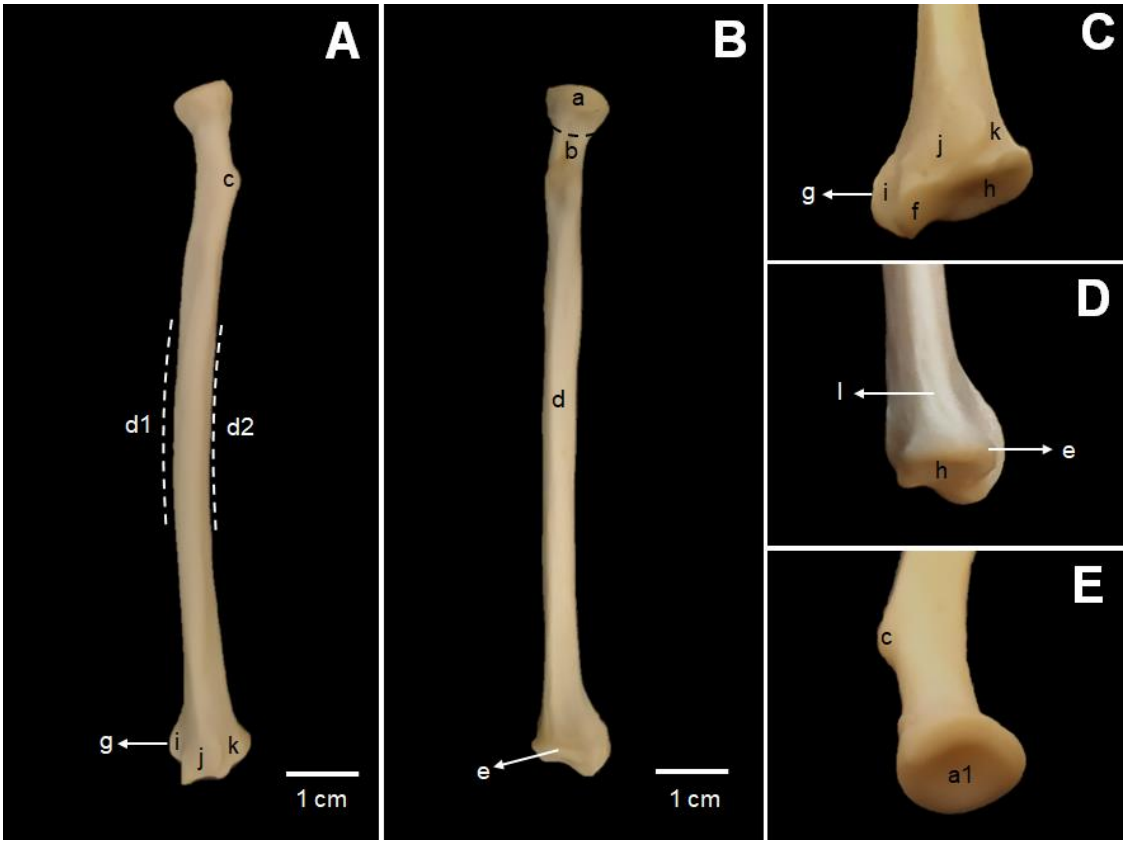

FIGURE 9 Left radius. Cranial view (A), Caudal view (B), Cranioventral view of the distal epiphysis (C), Lateral view of the distal epiphysis (D), View of the articular surface of the proximal epiphysis (E). a. Radial head (*Caput radii*); a1. Fovea of the radial head (*Fovea capitis radii*); b. Radial neck (*Collum radii*); c. Radial tuberosity (*Tuberositas radii*); d. Radial body (*Corpus radii*); d1. Medial margin (*Margo medialis*); d2. Lateral margin (*Margo lateralis*); e. Transverse ridge (*Crista transversa*); f. Carpal articular surface (*Facies articularis carpea*); g. Medial styloid process (of the radius) (*Processus styloideus medialis*); h. Ulnar notch (*Incisura ulnaris*); i. Sulcus for the tendon of the extensor carpi oblique muscle (*Sulcus musculi extensor carpi obliquus*); j. Sulcus for the tendon of the extensor carpi radialis muscle (*Sulcus musculi extensor carpi radialis*); k. Sulcus for the tendon of the common digital extender muscle (*Sulcus musculi extensor digitalis communis*); l. Sulcus for the tendon of the lateral digital extensor muscle (*Sulcus musculi extensor digitalis lateralis*).

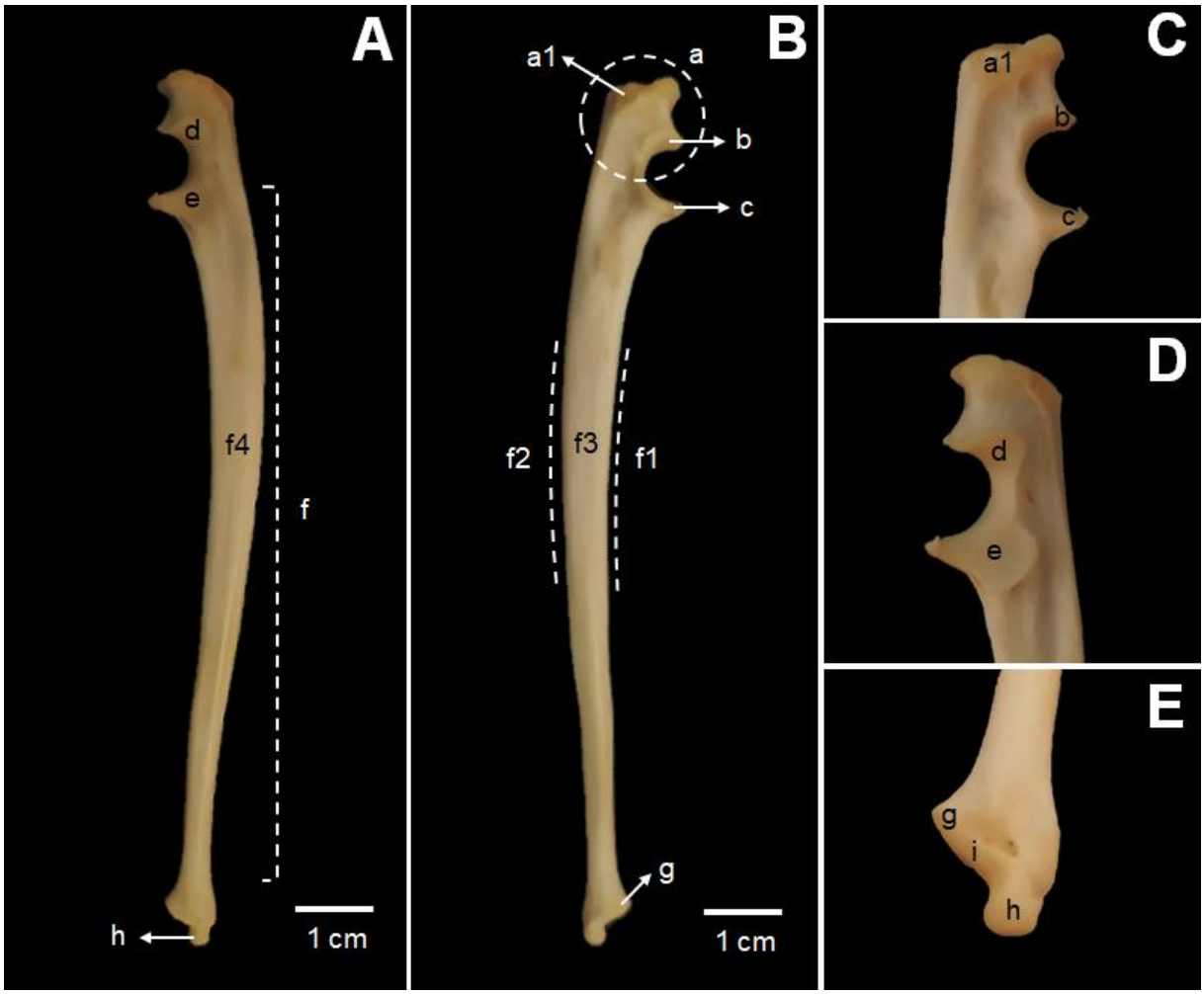

FIGURE 10 Left ulna. Lateral view (A), Medial view (B), Lateral view of the proximal epiphysis (C), Medial view of the proximal epiphysis (D), Lateral view of the distal epiphysis (E). a. Olecranon (*Olecranon*); a1. Olecranon tubercle (*Tuber olecrani*); b. Anconeus process (*Processus anconeus*); c. Coronoid process (*Processus coronoideus*); d. Trochlear notch (*Incisura trochlearis*); e. Radial notch (*Incisura radialis*); f. Body of the ulna (*Corpus ulnae*); f1. Cranial margin (*Margo cranialis*); f2. Caudal margin (*Margo caudalis*); f3. Medial face (*Facies medialis*); f4. Lateral face (*Facies lateralis*); g. Head of the ulna (*Caput ulnae*); h. Styloid process of the ulna (*Processus styloideus*); i. Carpal articular surface (*Facies articularis carpea*).

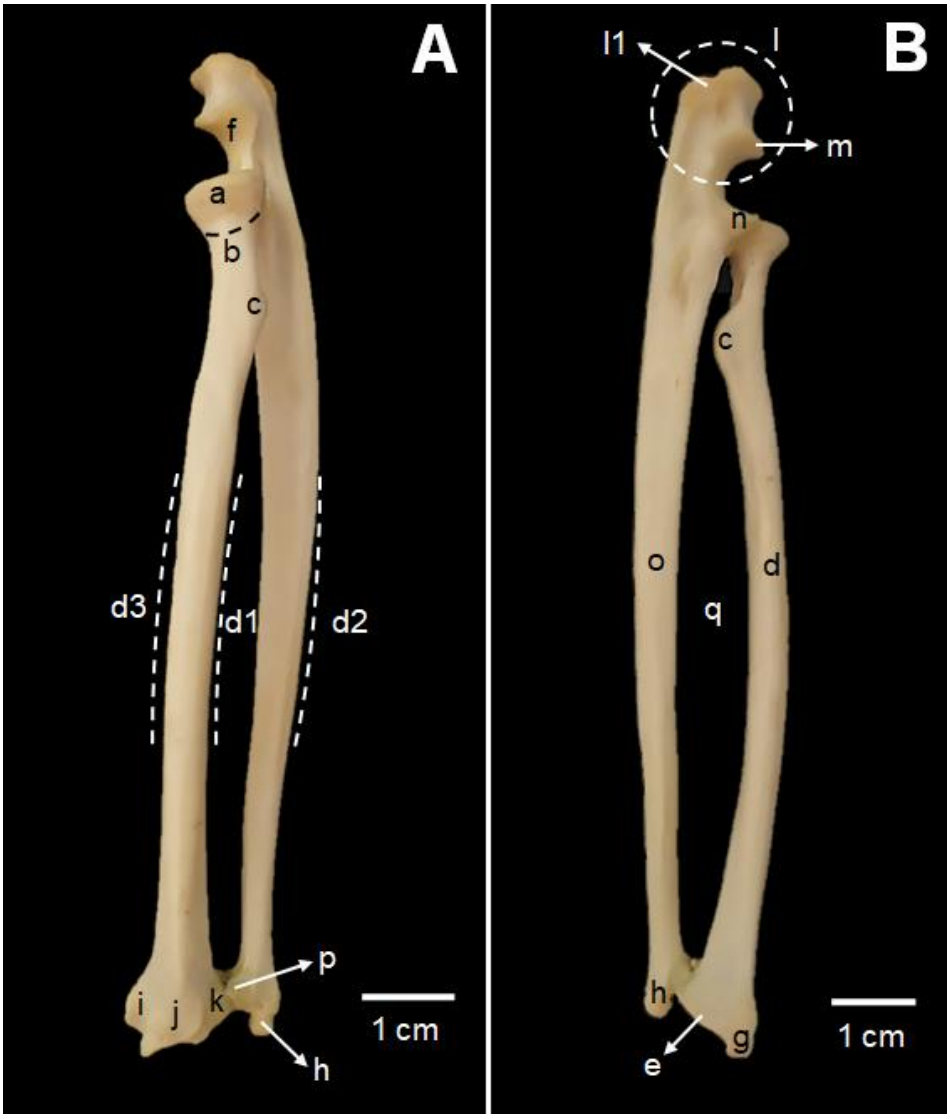

FIGURE 11 Radius and ulna, left antimere. Craniocaudal view (A), Caudal view (B). a. Radial head (*Caput radii*); b. Radial neck (*Collum radii*); c. Radial tuberosity (*Tuberositas radii*); d. Radial body (*Corpus radii*); d1. Interosseous margin (*Margo interosseus*); d2. Caudal margin (*Margo caudalis*); d3. Cranial margin (*Margo cranialis*); e. Transverse ridge (*Crista transversa*); f. Trochlear notch (*Incisura trochlearis*); g. Medial styloid process (of the radius) (*Processus styloideus medialis*); h. Lateral styloid process (of the ulna) (*Processus styloideus lateralis*); i. Sulcus for the tendon of the extensor carpi oblique muscle (*Sulcus musculi extensor carpi obliquus*); j. Sulcus for the tendon of the extensor carpi radialis muscle (*Sulcus musculi extensor carpi radialis*); k. Sulcus for the tendon of the common digital extensor muscle (*Sulcus musculi extensor digitalis communis*); l. Olecranon (*Olecranon*); l1. Olecranon tuber (*Tuber olecrani*); m. Anconeal process (*Processus anconeus*); n. Coronoid process (*Processus coronoideus*); o. Body of the ulna (*Corpus ulnae*); p. Head of the ulna (*Caput ulnae*); q. Antebrachial interosseous space (*Spatium interosseum antebrachii*).

In its proximal epiphysis, the humerus was better visualized in the ventrodorsal projection, in which few structures of the medial face were identified by the 3D reconstruction (Fig. 6A). The mediolateral radiograph of the humerus showed better visualization of structures (Fig. 12). The dorsoventral projection suffered overlapping of the clavicle and scapula in the

3D reconstruction and structures of the proximal epiphysis were not identified (Fig. 6B). Particularities such as the head, neck, lesser tubercle, and ridges of the greater and lesser tubercles could be seen (Figs. 6A and 12). In the distal epiphysis of the bone, the radiographic image also presented limitations regarding the number of structures observed, however, it was widely described through the 3D reconstruction. Only two structures could not be visualized by this method, the olecranon fossa and the trochlea, due to the image of the bone articulated with the ulna (Figs. 12 and 13).

All structures previously identified in the macroscopic study of the radius and ulna were well described in their epiphyses through 3D reconstruction. Only structures on the articular surface of the distal epiphysis of the radius, such as the ulnar notch and the carpal articular surface, could not be visualized (Figs. 13 and 17). Structures of the distal epiphysis of the radius and the proximal and distal epiphysis of the ulna were poorly identified through the radiographic image (Figs. 12 and 15).

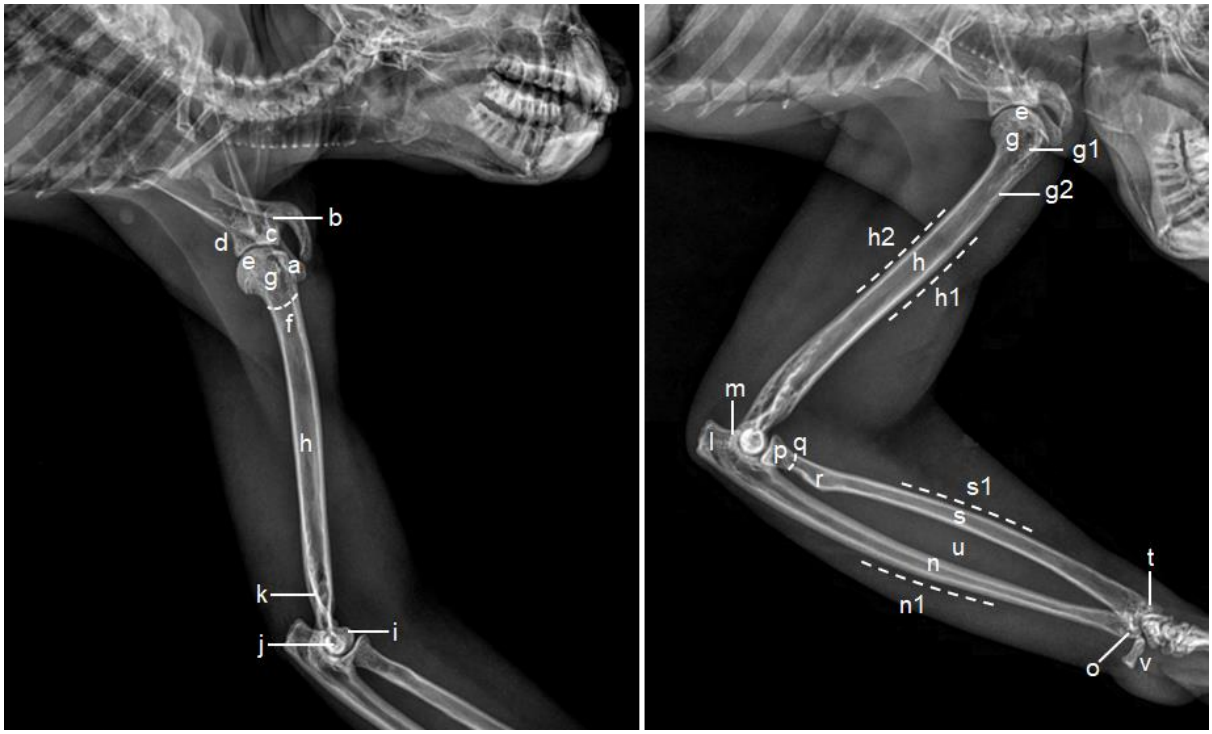

FIGURE 12 Radiographic image in mediolateral projection of the left antimere, highlighting the scapula, humerus, radius, ulna and carpus. a. Acromion; b. Coracoid process; c. Supraglenoid tubercle; d. Infraglenoid tubercle; e. Humeral head; f. Humeral neck; g. Lesser tubercle; g1. Lesser tubercle crest; g2. Greater tubercle crest; h. Humeral body; h1. Cranial surface of the humerus; h2. Caudal surface of the humerus; i. Capitulum of the humerus; j. Medial epicondyle; k. Medial supra-epicondylar crest; l. Olecranon/Olecranon tubercle; m. Anconeus process; n. Body of the ulna; n1. Caudal margin of the ulna; o. Lateral styloid process (of the ulna); p. Radial head; q. Radial collar; r. Radial tuberosity; s. Radial body; s1. Cranial margin of the radius; t. Medial styloid process (of the radius); u. Forearm interosseous space; v. Accessory carpal bone or pisiform bone.

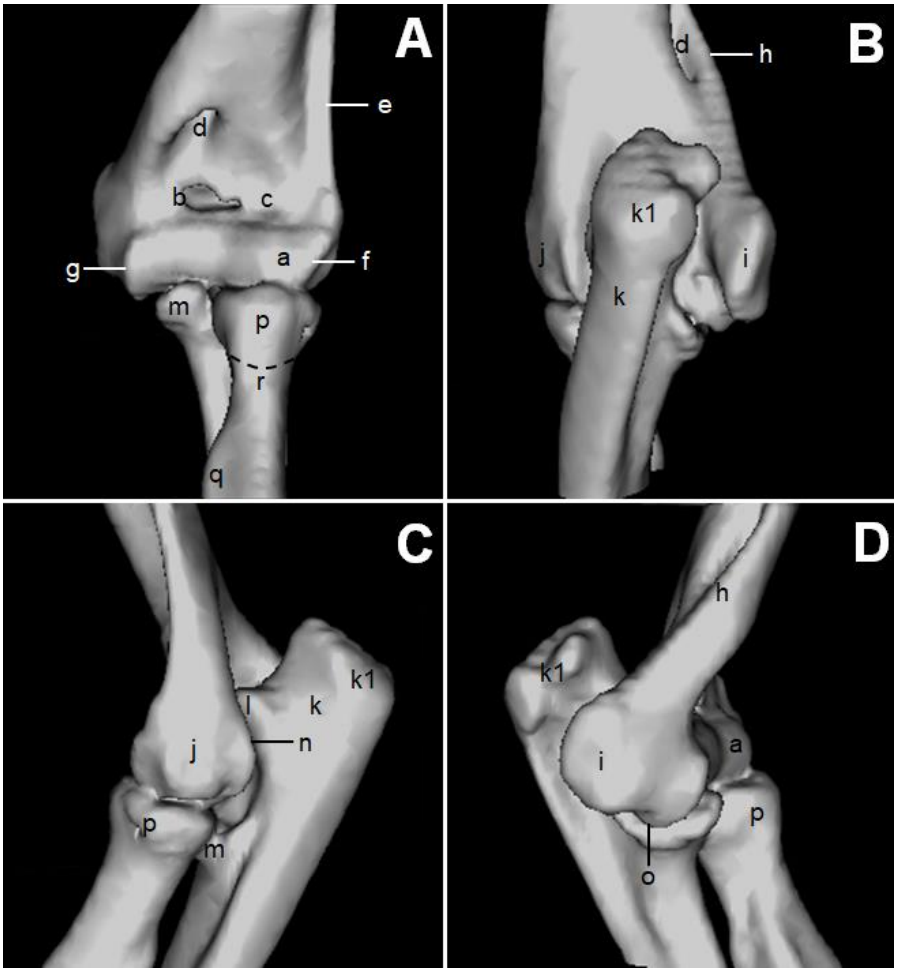

FIGURE 13 Image in 3D reconstruction of the cranial (A), caudal (B), lateral (C) and medial (D) face, of the distal epiphysis of the humerus and proximal epiphysis of the radius and ulna. a. Capitulum of the humerus; b. Coronoid fossa; c. Radial fossa; d. Entepicondylar foramen; e. Lateral supra-epicondylar crest; f. Lateral condyle; g. Medial condyle; h. Medial supra-epicondylar crest; i. Medial epicondyle; j. Lateral epicondyle; k. Olecranon; k1. Olecranon tubercle; l. Anconeus process; m. Coronoid process; n. Trochlear notch; o. Radial notch; p. Radial head; q. Radial tuberosity; r. Radial neck.

The carpus contains ten bones, four in the proximal (antebrachial) and four in the distal (metacarpal) rows, a central carpal bone inserted between both rows, between the radial carpal bone and the carpal bone II, and a sesamoid bone located in the abductor pollicis longus of the thumb (sesamoid bone of the abductor pollicis longus muscle). Ovoid sesamoid axial and abaxial bones articulate on the palmar surface at the distal trochlea of each of the five metacarpal bones. Comma-shaped sesamoid bones are found in the proximal interphalangeal joints of the last four digits and the distal interphalangeal joint of the thumb. The thumb has only two phalanges, while the other four digits contain three. Each finger has a distal phalanx covered by a keratin nail plate, rectangular and unsharpened. No sesamoid bones are present on the palmar surface of the distal interphalangeal joints of fingers II to V (Fig. 14).

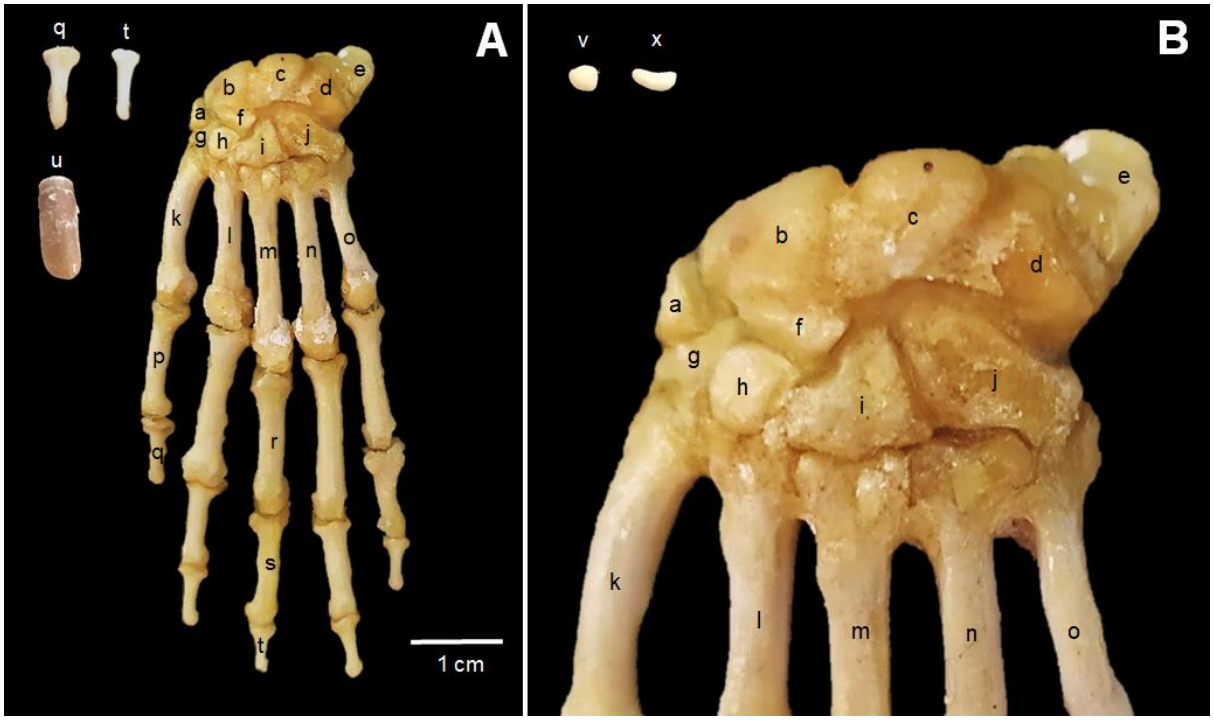

FIGURE 14 Carpal bones, metacarpal and phalanges, left antimere. Cranial view (A), Cranial view of the carpal and metacarpal bones (B). a. Sesamoid bone of the musculus abductor pollicis longus (*Os sesamoideum m. abductoris digiti primi (pollicis) longi*); b. Radial carpal bone (*Os carpi radiale* or *scaphoideum*); c. Intermediate carpal bone (*Os carpi intermedium* or os *lunatum*); d. Ulnar carpal bone (*Os carpi ulnare* or *os triquetrum*); e. Accessory carpal bone (*Os carpi accessorium* or *os pisiforme*); f. Central carpal bone (*Os carpi centrale*); g. Carpal bone I (*Os carpale primum* or *os trapezium*); h. Carpal bone II (*Os carpale secundum* or *os trapezoidum*); i. Carpal bone III (*Os carpale tertium* or *os capitatum*); j. Carpal bone IV (*Os carpale quartum* or *os hamatum*); k. Metacarpal bone I (*Os metacarpale primum*); l. Metacarpal bone II (*Os metacarpale secundum*); m. Metacarpal bone III (*Os metacarpale tertium*); n. Metacarpal bone IV (*Os metacarpale quartum*); o. Metacarpal bone V (*Os metacarpales quintum*); p. Proximal phalanx of the first digit (*Phalanx proximalis digiti primi*); q. Distal phalanx of the first digit (*Phalanx distalis digiti primi*); r. Proximal phalanx of the third digit (*Phalanx proximalis digiti tertii*); s. Middle phalanx of the third digit (*Phalanx media digiti tertii*); t. Distal phalanx of the third digit (*Phalanx distalis digiti tertii*); u. Unguicula (*Unguicula*); v. Proximal sesamoid or metacarpal bone (*Ossa sesamoidea proximalia*); x. Distal sesamoid or interphalangeal bone (*Os sesamoidum distale*).

All structures described in the macroscopic carpal and metacarpal images could be identified using both imaging methods (Figs. 15 and 17). In the radiographic image, it was possible to visualize the metacarpal and interphalangeal sesamoid bones, as well as the entire phalangeal region (Fig. 15). The 3D reconstruction image was limited to the carpal and carpo-metacarpal joint areas (Fig. 17). A radiographic examination of this region is an excellent method of identifying fractures. In three females studied, we have found fractures in the phalangeal region, which were clear in the radiographic image (Fig. 16).

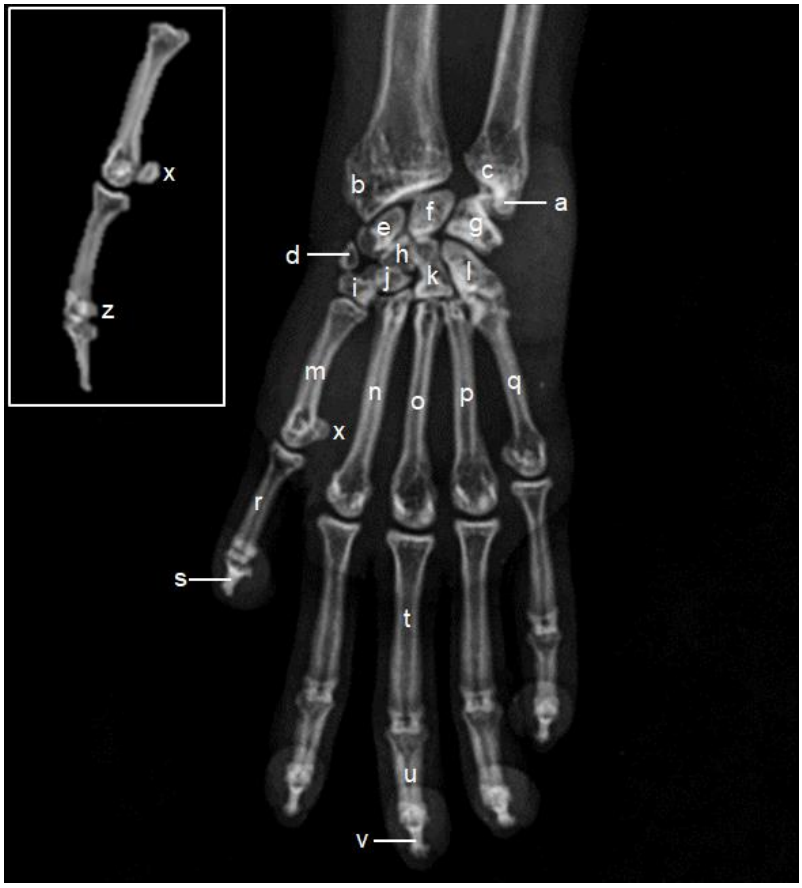

FIGURE 15 Radiographic image of the left antimere in dorsoventral projection of the radius and ulna and dorsopalmar projection of the carpus, metacarpal and phalanges. a. Lateral styloid process (of the ulna); b. Medial styloid process (of the radius); c. Head of the ulna; d. Sesamoid bone of the musculus abductor pollicis longus; e. Radial carpal bone or scaphoid bone; f. Intermediate carpal bone or lunatu bone; g. Ulnar carpal bone or triquetral bone; h. Central carpal bone; i. Carpal bone I or trapezius bone; j. Carpal bone II or trapezoid bone; k. Carpal bone III or capitate bone; l. Carpal bone IV or hamate bone; m. Metacarpal bone I; n. Metacarpal bone II; o. Metacarpal bone III; p. Metacarpal bone IV; q. Metacarpal bone V; r. Proximal phalanx of the first digit; s. Distal phalanx of the first digit; t. Proximal phalanx of the third digit; u. Middle phalanx of the third digit; v. Distal phalanx of the third digit; x. Proximal sesamoid or metacarpal bone; z. Distal sesamoid or interphalangeal bone.

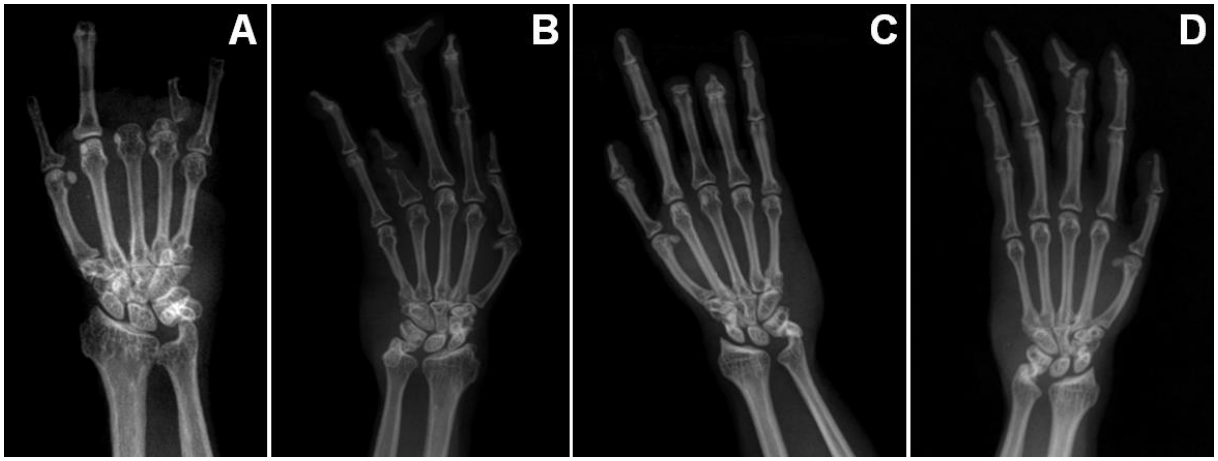

FIGURE 16 Fracture and bone loss in the phalangeal region, identified in the right antimere of F2 (A), left antimere of F3 (B), right antimere of F4 (C) and left antimere of F4 (D).

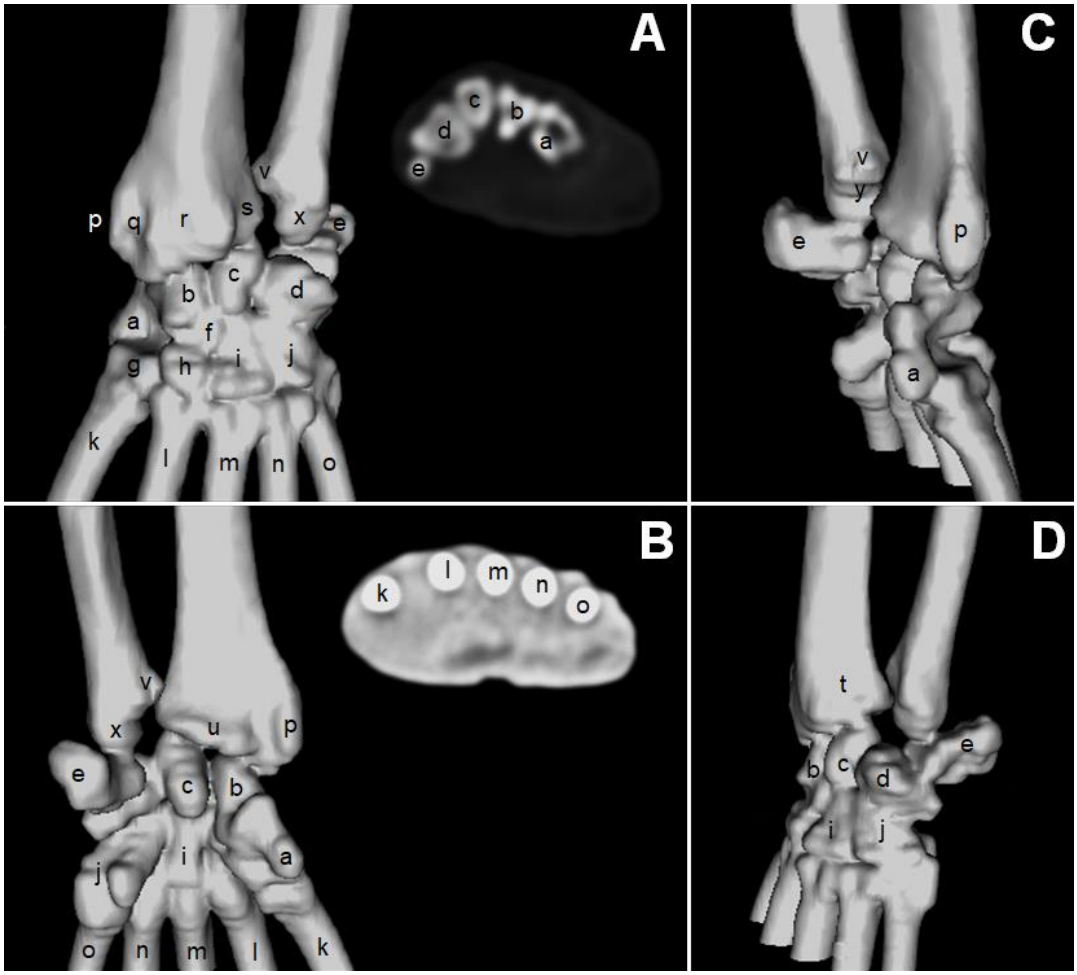

FIGURE 17 Image in 3D reconstruction of the cranial face and cross section at the level of the carpal region (A), caudal face and cross section at the level of the metacarpal region (B), medial face (C) and lateral face (D) of the distal epiphysis of the radius and ulna, and bones from carpus, metacarpus and phalanges. a. Sesamoid bone of the musculus abductor pollicis longus; b. Radial carpal bone or scaphoid bone; c. Intermediate carpal bone or lunatu bone; d. Ulnar carpal bone or triquetral bone; e. Accessory carpal bone; f. Central carpal bone; g. Carpal bone I or trapezius bone; h. Carpal bone II or trapezoid bone; i. Carpal bone III or capitate bone; j. Carpal bone IV or hamate bone; k. Metacarpal bone I; l. Metacarpal bone II; m. Metacarpal bone III; n. Metacarpal bone IV; o. Metacarpal bone V; p. Medial styloid process (of the radius); q. Sulcus for the tendon of the extensor carpi oblique muscle; r. Sulcus for the tendon of the radial carpal extensor muscle; s. Sulcus for the tendon of the common digital extender muscle; t. Sulcus for the tendon of the lateral digital extender muscle; u. Transverse crest; v. Head of the ulna; x. Styloid process of the ulna; y. Carpal articular surface.

4 DISCUSSION

The forelimb bones of *Sapajus libidinosus* showed, in general, an anatomical pattern that was more similar to that found in New World monkeys and man. Some features are common to Old World monkeys, such as aspects of the hand, and others, to Strepsirrhini primates, such as the presence of a sesamoid of the abductor longus pollicis muscle between the carpal bones, considered a primitive feature.

There was no statistical difference regarding the lengths of the bones of the forelimb between males and females, corroborating what is described in the literature. Kinzey (1997) reports an average of 1.5 to 4 kg for both males and females, while Silva et al. (2009) describe a more assertive mean of 3165.09 ± 404.94 g for males and 2046.82 ± 362.60 g for females. However, despite the discrepancy regarding body weight, body and head lengths are very similar between genders, with 465 mm for males and females (Kinzey, 1997), 340-440 mm also for males and females (Groves, 2001), and 377.95 ± 43.19 mm for males and 350.30 ± 35.19 mm for females (Silva et al., 2009).

In other primate species, such as *Callithrix jacchus*, females are reported to have superior bone size by about 10%, compared to males (Leutenegger & Larson, 1985). Despite the numerical superiority of bone length in females of *Sapajus libidinosus*, the data was not statistically significant. Additionally, this difference may have been observed due to the limited number of animals studied, besides different genetic backgrounds, health status, food, and environmental enrichment (Casteleyn et al., 2012). Another point to be analyzed is that, among the four males of the *Sapajus libidinosus* species, two juveniles were identified according to the dental parameters, basisphenoid and basioccipital synostosis, and because they had coronal and lambdoid sutures still open, and consequently the long bones were not yet fully developed, presenting lower measurements.

The scapula, throughout the Primates Order, has a well-developed spine, and a large acromion and coracoid process (Mivart, 1867). Structurally, the scapula of *Sapajus libidinosus* resembles that of *Callithrix jacchus* (Casteleyn et al., 2012), *Callimico goeldii* (Hill, 1959), *Alouatta seniculus* (Mesquita et al., 2019) and man (Sobotta, 2000), presenting, in the last two, a shorter dorsoventral length. Hill (1959) reports, in *Callimico goeldii*, a foramen in the ventral region of the supraspinatus fossa, which was not observed in this study nor described in any other study with primates.

The acromion, a well-developed structure identified in the *Sapajus libidinosus* in this study, is also observed in most arboreal primates, both New World and Old World ones, as well as in man (Senut et al., 2004). The same authors report that the characteristic of the elongated, triangular, and thickened acromion may be related to the degree of development of the deltoid muscle on the ventral surface and the trapezius muscle on the dorsal surface of the scapula.

The presence of a well-developed coracoid process is also portrayed in several primate species, from lemurs to Old World monkeys, including man (Senut et al., 2004). Martin & O'brien (1939) describe that the process is related to two important purposes: first, it is the main support by which the clavicle is attached to the scapula and, second, together with the acromion

and the coracoacromial ligament, it forms the arch above of the glenoid cavity. However, the authors report that its most important function appears to provide a strong fixation for the ligaments, connecting them to the clavicle and assisting in the abduction of the arm, since in almost all animals in which the clavicle has disappeared and the power to abduct the forelimb was lost, the coracoid process was also reduced to a small bulge hardly distinguishable from the rest of the bone.

Studies that portray the scapula of primates are more focused on the shape and position of the bone involved in the locomotor behavior of the species (Ashton et al., 1967; Chan, 2007; Oxnard, 1968). Chan (2007) reports that the scapular position affects shoulder mobility, which plays an important role in this type of behavior. These studies find a relationship between specific measurements, such as the angle between the glenoid cavity and the lateral edge of the scapula, in which the smaller angle determines species with greater brachiation behavior (Oxnard, 1968).

The 3D reconstruction image showed us that *in Sapajus libidinosus* the position of the scapula is quite dorsal, closer to the midsagittal axis, as in *Callithrix jacchus* (Casteleyn et al., 2012). Studies explain a relationship between scapular position and greater shoulder mobility, comparing primates and non-primate mammals, in which primates have greater mobility, and among arboreal and terrestrial primates, the former stand out (Jenkins Jr., 1974; Larson, 1974; Larson, 1993; Le Gros Clark, 1959; Rose, 1973). Chan (2007) reports that the scapula is significantly more dorsally oriented in New World arboreal quadrupedal monkeys when compared to terrestrial ones, and the same is true for Old World monkeys.

What is observed in humans is the opposite of what is being discussed, with the scapula situated much more dorsally than in other primates such as Lorinae, *Ateles* and *Alouatta* (Erikson, 1963; Cartmill & Milton, 1977; Cartmill, 1985; Gebo, 1996; Roberts & Davidson, 1975). However, Chan (2007) reports that the shorter scapular spine and longer clavicle contribute to this positioning in hominoids, and Jenkins Jr. et al. (1978) agree with the statement, reporting that the dorsal position of the scapula increases the distance between the acromion and the sternum, which must be compensated by a longer clavicle.

In the clinical-surgical aspect, scapular fractures are uncommon in humans, representing only 1% of all fractures, 3% of scapular girdle injuries and 5% of all shoulder fractures, being, of the total, 50% of the scapular body, 25% from the neck, 10% from the glenoid cavity and 14% from the acromion and coracoid processes. Goss (1995) associates this with the arrangement of the bone, protected by the rib cage and covered by a thick layer of soft tissues, in addition, its mobility allows considerable dissipation of traumatic forces. Despite the exposed

percentage, glenoid cavity fractures (Goss, 1992; Ideberg, 1984), scapular neck fractures (Goss, 1994; Miller & Ada, 1992) and displacement of the scapulohumeral joint (Ebraheim et al., 1988) are described in the literature. Goss (1995) reports that in case of a scapular fracture, radiographic projections are always requested, however, due to the complex bone anatomy of the area, computed tomography with reconstructions is often necessary to accurately detect and define the extent of the lesion, making clear the importance of knowledge of macroscopic structures and imaging methods for diagnosing scapular injuries.

The clavicle is intimately articulated with the scapular acromion. Despite its importance for forelimb movements, this is still a rarely studied bone of the shoulder and most studies come from observations of human anatomy (Longia et al., 1982; Olivier & Capliez, 1957; Ray, 1959; Schultz , 1937). However, 2D studies (Voisin, 2006) and 3D technology (Squyres & DeLeon, 2015) were used to analyze differences in the shape of clavicle curvatures in different locomotor groups of anthropoid primates, and a comparison of the studies shows that the image in 3D reconstruction brings anatomical details that are often not seen in the 2D image, which can be very valuable in terms of surgical planning, due to the visualization of all faces. Our study identified that the analysis of the clavicle bone piece proved to be more enlightening when compared to imaging methods, contributing to surgical planning.

The clavicle, structurally, presents a remarkable similarity to what is observed in men (Sobotta, 2000). Morphologically, it presents a lot of distinction among primate species. The sigmoid form observed in *Sapajus libidinosus* corroborates what was identified in *Callithrix jacchus* (Casteleyn et al., 2012), *Callimico goeldii* (Hill, 1959), *Pan* (Schultz, 1930) and man (Sobotta, 2000). However, the interpretation must go much further. According to Voisin (2006), curvatures in the cranial view have information about the parameters of elevation of the arm, while the dorsal view is focused on the position of the scapula related to the thorax.

The results of the study by Voisin (2006) report that, in the cranial view, *Gorila* and *Papio* presented pronounced external curvature and a slight, or even absent, internal curvature; *Hylobates* and *Ateles* are characterized by a pronounced inner and slightly pronounced outer curvature, contrary to the first group, and *Pan*, *Homo*, *Pongo*, *Procolobus* and *Colobus* showed the two curvatures equally pronounced, as did the animals in this study. This information led the authors to analyze that only a few primate species had a clavicle with marked internal curvature in cranial view and that all of them needed rapid and powerful elevation of the arm. Among these, only *Ateles* did not have a superficial pectoral insertion in the clavicle, but the deltoid, which takes the place and function of the pectoral in these animals. This superficial pectoral insertion, according to Stern et al. (1980), represents a unique feature among primates.

631 The action of this muscle is assisted by the pronounced internal curvature that acts as a "crank",
632 which helps the glenoid cavity of the scapula to rotate cranially, and the greater the curvature,
633 the more pronounced the cranking effect can be.
634 In the dorsal view, the *Sapajus libidinosus* in this study showed a clavicle with two
635 prominent curvatures, which most resembles those of great apes and spider monkeys, which
636 have clavicles with two curvatures, a ventral one, always more pronounced, and a dorsal one.
637 Baboons, *Colobus* and *Procolobus* monkeys have a ventral curvature and a dorsal curvature
638 that is slightly pronounced or absent; gibbons have only the dorsal curvature, and humans have
639 only the lower curvature, which is less pronounced than that found in apes. A clavicle with two
640 curvatures, as observed in the animals in this study, is associated with a dorsal scapula that is
641 high in relation to the thorax, a fact confirmed by the image in the 3D reconstruction (Voisin,
642 2006).
643 The sternoclavicular joint is supported by the costoclavicular ligament, found only in
644 monkeys and humans (Cave, 1961), and limits horizontal and vertical movement of the clavicle.
645 In this case, the elongation of the costoclavicular ligament increases the mobility and weakness
646 of the sternoclavicular joint, requiring greater muscle control, exercised by the subclavian
647 muscle. This condition of dorsal and high scapula, in relation to the thorax observed in *Sapajus*
648 *libidinosus*, great apes and spider monkeys, prevents stretching of the costoclavicular ligament,
649 making the scapula/clavicle complex relatively rigid, and preventing clavicle dislocation
650 because of suspension movements performed by brachiating and arboreal species, such the one
651 under study (Squyres & DeLeon, 2015). This interpretation is confirmed by electromyographic
652 studies in spider monkeys, which show that the subclavius is not activated when the animal
653 promotes brachiation movement (Konstant et al., 1982).
654 The humerus is articulated to the scapula. Structurally, the humerus of *Sapajus*
655 *libidinosus* presented a cranially arranged deltoid tuberosity, as a subtle projection derived from
656 the prolongation of the crest of the greater tubercle. This same observation was found in
657 *Callimico goeldii* (Hill, 1959), *Alouatta seniculus* (Mesquita et al., 2019), man (Sobotta, 2000),
658 *Saxonella crepaturae, Plesiadapis walbeckensis*, ancestral primates (Szalay & Dagosto, 1980)
659 and in *Callithrix jacchus* (Casteleyn et al., 2012), being more pronounced in the latter. Well-
660 developed supra-epicondylar ridges, increasing towards the epicondyles, described in *Sapajus*
661 *libidinosus*, have also been observed in *Callimico goeldii* (Hill, 1959), man (Sobotta, 2000) and
662 in *Callithrix jacchus* (Casteleyn et al., 2012); not being described in *Alouatta seniculus*
663 (Mesquita et al., 2019). The coronoid fossa was not observed in *Callimico goeldii* (Hill, 1959)
664 and *Alouatta seniculus* (Mesquita et al., 2019), but it was identified in man (Sobotta, 2000) and

the animals of this study. The radial nerve does not produce a spiral groove in *Callimico goeldii* (Hill, 1959), *Callithrix jacchus* (Casteleyn et al., 2012) and *Alouatta seniculus* (Mesquita et al., 2019). It was only seen in humans (Sobotta, 2000) and *Sapajus libidinosus*.

Despite the identification of a thin septum in the supratrochlear region, a supratrochlear foramen was not identified in any of the studied animals, corroborating studies with *Callimico goeldii* (Hill, 1959), *Alouatta seniculus* (Mesquita et al., 2019), *Callithrix jacchus* (Casteleyn et al., 2012) and humans (Sobotta, 2000). However, Benfer & Tappen (1968) conducted a study on the occurrence of humeral septal perforation in three Old World monkeys: *Cercocebus albigena*, *Cercopithecus aethiops* and *Cercopithecus ascanius*, concluding three possibilities, the first being that the angulation and robustness of the anconeal process are associated with the occurrence of septal perforation of the humerus, the second is that the relative protrusion of the anconeal process is associated with advancing age, in which younger individuals have a more protuberant process and a higher percentage of septal perforation than older ones, and the third point is the association of the shape of the anconeal process with the size of the humerus, in which the occurrence of perforation is less likely in individuals with larger and more robust humerus. Considering, in *Sapajus libidinosus*, the presence of a shorter anconeal process, a well-developed and robust humerus, and that the studied animals had an age range between juvenile/adult and elderly, the three possibilities discussed by Benfer & Tappen (1968) can be confirmed.

Another structure brings attention to the particularities of this bone, the entepicondylar foramen. This structure, observed in the humerus, is consistently present in most platyrrhines, but its absence is also common (Meldrum et al., 1990). According to Landry (1958), this foramen is traversed by the median nerve and usually also by the brachial artery and, although its presence or absence may vary even intraspecifically in some species, in most Anthropoidea the structure shows a more consistent pattern. Its presence or absence was used as a method of morphological identification in two phylogenetic studies of platyrrhine monkeys (Ford, 1986; Rosenberger & Coimbra-Filho, 1984) for diagnosing subfamilies that are included in other groups of mammals (Carleton, 1980), proving to be of great taxonomic significance, a fact that only a few primatologists have noticed (Hershkovitz, 1990).

In all *Sapajus libidinosus* in this study, a large and oblique entepicondylar foramen was identified crossing the medial supra-epicondylar crest. This structure was not identified in *Alouatta seniculus* (Mesquita et al., 2019), in a large part of the Callitrichidae family (Hill, 1959) and in man (Sobotta, 2000), however, it was observed in *Tarsius* (Hill, 1955), lemurs (Murie & Mivart, 1872) and *Callimico goeldii* (Hill, 1959). According to Garbino & Aquino

(2017), the absence of this foramen is probably due to the vertical positioning of the species, which presupposes intense abduction of the forelimbs. However, before highlighting any adaptationist investigation into the function of the entepicondylar foramen or any adaptive advantage over its disappearance, Gould & Lewontin (1979) emphasized that the presence of a certain structure does not always mean that there is a function allied to it.

Garbino & Aquino (2017; 2018) studied the entepicondylar foramen in a range of primate species and observed that the foramen is absent in Atelidae and most Callitrichinae, - except for some species such as *Callimico goeldii* -, possibly associated with brachiation and the considerable amount of time in the vertical grasping posture, respectively. In *Aotus* and *Callicebus*, some species presented it and others did not, which may be reflected in some adaptive value, and the foramen was present in Cebinae and Pitheciidae, probably due to the maintenance of the basal condition present in the Platyrrhini ancestors.

Regarding morphological aspects of the humerus, found in *Sapajus libidinosus,* it is very similar to that observed in humans (Sobotta, 2000) and *Alouatta seniculus* (Mesquita et al., 2019) in terms of robustness and bone development. Casteleyn et al. (2012) describe a thinner humerus in *Callithrix jacchus*. In this regard, Burr et al. (1989) report that the structural stiffness of the humerus is greater per unit of body weight in primates that spend more time in terrestrial environments than in those that are more restricted to climbing in arboreal environments. This may be one of the explanations for the morphology observed in the humerus of *Sapajus libidinosus* which, despite being classified as arboreal primates, many go to the ground in search of tools and for foraging (Falótico, 2011).

The radius and ulna are the representative bones of the forearm. Contrary to the findings in *Hapale* (Hill, 1959), the radius is not considerably more robust than the ulna, the main distinction between them, apart from their epiphyses, lies in the cylindrical shape of the diaphysis of the radius, in contrast to the laterally compressed character from the ulna. This same conformation observed in *Sapajus libidinosus* was also described in *Alouatta seniculus* (Mesquita et al., 2019) and *Callimico goeldii* (Hill, 1959).

The radius also structurally presents a long neck; considering the distance from the head to the radial tuberosity, as observed in *Callimico goeldii* (Hill, 1959), *Callithrix jacchus* (Casteleyn et al., 2012) and humans (Sobotta, 2000), being slightly smaller in *Alouatta seniculus* (Mesquita et al., 2019), and a pronounced radial tuberosity, corroborating the study on *Callithrix jacchus* (Casteleyn et al., 2012). In humans, a less developed tuberosity is observed (Sobotta, 2000), being even smaller in *Alouatta seniculus* (Mesquita et al., 2019). Considering that this structure is related to the insertion of the tendon of the biceps brachii

muscle (Storti et al., 2017), and due to its function of extending the shoulder joint and flexing the elbow joint, arboreal primates, which present great intensity of locomotion, end up needing further development of this muscle, and consequently the projection in which it is inserted (Rinker, 1954), explaining the more robust tuberosity in these animals.

The distal sulcus for insertion of the tendons of the extensor muscles were well delimited in this study, as well as in humans (Sobotta, 2000), but they were not described in *Alouatta seniculus* (Mesquita et al., 2019) and *Callithrix jacchus* (Casteleyn et al., 2012), perhaps because they present themselves more subtly. Ulna structures follow the pattern described in Callitrichideos (Casteleyn et al., 2012; Hill, 1959) and *Alouatta seniculus* (Mesquita et al., 2019).

The morphology of the radius and ulna does not differ much between primates. The slight curvature observed at the interosseous margin in *Sapajus libidinosus* is also seen in *Callithrix jacchus* (Casteleyn et al., 2012) and *Callimico goeldii* (Hill, 1959). In man, (Sobotta, 2000) and *Alouatta seniculus* (Mesquita et al., 2019), the radius and ulna are more rectilinear and, in the former, the distal epiphysis of the ulna does not articulate with the carpus (Sobotta, 2000), contrary to what was observed in platyrrhines (Casteleyn et al., 2012; Hill, 1959; Mesquita et al., 2019). The tomographic image performed on the *Sapajus libidinosus* of this study shows that the only joint contact between the ulna and the carpus occurs with the styloid process of the ulna and the accessory bone.

Godinot & Beard (1993) reported that the lack of ulno-carpal contact is one of the striking adaptations of the pulses of extant hominoids compared to that of most other Simiiformes, and that this lack of direct contact is a structural adaptation to allow a greater range of motion, being, *a priori*, considered an indication of increased capacity for ulnar deviation. Jouffroy & Medina (2002) tested this hypothesis through radiography, comparing the displacement of the carpal bones along the radioulnar deviation in eight genera with or without ulno-carpal contact, and concluded that the deviation is not directly correlated with its presence or absence, and that most ulnar deviations occur at the antebrachiocarpal joint in primates that do not have ulno-carpal contact, as is the case with hominoids, and at the middle carpal joint in primates whose ulna articulates with the ulnar carpal bone, which includes cercopithecines, platyrrhines and most strepsirrhines. On the other hand, in the animals of this study, and by evaluation of the 3D reconstruction, the ulnar contact occurs with the accessory carpal bone. Because of this, Yalden (1972) described that radiography and cineradiography are the most appropriate techniques to investigate carpal movements *in situ*, since the impediment of superimposing bone images can be eliminated using incidence angles.

Radiographic examination was also used to evaluate comminuted and diaphyseal fracture of the radius, associated with a transverse fracture of the ulna in a Mandrel (*Mandrillus sphinx*), which underwent a minimally invasive plate osteosynthesis. From the examination, the researchers were able to see that, in addition to the fracture, the animal presented moderate radiographic signs of osteoarthritis in the elbow (Tong & Guiot, 2013), highlighting the importance of performing complementary imaging tests in case of suspected fracture of the radius and ulna, for better clinical-surgical planning.

The primate hand is a well-studied structure among primatological researchers, in particular, the hand skeleton includes features thought to reflect foraging, locomotion, and posture, and presents a distinction between species. Overall, the primate hand skeleton, including lemurs, monkeys and humans, consists of more than 27 bones, consisting of eight carpals, five metacarpals and 14 phalanges, and in some primates, the central bone arranged between the proximal and distal row of the carpus is observed. The number of sesamoids varies among individuals, some have a distinctive thumb and exclusive characteristics of primates, such as their extension and opposable nature, and the distal phalanges are classified into tegulas (claws) and ungulas (nails), which vary along the order (Boyer et al., 2013; Papademetriou et al., 2005).

Most studies of primate hands use imaging methods such as radiography and 3D reconstruction through tomography, additionally highlighting the importance of macroscopic anatomical knowledge for correct bone identification (Boyer et al., 2013; Cartmill & Milton, 1977; Jouffroy et al., 1991; Le Minor, 1994; Lewis, 1985).

Sapajus libidinosus presented a hand with ten carpal bones, composed of two rows with four bones each; a central one, arranged between the radial or scaphoid carpal bone and a second carpal bone, or trapezoid and a sesamoid bone in a medial position. The central carpal bone is a remnant of the primitive autopodium, in which a central row of four bones is present (Hildebrand, 1995). The number and composition of carpal bones in *Sapajus libidinosus* contrasts with those of hominoids and a specimen of *Alouatta seniculus* (Mesquita et al., 2019), but show similarities with those of Old World monkeys (Swindler & Wood, 1973), *Callithrix jacchus* (Casteleyn et al., 2012), *Callimico goeldii* (Hill, 1959) and small domestic mammals, including laboratory animals (Barone, 1966; Bertolini & Leutert, 1978).

This same general structure is also observed in most primates, from fossils such as *Plesiadapis*, *Nannodectes*, *Notharctus*, *Smilodectes*, *Adapis*, *Proconsul*, *Mesopithecus*, *Proconsulidae* (Godinot & Beard, 1991; Harrison, 1987), to Lemuriformes (Godinot & Beard, 1991) and the Simiiformes (Hoffstetter, 1982), changing only in shape and anatomical

disposition. Godinot & Beard (1991) report that in *Homo*, pongidae and *Indri*, there was a fusion of this bone with the scaphoid during evolution. The central bone was also identified in *P. lowii*, *Cynocephalus volans*, *Tarsius pumilus*, *Mirza coquereli*, *Cebus* and *Tupaia glis*. The difference between the carpus of the first ones and that of the genus *Cebus* and *Tupaia glis*, as well as that of other more modern primates, is the presence of the extensive central-fourth carpal bone contact, which separates modern Strepsirrhini, *Ptilocercus* and *Papio cynocephalus* from Haplorrhini and Tupaiids (Beard & Godinot, 1988; Sargis, 2002; Stafford & Thorington, 1998). These alterations, according to Godinot & Beard (1991), may be related to prehensile and locomotor development, hand specializations of different primate groups.

Between the radial carpal bone, or scaphoid, and the first carpal bone, or trapezium, a small sesamoid bone, named the sesamoid of the muscle abductor pollicis longus, was observed. Le Minor (1994) investigated this bone in a series of 276 non-human primates representing 37 genera, in addition to humans, in a series of 300 radiographs, including *Galago*, *Lemur*, *Cebus*, *Macaca*, *Cercopithecus*, *Pongo pygmaeus* and *Homo*. According to the author, the presence of this ossicle in primates is a primitive characteristic and is present in all non-human primates and usually articulates with the scaphoid and trapezius, as identified in this study. The author also reports changes in the general pattern of mammals only in *Gorilla gorilla*, in which the sesamoid bone is observed in about half of the individuals, and in *Homo*, where this ossicle is normally absent.

The metacarpals are five in number and basically differ in size in primates. The first Euprimates had a short metacarpal and long phalanges. The first Simiiformes had longer metacarpals and acquired relatively shorter digits as a result of their emphasis on horizontal quadrupedalism, which the genus *Sapajus* falls into. Early Cercopithecines, as they further emphasized horizontal quadrupedalism or even semi-terrestriality, have relatively shorter digits and longer metacarpals, compared to Simiiformes (Godinot & Beard, 1991). Several authors explain this, exposing that primates with longer metacarpals are often associated with animals that habitually adopt digitigrade postures during terrestrial locomotion (Brown & Yalden, 1973; Coombs, 1978; Gregory, 1912; Hildebrand, 1985; Howell, 1944). ; Polly, 2007), conferring several biomechanical advantages over shorter metacarpals, considering that, in a digitigrade posture, longer metacarpals would increase the effective length of the forelimb, increasing the stride length and, therefore, generating lower locomotor costs associated with high-speed or long-distance travel (Patel, 2009).

The metacarpal I, associated with the thumb, is relatively shorter in non-human primates, as observed in studies in gibbons (Baker, 2011), *Callithrix jacchus* (Casteleyn et al.,

2012), *Callimico goeldii* (Hill, 1959) and *Alouatta seniculus* (Mesquita et al., 2019). It is so small in *Ateles* that they seem to have no thumbs (Baker, 2011). In the latter, length, reduction, or atrophy is associated with a delay in ossification and even chondrification (Jouffroy & Lessertisseur, 1977). The baboons - the most terrestrial of all catarrhine primates - are the ones with the thumb and proportion of fingers closest to humans (Schultz, 1930).

In addition to the variation in the length of the thumb bones, most primates have opposable thumbs. The opposition, according to Reghem et al. (2009), is the ability of the thumb to touch the other fingers of the same hand, especially the last digit, helping in activities such as grasping and swinging from trees. Gebo (2014) highlights that all Old-World monkeys, including humans, the New World ones, and some prosimians, have opposable thumbs, with few exceptions, such as *Tarsius*, marmosets, and spider monkeys. The same authors also report that animals that do not have opposable thumbs end up compensating in another way, such as the *Atelidae*, which use their tails as a tool for feeding and/or locomotion.

The arranged protuberances of the distal phalanges, tegulae (claws) and ungulae (nails), vary in the Order classification and are differentiated based on shape. Claws are laterally compressed and longitudinally curved, and have sharp, pointed distal ends, seen in tamarins and marmosets (Callitrichidae) and *Aye-aye* (Daubentonidae) (Boyer et al., 2013; Casteleyn et al., 2012; Hill, 2012; Hill, 1959), while nails are mostly flat, as in the animals in this study, *Alouatta seniculus* (Mesquita et al., 2019) and Old World monkeys (Andrade et al., 2002).

Among the animals analyzed in this study, three females presented hand fractures, all in the phalangeal region. In this regard, authors report that despite the attention to the construction and selection of more suitable housing for non-human primates in captivity (Martin et al., 2002; Nystrom et al., 2001; Tardif et al., 2013), fractures in the hands are commonly observed as a result of falling, jumping from excessive heights, attempts to remove a limb trapped in faulty cages, or even improper catching techniques (Pritzker & Kessler, 2012). Given this, females may be more affected by participating in the defense of the group and often get injured when trying to protect their babies from infanticidal males, cases that occur both in captivity and in the wild (Harris, 2002). Pig et al. (2016) reported a case of a female Siamang (*Hylobates syndactilus*), raised in captivity, which suffered a closed fracture of the proximal phalanx of the middle finger, resulting in finger deformity and functional disability of the hand, and radiography was used as a diagnostic method for correct surgical planning. However, knowledge of hand anatomy is important in clinical interventions.

5 CONCLUSION

By bringing detailed anatomical and image data on the forelimb of *Sapajus libidinosus* and considering the aforementioned studies, and many others conducted on primates, which are still so scarce in this species, we open the door to a range of experiments aimed at skeletal and clinical pathologies, surgery, surgical planning and paleontology, in addition to serving as a scientific collection for primatologists and contributing to the education in the science of laboratory animals. It was possible to verify the efficiency of the imaging methods, demonstrating that it is possible to identify bone structures with precision, mainly through 3D reconstruction, when compared to images of bone pieces. *Sapajus libidinosus* presented anatomical characteristics, structurally and morphologically, more similar to those of neotropical primates and man, being an excellent indicator of an experimental model for studies in these species. This material, with knowledge of macroscopic bone anatomy and through tomographic and radiological exams, generates a basis for research that may contribute to the refinement of research protocols and possibly also to the reduction of animals in experiments.

ACKNOWLEDGMENTS

The authors would like to thank CETAS/IBAMA-Natal, on behalf of the environmental analyst and Veterinary Doctor Tiago Saulo Freire Costa, for their help and agreement in the use of animals and the Coordination for the Improvement of Higher Education Personnel (CAPES), for the doctoral scholarship. They would also like to thank the staff of the Instituto de Radiologia de Natal (IRV), for all the support in performing the tomography and Rx exams, and the Potiguar University (UnP), for the partnership established and competence in performing the radiographic exams.

AUTHOR CONTRIBUTIONS

Ana Yasha F. de La Salles: conceptualization; data curation; formal analysis; investigation; methodology; project administration; resources; software; supervision; validation; visualization; writing the original draft; writing-reviewing and editing. **Jéssica K. de Andrade:** conceptualization; formal analysis; investigation; resources; visualization. **Joyce G. de Souza:** conceptualization; formal analysis; investigation; resources; visualization. **Kelvis de B. Freitas:** conceptualization; formal analysis; investigation; visualization. **Artur da N. Carreiro:** conceptualization; formal analysis; investigation; visualization. **Edson Vinícius L. Veloso:** conceptualization; formal analysis; investigation; visualization. **Ediane F. Rocha:**

conceptualization; formal analysis; investigation; visualization. **Marcius Alessandro P. Klem:** conceptualization; data curation; formal analysis; methodology; resources; software; supervision; visualization. **Felipe V. Câmara:** conceptualization; formal analysis; investigation; visualization. **Danilo José A. de Menezes:** conceptualization; data curation; formal analysis; investigation; methodology; project administration; resources; software; supervision; validation; visualization; writing-reviewing and editing.

REFERENCES

Andrade A, Pinto SC, Oliveira RS. 2002. Animais de laboratório: Criação e experimentação [online]. Rio de Janeiro: Editora Fiocruz.

Armbrust LJ. 2010. Imagens digitais e captura digital de imagens radiográficas. In: Thrall DE, editor. *Diagnóstico de radiologia veterinária*. Rio de Janeiro: Elsevier. p 22-37.

Ashton EH, Oxnard C, Spence TF. 1967. Scapular shape and primate classification. *Proceedings of the Zoological Society of London* 145: 125–142.

Baker, SN. 2011. The primate reticulospinal tract, hand function and functional recovery. *Journal of Physiology* 589: 5603–612.

Barone R. 1966. Anatomie comparée des mammiféres domestiques, tome troisième: Ostéologie. Paris: Editions Vigot.

Beard KC, Godinot M. 1988. Carpal anatomy of *Smilodectes gracilis* (Adapiformes, Notharetinae) and its significance for lemuriform phylogeny. *Journal of Human Evolution* 17: 71-92.

Benfer RA, Tappen NC. 1968. The occurrence of the septal perforation of the humerus in three non-human primate species. *American Journal of Physical Anthropology* 29: 19-28.

Bertolini R, Leutert G. 1978. Atlas der anatomie des menschen, band 1: Arm und bein. Berlin: Springer-Verlag.

Bicca-Marques JC, Silva VM, Gomes DF. 2006. Ordem Primates. In: Reis NR, Peracchi AL, Pedro WA, Lima IP, editores. *Mamíferos do Brasil*. Londrina: UEL. p 101-148.

Bortolini Z. 2013. Ressonância magnética na avaliação das estruturas encefálicas do *Alouatta fusca* (Bubio-ruivo – Geoffroy Saint-Hilaire, 1812). Tese de doutorado. Universidade Estadual Paulista, Faculdade de Medicina Veterinária e Zootecnia, Botucatu, Brasil.

Bortolini Z, Matayoshi PM, Santos RV, Doiche DP, Machado VMV, Teiceira CR., Vulcano LC. 2013. Casuística dos exames de diagnóstico por imagem na medicina de animais selvagens - 2009 a 2010. *Arquivo Brasileiro de Medicina Veterinária e Zootecnia* 65: 1247-1252.

Boyer DM, Yapuncich GS, Chester SGB, Bloch JI, Godinot M. 2013. Hands of early primates. *American Journal of Physical Anthropology* 57: 33-78.

Brown JC, Yalden DW. 1973. The description of mammals – 2: limbs and locomotion of terrestrial mammals. *Mammal Review* 3: 107–134.

Burr DB, Ruff CB, Johnson C. 1989. Structural adaptations of the femur and humerus to arboreal and terrestrial environments in three species of macaque. *American Journal of Physical Anthropology* 79: 357-367.

Carleton MD. 1980. Phylogenetic relationships in Neotomine-*Peromyscine* rodents (Muroidea) and a reappraisal of the dichotomy within New World Cricetinae. *Miscellaneous Publications, Museum of Zoology, University of Michigan* 157: 1–146.

Cartmill M, Milton K. 1977. The lorisiform wrist joint and the evolution of "brachiating" adaptations in the Hominoidea. *American Journal of Physical Anthropology* 47: 249-272.

Cartmill M. 1985. Climbing. In: Hildebrand M, Bramble DM, Liem KF, Wake DB, editores. *Functional Vertebrate Morphology*. Cambridge: The Belknap Press of Harvard University Press. p 73–88.

Casteleyn C, Bakker J, Breugelmans S, Kondova L, Saunders J, Langermans JAM, Cornillie P, Van den Broeck W, Van Loo D, Van Hoorebeke L, Bosseler L, Chiers K, Decostere A. 2012.

968 Anatomical description and morphometry of the skeleton of the common marmoset (*Callithrix*
969 *jacchus*) *Laboratory Animals* 46: 152-63.
970
971 Cave AJE. 1961. Nature and morphology of the costoclavicular ligament. *Journal of Anatomy*
972 95:170–179.
973
974 Chan LK. 2007. Scapular Position in Primates. *Folia Primatologica* 78: 19–35.
975
976 Coombs WP. 1978. Theoretical aspects of cursorial adaptations in dinosaurs. *The Quarterly*
977 *Review of Biology* 53: 393–418.
978
979 Dangelo JG, Fattini CA. 2011. Anatomia humana e sistema segmentar. São Paulo: Atheneu.
980
981 Ebraheim NA, An HS, Jackson WT, Pearlstein SR, Burgess A, Tscherne H, Hass N, Kellam J,
982 Wipperman BU. 1988. Scapulothoracic dissociation. *The Journal of Bone and Joint Surgery*
983 70: 428-432.
984
985 Erikson GE. 1963. Brachiation in New World monkeys and in anthropoid apes. *Symposia of*
986 *the Zoological Society of London* 10: 135–164.
987
988 Falótico T. 2011. Uso de ferramentas por macacos-prego (*Sapajus libidinosus*) do Parque
989 Nacional Serra da Capivara - PI. Tese de Doutorado. Programa de Pós-Graduação em
990 Psicologia, Instituto de Psicologia da Universidade de São Paulo, São Paulo, Brasil.
991
992 Federative International Programme on Anatomical Terminologies, Verlag GT. 1998.
993 Terminologia Anatomica: International anatomical terminology. New York: Stuttgart.
994
995 Ford SM. 1986. Systematics of the New World Monkeys. In: Swindler DR, Erwin J, editors.
996 *Comparative Primate Biology, Volume 1: Systematics, Evolution and Anatomy*. New York:
997 Alan R. Liss, Inc. p 73-135.
998
999 Garbino GST, Aquino CC. 2017. The entepicondylar foramen of the humerus in Platyrrhini. In:
1000 Silva VL, Ferreira RG, Oliveira MAB, editores. *A primatologia no Brasil, volume 14, Anais do*
1001 *Congresso Brasileiro de Primatologia*. Recife: Editora UFPE.

1002 Garbino GST, Aquino CC. 2018. Evolutionary significance of the entepicondylar foramen of
1003 the humerus in New World Monkeys (Platyrrhini). *Journal of Mammalian Evolution* 25: 141–
1004 151.
1005
1006 Gebo DL. 1996. Climbing, brachiation, and terrestrial quadrupedalism: historical precursors of
1007 hominid bipedalism. *American Journal of Physical Anthropology* 101: 55–92.
1008
1009 Gebo, DL. 2014. Primate Comparative Anatomy. Baltimore: Johns Hopkins University Press.
1010
1011 Godinot M, Beard KC. 1991. Fossil primate hands: A review and an evolutionary inquiry
1012 emphasizing early forms. *Human Evolution* 6: 307–354.
1013
1014 Godinot M, Beard KC. 1993. A survey of fossil primate hands. In: Preuschoft H, Chivers DJ,
1015 editores. *Hands of Primates*. Wien: Springer. p 335-378.
1016
1017 Goss TP. 1992. Fractures of the glenoid cavity. *The Journal of Bone and Joint Surgery* 74: 299-
1018 305.
1019
1020 Goss TP. 1994. Fractures of the glenoid neck. *Journal of Shoulder and Elbow Surgery* 3: 42-
1021 52.
1022
1023 Goss TP. 1995. Scapular fractures and dislocations: Diagnosis and treatment. *Journal of the*
1024 *American Academy of Orthopaedic Surgeons* 3: 22-33.
1025
1026 Gould SJ, Lewontin RC. 1979. The spandrels of San Marco and the Panglossian paradigm: a
1027 critique of the adaptationist programme. *Proceedings of the Royal Society B: Biological*
1028 *Sciences* 205: 581–598.
1029
1030 Gregory WK. 1912. Notes on the principles of quadrupedal locomotion and on the mechanics
1031 of the limbs in hoofed animals. *Annals of the New York Academy of Sciences* 22: 267–294.
1032
1033 Gros-Louis J, Perry S, Manson JH. 2003. Violent coalitionary attacks and intraspecific killing
1034 in wild white-faced capuchin monkeys (*Cebus capucinus*). *Primates* 44: 341–346.

Groves CP. 2001. Primate taxonomy. Washington: Smithsonian Institution Press.

Harris TR. 2002. Infanticide and subsequent mating behavior in a black and white colobus monkey group. AAPA poster and presentation schedule. *American Journal of Physical Anthropology* 117: 17-67.

Harrison T. 1987. The phylogenetic relationships of the early catarrhine primates: A review of the current evidence. *Journal of Human Evolution* 16: 41-80.

Hershkovitz P. 1990. Titis, New World monkeys of the genus *Callicebus* (Cebidae, Platyrrhini): A Preliminary Taxonomic Review. *Fieldiana Zoology* 55: 1-109.

Hildebrand M. 1985. Walking and running. In: Hildebrand M, Bramble DM, Liem KF, Wake DB, editores. *Functional vertebrate morphology*. Cambridge: Belknap Press. p 38–57.

Hildebrand M. 1995. Analysis of vertebrate structure. New York: John Wiley & Sons Inc.

Hill WCO. 1955. Primates II, Haplorhini: Tarsioidea. Edinburgh: Edinburgh University Press

Hill WCO. 1959. The anatomy of *Callimico goeldii* (Thomas): A primitive american primate. *Transactions of the American Philosophical Society, New Series* 49: 1-116.

Hoffstetter R. 1982. Les Primates Simiiformes (= Anthropoidea) (Compréhension, phylogénie, histoire biogéographique). *Annales de Paléontologie* 68: 241–290.

Howell AB. 1944. Speed in Animals. New York: Hafner Publishing Company.

Ideberg R. 1984. Fractures of the scapula involving the glenoid fossa. In: Bateman JE, Welsh RP, editores. *Surgery of the Shoulder*. Philadelphia: BC Decker. p 63-66.

International Committee on Veterinary Gross Anatomical Nomenclature. 2017. Nomina Anatomica Veterinária. 6 ed. Hanover, Ghent, Columbia, MO, Rio de Janeiro: Editorial Committee.

1068 Jenkins Jr. FA. 1974. Tree shrew locomotion and the origins of primate arborealism. In: Jenkins
1069 Jr. FA, editor. *Primate Locomotion*. New York: Academic Press. p 85–115.
1070
1071 Jenkins Jr. FA, Dombrowski PJ, Gordon EP. 1978. Analysis of the shoulder in brachiating
1072 spider monkeys. *American Journal of Physical Anthropology* 48: 65–76.
1073
1074 Johnson-Delaney CA. 1994. Primates. Veterinary clinics: Small animal practice 24: 121-152.
1075
1076 Jouffroy FK, Godinot M, NakanoY. 1991. Biometrical characteristics of primate hands. Journal
1077 of Human Evolution 6: 269-306.
1078
1079 Jouffroy FK, Lessertisseur J. 1977. Processus de réduction des doigts (main et pied) chez les
1080 primates. In: Raynaud A, editor. *Mécanismes de la Rudimentation des Organes chez les*
1081 *Embryons de Vértebrés*. Paris: Editions du CNRS. p 381-392.
1082
1083 Jouffroy FK, Medina MF. 2002. Radio-ulnar deviation of the primate carpus: an X-ray study.
1084 *Zeitschrift für Morphologie und Anthropologie* 83: 275-89.
1085
1086 Kinzey WG. 1997. *Cebu*s. In: Kinzey WG, editor. *New World Primates: Ecology, Evolution,*
1087 *and Behavior*. New York: Aldine de Gruyter. p 248-257.
1088
1089 Konstant W, Stern JT, Fleagle JG, Jungers WL. 1982. Function of the subclavius muscle in a
1090 nonhuman primate, the Spider monkey (*Ateles*). Folia Primatologica 38: 170–182.
1091
1092 Krautwald-Junghanns ME, Zebisch K, Enders F, Pees M, Willuhn J. 2001. Diagnoses of liver
1093 disease in birds by radiography and ultrasonography: under special consideration of ultrasound-
1094 guided liver biopsies. *Seminars in Avian and Exotic Pet Medicine* 10: 153-161.
1095
1096 La Salles AYF, Cordeiro JF, Santos JRS, Carreiro AN, Medeiros GX, Menezes DJA. 2017.
1097 Anatomical description of the main vessels for venipuncture in the black-striped capuchin
1098 monkey (*Sapajus libidinosus*, Silva Junior, 2002). *Journal of Medical Primatology* 46: 320-
1099 326.

La Salles AYF, Andrade JK, Lemos KKA, Carreiro AN, Souza JG, Costa TSF, Reinaldo MPOS, Souza AP, Menezes DJA. 2019. Electrocardiographic parameters of *Sapajus libidinosus* (SPIX, 1823) after chemical immobilization with tiletamine-zolazepam. *Journal of Medical Primatology* 48: 154-160.

La Salles AYF, Andrade JK, Cordeiro JF, Carreiro AN, Falcão BMR, Freitas KB, Menezes DJA. 2021. Assessment of the technique of the anesthetic block of the Brachial Plexus by Supraclavicular approach in *Sapajus libidinosus* (SPIX, 1823). *Journal of Medical Primatology* 50: 29-35.

Ladeira LMCEB, Höfling E. 2007. Osteologia craniana de Bucconidae. *Boletim do Museu Paraense Emílio Goeldi Ciências Naturais* 2: 117-153.

Landry SO. 1958. The Function of the entepicondylar foramen in mammals. *American Midland Naturalist* 60: 100-112.

Larson SG. 1993. Functional morphology of the shoulder in primates. In: Gebo DL, editor. *Postcranial Adaptation in Nonhuman Primates*. De Kalb: Northern Illinois University Press. p 45–69.

Le Gros Clark WE. 1959. The antecedents of man. Edinburgh: Edinburgh University Press.

Le Minor JM. 1994. The sesamoid bone of musculus abductor pollicis longus (os radiale externum or prepollex) in primates. *Acta anatomica* 150: 227-231.

Leutenegger W, Larson S. 1985. Sexual dimorphism in the postcranial skeleton of New World primates. *International Journal of Primatology* 44: 82–95.

Lewis OJ. 1985. Derived morphology of the wrist articulations and theories of hominoid evolution. Part I. The lorisine joints. *Journal of Anatomy* 140: 447-460.

Longia GS, Agarwal AK, Thomas RJ, Jain PN, Saxena SK. 1982. Metrical study of rhomboid fossa of clavicle. Anthropologischer Anzeiger 40: 111–115.

Martin CP, O'Brien HD. 1939. The coracoid process in the primates. Journal of Anatomy 73: 630–642.

Martin DP, Gilberto T, Burns C, Pautler HC. 2002. Nonhuman primate cage modifications for environmental enrichment. *Contemporary Topics in Laboratory Animal Science* 41: 47–49.

Martins AB, Fialho MS, Jerusalinsky L, Valença-Montenegro MM, Bezerra BM, Laroque PO, Melo FR, Lynch Alfaro, JW. 2021. *Sapajus libidinosus* (amended version of 2019 assessment). *The IUCN Red List of Threatened Species*. 10.2305/IUCN.UK.2021-1.RLTS.T136346A192593226.en.

Meldrum DJ, Fleagle JG, Kay RF. 1990. Partial humeri of two Miocene Colombian primates. *American journal of physical anthropology* 81: 413-422.

Mesquita VA, Souza ANA, Sousa EL, Pinheiro GG, Silva WA, Marques DA. 2019. Atlas simplificado de osteologia de *Alouatta seniculus*. Manaus: Instituto Federal de Educação, Ciência e Tecnologia do Amazonas.

Miller ME, Ada JR. 1992. Fractures of the scapula, clavicle, and glenoid. In: Rowner BD, Jupiter JB, Levine AM, editores. *Skeletal Trauma: fractures, dislocations, ligamentous injuries.* Philadelphia: WB Saunders. p 1291-1310.

Mivart G. 1867. XIII. On the Appendicular Skeleton of the Primates. *Philosophical transactions of the roya society of London* 157: 299-429.

Murie J, Mivart G. 1872. On the anatomy of the Lemuroidea. *Transactions of the Zoological Society of London* 7: 1-113.

Nyström P, Schapiro SJ, Hau J. 2001. Accumulated means analysis: a novel method to determine reliability of behavioral studies using continuous focal sampling. *In Vivo* 15: 29–34.

Olivier G, Capliez S. 1957. Anthropologie de la clavicule. *Bull Me´m Soc Anthrop* 10: 225–261.

1166 Oxnard CE. 1968. A note on the fragmentary sterkfontein scapula. *American Journal of*
1167 *Physical Anthropology* 28: 213-217.
1168
1169 Papademetriou E, Ching-Fan S, George FM. 2005. A meta-analysis of primate hand
1170 preferences, particularly for reaching. *Journal of Comparative Psychology* 119: 33–48.
1171
1172 Patel BA. 2009. Not so fast! – Speed effects on forelimb kinematics in cercopithecine monkeys
1173 and implications for digitigrade postures in primates. *American Journal of Physical*
1174 *Anthropology* 140: 92–112.
1175
1176 Piga S, Negro F, Meda S, Bertuglia A. 2016. A simple technique to repair a hand fracture in a
1177 captive Siamang. *Journal of Medical Primatology* 45: 324-326.
1178
1179 Polly PD. 2007. Limbs in mammalian evolution. In: Hall BK, editor. Fins into Limbs:
1180 Evolution, Development, and Transformation. Chicago: University of Chicago Press. p 245–
1181 268.
1182
1183 Pritzker KPH, Kessler MJ. 2012. Arthritis, muscle, adipose tissue and bone diseases. In: Abee
1184 CR, Mansfield K, Tardif S, Morris T, editores. Nonhuman Primates in Biomedical Research,
1185 volume 2: Diseases. San Diego: Elsevier-Academic Press. p 629–697.
1186
1187 Rangel CH, Adler JGV, Heliodor GC, Santos Jr. A, Verona CE. 2013. Relato de caso de morte
1188 por agressão entre macacos-prego *Sapajus nigritus* (Primates: Cebidae) no Jardim Botânico do
1189 Rio de Janeiro. *Neotropical Primates* 20: 48-52.
1190
1191 Ray LJ. 1959. Metrical and non-metrical features of the clavicle of the Australian aboriginal.
1192 *American Journal of Physical Anthropology* 17: 217–226.
1193
1194 Reghem E, Pouydebat E, Bels V, Gorce P. 2009. Function and strategies of a primate hand
1195 (*Microcebus murinus*) in climbing: evolutionary implications. *Comparative Biochemistry and*
1196 *Physiology Part A: Molecular & Integrative Physiology* 153: 114-133.

1197 Rinker GC. 1954. The comparative myology of the mammalian genera Sigmodon, Oryzomys,
1198 Neotoma, and Peromyscus (Cricetinae), with remarks on intergeneric relationships.
1199 *Miscellaneous Publications, Museum of Zoology, University of Michigan Press* 83:1-24.
1200
1201 Roberts D, Davidson I. 1975. The lemur scapula. In: Tattersall I, Sussman RW, editores. *Lemur*
1202 *Biology*. New York: Plenum Press.
1203
1204 Rose MD. 1973. Quadrupedalism in primates. *Primates* 14: 337–358.
1205
1206 Rosenberger AL, Coimbra-Filho AF. 1984. Morphology, taxonomic status and affinities of the
1207 lion tamarins, *Leontopithecus* (Callitrichinae, Cebidae). *Folia Primatologica* 42: 149-179.
1208
1209 Sargis EJ. 2002. Functional morphology of the forelimb of tupaiids (Mammalia, Scandentia)
1210 and its phylogenetic implications. *Journal of Morphology* 253: 10–42.
1211
1212 Schultz AH. 1930. The skeleton of the trunk and limbs of higher primates. *Human Biology* 2:
1213 303-438.
1214
1215 Schultz AH. 1937. Proportion, variability and asymmetries of the long bones of the limbs and
1216 the clavicles in man and apes. *Human Biology* 9: 281–328.
1217
1218 Senut B, Nakatsukasa M, Kunimatsu Y, Nakano Y, Takano T, Tsujikawa H, Shimizu D,
1219 Kagaya M, Ishida H. 2004. Preliminary analysis of *Nacholapithecus* scapula and clavicle from
1220 Nachola, Kenya. *Primates* 45: 97–104.
1221
1222 Silva TCF, Valença-Montenegro MM, Lucas JLB, Wagner PGC, Ferreira JG, Ferreira DRA,
1223 Jerusalinsky L, Martins AB, Senna MB, Laroque PO. 2009. Morfometria de *Cebus libidinosus*
1224 SPIX, 1823 (Primates, Cebidae). In: XIII Congresso Brasileiro de Primatologia. Livro de
1225 Resumos do XIII Congresso Brasileiro de Primatologia.
1226
1227 Sobotta J. 2000. Atlas de Anatomia Humana. Rio de Janeiro: Guanabara Koogan.

1228 Squyres N, DeLeon VB. 2015. Clavicular curvature and locomotion in anthropoid primates: a
1229 3D geometric morphometric analysis. *American Journal of Physical Anthropology* 158: 257–
1230 268.
1231
1232 Stafford BJ, Thorington RWJ. 1998. Carpal development and morphology in archontan
1233 mammals. *Journal of Morphology* 235: 135–155.
1234
1235 Stern JT, Wells JP, Jungers WL, Vangor AK, Fleagle JG. 1980. An electromyographic study
1236 of the pectoralis major in Atelines and Hylobates with special references to the evolution of a
1237 pars clavicularis. *American Journal of Physica Anthropology* 52: 13–25.
1238
1239 Storti TM, Paniago AF, Faria RLS. 2017. Reconstrução do tendão distal do bíceps com enxerto
1240 do tríceps: nota técnica. *Revista Brasileira de Ortopedia* 52: 354-358.
1241
1242 Swindler DR, Wood CD. 1973. Osteology/Appendicular skeleton. In: Swindler DR, Wood CD,
1243 editores. *An atlas of primate gross anatomy – baboon, chimpanzee, and man*. London:
1244 University of Washington Press.
1245
1246 Szalay F, Dagosto M. 1980. Locomotor adaptations as reflected on the humerus of paleogene
1247 primates. *Folia Primatologica* 34: 1–45.
1248
1249 Tardif SD, Coleman K, Hobbs TR, Lutz C. 2013. IACUC Review of nonhuman primate
1250 research. *ILAR Journal* 54: 234–245.
1251
1252 Tidwell AS. 2010. Princípios da tomografia computadorizada e da imagem por ressonância
1253 magnética. In: Thrall DE, editor. *Diagnóstico de radiologia veterinária*. Rio de Janeiro:
1254 Elsevier. p 50.
1255
1256 Tong K, Guiot LP. 2013. Minimally invasive plate osteosythesis of fractures of the radius and
1257 ulna in a primate. *Veterinary and Comparative Orthopaedics and Traumatology* 26: 416-420.
1258
1259 Tranquilim MV. 2012. Análise do líquido cefalorraquidiano, tomografia computadorizada
1260 craniana e angiotomografia cerebral de *Alouatta guariba* – Geoffroy Saint-Hilaire, 1812 (Bugio

1261 Ruivo). Tese de Doutorado. Faculdade de Medicina Veterinária e Zootecnia, Universidade
1262 Estadual Paulista, Botucatu, Brasil.
1263
1264 Voisin J. 2006. Clavicle, a neglected bone: Morphology and relation to arm movements and
1265 shoulder architecture in primates. *The anatomical record* 288A: 944-953.
1266
1267 Watts ES. 1990. A Comparative study of neonatal skeletl development in *Cebus* and other
1268 primates. *Folia Primatologica* 54: 217-224.
1269
1270 Yalden DW. 1972. The form and function of the carpal bones in some arboreally adapted
1271 mammals. Acta anatomica 82: 383-406.
1272
1273 Young JW, Heard-Booth AN. 2016. Grasping primate development: Ontogeny of intrinsic hand
1274 and foot proportions in capuchin monkeys (*Cebus albifrons* and *Sapajus apella*). *American*
1275 *Journal of Physical Anthropology* 161: 104-115.

CAPÍTULO III:

Anatomy applied to image diagnosis of the hind limb in the black-striped capuchin (*Sapajus libidinosus* Spix, 1823)

Trabalho submetido à revista American Journal of Primatology
ISSN: 1932-8494; Fator de Impacto: 2.371; Qualis A1

Anatomy applied to image diagnosis of the hind limb in the black-striped capuchin (*Sapajus libidinosus* Spix, 1823)

Running title: Anatomy of the hind limb in the black-striped capuchin

Ana Yasha F. de La Salles[1], Jéssica K. de Andrade[2], Joyce G. de Souza[1], Kelvis de B. Freitas[3], Artur da N. Carreiro[1], Edson Vinícius L. Veloso[1], Ediane F. Rocha[1], Marcius Alessandro P. Klem[4], Fábio Tatian M. Mendonça[5], Danilo José A. de Menezes[1,6*]

[1]Postgraduate program in Animal Science and Health, Federal University of Campina Grande, Center for Rural Health and Technology, Patos, Paraíba, Brazil.

[2]Veterinary Doctor, Postgraduate in Veterinary Anesthesiology at Instituto Qualittas, Fortaleza, Ceará, Brazil.

[3]Graduate Program in Structural and Functional Biology, Federal University of Rio Grande do Norte, Natal, Rio Grande do Norte, Brazil.

[4]Veterinary Doctor specialized in Diagnostic Imaging, managing partner of the Institute of Veterinary Radiology, Natal, Rio Grande do Norte, Brazil.

[5]Veterinary Doctor, Tutor of Diagnostic Imaging Practices, Veterinary Health Center, Universidade Potiguar, Natal, Rio Grande do Norte, Brazil.

[6]Department of Morphology, Federal University of Rio Grande do Norte, Natal, Rio Grande do Norte, Brazil.

*Corresponding author: Danilo José Ayres de Menezes, Campus Universitário UFRN, Av. Senador Salgado Filho, 3000, Lagoa Nova, Natal/RN, 59064-741, Brazil. Telephone: +55 84 98101-9198. Email: mdanayres@gmail.com

Abstract

The knowledge of anatomy and imaging exams emerges as an important tool in the study of evolutionary processes of a species, in the elaboration of diagnosis, and the successful choice of the appropriate clinical and surgical procedures. Therefore, this study aims at describing the structures of the hind limb of *Sapajus libidinosus* in anatomical pieces, identifying them in radiographic and tomographic images. For this, four cadavers were used in the macroscopic analysis and five animals for the imaging exams, of which four were euthanized and added to the macroscopic stage. For imaging exams, they were kept anesthetized. All bones were documented, structures described, and compared with data in the literature from human and non-human primates. We have performed Student's t-test for independent samples. There was no statistical difference between the sexes regarding the length of the hind limb bones. The coxal bone was largely well described using imaging methods. A small penile bone is present at the tip of the penis, and it could be identified by all analyzed methods. The femur, as well as the tibia and fibula, were not well portrayed in their proximal and distal epiphyses by radiography, however, they were well identified on tomography. No third trochanter was observed in the femur, and the patella had a triangular shape. All the structures described in the macroscopic image of the tarsus and metatarsus could be identified through radiography and tomography. More subtle structures, such as the popliteal notch, on the tibia and gluteal tuberosity; pectineal line and facies aspera, on the coxal bone, were not identified through imaging. The *Sapajus libidinosus* presented anatomical characteristics more similar to those of larger New World and Old World monkeys, including man, being a great indicator of an experimental model for studies in recent primates.

Key words

3D reconstruction, anatomy, Cebidae, digital radiology, skeleton

1 INTRODUCTION

Brazil has the greatest diversity of primates in the world, with 70% of the total species found in the Amazon. According to Del-Claro (2003), this attracts studies focused on biodiversity. Among the most common primate species kept under human care in Brazil, the black-striped capuchin monkey stands out. Belonging to the Cebidae family, this species is medium-sized, arboreal, diurnal, and has the widest geographic distribution among New World monkeys (Kinzey, 1997; Martins et al., 2021).

Although illegal in Brazil, these animals are still the target of hunting and illegal wildlife trade, being subjected to inadequate breeding and management (Nascimento et al., 2013). This maintenance in illegal captivity can favor the occurrence of several conditions, among which are those affecting bone structures, as well as fractures resulting from traumatic events and joint degenerative processes (Gros-Louis et al., 2003; Johnson-Delaney, 1994; Rangel et al., 2013).

Neotropical primates have been studied in various morphological aspects and, considering the current state of science, knowledge about wild animals in general is important, whether aiming at their preservation or protecting their reproduction, promoting the continuation of the potential ability to use these animals as biological models.

Black-striped capuchin monkeys have been one of the most used Cebidae in biomedical research (Alfaro et al., 2014; Gros-Louis et al., 2003; Lima et al., 2017; Martins Jr. et al., 2015; Nieves et al., 2021; Watts, 1990). Their easy handling and ease of breeding in captivity contribute to this (Diniz, 1997). For osteological studies, these primates resemble humans in terms of bone structure and remodeling, making them an excellent animal model for this line of research (Pritzker & Kessler, 2012).

Radiology and, later, computed tomography, in veterinary medicine, particularly in primatology, represented a great evolution in the imaging exams of the appendicular skeleton,

allowing direct vision and diagnosis, with wide prognostic and therapeutic implications of many diseases that affect this region, besides enabling anatomical studies and proving to be an excellent model for morphofunctional investigation (Fonteles et al., 2010; Young & Schneider, 1981; Pritzker & Kessler, 2012; Rodman, 1979; Ruff & Leo, 1986; Silverman et al., 2005; Tong & Guiot, 2013). However, the number of studies on *Sapajus libidinosus*, focused on the area of gross anatomy, compared to imaging methods, is still limited.

Basic anatomical studies, aimed at describing structures, are often neglected, and, as a result, they are scarce in the literature, despite representing the foundation for many other areas of medicine. Therefore, to contribute to the formation of an osteological and image database that serves as a reference for the species under study, this research sought to recognize the structures of the hind limb of the black-striped capuchin monkey (*Sapajus libidinosus*) in anatomical parts, and radiographic and tomographic images.

2 MATERIAL AND METHODS

2.1 Animals and Study Site

The study was conducted respecting the principles of the American Society of Primatologists (ASP) for the ethical treatment of non-human primates. The methodological protocols were approved by the Ministry of the Environment, through the Biodiversity Authorization and Information System-SISBIO of the Chico Mendes Institute-ICMBio (n.º 70606-2), CEUA/UFCG (n.º 121/2019) and CEUA/UFRN protocol 074/2019, certificate n.º 209.074/2019.

The macroscopic stage of the study was conducted at the Laboratory of Animal Anatomy, Department of Morphology, Federal University of Rio Grande do Norte (UFRN),

Natal-RN Campus. The CT scans and part of the radiographs were performed at the Institute of Veterinary Radiology (IRV), Natal-RN, and the other radiographs, in partnership with the Potiguar University (UnP), Natal-RN.

Four animal cadavers, males, two juveniles aged less than 10 years, and two adults estimated to be 10-15 years old, kept frozen, donated by CETAS/IBAMA/Natal-RN, were used for the macroscopic study of the hind limb.

For the radiography (RX) and tomography (CT), five specimens of *Sapajus libidinosus* were selected, an adult male, with estimated age at 10-15 years, and four elderly females, with age estimated at 20-30 years, weighing in average 2.21 kg, from the Wild Animal Screening Center (CETAS/IBAMA), in the city of Natal/RN. The monkeys were submitted to four hours of water fasting and eight hours of food fasting before the anesthetic procedure. After the imaging tests, the females were euthanized with 19.1% potassium chloride (Equiplex®, Brazil), at a dose of 1 mL/kg, intravenously, and added to the macroscopic study, totaling eight animals at this stage. The adult animal was used only for the examinations and returned to CETAS.

2.2 Preparation of parts and bone description

In the eight animals destined for the macroscopic stage, a dissection technique associated with maceration was performed, according to Ladeira & Höfling (2007). The region of interest was separated into the thigh bone, penile bone, and right and left pelvic limbs, and stored in bags made with mesh-like tissue, to facilitate their identification after maceration. The bones were separated by animal and, to join them together, we have used Araldite® Hobby epoxy glue and instant superglue (Tekbond®, Brazil).

The lengths of the pelvic limb bones, from the most cranial to the most caudal extremity or the most proximal to the most distal, were determined in the eight animals destined for macroscopic description. The right antimere was defined as the standard for measurement.

All bones were described, following the recommendations of the *Nomina Anatomica Veterinaria* (International Committee On Veterinary Gross Anatomical Nomenclature, 2017).

2.3 Imaging exams

Five animals were used in this stage. One adult male and one female were destined for tomography and radiography exams, and the other females, only for radiography exams. For the examinations, the animals were captured with a catching net, sent to the IRV and UnP, and sedated with an association of tiletamine hydrochloride and zolazepam hydrochloride (Telazol® 10%, Zoetis, Brazil) at a dose of 6 mg/kg, administered intramuscularly (La Salles et al., 2019, 2021). Upon arrival, access to the caudal saphenous vein was obtained (La Salles et al., 2017) for anesthetic induction, which was performed with intravenous propofol (Provive 1%, União Química, Brazil) in a target-controlled infusion (IAC), with a VP50 infusion pump (MedRena®, Guangdong, China), at a dose of 2-5mg/kg, followed by anesthetic maintenance at an initial dose of 0.25-0.5 mg/kg/min, reduced during the experiment. The animal was kept breathing room air, and in the 3rd anesthetic stage, between the 2nd and 3rd plane, so that there was no movement during the exams. Monitoring was performed using a multiparameter monitor (Model DL 1000, Deltalife, Brazil).

After the exams, euthanasia was performed. One male animal was donated only for the examinations and was not euthanized. The corpses of the four euthanized females were sent to the Animal Anatomy Laboratory/UFRN to be added to the macroscopic study.

2.3.1 Radiography

At the Veterinary Hospital of UnP, radiographic examinations were performed using a conventional radiodiagnostic device, model VET500, (X-RAD X-Ray equipment, Brazil), with a capacity of 500 mA and 125 kV, equipped with a radiographic table with an anti-diffusion device and X-ray tube, and the images were acquired with the CR digital system, with an IP cassette plate, CC type (24 cm x 30 cm) (Fujifilm, Japan) and FCR PRIMA T2 Image Reader photostimulable phosphor plate scanner, model CR-IR 392 (Fujifilm, Japan). The radiographic technique used was 44-46 kV, 0.045-0.05 s and 200 mA, under the same focus-film distance. The images were saved in PDS files and analyzed using the PD-S Viewer software, version 1.4.0.0.

To obtain better image definition, two animals were referred to the IRV, and the images were performed using a conventional radiodiagnostic device, Intecal, CR 500 mAs – Casa do Radiologista, equipped with a radiographic table with anti-diffusion grid, "Potter-Bucky ", and IAE X-ray tube (Italy) with a rotating anode and the images were acquired using the DR digital system, with a VIEWORKS digitizer plate, model CESIO 1417WA, with 2560 x 3072 pixels. The radiographic technique used was 55 kV, 0.06 s and 300 mA. After the acquisition, the radiographic images were saved in DICOM files, and transferred and analyzed online using the postDICOM program (Herten, Netherlands). All radiographic examinations were performed in compliance with the radiological protection standards.

The animals were positioned directly on the radiographic tables. The pelvic limb was radiographed under the mediolateral and craniocaudal projections, in the thigh and leg regions, and dorsoplantar, in the foot region. Ventrodorsal and laterolateral projections were also made to visualize the pelvis and penile bone.

The radiographic exams were individually analyzed, identifying all the bones and particularities observed in the skeletal system already described in the macroscopic stage, and a comparison of the three study methods was performed.

2.3.2 Computed tomography

For the examination in question, a helical computed tomography device, model XVision EX, single slice (Toshiba, Japan) was used. Before the scan, sagittal radiographic images of each region and sub-region to be studied of each animal were acquired (topogram), to define the extent of the study (the beginning and end of the scan) and the slice variation. Once the area was defined, transverse planes with predetermined section thickness and table increment were performed.

The imaging parameters used for the pelvic limb were: 2.0 mm slice thickness, 2.0 table increment, 100 mA and 120 kV, for the coxofemoral region; 2.0 mm slice thickness, 1.5 table increment, 150 mA and 120 kV, for the femorotibial and patellofemoral regions, and 1.0 mm of slice thickness, 1.0 table increment, 150 mA and 120 kV, for the tarsal, metatarsal, phalangeal and penile bone regions. To perform the CT, the animals were positioned in sternal recumbency, with caudal extension of the thoracic and hind limbs.

We have transferred the tomographic images to the Horos software version 1.1.7 (United States) for the analysis of transverse plane images and multi-planar reconstructions (MPR) in sagittal and dorsal planes. 3D reconstruction to illustrate bone anatomy was also obtained.

The tomographic images were individually analyzed, and we have also performed the identification of the bones and particularities, already described macroscopically, and a comparison of the three methods of study.

2.4 Statistical analysis

During the study, the results obtained were documented with a digital camera, and, later, described and compared with data from the literature about human and non-human primates. Mean and standard deviation of the lengths of the bones of the right antimere of the hind limb were determined. Student's t-test was performed for independent samples using the Past software, version 4.03.

3 RESULTS

The bones of the hind limb comprise the coxal, femur, tibia, fibula, tarsus, metatarsal and phalanges. Measurements of bone lengths, of the right antimere, from the most cranial to the most caudal end of the coxal bone, and the most proximal to the most distal end of the long bones, are described in Table 1.

TABLE 1 Length in millimeters (mm) of the bones of the right antimere of the hind limb, of four males (M1-M4) and four females (F1-F4) of *Sapajus libidinosus*, arranged in mean (Mean) and standard deviation (SD).

	Mean	**SD**	**Mean M***	**Mean F****
Coxal	86.1	7.92	82.3	89.9
Femur	124.6	8.33	120.5	128.6
Tibia	118.4	7.99	114.8	122.0
Fibula	110.1	8.77	106.0	114.1
Value of t			0.2103	
Value of p			2.056	

† * Mean of males, **Mean of females.

† Means do not differ statistically from each other when compared by the t test ($p < 0.05$).

Data from table 1 demonstrate that there was no statistically significant difference between males and females regarding the length of the hind limb bones. No differences were observed among the studied specimens regarding the analyzed bones.

The coxal bone is composed of three bones: ilium, ischium and pubis, and contains a large obturator foramen (Figure 2). The acetabulum is deep and contains a margin, a fossa and a semilunar articular surface, which is interrupted by an acetabular notch. Dorsal to the acetabulum, a discrete ischial spine is present. There are discreet coxal and sacral tuberosities and a clearly visible ischial tuberosity. The iliac surface has a tuberosity and a fossa and, together with the auricular surface, forms the sacropelvic surface, to which the sacrum articulates. Forming the cranial border is the iliac crest. Iliac spines and inner and outer lips are also seen in the ilium. An arcuate line is seen on the medial aspect, opposite to the greater sciatic notch. Through the symphysis surface of the pubis and ischium, the two halves of the coxal bone articulate, forming the pubic and ischial symphysis, which together represent the pelvic symphysis (Figure 1). The pubis still forms, through this union, a central pubic tubercle, and its cranial margin is called the pecten. The sciatic arch is in the shape of an “inverted V”. The tubercle to the psoas minor muscle was also seen (Figure 2). Iliopubic eminence was not identified.

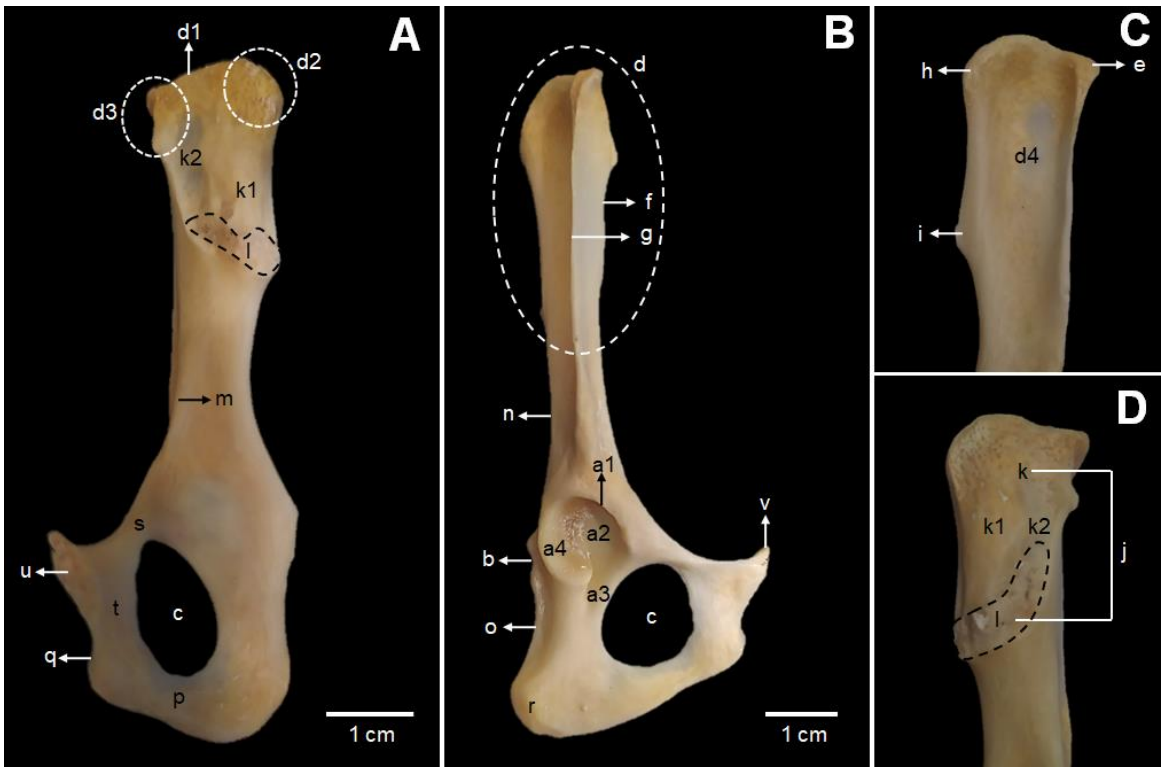

FIGURE 1 Coxal bone. Medial view of the right antimere (A), Lateral view of the right antimere (B), Lateral view of the right ilium bone (C), Medial view of the left ilium bone (D). a. Acetabulum (*Acetabulum*); a1. Acetabulum margin (*Margo acetabuli*); a2. Acetabulum fossa (*Fossa acetabuli*); a3. Acetabular notch (*Incisura acetabuli*); a4. Semilunar face (*Facies luneta*); b. Ischial spine (*Spina ischiadica*); c. Obturator foramen (*Foramen obturatum*); d. Wing of ilium (*Ala ossis ilii*); d1. Iliac crest (*Crista iliaca*); d2. Coxal tuber (*Tuber coxae*); d3. Sacral tuber (*Tuber sacrale*); d4. Gluteal surface (*Facies glutaea*); e. Cranial ventral iliac spine (*Spina iliaca ventralis cranialis*); f. Inner lip (*Labium internum*); g. Outer lip (*Labium externum*); h. Cranial dorsal iliac spine (*Spina iliaca dorsalis cranialis*); i. Caudal dorsal iliac spine (*Spina iliaca dorsalis caudalis*); j. Sacropelvic surface (*Facies sacropelvina*); k. Iliac surface (*Facies iliaca*); k1. Iliac tuberosity (*Tuberositas iliaca*); k2. Iliac fossa (*Fossa iliaca*); l. Auricular surface (*Facies auriculares*); m. Arcuate line (*Linea arcuata*); n. Greater sciatic notch (*Incisura ischiadica major*); o. Lesser sciatic notch (*Incisura ischiadica minor*); p. Ramus ossis ischii (*Ramus ossis ischii*); q. Symphyseal face of the ischium (*Facies symphysialis ossis ischii*); r. Ischial tuberosity (*Tuber ischiadicum*); s. Cranial ramos of pubic bone (*Ramus cranialis ossis púbis*); t. Caudal ramus of pubic bone (*Ramus caudalis ossis púbis*); u. Sympyseal surface of the pubis (*Facies symphysialis ossis pubis*); v. Pubic tubercle (*Tuberculum pubicum*).

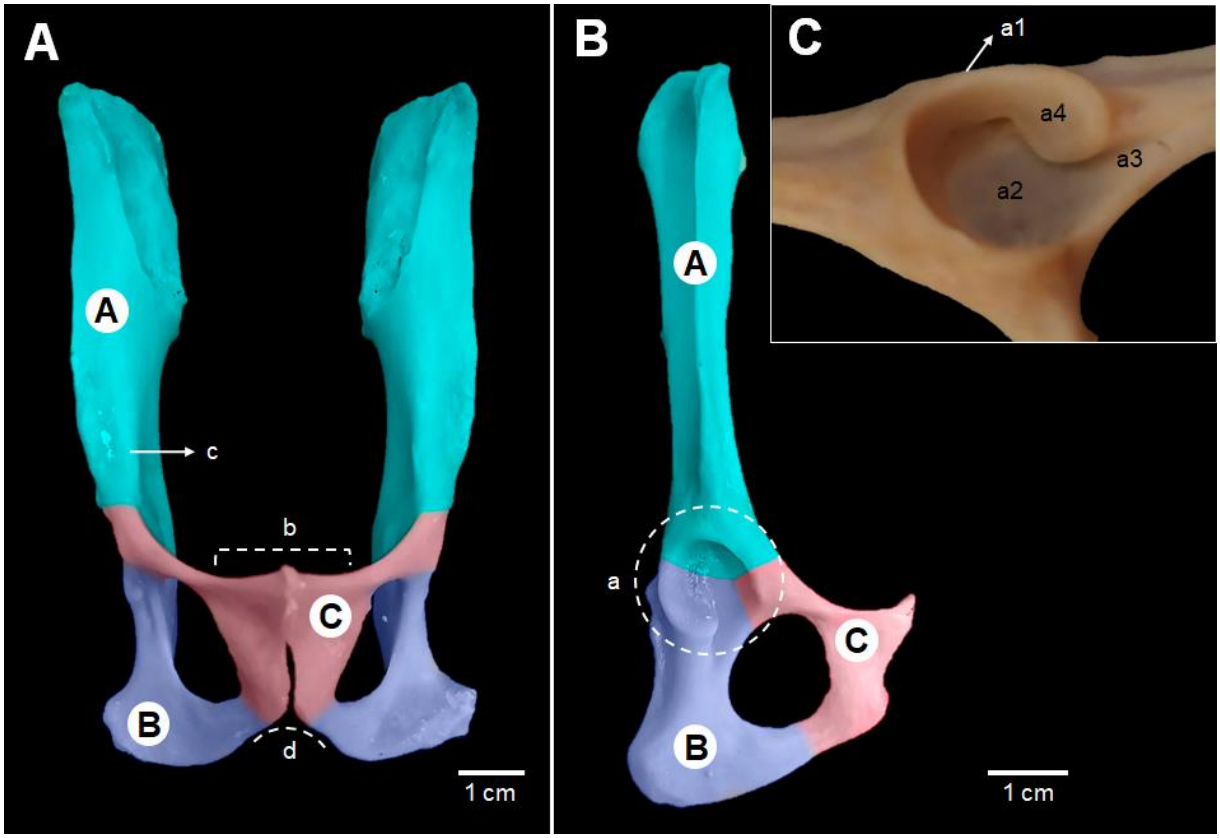

FIGURE 2 Coxal bone. Ventral view (A), Lateral view of the right antimere (B), Close-up of the acetabulum (C). A. Body of the ilium bone (*Corpus ossis ilii*); B. Ischial bone body (*Corpus ossis ischii*); C. Pubic bone body (*Corpus ossis púbis*); a. Acetabulum (*Acetabulum*); b. Pectineal line of the pubis (*Pecten ossis púbis*); c. Tubercle for minor psoas (*Tuberculum m. psoas minoris*); d. Ischial arch (*Arcus ischiadicus*).

The coxal bone was largely well described through radiographic imaging and 3D reconstruction, with most of its structures identified, with the tomographic image providing the best visualization. Internal structures of the acetabulum, the symphysis surfaces of the pubis and ischium, and structures of the articular surface with the sacrum could not be identified by imaging methods, because of the articulation with the corresponding bones. The arcuate line was also not identified by these methods (Figures 3, 5, 6). The cross-sectional tomographic image of the region allowed identification of the sacrum, coxal bone, femur and caudal vertebra (Figure 4).

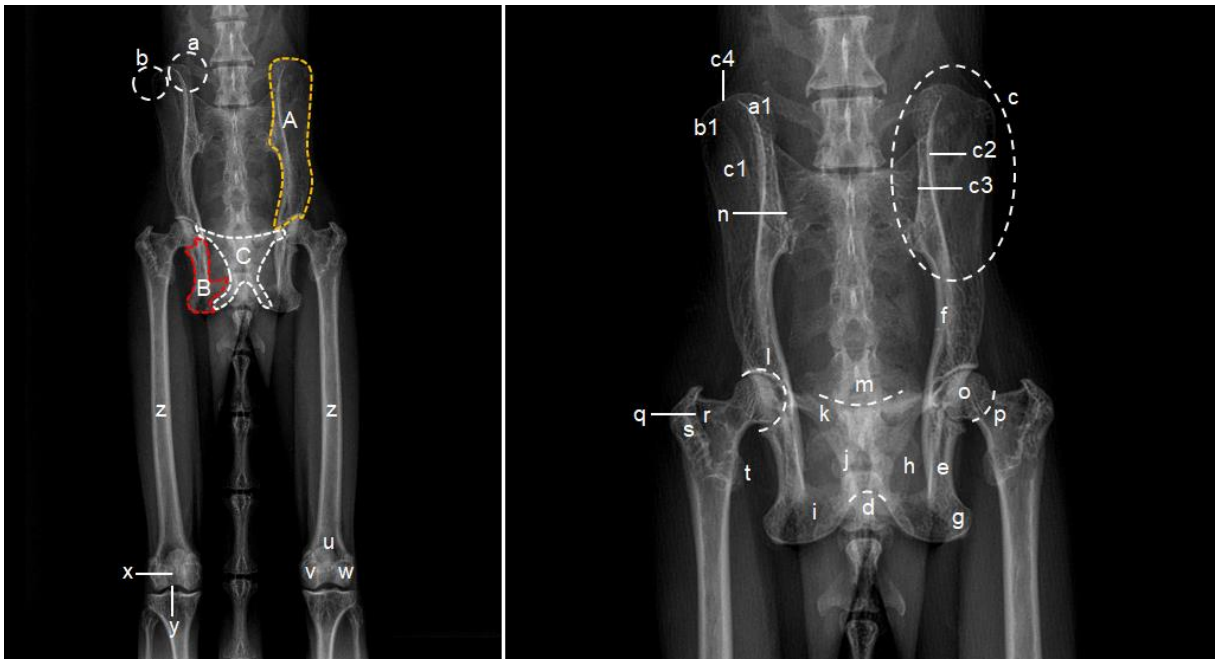

FIGURE 3 Radiographic image in dorsoventral projection, highlighting the coxal bone and femur. A. Ilium; B. Ischium; C. Pubis. a. sacral tuber; a1. Cranial dorsal iliac spine; b. Coxal tuber; b1. Cranial ventral iliac spine; c. Wing of ilium; c1. Gluteal surface; c2. Outer lip; c3. Inner lip; c4. Illiac crest; d. Sciatic arch; e. Lesser sciatic notch; f. Greater sciatic notch; g. Ischial tuberosity; h. Obturator foramen; i. Ramus of the Ischium; j. Caudal ramus of the pubic bone; k. Cranial ramus of the pubis; l. Acetabulum; m. Pectineal line; n. Sacroiliac joint; o. Head of the femur; p. Neck of the femur; q. Intertrochanteric crest; r. Trochanteric fossa; s. Caudal part of the greater trochanter; t. Lesser trochanter; u. Popliteal face; v. Medial condyle; w. Lateral condyle; x. Intercondylar fossa; y. Intercondylar line; z. Body of the femur.

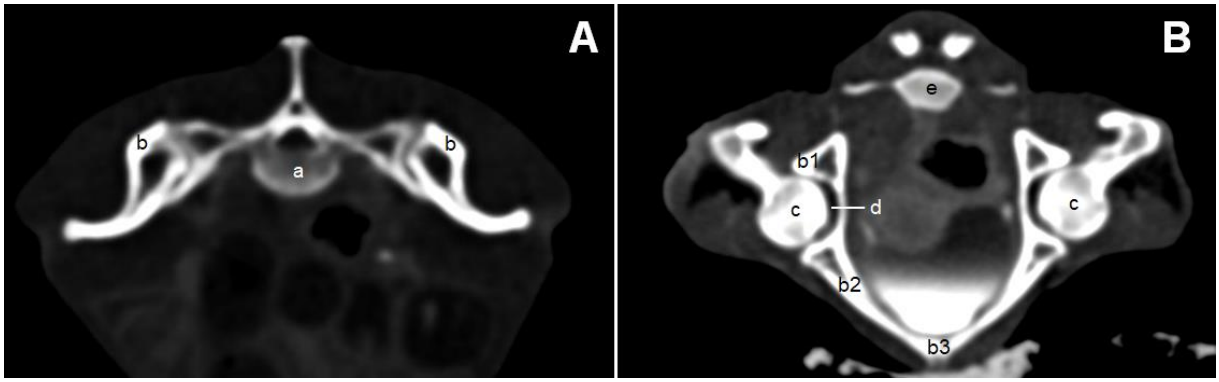

FIGURE 4 Cross-sectional tomographic image of the sacrocaudal region at the level of the sacral vertebra (A) and Ca2 (B). a. Sacrum; b. Coxal; b1. Ilium; b2. Ischium; b3. Pubis; c. Femur; d. Acetabulum; e. Caudal vertebra.

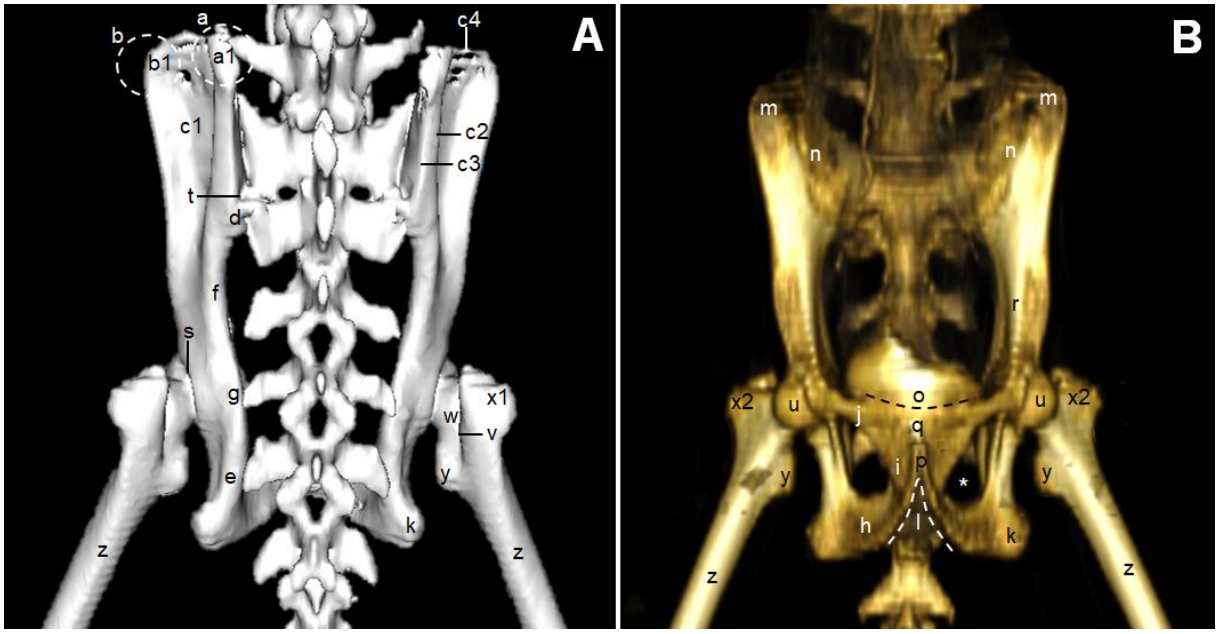

FIGURE 5 Image in 3D reconstruction in dorsoventral (A) and ventrodorsal (B) projection, highlighting the coxal bone and femur. a. Sacral tuberosity; a1. Cranial dorsal iliac spine; b. Coxal tuberosity; b1. Cranial ventral iliac spine; c. Wing of ilium; c1. Gluteal surface; c2. Outer lip; c3. Inner lip; c4. Iliac crest; d. Caudal dorsal iliac spine; e. Lesser sciatic notch; f. Greater sciatic notch; g. Ischial spine; h. Ramus of the ischium bone; i. Caudal ramus of the pubic bone; j. Cranial ramus of the pubic bone; k. Tuber ischium; l. Sciatic arch; m. Coxal tuberosity; n. Sacropelvic surface; o. Pectineal line of the pubis; p. Ischial symphysis; q. Pubic symphysis; r. Tubercle for minor psoas; s. Acetabulum; t. Sacroiliac joint; u. Head of the femur; v. Intertrochanteric crest; w. Trochanteric fossa; x. Greater trochanter; x1. Caudal part of the greater trochanter; x2. Cranial part of the greater trochanter; y. Lesser trochanter; z. Body of the fêmur bone; * Obturator foramen.

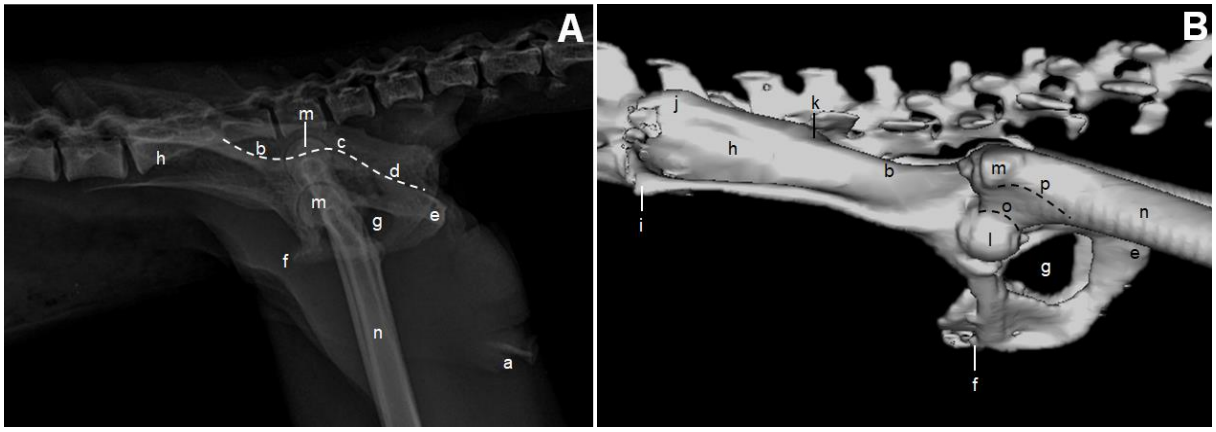

FIGURE 6 Radiographic image (A) and 3D reconstruction (B), in laterolateral projection, highlighting the coxal, femur and penile bone. a. Penile bone; b. Greater sciatic notch; c. ischial spine; d. Lesser sciatic notch; e. Sciatic tuberosity; f. Pubic tubercle; g. Obturator foramen; h. Wing of the ilium/Gluteal surface; i. Cranial ventral iliac spine; j. Cranial dorsal iliac spine; k. Caudal dorsal iliac spine; l. Head of the femur; m. Greater trochanter (cranial part); n. Body of the femur; o. Neck of the femur; p. Intertrochanteric line.

A small penile bone, averaging 5 mm in length, is present at the tip of the penis. It was noted that, in young animals, thus characterized according to dental parameters, basisphenoid and basioccipital synostosis, and for presenting coronal and lambdoid sutures still open, the penile bone presented a larger size, reaching up to 8 mm, and in adult animals, it presented a reduced size, reaching a minimum of 3 mm. In addition, its morphology was different, being more rectilinear in young animals, whereas, in adult ones, it presented a thin cranial process extending to the glans penis and a more voluminous caudal part (Figura 7).

FIGURE 7 Macroscopic image of penile bone (*Os penis*) from an adult animal (A), and a young animal (B).

The penile bone can be observed both through radiographic imaging (Figure 6), and different tomographic imaging methods (Figure 8C), in which the penile region is visualized, and in 3D reconstruction (Figures 8A, B, D). Figures 8A and 8D show the bone structure clearly detailed, and Figure 8B depicts the marking of the approximate location of the penile bone, based on the shape observed macroscopically.

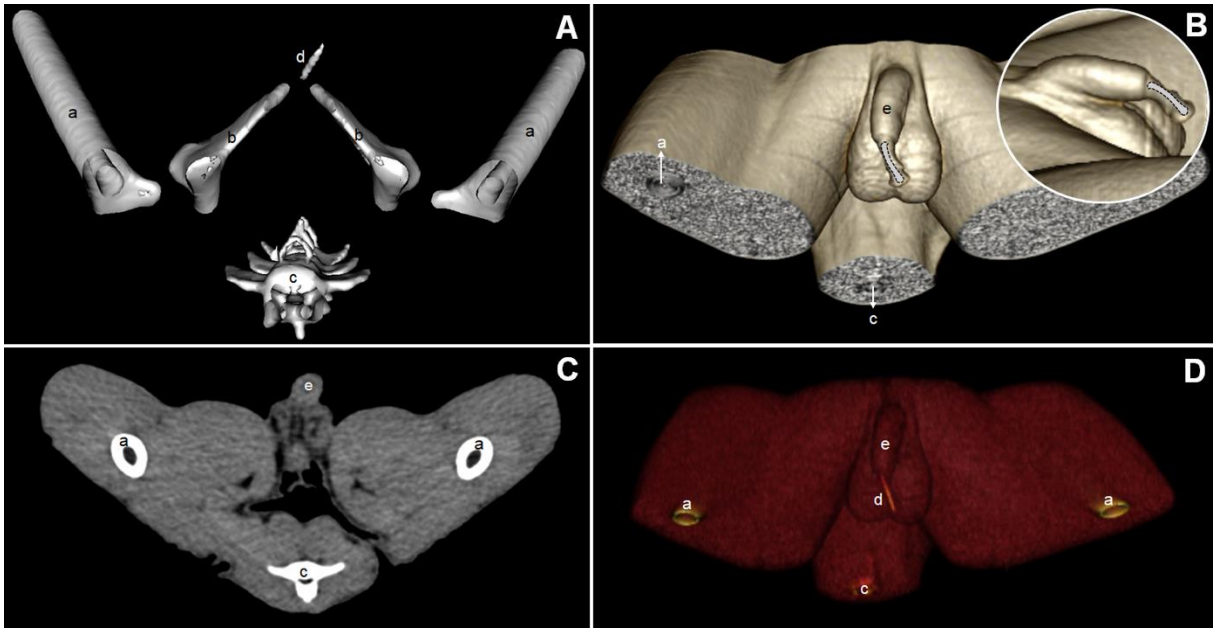

FIGURE 8 Tomographic and 3D reconstruction images, highlighting the penile region. a. Femur; b. Coxal bone; c. Caudal vertebra; d. Penile bone; e. Penis.

The femur is quite long, being the largest bone in the body, and shows a well-delineated head with the presence of a fovea, a very distinct neck, and pronounced greater and lesser trochanters (Figures 9, 10C). No third trochanter was observed. An intertrochanteric line connects the two trochanters on the cranial surface (Figure 10A). A small gluteal tuberosity was identified. A subtle dentate line was observed and continued by a facies aspera ventrally. The condyles are separated by an intercondylar fossa, bounded ventrally by an intercondylar line, and the epicondyles are surrounded by an extensor fossa (Figures 9B, 10B, 10C). The patella is triangular, with rounded edges, a narrower apex, a wider base with a central tubercle, and

articulates with a well-defined trochlea (Figures 10E, 10F). A small, round to oval fabella articulates on the dorsal surface of each femoral condyle (Figure 14).

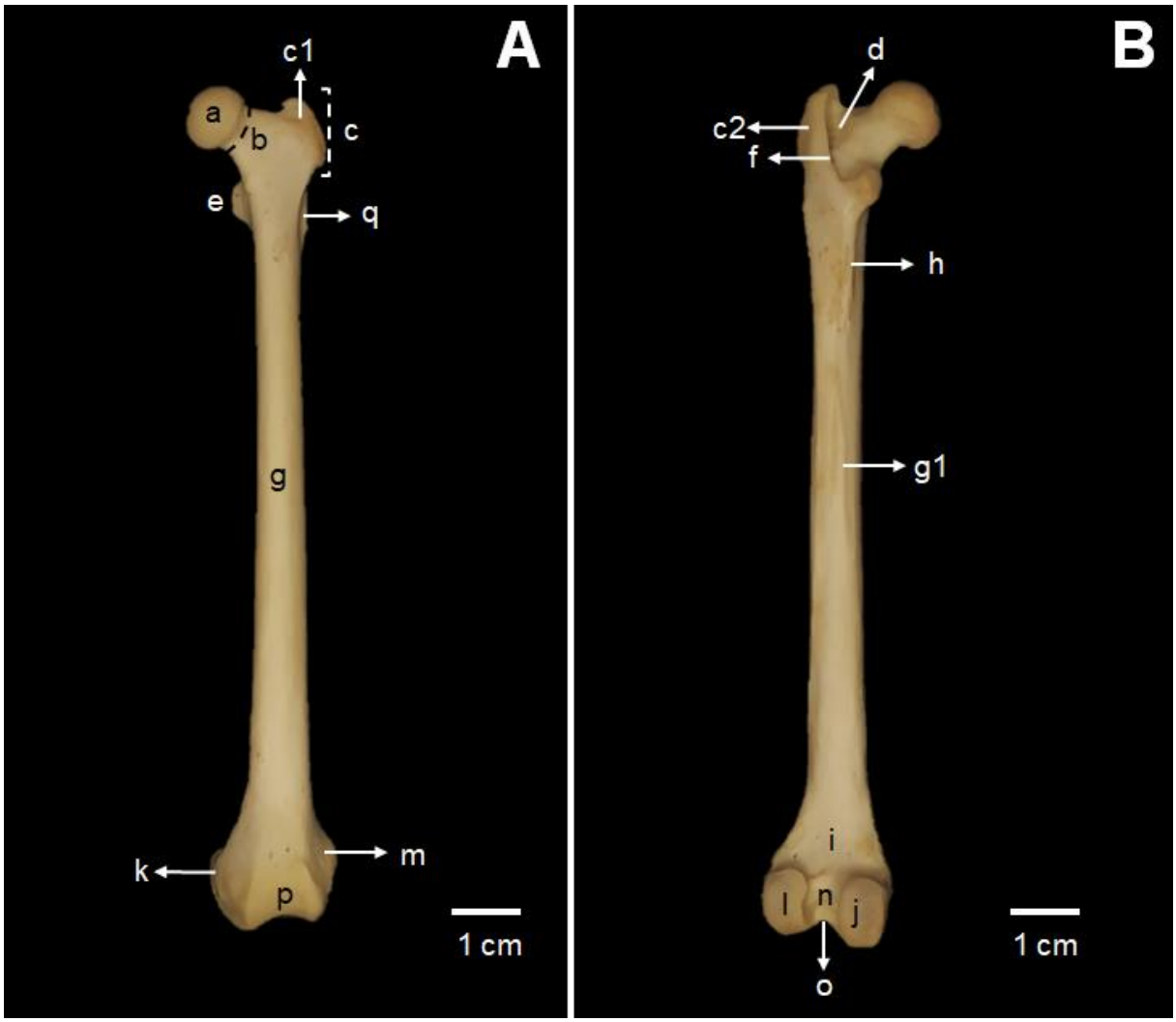

FIGURE 9 Left femur. Cranial view (A), Caudal view (B). a. Head of the femur (*Caput ossis femoris*); b. Neck of the femur bone (*Collum ossis femoris*); c. Greater Trochanter (*Trochanter major*); c1. Cranial part (*Pars cranialis*); c2. Caudal part (*Pars caudalis*); d. Trochanteric fossa (*Fossa trochanterica*); e. Lesser Trochanter (*Trochanter minor*); f. Intertrochanteric crest (*Crista intertrochanterica*); g. Body of the femur bone (*Corpus ossis femoris*); g1. Facies aspera (*Facies aspera*); h. Pectineal line (*Linea pectineus*); i. Popliteal face (*Facies poplitea*); j. Medial condyle (*Condylus medialis*); k. Medial epicondyle (*Epicondylus medialis*); l. Lateral condyle (*Condylus lateralis*); m. Lateral epicondyle (*Epicondylus lateralis*); n. Intercondylar fossa (*Fossa intercondylaris*); o. Intercondylar line (*Linea intercondylaris*); p. Trochlea of the femur bone (*Trochlea ossis femoris*); q. Gluteal tuberosity (*Tuberositas glutea*).

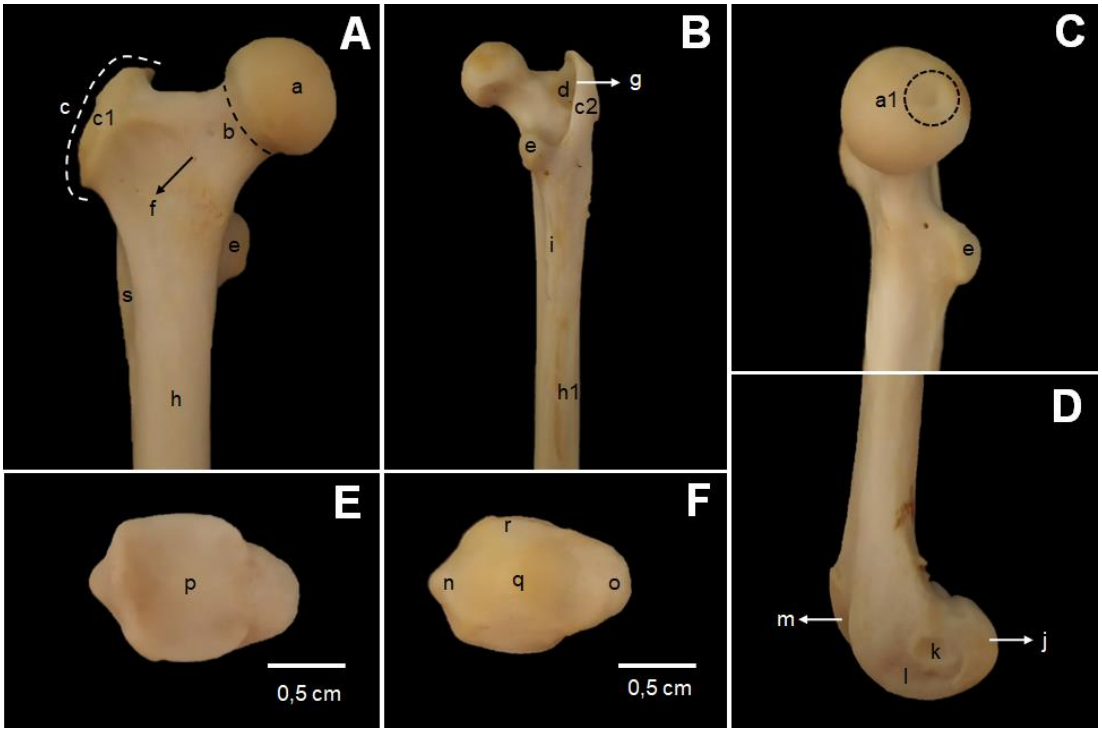

FIGURE 10 Right femur. Cranial view of the proximal epiphysis (A), Caudal view of the proximal epiphysis (B), Medial view of the proximal epiphysis (C), Medial view of the distal epiphysis (D). Patella. Ventral view (E), Dorsal view (F). a. Head of the femur (*Caput ossis femoris*); a1. Fovea capitis femoris (*Fovea capitis*); b. Neck of the femur bone (*Collum ossis femoris*); c. Greater Trochanter (*Trochanter major*); c1. Cranial part (*Pars cranialis*); c2. Caudal part (*Pars caudalis*); d. Trochanteric fossa (*Fossa trochanterica*); e. Lesser Trochanter (*Trochanter minor*); f. Intertrochanteric line (*Linea intertrochanterica*); g. Intertrochanteric crest (*Crista intertrochanterica*); h. Body of the femur bone (*Corpus ossis femoris*); h1. Facies aspera (*Facies aspera*); i. Pectineal line (*Linea pectineus*); j. Medial condyle (*Condylus medialis*); k. Medial epicondyle (*Epicondylus medialis*); l. Extensor fossa (*Fossa extensoria*); m. Trochlea of the femur bone (*Trochlea ossis femoris*); n. Base of the patella (*Basis patellae*); o. Apex of the patella (*Apex patellae*); p. Articular surface (*Facies articularis*); q. Cranial surface (*Facies cranialis*); r. Cartilaginous process (*Processus cartilagineus*); s. Gluteal tuberosity (*Tuberositas glutea*).

The tibia, the second largest bone in the body, and the complete fibula, are well-developed bones, separated by a large interosseous space and not fused. The fibular articular surface and fibular notch of the tibia articulate with the articular surface of the fibular head, and the malleolar articular surface of the fibula, respectively. The tibia has a very prominent cranial tuberosity, in which, laterally, passes the extensor sulcus. A popliteal notch was identified (Figure 12). Cranial and caudal to the intercondylar eminence, well-delimited intercondylar areas are observed. Very prominent malleolus and subtle malleolar grooves are seen in the distal epiphysis (Figure 11).

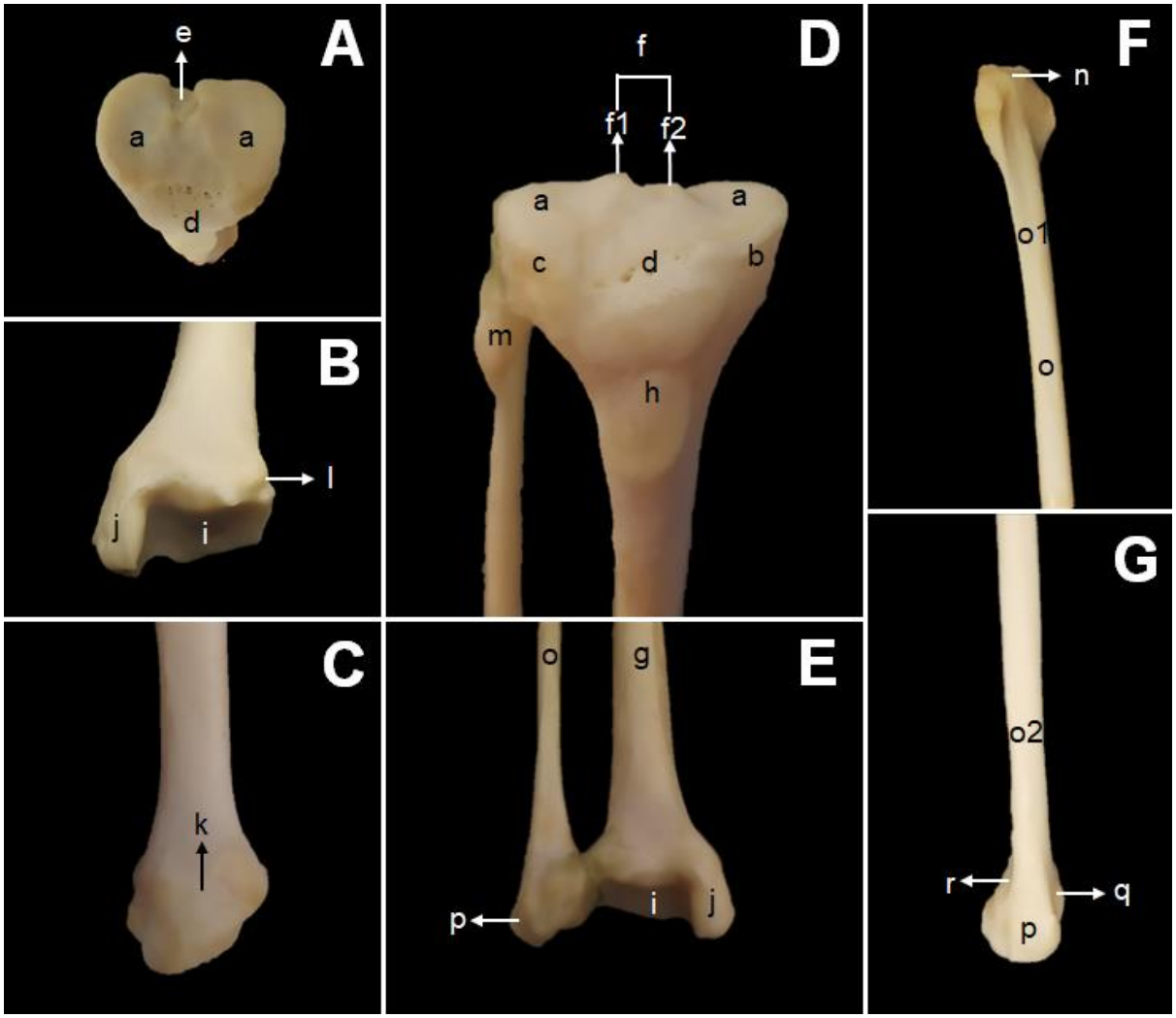

FIGURE 11 Tibia and fibula. View of the articular surface of the proximal epiphysis of the tibia (A), View of the articular surface of the distal epiphysis of the tibia (B), Medial view of the distal epiphysis of the tibia (C), Cranial view of the proximal epiphysis of the tibia and fibula (D), Cranial view of the distal epiphysis of the tibia and fibula (E), Medial view of the proximal epiphysis of the fibula (F), Lateral view of the distal epiphysis of the fibula (G). a. Proximal articular surface (*Facies articularis proximalis*); b. Medial condyle (*Condylus medialis*); c. Lateral condyle (*Condylus lateralis*); d. Cranial intercondylar area (*Area intercondylaris cranialis*); e. Caudal intercondylar area (*Area intercondylaris caudalis*); f. Intercondylar eminence (*Eminentia intercondylaris*); f1. Medial intercondylar tubercle (*Tuberculum intercondylare mediale*); f2. Lateral intercondylar tubercle (*Tuberculum intercondylare laterale*); g. Body of the tibia (*Corpus tibiae*); h. Tibial tuberosity (*Tuberositas tibiae*); i. Cochlea of tibia (*Cochlea tibiae*); j. Medial malleolus (*Malleolus medialis*); k. Medial malleolar sulcus (*Sulcus malleolaris medialis*); l. Fibular notch (*Incisura fibularis*); m. Head of the fibula (*Caput fibulae*); n. Articular surface of the fibular head (*Facies articularis capitis fibulae*); o. Body of the fibula (*Corpus fibulae*); o1. Medial surface (*Facies medialis*); o2. Lateral surface (*Facies lateralis*); p. Lateral mallelous (*Malleolus lateralis*); q. Articular face of the malleolous (*Facies articular malleoli*); r. Lateral malleolar sulcus (*Sulcus malleolaris lateralis*).

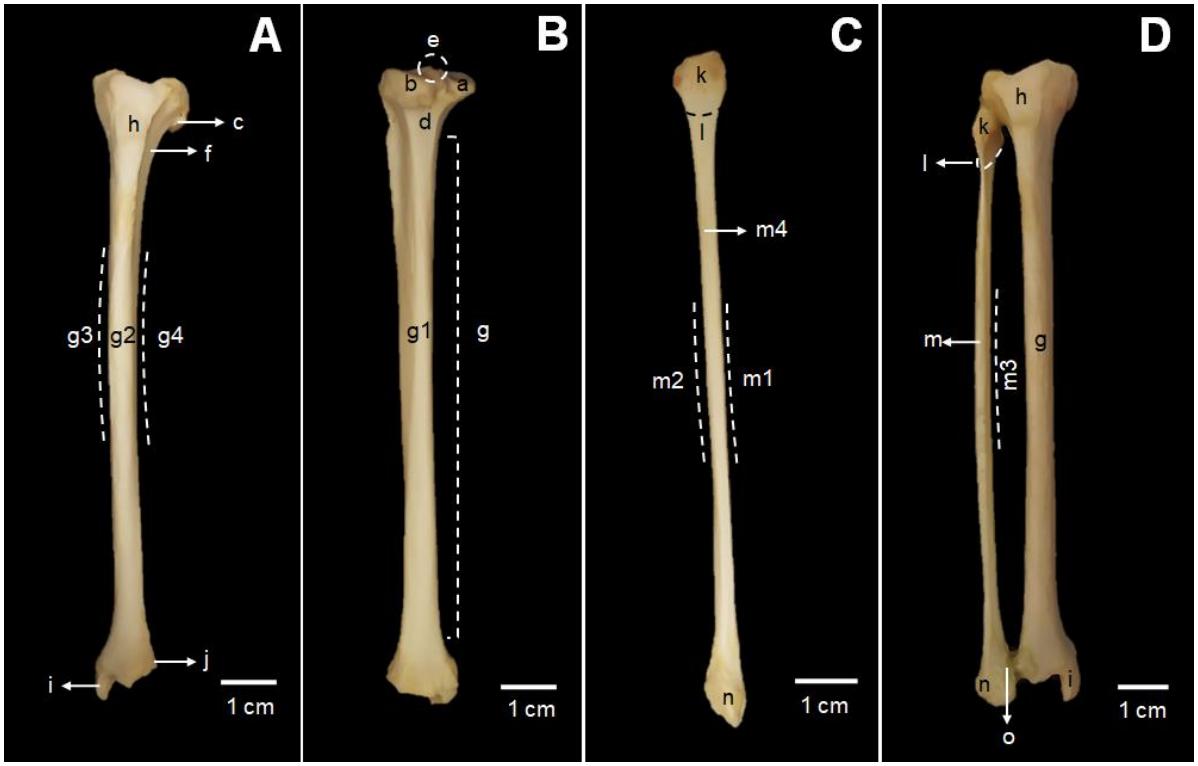

FIGURE 12 Left tibia. Cranial View (A), Caudal View (B). Right tibia and fibula. Lateral view of the fibula (C), Cranial view of the tibia and fibula (D). a. Medial condyle (*Condylus medialis*); b. Lateral condyle (*Condylus lateralis*); c. Fibular articular surface (*Facies articularis fibularis*); d. Popliteal notch (*Incisura poplitea*); e. Intercondylar eminence (*Eminentia intercondylaris*); f. Extensor sulcus (*Sulcus extensorius*); g. Body of the tibia (*Corpus tibiae*); g1. Caudal surface (*Facies caudalis*); g2. Cranial surface (*Facies cranialis*); g3. Medial margin (*Margo medialis*); g4. Lateral/interosseous margin (*Margo lateralis/Margo interosseus*); h. Tibial tuberosity (*Tuberositas tibiae*); i. Medial malleolus (*Malleolus medialis*); j. Fibular notch (*Incisura fibularis*); k. Head of the fibula (*Caput fibulae*); l. Neck of the fibula (*Collum fibulae*); m. Body of the fibula (*Corpus fibulae*); m1. Cranial margin (*Margo cranialis*); m2. Caudal margin (*Margo caudalis*); m3. Interosseous margin (*Margo interosseus*); m4. Lateral surface (*Facies lateralis*); n. Lateral malleolus (*Malleolus lateralis*); o. Malleolar articular surface (*Facies articular malleoli)*.

We could identify all structures of the proximal femoral epiphysis through the 3D reconstruction, in laterolateral (Figure 6), ventrodorsal and dorsoventral (Figure 5) projections, making it possible to visualize their various surfaces. More subtle structures, such as the gluteal tuberosity, dentate line and facies aspera were not identified. The fovea of the femoral head was also not observed because of the articulation with the acetabulum. In the radiographic image of dorsoventral projection, it was possible to identify most of the structures of the proximal epiphysis (Figure 3), while in the laterolateral projection, due to bone overlap of the coxal bone, the structures were not well identified (Figure 6A). All structures of the distal femoral epiphysis

could also be identified through 3D reconstruction (Figure 14), since the radiographic image was limited in terms of identification, being restricted in the dorsoventral projection to the visualization of the caudal aspect of the bone (Figure 3), and in the mediolateral projection to the patella, sesamoid and medial epicondyle (Figure 13).

Except for structures on the articular surface of the proximal epiphysis, such as the caudal intercondylar area, and on the articular surface of the distal epiphysis of the tibia, such as the cochlea, all other structures of the tibia and fibula were identified by imaging methods and were more clearly observed by 3D reconstruction, and with more limited visibility of structures in the radiographic image. It was not possible to identify the popliteal notch by radiography.

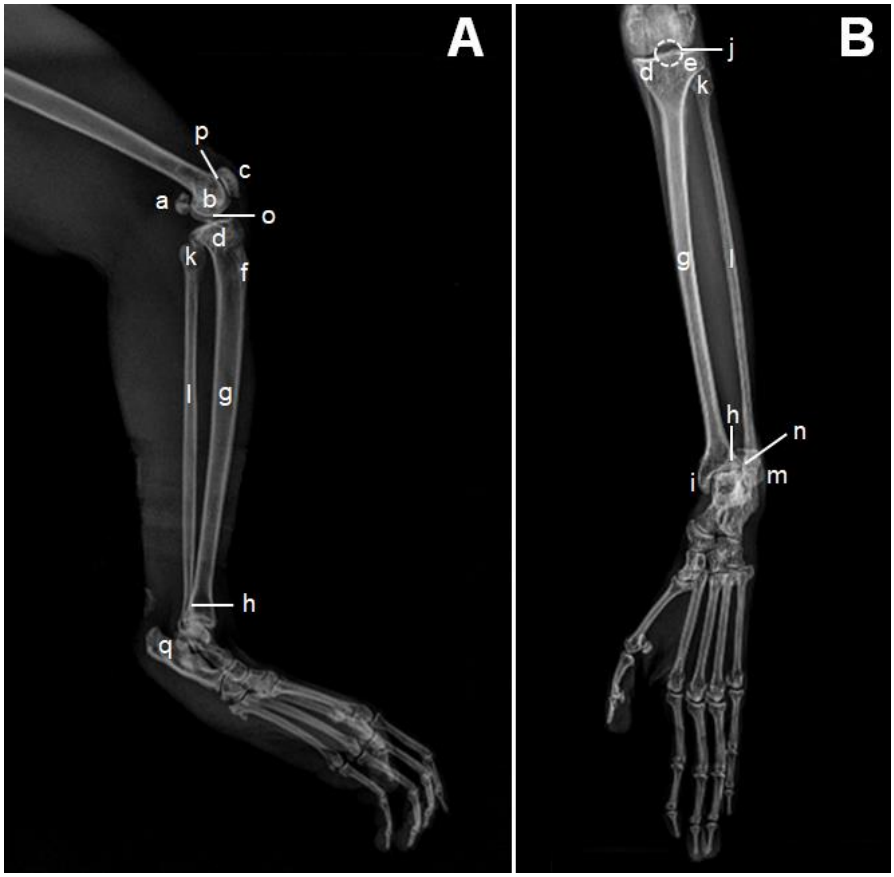

FIGURE 13 Radiographic image in mediolateral (A) and dorsoventral (B) projection of the left antimere, highlighting the femur, patella, tibia and fibula. a. Medial sesamoid bone of the gastrocnemius muscle; b. Medial epicondyle; c. Patella; d. Medial condyle of the tibia; e. Lateral condyle of the tibia; f. Tibial tuberosity; g. Body of the tibia; h. Fibular notch; i. Medial malleolus; j. Intercondylar eminence; k. Head of the fibula; l. Body of the fibula; m. Lateral malleolus; n. Malleolar articular surface; o. Femorotibial joint; p. Patellofemoral Joint; q. Calcaneus.

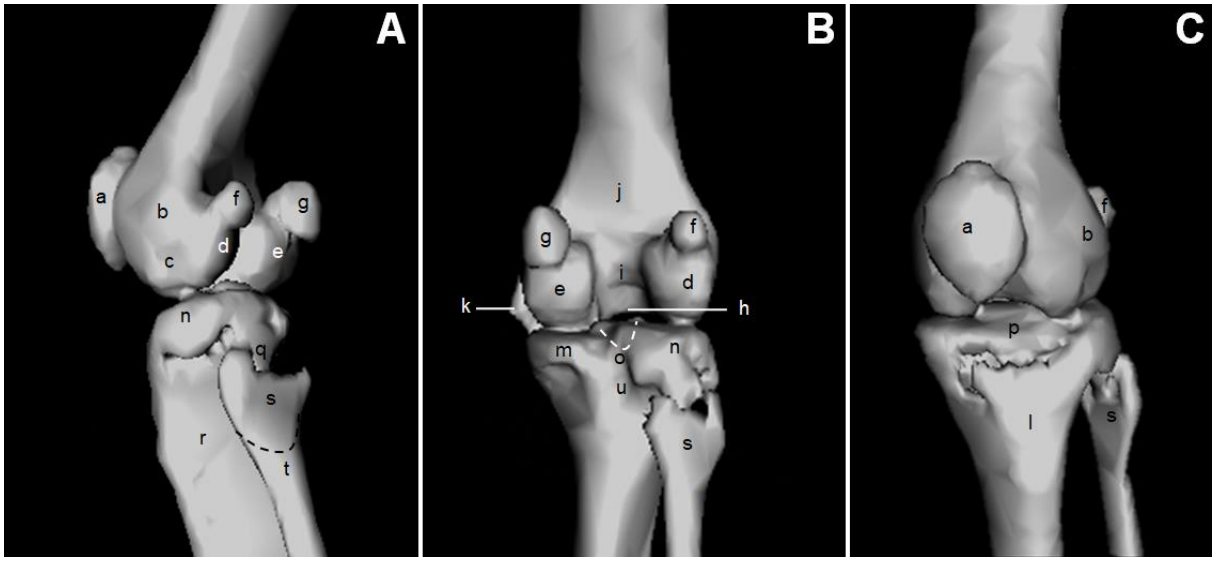

FIGURE 14 Image in 3D reconstruction of the lateral (A), caudal (B) and cranial (C) face of the distal epiphysis of the femur and proximal epiphysis of the tibia and fibula. a. Patella; b. Lateral epicondyle; c. Extensor fossa; d. Lateral condyle of the femur; e. Medial condyle of the femur; f. Lateral sesamoid bone of the gastrocnemius muscle; g. Medial sesamoid bone of the gastrocnemius muscle; h. Intercondylar line; i. Intercondylar fossa; j. Popliteal face; k. Medial epicondyle; l. Tibial tuberosity; m. Medial condyle of the tibia; n. Lateral condyle of the tibia; o. Intercondylar eminence; p. Cranial intercondylar area; q. Fibular articular surface; r. Extensor sulcus; s. Head of the fibula; t. Neck of the fibula; u. Popliteal notch.

The tarsus contains seven bones, the talus and calcaneus in the crural row, the central tarsal bone, forming a reduced intermediate row, and four bones in the metatarsal row that increase in size from medial to lateral. Five digits are present. The finger I, known as the hallux, contains two phalanges, while the other four have three (Figure 15). The distal phalanx of the finger I has a wider and flatter base, but all the distal phalanges are covered by a nail (unguis) (Figure 15A). A prominent lateral process of the talus and a lateral process of the calcaneal tuberosity were identified (Figure 15B). Axial and ovoid abaxial sesamoid bones are present on the plantar surface in the distal trochlea of the metatarsal bones. Comma-shaped sesamoid bones are found in the proximal interphalangeal joints of the last four digits and the distal interphalangeal joint of the thumb. No sesamoid bone is present on the plantar surface at the distal interphalangeal joints of fingers II to V (Figure 16).

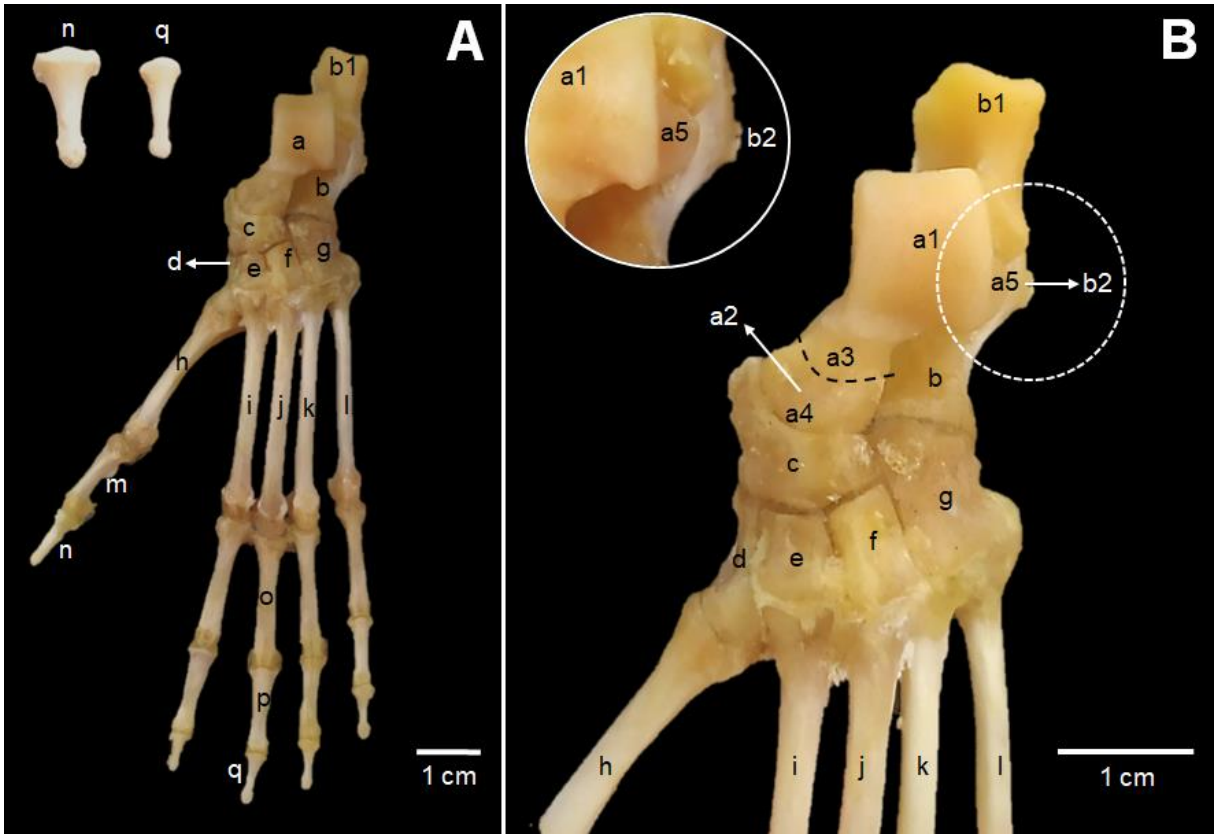

FIGURE 15 Tarsal bones, metatarsus and phalanges, left antimere. Cranial view (A), Cranial view of the tarsal and metatarsal region (B). a. Talus (*Talus*); a1. Trochlea of the talus (*Trochlea tali*); a2. Talus head (*Caput tali*); a3. Talus neck (*Collum tali*); a4. Navicular articular surface (*Facies articularis navicularis*); a5. Lateral process of the talus (*Processus lateralis tali*); b. Calcaneus (*Calcaneus*); b1. Calcaneal tuberosity (*Tuber calcanei*); b2. Lateral process of the calcaneal tuberosity (Pro*cessus lateralis tuber calcanei*); c. Central tarsal bone (*Os tarsi centrale* or *os naviculare*); d. First tarsal bone (*Os tarsale primum* or *os cuneiformes mediale*); e. Second tarsal bone (*Os tarsale secundum* or *os cuneiformes intermedium*); f. Third tarsal bone (*Os tarsale tertium* or *cuneiformes laterale*); g. Fourth tarsal bone (*Os tarsale quartum* or *os cuboideum*); h. The first metatarsal (*Os metatarsale primum*); i. The second metatarsal (*Os metatarsale secundum*); j. The third metatarsal (*Os metatarsale tertium*); k. The fourth metatarsal (*Os metatarsale quartum*); l. The fifth metatarsal (*Os metatarsale quintum*); m. First digit proximal phalanx (*Phalanx proximalis digiti primi*); n. First digit distal phalanx (*Phalanx distalis digiti primi*); o. Third digit proximal phalanx (*Phalanx proximalis digiti tertii*); p. Third digit middle phalanx (*Phalanx media digiti tertii*); q. Third digit distal phalanx (*Phalanx distalis digiti tertii*).

All structures described in the macroscopic image of the tarsus and metatarsus were also identified using the two imaging methods (Figures 16, 17). In the radiographic image, it was possible to visualize the metatarsal and interphalangeal sesamoid bones, as well as the entire phalangeal region (Figure 16). The 3D reconstruction image was limited to the tarsal and tarsal-

476 metatarsal joint areas. The talar support, a structure observed in the calcaneus in caudal view,
477 which forms an articulation with the talus bone, was observed exclusively through 3D
478 reconstruction (Figure 17).
479

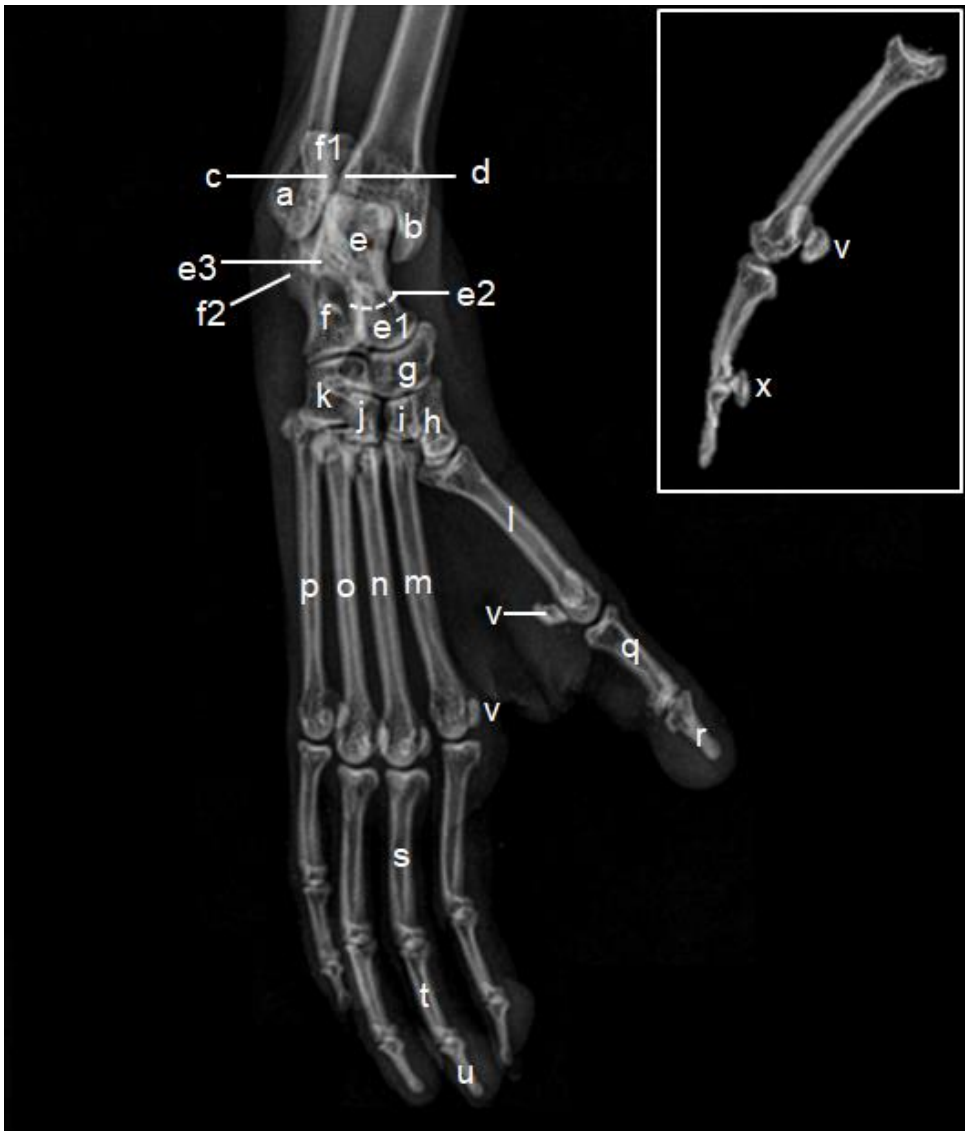

480
481 **FIGURE 16** Radiographic image of the right antimere in dorsoventral projection of the distal
482 epiphysis of the tibia and fibula and dorsoplantar of the tarsus, metatarsus and phalanges. a.
483 Lateral malleolus; b. Medial malleolus; c. Malleolar articular face; d. Fibular notch; e.
484 Talus/Trochlea of the Talus; e1. Talus head; e2. Talus neck; e3. Lateral process of talus; f.
485 Calcaneus; f1. Calcaneal tuberosity; f2. Lateral process of the calcaneal tuberosity; g. Central
486 tarsal bone or navicular bone; h. Tarsal bone I or medial cuneiform bone; i. Tarsal bone II or
487 intermediate cuneiform bone; j. Tarsal bone III or lateral cuneiform bone; k. Tarsal bone IV or
488 cuboid bone; l. Metatarsal bone I; m. Metatarsal bone II; n. Metatarsal bone III; o. Metatarsal
489 bone IV; p. Metatarsal bone V; q. Proximal phalanx of the first digit; r. Distal phalanx of the
490 first digit; s. Proximal phalanx of the third digit; t. Middle phalanx of the third digit; u. Distal
491 phalanx of the third digit; v. Proximal or metatarsal sesamoid bone; x. Distal sesamoid or
492 interphalangeal bone.

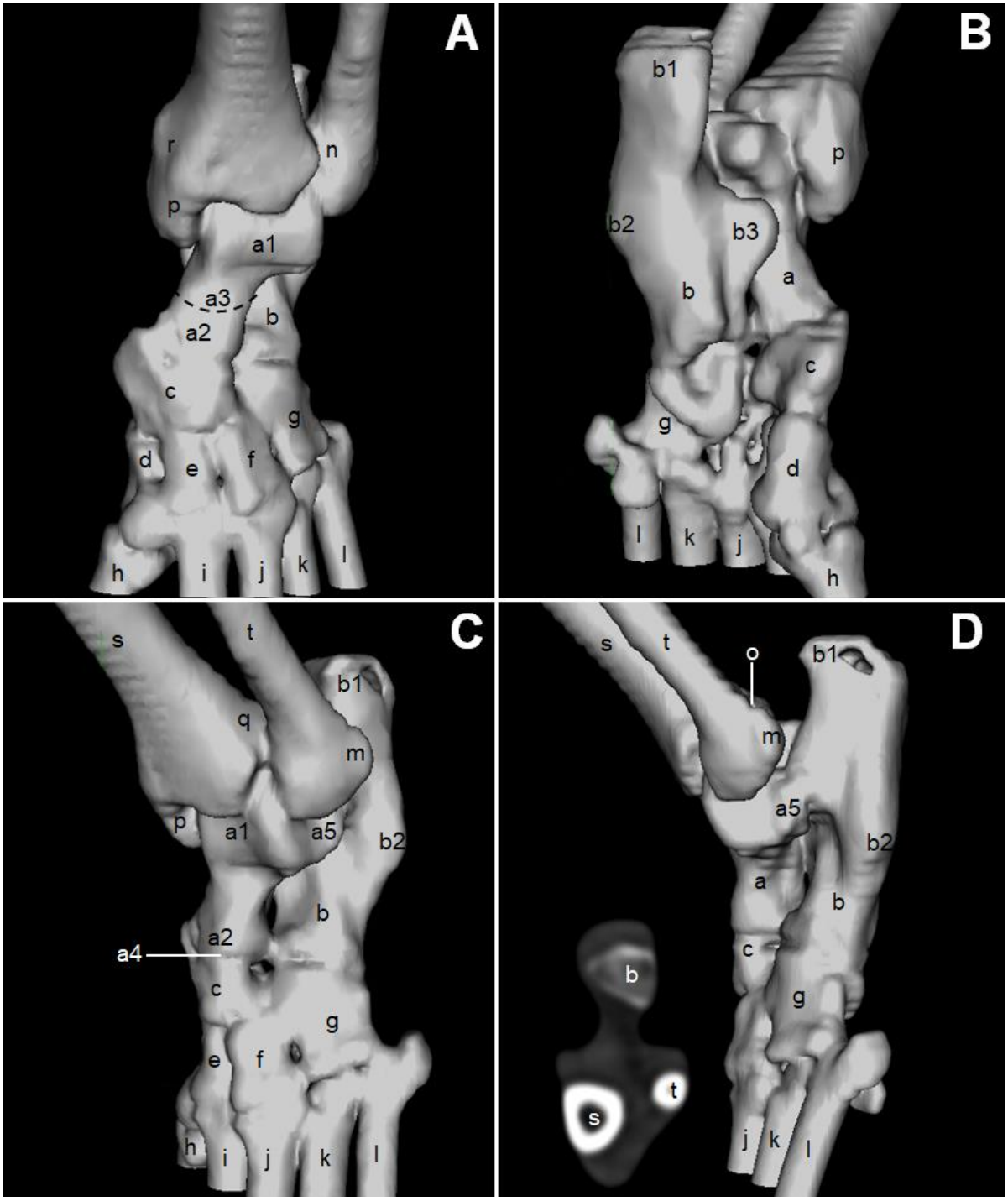

FIGURE 17 Image in 3D reconstruction of the cranial (A), caudal (B), medial (C) and lateral face, with a cross-sectional image at the level of the talocrural joint (D) of the distal epiphysis of the tibia and fibula and bones of the tarsus, metatarsal and phalanges. a. Talus; a1. Trochlea of the talus; a2. Talus head; a3. Talus neck; a4. Articular surface; a5. Lateral process of the talus; b. Calcaneus; b1. Calcaneal tuberosity; b2. Lateral process of the calcaneal tuberosity; b3. Support of the talus; c. Central tarsal bone or navicular bone; d. First tarsal bone or medial cuneiform bone; e. Second tarsal bone or intermediate cuneiform bone; f. Third tarsal bone or lateral cuneiform bone; g. Fourth tarsal bone or cuboid bone; h. The first metatarsal; i. The second metatarsal; j. The third metatarsal; k. The fourth metatarsal; l. The fifth metatarsal; m. Lateral malleolus; n. Malleolar articular surface; o. Lateral malleolar sulcus; p. Medial malleolus; q. Fibular notch; r. Medial malleolar sulcus; s. Body of the tibia; t. Body of the fibula.

4 DISCUSSION

The pelvic limb bones of the *Sapajus libidinosus*, in general, showed an anatomical pattern that was more similar to that observed in larger New-World monkeys, men and Old-World monkeys, in increasing order of proximity, maintaining more distant characteristics from those reported in primates Strepsirrhini and *Tarsius*.

There was no statistical difference regarding the lengths of the bones of the hind limb between males and females, corroborating what was described in the literature, in which, despite discrepancy regarding body weight being reported, with an average of 1.5 to 4 kg for males and females (Kinzey, 1997) and 3165.09 ± 404.94 g for males and 2046.82 ± 362.60 g for females (Silva et al., 2009), the body and head lengths are very similar between the genera, with 465 mm for males and females (Kinzey, 1997), 340-440 mm also for males and females (Groves, 2001) and 377.95 ± 43.19 mm for males and 350.30 ± 35.19 mm for females (Silva et al., 2009).

Leutenegger & Larson (1985), regarding *Callithrix jacchus,* describe that females outnumber males in bone size by about 10%. Despite the numerical superiority of bone size in females of *Sapajus libidinosus*, the results were not statistically significant. In a complementary way, this difference may have been observed because of the limited number of subjects. In addition, different genetic backgrounds, health status, food, and environmental enrichment may also explain this (Casteleyn et al., 2012). Another point to be analyzed is that, among the four male *Sapajus libidinosus*, two juveniles were identified according to the dental parameters, basisphenoid and basioccipital synostosis, and because they presented coronal and lambdoid sutures that were still open and, consequently, the long bones were not fully developed yet, showing lower lengths.

529 The junction between the two coxal bones with the sacrum, through the pelvic
530 symphysis, forms the pelvic cingulum, formed by three bones: ilium, ischium and pubis.
531 Structurally, the thigh bone of *Sapajus libidinosus* was very similar to that of man (Sobotta,
532 2000), *Callimico goeldii* (Hill, 1959), *Callithrix jacchus* (Casteleyn et al., 2012) and *Alouatta*
533 *seniculus* (Mesquita et al., 2019), although the last two are described more superficially. As for
534 morphology, the pelvis of *Sapajus libidinosus* is more similar to that of non-human primates,
535 specifically platyrrhines (Casteleyn et al., 2012; Hill, 1959; Mesquita et al., 2019) than man,
536 which has a shorter upper-lower length (Sobotta, 2000).

537 The pelvic morphology is largely shaped by locomotor and obstetric functions. The
538 pelvis is characterized by being a critical link in the locomotor system of the hind limbs, as the
539 propulsion muscles attach to it, and forces from the limb are transmitted through it to the trunk.
540 For many years there has been discussion about the evolution of bipedal behaviors in hominid
541 fossils, and how the pelvis adapted to this form of locomotion in primates (Ashton et al., 1981;
542 Kibii et al., 2011; Le Gros Clark, 1955; Lovejoy, 2005; Marchal, 2000; Rak & Arensburg, 1987;
543 Reynolds, 1931; Rosenberg, 1992; Weaver & Hublin, 2009).

544 The *Sapajus libidinosus* had a long symphysis, with a relatively open area between the
545 two ischia. Data corroborate with other New World monkeys, and distinguish them from
546 lemurs, in which the pelvis is characterized by a very short symphysis and a long pubic arch
547 and, since the pelvis does not narrow caudally, it does not have much direct support for the
548 viscera when the animal assumes the upright position. The same characteristics are observed in
549 *Tarsius*. Another particularity of this genus is a very long ilium, as observed in the animals in
550 this study, most likely a characteristic of jumping habits (Schultz, 1930; Elftman, 1932). The
551 same authors report a discrepancy between New-World and Old-World monkeys. In the latter,
552 the pubic symphysis is longer, however, the pelvic outlet is relatively smaller. The observation
553 brings the fact that the pelvis of a gibbon, orangutan, chimpanzee, or gorilla has features in

554 which it resembles that of man, rather than that of an ape, and the main feature is a wide iliac
555 plate, commonly considered advantageous for supporting the viscera, as both species often
556 assume an erect or semi-erect position.

557 A penile bone was identified in the four male specimens analyzed in the study, with
558 differences in size and morphology. It was noted that in young animals, it presented a larger
559 size, reaching up to 8 mm and, in adult ones, it presented a reduced size, reaching a minimum
560 of 3 mm. In addition, the morphology of the bone was different, assuming a more rectilinear
561 structure in young subjects, and, in adults, there was a thin cranial process that extends to the
562 glans penis and a more voluminous caudal part. No studies have discussed differences in the
563 penile bone between young and adult primates.

564 The penile bone, also called the baculum, occurs in the distal portion of the penis of
565 placental mammals and develops in the distal septum of the cavernous bodies of the penis,
566 dorsal to the urethra, under partial androgen control during puberty, being classified as a
567 heterotopic bone, or that is, an accessory structure which does not belong to the skeleton (Carosi
568 & Scalici, 2017). Considering that it suffers direct interference from androgens and that with
569 age there is a progressive decline in androgen production (Bonaccorsi, 2001), it is acceptable
570 that there is also a decline in bone structure.

571 This penile bone is widely observed among primates, being found in all families of all
572 infraorders (Simiiformes, including New and Old World monkeys, Lemuriformes,
573 Lorisiformes, Chiromyiformes), except for *Tarsius*. As for the genera, it is absent in some New
574 World monkeys. In the family *Atelidae*, none of the genera have this bone, including *Lagothrix*
575 spp., *Ateles* spp. and *Alouatta* spp. (Dixson, 1987; Horácio & Sampaio, 2015), with a particular
576 exception found by Dixson et al. (2004a) in a hybrid of Muriqui (*Brachyteles hypoxanthus* ×
577 *Brachyteles arachnoides*). Furthermore, in the family Pithecidae, two of the four genera,
578 *Cacajao* spp. and *Chiropotes* spp., also lack the penile bone (Dixson, 1987). Finally, the only

579 representative of Old World monkeys without a penile bone is the man (*Homo sapiens*)
580 (Sobotta, 2000).

581 As for morphology, this is the most varied bone in size and shape, and its variability is
582 particularly useful in identifying species in some taxa (Carosi & Scalici, 2017). In some
583 prosimian species, such as *Cheirogaleus* and *Microcebus*, the penile bone is elongated and
584 emerges slightly from the tip of the penis, where it is covered by a horny pad. When analyzing
585 a ratio between penile bone length and body size, although several primate species show a
586 relationship, notable exceptions are observed. Length varies from 1.5 mm in *Saguinus inustus*,
587 a primate with about 500 g of body weight, to 53.1 mm in *Macaca arctoides*, a primate with
588 about 10 kg of body weight, and much smaller species such as *Galagoides*, which have 63 g of
589 body weight, have a penile bone nine times that of the *Saguinus*, and much larger species, such
590 as the *Gorilla gorilla*, with 160 kg of body weight, can have a penile bone up to four times
591 smaller than that in *Macaca* (Dixson, 1987; Dixson et al., 2004b; Eberhard, 1985).

592 Older and newer primate families show an inverse relationship between penile bone
593 length and body mass. Some prosimian species have a longer than expected penile bone based
594 on body mass, while all great ape species (Hominidae) have a shorter than expected penile bone.
595 New World primates are marked by their small penile bone, in relation to body size, without
596 considering that, except for *Homo* and *Tarsius*, all other genera of primate without penile bone
597 belong to this clade (Carosi & Scalici, 2017). Dixson (1987) reports that, except for *Cebus*,
598 *Sapajus* and *Saimiri*, the other New World monkeys have, in general, the smallest penile bones
599 of the Primate Order. However, this exception contradicts data from this study, in which this
600 bone in *Sapajus libidinosus* measured an average of 5 mm in length, close to that observed in
601 *Callithrix jacchus*, a primate weighing on average 350 g, with a penile bone of 2.5 mm
602 (Casteleyn et al., 2012) and *Cebuella pygmaea*, weighing on average 130 g, with a penile bone
603 of 1.7 mm (Dixson, 1987).

Clinically, a study has shown that the absence of the penile bone in humans makes them more susceptible to erectile dysfunction, considering that men entirely depend on increased blood flow to the penis to maintain an erection, while most primates receive additional assistance from this bone (Schultz et al., 2016). Other studies also describe this relationship between erectile dysfunction and absence of penile bone in men with a multi-case approach and highlight that the appreciation of any physiological process and the subsequent institution of treatment strategies totally depend on a correct understanding of anatomy and physiology (Hsieh et al., 2012; Nicolini et al., 2019). Clinical analyzes report that species with an elongated penile bone have longer intromission times and maintain it after ejaculation, e.g. *Galago crassicaudatus*, *G. senegalensis*, *G. demidouii*, *Loris tardigradus* and *Macaca arctoides*, and species with a short penile bone have relatively brief copulations, with immediate termination of intromission, as, for example, *Callitrichidae* and *Colobinae* (Dixon, 1987).

The femur of *Sapajus libidinosus* was the largest bone in length identified in the body, with an average of 126.5 mm, a characteristic consistent with humans (Sobotta, 2000). Hill (1959) described a 75 mm femur in *Callimico goeldii* and a 57 mm femur was identified in *Callithrix jacchus* (Casteleyn et al., 2012), however, it did not represent the largest bone in length in these animals. A small third trochanter was reported in *Callimico goeldii* (Hill, 1959), opposing this study with *Sapajus libidinosus*, *Alouatta seniculus* (Mesquita et al., 2019), *Callithrix jacchus* (Casteleyn et al., 2012) and man (Sobotta, 2000). A smaller trochanter was not observed in *Presbytis rubicunda*, a primate of the Cercopithecidae family (Rafferty, 1998). More subtle structures identified in *Sapajus libidinosus*, such as the intertrochanteric line, *linea aspera* and pectineal line, were not clearly represented in *Callimico goeldii* (Hill, 1959) and *Callithrix jacchus* (Casteleyn et al., 2012), in contrast to what was observed in humans (Sobotta, 2000) and in *Alouatta seniculus* (Mesquita et al., 2019), in which only the intertrochanteric line was not identified. A small gluteal tuberosity was identified in this study, corroborating data

629 from man (Sobotta, 2000) and *Alouatta seniculus* (Mesquita et al., 2019), and it presented as a
630 robust structure in *Propithecus diadem*, a lemur (Rafferty, 1998) and in *Galago senegalensis*
631 (Burr et al., 1982).

632 In terms of shape, the femur of *Sapajus libidinosus*, as well as of other primates, in
633 general, shows similarities, presenting both a proximal and distal epiphysis with larger well-
634 delimited structures in *Pongo pygmaeus*, *Hylobates syndactylus*, *Ateles fusciceps*, *Colobus*
635 *guereza*, *Trachypithecus cristatus*, *Propithecus diadema* (Rafferty, 1998), *Galago senegalensis*
636 (Burr et al., 1982), *Callimico goeldii* (Hill, 1959), *Callithrix jacchus* (Casteleyn et al., 2012),
637 *Alouatta seniculus* (Mesquita et al., 2019) and baboon (Yamanaka et al., 2005). However,
638 differences are identified when a detailed comparative study of bone morphometry and the size
639 of structures is performed (Hershkovitz, 1988).

640 Burr (1989) conducted a study comparing the transverse geometry of the femur in three
641 species of monkeys with different behaviors, *Macaca nemestrina* and *M. mulatta*, which behave
642 in terrestrial and arboreal environments, the first being almost completely quadrupedal in
643 locomotion (Rodman, 1979; Rodman & McHenry, 1980) and *M. fascicularis*, which is more
644 arboreal than the other species, spending less than 2% of its time on the ground, with
645 quadrupedal locomotion (Cant, 1988; Rodman, 1979), and concluded that the "barrel-shaped"
646 femur - in which flexion and torsional stiffness are greater in the mid-axis of the bone, compared
647 to the proximal and distal areas - may be associated, but not restricted, to jumping behaviors,
648 as well as the structural rigidity of the femur is greater in primates that spend more time in
649 terrestrial environments.

650 The patella articulates in the supratrochlear region of the femur. Primates show varying
651 degrees of specialization of this bone morphology, whether associated with locomotion posture
652 or knee range of motion and patellar mechanics (Lovejoy, 2007). This triangular-shaped
653 sesamoid with a well-rounded apex in *Sapajus libidinosus* differs from the ovoid patella of

654 *Callithrix jacchus* (Casteleyn et al., 2012), subsquare with rounded angles in *Callimico goeldii*
655 (Hill, 1959), and triangular with an acute apex in man. (Sobotta, 2000).

656 The second-longest bone in the body of *Sapajus libidinosus* is the tibia, measuring an
657 average of 118.5 mm. On the other hand, data from *Callimico goeldii*, with 75.5 mm (Hill,
658 1959) and *Callithrix jacchus*, with 60 mm (Casteleyn et al., 2012), highlight the tibia as the
659 largest bone in the body in these animals, with length superior to the femur. Hill (1959) reports
660 that this statement is true among the Callithrichids. The fibula had a length of 111.5 mm in
661 *Sapajus libidinosus*, 71 mm in *Callimico goeldii* (Hill, 1959) and 58 mm in *Callithrix jacchus*
662 (Casteleyn et al., 2012), even higher, in the latter, than that described for the femur.

663 Both in terms of shape and structures, the tibia and fibula of *Sapajus libidinosus*
664 resemble those of men (Sobotta, 2000), chimpanzees (Marchi, 2015), *Callimico goeldii* (Hill,
665 1959), *Callithrix jacchus* (Casteleyn et al., 2012) and *Alouatta seniculus* (Mesquita et al., 2019),
666 being more robust in the first two. In *Tarsius*, Marchi (2015) reports a thinner and more
667 incomplete fibula, which runs only up to the middle third of the tibia where it fuses, different
668 from the previously described primates. The same author reports it is characteristic of jumping
669 mammals.

670 The tibia, together with the femur, carries most of the body weight during locomotion,
671 whereas the fibula is often relegated, by anatomists and anthropologists, to an inferior position
672 and has even been described as having a vestigial function in humans (Moore and Dalley, 2006).
673 As a result, bone assessment studies focused on locomotion generally neglect the fibula,
674 however, studies performed on human samples have shown that, of all the weight carried by
675 the leg during plantigrade locomotion, the load imposed on the fibula is considerable,
676 representing 6% to 19% depending on ankle position (Funk et al., 2004; Goh et al., 1992;
677 Lambert, 1971; Takebe et al., 1984; Wang et al., 1996).

678 In contrast, in non-human mammals, the fibula is one of the most important supporting
679 structures of the leg (Walmsley, 1918; Barnett and Napier, 1953). Mainly arboreal hominoids
680 such as gibbons, orangutans and chimpanzees have greater relative fibular robustness compared
681 to essentially terrestrial hominoids such as gorillas and humans. These differences are likely a
682 consequence of three factors: the degree of leg adduction (Schmitt, 2003; Carlson et al., 2005),
683 the degree of ankle dorsiflexion (DeSilva, 2009), and the degree of peroneal mobility (Barnett
684 & Napier, 1953), which are greater in animals that move on uneven terrains, such as carnivores,
685 and especially in primates that live in an arboreal environment, probably subjecting them to
686 greater load than that received by the fibula of terrestrial hominoids (Carleton, 1941; Walmsley,
687 1918).

688 Barnett & Napier (1953) follow the same line as the previous authors regarding the
689 relative proportions of the tibia and fibula and emphasize that, in burrowing and swimming
690 mammals, the fibula is more robust in relation to the tibia. In jumping mammals, it is less robust
691 and more flexible, and of intermediate size in those adapted to uneven surfaces in trees or on
692 the ground, such as primates and carnivores. Carlson et al. (2005) found that during quadrupedal
693 arboreal locomotion, lemurs exerted laterally directed forces more often than when moving on
694 the ground, generating a greater fibular load.

695 Le Minor (1992) performed a radiographic study with 246 adult non-human primates
696 belonging to 34 genera and observed, in some species, a popliteal sesamoid bone in the
697 popliteus muscle tendon, which articulates caudally in the lateral condyle of the tibia, very close
698 to the fibular articular surface and the fibular head, being considered, in primates, a primitive
699 character. The author reports that the popliteal bone has been identified in all prosimians and
700 Callitrichids, variably observed in Atelidae and *Pongo*, commonly absent in *Gorilla*, and absent
701 or very rare in *Cebus*, Cercopithecidae, Hylobatidae, *Pan* and man. The statement made
702 regarding the genera *Cebus* corroborates the data of our study and works conducted by Forster

703 (1903), Pearson & Davin (1921), Taylor & Bonney (1905) and Vallois (1914), who report that
704 it is a bone always absent in the genera.

705 The oldest tarsal remains of mammals are those of trichodondons, which were the first
706 known mammals nearly 200 million years ago, possibly evolved from cynodonts, mammal-like
707 reptiles of the early Middle Triassic (Szalay, 1982; Szalay & Decker, 1974). Probably the most
708 significant functional change in the early evolution of the foot of a mammal of reptilian ancestry
709 was the progressive development of the superposition of the talus over the calcaneus, which in
710 the ancestors was positioned medially to each other, with a joint between the fibula and the
711 calcaneus, causing the fibula to have a greater weight-bearing function. This function of the
712 fibula was reduced with the evolution of the talus superposition, leaving the tibia as the main
713 weight-bearing structure of the leg. This evolution of talar superposition also promoted a
714 functional change in the foot, making pronation-supination movements possible and extensive
715 in the subtalar joint complex (Lewis, 1964, 1980).

716 The tarsal bones are equal in number and general arrangement to those of men (Sobotta,
717 2000), *Callimico goeldii* (Hill, 1959), *Callithrix jacchus* (Casteleyn et al., 2012), *Alouatta*
718 *seniculus* (Mesquita et al., 2019), baboons and chimpanzees (Swindler & Wood, 1973).
719 However, the modern human foot, compared to all other primates, is functionally and
720 morphologically distinct, and very short regarding the total length of the lower limb (Gebo,
721 1992; Klenerman & Wood, 2006; Lewis, 1989). Nowak et al. (2010) report that humans are
722 unique as they, compared to other primates, lack mobility in the mid and distal region of the
723 foot. This greater rigidity in our species is often attributed to stability during bipedalism,
724 however, medial and distal mobility in the foot of non-human primates facilitates the diversity
725 of postural modes observed, such as digitigrade, semiplantigrade and plantigrade, as well as the
726 locomotion they exhibit in arboreal environments and highly variable terrain (Gebo, 1992;
727 Meldrum, 1993).

Olson & Seidel (1983) describe that, among the characteristics included in the initial definition of the order Primates, are pentadactyly and independently mobile digits, anatomical characteristics that make possible the arboreal way of life, and the adaptation to grab, climb and jump between trees. They also report that primates have at least one pair of gripping extremities, of which the foot is usually the most adapted to the function, with the finger I being generally opposable as well, and as a facilitating method, the distal phalanges of the primate feet normally have flat and short nails, instead of pointed claws, allowing greater contact between the substrate and the plantar surface.

While the foot anatomy of Cebidae, such as *Sapajus libidinosus*, differs little from that observed in Old World monkeys (Swindler & Wood, 1973) and *Alouatta seniculus* (Mesquita et al., 2019), which have nails in all digits, Callitrichids are a notable exception, as they have claws on all toes, except digit I (Olson & Seidel, 1983), corroborating a study on *Callimico goeldii* (Hill, 1959) and *Callithrix jacchus* (Casteleyn et al. , 2012).

The last common ancestor of primates differed from other mammals as it had nails on all known digits except the second toe (Patel et al., 2015). Some other primates, such as prosimians (*Lemur*, *Lorinae*, *Galago* and *Tarsius*), have developed this same specialized claw on the second or third toe, known as the cleaning claw (Paciulli & Chennu, 2018). This feature was not identified in the animals of this study, in *Callimico goeldii* (Hill, 1959), *Callithrix jacchus* (Casteleyn et al., 2012), *Alouatta seniculus* (Mesquita et al., 2019) and in Old World primates (Swindler & Wood, 1973).

Le Minor & Winter (2003) have investigated a series of 306 non-human primates of 40 different genera, a series of 412 human metatarsal bones, and addressed the occurrence and morphology of an intermetatarsal articular facet in the first metatarsal bone in 30.8% of humans, with no occurrence in any of the non-human primates. *Callimico goeldii* (Hill, 1959), *Callithrix jacchus* (Casteleyn et al., 2012) and *Alouatta seniculus* (Mesquita et al., 2019) corroborate with

753 this study. The authors attributed the appearance of this new articular facet in humans to an
754 adaptation related to general morphological changes of the foot, resulting from bipedalism.

755 In addition to the importance of discussing studies focused on anatomomorphological
756 and evolutional characteristics, bone anatomical knowledge and the identification of normal
757 and abnormal, associated with diagnostic imaging methods, have been addressed in a series of
758 studies and have largely contributed to the recognition of malformation patterns, in the
759 diagnosis of constitutional diseases of the bones, identification of abnormalities, clinical
760 evaluation and development of the course of the disease, determination of morphometric
761 characteristics, number of bones, density, ossification time, etc., which may provide
762 indispensable signs in the recognition of several pathologies, contributing, at the same time, to
763 a better approach and clinical-surgical planning, besides the institution of adequate treatment.

764 In this regard, Caffey (1958) reported the importance of anatomical knowledge of the
765 pelvis in the diagnosis of bone dysplasias. Jana et al. (2017) discussed several common, and
766 some uncommon, radiological findings on pelvic radiographs and concluded that this exam is
767 an important component of the skeletal examination in suspected dysplasia. Fonteles et al.
768 (2010) reported the occurrence of hip dysplasia in a female *Cebus libidinosus,* and Kealy (2005)
769 stated that radiography is the only method available to conclusively demonstrate the presence
770 or absence of anatomical changes associated with this disease in live animals.

771 The genital region was also explored by Spani et al. (2020), in which, through a 3D
772 study of 13 different species of primates, reported that the high resolution of 3D micro-CT
773 images revealed variability in addition to that available in 2D images from previous studies,
774 and showed for the first time new internal and external morphological structures.

775 Link et al. (1998) used high-resolution magnetic resonance and computed tomography
776 to study the trabecular vertebral and femoral structure of humans and compare these techniques
777 with bone mineral density in predicting bone strength, and concluded that these techniques can

778 be widely used clinically, whether to assess the course of osteoporosis or other metabolic bone
779 diseases, as they are decisive in the texture analysis of trabecular bone images, in the prediction
780 of bone strength, risk of fracture, measurement of bone histomorphometry in vivo,
781 understanding the pathophysiology of the disease, and monitoring new forms of treatment.

782 Tomography was also used by Ryan & Sukhdeo (2016), allowing the reconstruction of
783 the pelvic girdle and the distal epiphysis of the fragmented femur through rigid transformations
784 of isosurface reconstructions, highlighting the macroscopic knowledge and the use of more
785 advanced imaging methods as an excellent basis for the anatomical study, determination of
786 pathologies, and establishment of appropriate treatments.

787 There was a study using radiography aimed at determining whether natural osteoarthritis
788 of the knee joints, similar to the condition in humans, developed in *Macaca fasciculares*. The
789 research involved 58 animals and concluded that the species can be a useful model for the study
790 of osteoarthritis in humans (Carlson et al., 1994), increasing the importance of a knowledge of
791 bone anatomy in research, seeking to have primates as biological models.

792 Radiological techniques and images reconstructed with computed tomography have also
793 been used to monitor progressive changes in the compact bone in the tibia, and to assess loss of
794 tibial bone mass during restraint in monkeys during experimentally induced osteopenia (Young
795 & Schneider, 1981). Jungers & Minns (1979) stated that computed tomography is an ideal
796 technique for analyzing the transverse geometry of long bones from intact fossils, even when
797 they are highly mineralized, and their medullary cavities are occluded by the matrix. These
798 same authors conducted a study with the tomography of the femur and tibia of *Megaladapis*
799 *edwardsi* and *Indri indri*, in order to demonstrate the usefulness of this method in the evaluation
800 of the relationship between the fossil structure and function, geometric and biomechanical
801 properties of the bone, reaching a positive conclusion.

802 Mundinger et al. (2011) developed a fibular vascularized composite tissue
803 allotransplantation model in *Macaca fascicularis* to investigate the healing and rejection
804 patterns of bone and associated tissues and used serial radiographs during six months of follow-
805 up of the animals. The authors stated that, despite chronic rejection in two animals, serial
806 radiological images showed bone healing and donor-recipient bone union within 10 weeks in
807 all animals, proving to be an excellent method of allotransplantation evaluation.

808 Radiography was also used to follow the course of diseases that resembled osteitis
809 deformans in an adult male *Macaca Mulatta* (Hughes & Lang, 1971). Specific radiographic
810 criteria were used to analyze the maturation of the appendicular skeleton in a colony of rhesus
811 monkeys (Silverman et al., 2005). The first radiographic analysis comparing the secondary
812 ossification of the limbs of a newborn *Callimico goeldii* with representatives of marmosets
813 (*Callithrix jacchus*) and tamarins (*Saguinus oedipus*) was performed by Hofmann et al (2007).

814 Among many other aspects addressed in the literature, anatomy and imaging resources
815 also have their importance in paleontology. High-resolution computed tomography scan data
816 were collected to visualize and quantify the internal and external anatomical structures of each
817 element of the partial skeleton of *Australopithecus afarensis*, and the authors reported that the
818 use of the method is an excellent opportunity to reconstruct aspects of the paleobiology of the
819 species (Ryan & Sukhdeo, 2016). A macroscopic and radiographic evaluation was performed
820 on well-preserved skeletal remains of an animal of the genus *Macaca*, to investigate
821 hypertrophic osteoarthropathy (Hirst & Waldron, 2019). These and many other studies
822 highlight the importance of anatomical bone knowledge and efficiency in the identification of
823 anatomical structures in imaging methods for the various areas within primatology.

5 CONCLUSION

By describing the bone anatomy of the hind limb and identifying it in tomographic and radiographic images in *Sapajus libidinosus* and considering that the literature is still scarce in this species, especially regarding morphological aspects associated with imaging exams, this research enables a series of studies focused on bone malformation, skeletal pathologies, evaluation of disease development, clinic, surgery, surgical planning, treatment adequacy, skeletal morphophysiology, and paleontology, besides serving as a compilation within medicine and for primatologists. It was possible to verify the efficiency of diagnostic imaging methods, demonstrating that it is possible to identify the bone structures of the hind limb with precision, mainly through 3D reconstruction, when compared to images of bone parts. *Sapajus libidinosus* presented structurally and morphologically more similar anatomical characteristics to the primates of the infraorder Simiiformes, being an excellent indicator of an experimental model for studies in man. This material generates a basis for further research. It can also help in the refinement of research protocols and, at the same time, in the reduction of animals in experiments.

ACKNOWLEDGMENTS

The authors thank CETAS/IBAMA-Natal, on behalf of the environmental analyst and Veterinary Doctor Tiago Saulo Freire Costa, for the help and agreement in using the animals, and to the Coordination for the Improvement of Higher Education Personnel (CAPES) for the doctoral scholarship. They also thank the staff of the Instituto de Radiologia de Natal (IRV), for all the support in conducting the tomography and radiographic exams, and the Potiguar University (UnP), for the partnership established and competence in conducting the radiographic exams.

CONFLICT OF INTERESTS

All authors declare that there is no conflict of interest in the present study.

AUTHOR CONTRIBUTIONS

Ana Yasha F. de La Salles: Conceptualization (lead); data curation (lead); formal analysis (lead); research (lead); methodology (lead); project administration (support); resources (lead); software (lead); supervision (support); validation (equal); visualization (lead); original draft writing (lead); writing-reviewing and editing (lead). **Jéssica K. de Andrade:** Conceptualization (equal); formal analysis (support); research (support); resources (support); supervision (support); visualization (support). **Joyce G. de Souza:** Conceptualization (equal); formal analysis (support); research (support); resources (support); visualization (support). **Kelvis de B. Freitas:** Conceptualization (equal); formal analysis (support); research (support); resources (support); visualization (support). **Artur da N. Carreiro:** Conceptualization (equal); formal analysis (support); research (support); resources (support); visualization (support). **Edson Vinícius L. Veloso:** Conceptualization (equal); formal analysis (support); research (support); resources (support); visualization (support). **Ediane F. Rocha:** Conceptualization (equal); formal analysis (support); research (support); resources (support); visualization (support). **Marcius Alessandro P. Klem:** Conceptualization (support); data curation (support); formal analysis (support); methodology (support); resources (support); software (lead); supervision (support); visualization (support). **Fábio Tatian M. Mendonça:** Conceptualization (equal); formal analysis (support); research (support); resources (support); visualization (support). **Danilo José A. de Menezes:** Conceptualization (lead); data curation (lead); formal analysis (lead); research (lead); methodology (lead); project administration (lead); resources (lead); software (support); supervision (lead); validation (lead); visualization (lead); original draft writing (support); writing-reviewing and editing (lead).

DATA AVAILABILITY STATEMENT

Data supporting the results of this study are available from the corresponding author upon reasonable request.

ORCID

Ana Yasha Ferreira de La Salles https://orcid.org/0000-0003-2104-3539

Jéssica Kária de Andrade https://orcid.org/0000-0002-0039-8456

Joyce Galvão de Souza https://orcid.org/0000-0001-5492-6317

Kelvis de Brito Freitas https://orcid.org/0000-0002-4851-0734

Artur da Nóbrega Carreiro https://orcid.org/0000-0002-2131-7432

Edson Vinícius Leite Veloso https://orcid.org/0000-0002-1533-8499

Ediane Freitas Rocha https://orcid.org/0000-0003-4671-3906

Marcius Alessandro Pessanha Klem https://orcid.org/0000-0002-9097-6175

Fábio Tatian Moura Mendonça https://orcid.org/0000-0001-9770-2997

Danilo José Ayres de Menezes https://orcid.org/0000-0001-6089-3283

REFERENCES

Alfaro, J. W. L., Izar, P., & Ferreira, R. G. (2014). Capuchin monkey research priorities and urgent issues. *American Journal of Primatology*, 76 (8), 705-720. 10.1002/ajp.22269

Ashton, E. H., Flinn, R. M., Moore, W. J., Oxnard, C. E., & Spence, T. F. (1981). Further quantitative studies of form and function in the primate pelvis with special reference to Australopithecus. *Transactions of the Zoological Society of London*, 36 (1), 1–98. 10.1111/j.1096-3642.1981.tb00063.x

899 Barnett, C. H., & Napier, J. R. (1953). The rotatory mobility of the fibula in eutherian mammals.
900 *Journal of Anatomy*, 87 (1), 11-21. PMID: 13022578; PMCID: PMC1244562.
901
902 Bonaccorsi, A. C. (2001). Andropausa: Insuficiência androgênica parcial do homem idoso.
903 Uma Revisão. *Arquivos brasileiros de endocrinologia e metabologia*, 45 (2), 123-133.
904 10.1590/S0004-27302001000200003
905
906 Burr, D. B., Piotrowski, G., Martin, R. B., & Cook, P. N. (1982). Femoral mechanics in the
907 lesser bushbaby (*Galago senegalensis*): Structural adaptations to leaping in primates. *The*
908 *Anatomical Record*, 202 (3), 419-429. 0.1002/ar.1092020314
909
910 Burr, D. B., Ruff, C. B., & Johnson, C. (1989). Structural adaptations of the femur and humerus
911 to arboreal and terrestrial environments in three species of macaque. *American Journal of*
912 *Physical Anthropology*, 79 (3), 357-367. 10.1002/ajpa.1330790312.
913
914 Caffey, J. (1958). Achondroplasia of pelvis and lumbo-sacral spine: Some roentgenographic
915 features. *American Journal of Roentgenology*, 80 (3), 449–57. PMID: 13571498.
916
917 Cant, J. G. H. (1988). Positional behavior of long-tailed macaques (*Macaca fascicularis*) in
918 Northern Sumatra. *American Journal of Biological Anthropology*, 76 (1), 29-37.
919 10.1002/ajpa.1330760104.
920
921 Carleton, A. (1941). A comparative study of the inferior tibio-fibular joint. *Journal of Anatomy*,
922 76 (1), 45-55. PMCID: PMC1252714; PMID: 17104879

923 Carlson, C. S., Loeser, R. F., Jayo, M. J., Weaver, D. S., Adams, M. R., & Jerome, C. P. (1994).
924 Osteoarthritis in cynomolgus macaques: a primate model of naturally occurring disease.
925 *Journal of Orthopaedic Research*, 12 (3), 331-339. 10.1002/jor.1100120305.
926
927 Carlson, K.J., Demes, B., & Franz, T.M. (2005). Mediolateral forces associated with
928 quadrupedal gaits of lemurids. *Journal of Zoology*, 266 (3), 261-273,
929 10.1017/S0952836905006874
930
931 Carosi, M., & Scalici M. (2017). Baculum (Os Penis). In A. Fuentes (Ed.), *The International*
932 *Encyclopedia of Primatology* (pp. 1-5). Portugal: Porto Editora.
933
934 Casteleyn, C., Bakker, J., Breugelmans, S., Kondova, L., Saunders, J., Langermans, J. A. M.,
935 Cornillie, P., Van den Broeck, W., Van Loo, D., Van Hoorebeke, L., Bosseler, L., Chiers, K.,
936 & Decostere, A. (2012). Anatomical description and morphometry of the skeleton of the
937 common marmoset (*Callithrix jacchus*). *Laboratory Animals*, 46 (2), 152-63.
938 10.1258/la.2012.011167
939
940 Del-Claro, K. (2004). *Comportamento Animal - Uma introdução à ecologia comportamental*.
941 Jundiaí: Livraria Conceito.
942
943 DeSilva, J. M. (2009). Functional morphology of the ankle and the likelihood of climbing in
944 early hominins. *Proceedings of the National Academy of Sciences*, 106 (16), 6567-6572.
945 10.1073/pnas.0900270106

946 Diniz, L. S. M. (1997). *Primatas em cativeiro: Manejo e problemas veterinários, enfoque para*
947 *espécies neotropicais*. São Paulo: Ícone.
948
949 Dixson, A. F. (1987). Baculum length and copulatory behavior in Primates. *American Journal*
950 *of Primatology*, 13 (1), 51–60. 10.1002/ajp.1350130107
951
952 Dixson, A. F., Pissinatti, A., & Anderson, M. J. (2004a). Observations on genital morphology
953 and anatomy of a hybrid male muriqui (Genus *Brachyteles*). *Folia Primatologica*, 75 (2), 61-
954 69. 10.1159/000076264
955
956 Dixson, A. F., Nyholt, J., & Anderson, M. (2004b). A positive relationship between baculum
957 length and prolonged intromission patterns in mammals. *Acta Zoologica Sinica*, 50 (4), 490–
958 503.
959
960 Eberhard, W. G. (1985). *Sexual Selection and Animal Genitalia*. Cambridge: Harvard
961 University Press.
962
963 Elftman, H. O. (1932). The evolution of the pelvic floor of primates. *American Journal of*
964 *Anatomy*, 51 (2), 307-346. 10.1002/aja.1000510203
965
966 Fonteles, Z. G. C., Quessada, A. M., Alcantara, D. S., & Sousa, J. M. (2010). Aspectos
967 radiográficos da displasia coxofemoral em um *Cebus libidinosus*: Relato de caso. *Pubvet*, 4
968 (24), 872-878.

969 Forster, A. (1903). Die insertion des musculus semimembranosus. Eine
970 vergleichendanatomische Betrachtung. *Arch Anat Entw Gesch*, 1903, 257-320.
971
972 Funk, J. R., Rudd, R. W., Kerrigan, J. R., & Crandall, J. R. (2004). The effect of tibial curvature
973 and fibular loading on the tibia index. *Traffic Injury Prevention*, 5 (2), 164-172.
974 10.1080/15389580490436069
975
976 Gebo, D. L. (1992). Plantigrady and foot adaptation in African apes: implications for hominid
977 origins. *American Journal of Physical Anthropology*, 89 (1), 29–58. 10.1002/ajpa.1330890105
978
979 Goh, J. C. H., Lee, H. H., Ang, E. J., Bayon, P., & Pho, R. W. H. (1992). Biomechanical study
980 on the load-bearing characteristics of the fibula and the effects of fibular resection. *Clinical*
981 *Orthopaedics and Related Research*, 279, 223-228. 10.1097/00003086-199206000-00028
982
983 Gros-Louis, J., Perry, S., & Manson, J. H. (2003). Violent coalitionary attacks and intraspecific
984 killing in wild white-faced capuchin monkeys (*Cebus capucinus*). *Primates*, 44(4), 341–346.
985 10.1007/s10329-003-0050-z
986
987 Groves, C. P. (2001). *Primate taxonomy*. Washington: Smithsonian Institution Press.
988
989 Hershkovitz, P. (1988). The subfossil monkey femur and subfossil monkey tibia of the Antilles:
990 A review. *International Journal of Primatology*, 9 (4), 365–384. 10.1007/bf02737383

991 Hill, W. C. O. (1959). The Anatomy of *Callimico goeldii* (Thomas): A Primitive American
992 Primate. *Transactions of the American Philosophical Society, New Series*, 49 (5), 1-116.
993 10.2307/1005807
994
995 Hirst, C. S., & Waldron, T. (2019). Hypertrophic osteoarthropathy in an adult macaque.
996 *International Journal of Paleopathology*, 25, 39–45. 10.1016/j.ijpp.2019.04.002
997
998 Hofmann, M. I., Schradin, C., & Geissmann, T. (2007). Radiographic evaluation of neonatal
999 skeletal development in *Callimico goeldii* reveals closer similarity to *Callithrix jacchus* than to
1000 *Saguinus oedipus*. *American Journal of Primatology*, 69 (4), 420–433. 10.1002/ajp.20361.
1001
1002 Horácio, S., & Sampaio, I. (2015). The systematics and evolution of New World Primates - A
1003 Review. *Molecular Phylogenetics and Evolution*, 82, 348–357. 10.1016/j.ympev.2013.10.017.
1004
1005 Hsieh, C., Liu, S., Hsu, G., Chen, H., Molodysky, E., Chen, Y., & Yu, H. (2012). Advances in
1006 understanding of mammalian penile evolution, human penile anatomy and human erection
1007 physiology: clinical implications for physicians and surgeons. *Medical Science Monitor*, 18 (7),
1008 118-25. 10.12659/MSM.883201
1009
1010 Hughes, H. C., & Lang, C. M. (1971). Osteitis deformans in a macaque (*Macaca mulatta*).
1011 *Veterinary Pathology*, 8 (5-6), 414-420. 10.1177/0300985871008005-00603
1012
1013 International Committee on Veterinary Gross Anatomical Nomenclature. (2017). *Nomina*
1014 *Anatomica Veterinária.* 6 ed. Hanover, Ghent, Columbia, MO, Rio de Janeiro: Editorial
1015 Committee.

1016 Jana, M., Nair, N., Gupta, A. K., Kabra, M., & Gupta, N. (2017). Pelvic radiograph in skeletal
1017 dysplasias: An approach. *Indian Journal of Radiology and Imaging*, 27 (2), 187–199.
1018 10.4103/ijri.IJRI_367_16
1019
1020 Johnson-Delaney, C. A. (1994). Primates. *Veterinary Clinics of North America: Small Animal*
1021 *Practice*, 24 (1), 121-152. 10.1016/s0195-5616(94)50007-x
1022
1023 Jungers, W. L., & Minns, R. J. (1979). Computed tomography and biomechanical analysis of
1024 fossil long bones. *American Journal of Biological Anthropology*, 50 (2), 285-290.
1025 10.1002/ajpa.1330500219
1026
1027 Kealy, J. K. (2005). *Radiologia e ultra-sonografia do cão e gato*. São Paulo: Editora Manole.
1028
1029 Kibii, J. M., Churchill, S. E., Schmid, P., Carlson, K. J, Reed, N. D, Ruiter, D. J., & Berger, L.
1030 R. (2011). A partial pelvis of *Australopithecus sediba*. *Science*, 333 (6048), 1407–1411.
1031 10.1126/science.1202521
1032
1033 Kinzey, W. G. (1997). *Cebu*s. In W. G. Kinzey (Ed.), *New World Primates: Ecology, Evolution,*
1034 *and Behavior* (pp. 248-257). New York: Aldine de Gruyter.
1035
1036 Klenerman, L., & Wood, B. (2006). *The human foot: a companion to clinical studies*.
1037 Heidelberg: Springer.
1038
1039 La Salles, A. Y. F, Cordeiro, J. F., Santos, J. R. S, Carreiro, A. N., Medeiros, G. X., & Menezes,
1040 D. J. A. (2017). Anatomical description of the main vessels for venipuncture in the black-striped

capuchin monkey (*Sapajus libidinosus*, Silva Junior, 2002). *Journal of Medical Primatology*, 46 (6), 320-326. 10.1111/jmp.12291

La Salles, A. Y. F., Andrade, J. K., Lemos, K. K. A, Carreiro, A. N., Souza, J. G, Costa, T. S. F., Reinaldo, M. P. O. S., Souza, A. P., & Menezes, D. J. A. (2019). Electrocardiographic parameters of *Sapajus libidinosus* (SPIX, 1823) after chemical immobilization with tiletamine-zolazepam. *Journal of Medical Primatology*, 48 (3), 154-160. 10.1111/jmp.12403

La Salles, A. Y. F., Andrade, J. K., Cordeiro, J. F., Carreiro, A. N., Falcão, B. M. R., Freitas, K. B., & Menezes, D. J. A. (2021). Assessment of the technique of the anesthetic block of the Brachial Plexus by Supraclavicular approach in *Sapajus libidinosus* (SPIX, 1823). *Journal of Medical Primatology*, 50 (1), 29-35. 10.1111/jmp.12492

Ladeira, L. M. C. E. B., & Höfling, E. (2007). Osteologia craniana de Bucconidae. *Boletim do Museu Paraense Emílio Goeldi Ciências Naturais*, 2 (1), 117-153.

Lambert, K. L. (1971). The weight-bearing function of the fibula. A strain gauge study. *The Journal of Bone and Joint Surgery*, 53-A (3), 507-513. PMID: 5580009

Le Gros Clark, W. E. (1955). *The fossil evidence for human evolution*. Chicago: University of Chicago Press.

Le Minor, J. M. (1992). Brief communication: The popliteal sesamoid bone (Cyamella) in Primates. *American Journal of Physical Anthropology*, 87 (1), 107-110. 10.1002/ajpa.1330870109

1066 Le Minor, J. M., & Winter, M. (2003). The intermetatarsal articular facet of the first metatarsal
1067 bone in humans: a derived trait unique within primates. *Annals of Anatomy*, 185 (4), 359-365.
1068 10.1016/s0940-9602(03)80061-4
1069
1070 Leutenegger, W., & Larson, S. (1985). Sexual dimorphism in the postcranial skeleton of New
1071 World primates. *International Journal of Primatology*, 44 (2), 82–95. 10.1159/000156199
1072
1073 Lewis, O. J. (1964). The homologies of the mammalian tarsal bones. *Journal of Anatomy*, 98
1074 (2), 195-208. PMCID: PMC1261275; PMID: 14154422
1075
1076 Lewis, O. J. (1980). The joints of the evolving foot. Part II. The intrinsic joints. *Journal of*
1077 *Anatomy*, 130 (4), 833-857. PMCID: PMC1233206; PMID: 7429971
1078
1079 Lewis, O. J. (1989). *Functional morphology of the evolving hand and foot*. Oxford: Clarendon
1080 Press.
1081
1082 Lima, M. G. M., Buckner, J. C., Silva-Júnior, J. S., Aleixo, A., Martins, A. B., Boubli, J. P.,
1083 Link, A., Farias, I. P., Silva, M. N., Röhe, F., Queiroz, H., Chiou, K. L., Fiore, A. D., Alfaro,
1084 M. E., & Alfaro, J. W. L. (2017). Capuchin monkey biogeography: understanding *Sapajus*
1085 Pleistocene range expansion and the current sympatry between *Cebus* and *Sapajus*. *Journal of*
1086 *Biogeography*, 44 (4), 810-820. 10.1111/jbi.12945
1087
1088 Link, T. M., Majumdar, S., Lin, J. C., Newitt, D., Augat, P., Ouyang, X., Mathur, A., & Genant,
1089 H. K. (1998). A comparative study of trabecular bone properties in the spine and femur using

high resolution MRI and CT. *Journal of Bone and Mineral Research*, 13 (1), 122-132. 10.1359/jbmr.1998.13.1.122.

Lovejoy, C. O. (2005). The natural history of human gait and posture: part 1. Spine and pelvis. *Gait Posture*, 21 (1), 95–112. 10.1016/j.gaitpost.2004.01.001

Lovejoy, C. O. (2007). The natural history of human gait and posture. Part 3. The knee. *Gait and Posture*, 25 (3), 325-341. 10.1016/j.gaitpost.2006.05.001

Marchal, F. (2000). A new morphometric analysis of the hominid pelvic bone. *Journal of Human Evolution*, 38 (3), 347-365. 10.1006/jhev.1999.0360

Marchi, D. (2015). Variation in tibia and fibula diaphyseal strength and its relationship with arboreal and terrestrial locomotion: extending the investigation to non-hominoid primates. *Journal of Anthropological Sciences*, 93, 153-156. 10.4436/JASS.93005

Martins, A. B., Fialho, M. S., Jerusalinsky, L., Valença-Montenegro, M. M., Bezerra, B. M., Laroque, P. O., Melo, F. R., & Lynch Alfaro, J. W. (2021). *Sapajus libidinosus* (amended version of 2019 assessment). *The IUCN Red List of Threatened Species*. 10.2305/IUCN.UK.2021-1.RLTS.T136346A192593226.en.

Martins Jr., A. M. G., Amorim, N., Carneiro, J. C., Affonso, P. R. A. M., Sampaio, I., & Schneider, H. (2015). Alu elements and the phylogeny of capuchin (*Cebus* and *Sapajus*) monkeys. *American Journal of Primatology*, 77 (4), 368-375. 10.1002/ajp.22352

1114 Meldrum, D. J. (1993). On plantigrady and quadrupedalism. Notes and Comments. *American*
1115 *journal of physical anthropology*, 91, 379–385. 10.1002/ajpa.1330910310
1116
1117 Mesquita, V. A., Souza, A. N. A., Sousa, E. L., Pinheiro, G. G., Silva, W. A., & Marques, D.
1118 A. (2019). *Atlas simplificado de osteologia de Alouatta seniculus.* Manaus: Instituto Federal de
1119 Educação, Ciência e Tecnologia do Amazonas.
1120
1121 Moore, K. L., & Dalley, A. F. (2006). *Clinically Oriented Anatomy*. Baltimore: Lippincott
1122 Williams & Wilkins.
1123
1124 Mundinger, G. S., Nam, A. J., Hui-Chou, H. G., Stanwix, M. G., Jones, L. S., Drachenberg, C.
1125 B., Kukuruga, D., Shipley, S. T., Dorafshar, A. H., Panda, A., Bartlett, S. T., Barth, R. N., &
1126 Rodriguez, E. D. (2011). Nonhuman primate model of fibula vascularized composite tissue
1127 allotransplantation demonstrates donor-recipient bony union. *Plastic and Reconstructive*
1128 *Surgery*, 128 (6), 1193-204. 10.1097/PRS.0b013e318230c5d0
1129
1130 Nascimento, R. A., Schiavetti, A., & Montaño, R. A. M. (2013). An assessment of illegal
1131 capuchin monkey trade in Bahia State, Brazil. *Neotropical Biology and Conservation*, 8 (2),
1132 79-87. 10.4013/nbc.2013.82.03
1133
1134 Nicolini, Y., Tramacere, A., Parmigiani, S., & Dadomo, H. (2019). Back to stir it up: Erectile
1135 dysfunction in an evolutionary, developmental, and clinical perspective. *Journal of Sex*
1136 *Research*, 56 (3), 378-390. 10.1080/00224499.2018.1480743

1137 Nieves, M., Remis, M. I., Sesarini, C., Hassel, D. L., Argüelles, C. F., & Mudry, M. D. (2021).
1138 Assessment of genetic variability in captive capuchin monkeys (Primates: Cebidae). *Scientific*
1139 *Reports*, 11 (1), 7306. 10.1038/s41598-021-86734-w
1140
1141 Nowak, M. G., Carlson, K. J., & Patel, B. A. (2010). Apparent density of the Primate calcaneo-
1142 cuboid joint and its association with locomotor mode, foot posture, and the "midtarsal break".
1143 *American Journal of Physical Anthropology*, 142 (2), 180–193. 10.1002/ajpa.21210
1144
1145 Olson, T. R., & Seidel, M. R. (1983). The evolutionary basis of some clinical disorders of the
1146 human foot: a comparative survey of the living primates. *Journal of the Foot & Ankle*, 3 (6),
1147 322-41. 10.1177/107110078300300603
1148
1149 Paciulli, L. M., & Chennu, L. H. (2018). Hands (primate). In W. Trevathan (Ed.), *The*
1150 *International Encyclopedia of Biological Anthropology* (pp. 1-3). Hoboken: Wiley Blackwell.
1151
1152 Patel, B. A., Ian, J. W., Doug, M. B., Michael, C. G., Susan, G. L., & Jack, T. S. (2015). Distinct
1153 functional roles of primate grasping hands and feet during arboreal quadrupedal locomotion.
1154 *Journal of Human Evolution*, 88, 79–84. 10.1016/j.jhevol.2015.09.004
1155
1156 Pearson, K., & Davin, A.G. (1921). On the sesamoids of the knee joint. *Biometrika*, 13 (2-3),
1157 133-175. 10.2307/2331752
1158
1159 Pritzker, K. P. H., & Kessler, M. J. (2012). Arthritis, muscle, adipose tissue and bone diseases.
1160 In C. R. Abee, K. Mansfield, S. Tardif, T. Morris (Eds.), *Nonhuman Primates in Biomedical*
1161 *Research, volume 2: Diseases* (pp. 629-697). San Diego: Elsevier-Academic Press.

Rafferty, K. L. (1998). Structural design of the femoral neck in primates. *Journal of Human Evolution*, 34 (4), 361–383. 10.1006/jhev.1997.0202

Rak, Y., & Arensburg, B. (1987). Kebara 2 Neanderthal pelvis: first look at a complete inlet. *American Journal of Physical Anthropology*, 73 (2), 227–231. 10.1002/ajpa.1330730209

Rangel, C. H., Adler, J. G. V., Heliodor, G. C., Santos Jr., A., & Verona, C. E. (2013). Relato de caso de morte por agressão entre macacos-prego *Sapajus nigritus* (Primates: Cebidae) no Jardim Botânico do Rio de Janeiro. *Neotropical Primates*, 20 (1), 48-52. 10.1896/044.020.0108

Reynolds, E. (1931). The evolution of the human pelvis in relation to the mechanics of erect posture. In G. D. Williams (Ed.), *Papers of the Peabody Museum of American Archaeology and Ethnology*. Cambridge: The Bureau of International Research of Harvard University and Radcliffe College for the Museum University.

Rodman, P. S. (1979). Skeletal differentiation of *Macaca fascicularis* and *Macaca nemestrina* in relation to arboreal and terrestrial quadrupedalism. *American Journal of Physical Anthropology*, 51 (1), 51-62. 10.1002/ajpa.1330510107

Rodman, P. S., & McHenry, H. M. (1980). Bioenergetics and the origin of hominid bipedalism. *American Journal of Physical Anthropology*, 52 (1), 103-106. 10.1002/ajpa.1330520113

Rosenberg, K. R. (1992). The evolution of modern human childbirth. *Supplement: The American Journal of Physical Anthropology*, 35 (S15), 89–124. 10.1002/ajpa.1330350605

1186 Ruff, C. B., & Leo, F. P. (1986). Use of computed tomography in skeletal structure research.
1187 *Yearbook of Physical Anthropology*, 29 (S7), 181-196. 10.1002/ajpa.1330290508
1188
1189 Ryan, T. M., & Sukhdeo, S. (2016). KSD-VP-1/1: Analysis of the postcranial skeleton using
1190 high-resolution computed tomography. In Y. Haile-Selassie, D. F. Su (Eds.), *The postcranial*
1191 *anatomy of Australopithecus afarensis: New Insights from KSD-VP-1/1 (Vertebrate*
1192 *Paleobiology and Paleoanthropology)*. Alemanha: Springer.
1193
1194 Schmitt, D. (2003). Mediolateral reaction forces and forelimb anatomy in quadrupedal
1195 primates: implications for interpreting locomotor behaviour in fossil primates. *Journal of*
1196 *Human Evolution*, 44 (1), 47-58. 10.1016/S0047-2484(02)00165-3
1197
1198 Schultz, A. H. (1930). The skeleton of the trunk and limbs of higher primates. *Human Biology*,
1199 2 (3), 303-438.
1200
1201 Schultz, N., Lough-Stevens, M., Abreu, E., Orr, T., & Dean, M. (2016). The baculum was
1202 gained and lost multiple times during mammalian evolution. *Integrative and Comparative*
1203 *Biology*, 56 (4), 644-656, 10.1093/icb/icw034
1204
1205 Silva, T. C. F., Valença-Montenegro, M. M., Lucas, J. L. B., Wagner, P. G. C., Ferreira, J. G.,
1206 Ferreira, D. R. A., Jerusalinsky, L., Martins, A. B., Senna, M. B., & Laroque, P. O. 2009.
1207 Morfometria de *Cebus libidinosus* SPIX, 1823 (Primates, Cebidae). In *XIII Congresso*
1208 *Brasileiro de Primatologia. Livro de Resumos do XIII Congresso Brasileiro de Primatologia.*

1209 Silverman, S., Morgan, J. P., Ferron, R., McNulty, W., & Merten, D. (2005). Radiographic
1210 evaluation of appendicular skeletal maturation in the rhesus monkey. *Veterinary Radiology &*
1211 *Ultrasound*, 24 (1), 25-34. 10.1111/j.1740-8261.1983.tb01711.x
1212
1213 Sobotta, J. (2000). *Atlas de Anatomia Humana*. Rio de Janeiro: Guanabara Koogan.
1214
1215 Spani, F., Morigi, M. P., Bettuzzi, M., Scalici, M., & Carosi, M. (2020). A 3D journey on virtual
1216 surfaces and inner structure of ossa genitalia in Primates by means of a non-invasive imaging
1217 tool. *PLoS ONE*, 15 (1), e0228131. 10.1371/journal.pone.0228131
1218
1219 Swindler, D.R., & Wood, C.D. (1973). Osteology/Appendicular skeleton. In D. R. Swindler, C.
1220 D. Wood (Eds.), *An Atlas of Primate Gross Anatomy – Baboon, Chimpanzee, and Man*.
1221 London: University of Washington Press.
1222
1223 Szalay, F., & Decker, R. (1974). Origins, evolution and function of the tarsus in Late Cretaceous
1224 Eutheria and Paleocene primates. In F. Jenkins (Ed.), *Primate Locomotion* (pp. 223-259). New
1225 York: Academic Press.
1226
1227 Szalay, F. (1982). A new appraisal of marsupial phylogeny and classification. In M. Archer
1228 (Ed.), *Carnivorous Marsupials* (pp. 621-640). Sydney: Royal Zoological Society.
1229
1230 Takebe, K., Nakagawa, A., Minami, H., Kanazawa, H., & Hirohata, K. (1984). Role of the
1231 fibula in weight-bearing. *Clinical Orthopaedics and Related Research*, 184, 289-292. PMID:
1232 6705357

1233 Taylor, G., & Bonney, V. (1905). On the homology and morphology of the popliteus muscle:
1234 A contribution to comparative myology. *Journal of Anatomy*, 40 (1), 334-350. PMCID:
1235 PMC1287337; PMID: 17232661
1236
1237 Tong, K., & Guiot, L. P. (2013). Minimally invasive plate osteosythesis of fractures of the
1238 radius and ulna in a primate. *Veterinary and Comparative Orthopaedics and Traumatology*, 26
1239 (5), 416-420. 10.3415/VCOT-12-10-0134
1240
1241 Vallois, H. V. (1914). *Etude anatomique de l'articulation du genou chez les primates*.
1242 Montpellier: L'abeille.
1243
1244 Walmsley, T. (1918). The reduction of the mammalian fibula. *Journal of Anatomy*, 52 (3), 326-
1245 331. PMCID: PMC1262828; PMID: 17103842
1246
1247 Wang, Q., Whittle, M., Cunningham, J., & Kenwright, J. (1996). Fibula and its ligaments in
1248 load transmission and ankle joint stability. *Clinical Orthopaedics and Related Research*, 330,
1249 261-270. 10.1097/00003086-199609000-00034
1250
1251 Watts, E. S. (1990). A Comparative study of neonatal skeletl development in *Cebus* and other
1252 primates. *Folia Primatologica*, 54 (3-4), 217-224. 10.1159/000156446.
1253
1254 Weaver, T. D., & Hublin, J. (2009). Neandertal birth canal shape and the evolution of human
1255 childbirth. *Proceedings of the National Academy of Sciences*, 106 (20), 8151–8156.
1256 10.1073/pnas.0812554106

1257 Yamanaka, A., Gunji, H., & Ishida, H. (2005). Curvature, length, and cross-sectional geometry
1258 of the femur and humerus in anthropoid primates. *American Journal of Physical Anthropology*,
1259 127 (1), 46–57. 10.1002/ajpa.10439
1260
1261 Young, D. R., & Schneider, V. S. (1981). Radiographic evidence of disuse osteoporosis in the
1262 monkey (*M. nemestrina*). *Calcified Tissue International*, 33 (6), 631-639.
1263 10.1007/BF02409501.

CONCLUSÃO GERAL

Ao apresentar dados anatômicos e de imagem detalhados sobre o esqueleto de *Sapajus libidinosus*, este estudo contribui com a educação em ciência de animais de laboratório. Foi possível constatar a eficiência dos métodos de diagnósticos por imagem na espécie, demonstrando ser possível a identificação das estruturas ósseas com bastante precisão, quando comparada às peças ósseas. Ao todo, o conhecimento das estruturas anatômicas macroscopicamente e associadas ao reconhecimento em imagens, leva a uma melhor explanação de casos clínicos, conclusão de diagnósticos, instituição de tratamentos adequados, avaliação de agentes terapêuticos e intervenções cirúrgicas ósseas em primatas no geral, além de abrir margem para a realização de uma gama de experimentos voltados a patologias esqueléticas, anestesias regionais, doenças osteometabólicas, planejamentos cirúrgicos, paleontologia, dentre outros.

No geral, *Sapajus libidinosus* apresentou características anatômicas estruturalmente e morfologicamente mais semelhantes aos primatas da infraordem Simiiformes, sendo um ótimo indicador de modelo experimental para estudos no homem. Esse material vem, enfim, servir como acervo para futuras pesquisas com base morfológica e de saúde em primatas humanos, e não humanos, resultando no refinamento dos protocolos de pesquisa e possivelmente também em uma redução de animais em experimentos.